1-1-2018

Models and Algorithms to Solve Electric Vehicle Charging Stations Designing and Managing Problem under Uncertainty

Md Abdul Quddus

Models and algorithms to solve electric vehicle charging stations designing and managing problem under uncertainty.

By

Md Abdul Quddus

A Dissertation
Submitted to the Faculty of
Mississippi State University
in Partial Fulfillment of the Requirements
for the Degree of Doctor of Philosophy
in Industrial and Systems Engineering
in the Department of Industrial and Systems Engineering

Mississippi State, Mississippi

December 2018

Models and algorithms to solve electric vehicle charging stations designing and managing problem under uncertainty.

By

Md Abdul Quddus

Approved:

Mohammad Marufuzzaman
(Major Professor)

John M. Usher
(Committee Member)

Linkan Bian
(Committee Member)

Mihalis M. Golias
(Committee Member)

Stanley F. Bullington
(Graduate Coordinator)

Jason M. Keith
Dean
Bagley College of Engineering

Name: Md Abdul Quddus

Date of Degree: December 14, 2018

Institution: Mississippi State University

Major Field: Industrial and Systems Engineering

Major Professor: Dr. Mohammad Marufuzzaman

Title of Study: Models and algorithms to solve electric vehicle charging stations designing and managing problem under uncertainty.

Pages of Study: 217

Candidate for Degree of Doctor of Philosophy

This dissertation studies a framework in support electric vehicle (EV) charging station expansion and management decisions. In the first part of the dissertation, we present mathematical model for designing and managing electric vehicle charging stations, considering both long-term planning decisions and short-term hourly operational decisions (e.g., number of batteries charged, discharged through Battery-to-Grid (B2G), stored, Vehicle-to-Grid (V2G), renewable, grid power usage) over a pre-specified planning horizon and under stochastic power demand. The model captures the non-linear load congestion effect that increases exponentially as the electricity consumed by plugged-in EVs approaches the capacity of the charging station and linearizes it. The study proposes a hybrid decomposition algorithm that utilizes a Sample Average Approximation and an enhanced Progressive Hedging algorithm (PHA) inside a Constraint Generation algorithmic framework to efficiently solve the proposed optimization model. A case study based on a road network of Washington, D.C. is presented to visualize and validate the modeling results. Computa-

tional experiments demonstrate the effectiveness of the proposed algorithm in solving the problem in a practical amount of time. Finding of the study include that incorporating the load congestion factor encourages the opening of large-sized charging stations, increases the number of stored batteries, and that higher congestion costs call for a decrease in the opening of new charging stations.

The second part of the dissertation is dedicated to investigate the performance of a collaborative decision model to optimize electricity flow among commercial buildings, electric vehicle charging stations, and power grid under power demand uncertainty. A two-stage stochastic programming model is proposed to incorporate energy sharing and collaborative decisions among network entities with the aim of overall energy network cost minimization. We use San Francisco, California as a testing ground to visualize and validate the modeling results. Computational experiments draw managerial insights into how different key input parameters (e.g., grid power unavailability, power collaboration restriction) affect the overall energy network design and cost. Finally, a novel disruption prevention model is proposed for designing and managing EV charging stations with respect to both long-term planning and short-term operational decisions, over a pre-determined planning horizon and under a stochastic power demand. Long-term planning decisions determine the type, location, and time of established charging stations, while short-term operational decisions manage power resource utilization. A non-linear term is introduced into the model to prevent the evolution of excessive temperature on a power line under stochastic exogenous factors such as outside temperature and air velocity. Since the research problem is NP-hard, a Sample Average Approximation method enhanced with a

Scenario Decomposition algorithm on the basis of Lagrangian Decomposition scheme is proposed to obtain a good-quality solution within a reasonable computational time. As a testing ground, the road network of Washington, D.C. is considered to visualize and validate the modeling results. The results of the analysis provide a number of managerial insights to help decision makers achieving a more reliable and cost-effective electricity supply network.

Key words: Charging stations, electric vehicles, Vehicle-to-grid, renewable energy, constraint-generation algorithm, sample average approximation, scenario decomposition algorithm, rolling horizon heuristics

DEDICATION

Dedicated to my parents and my adorable daughter Ruqaiyah.

ACKNOWLEDGEMENTS

I am very grateful to everyone who has assisted me throughout my doctoral studies over the years. I would like to thank Dr. Mohammad Marufuzzaman, my major professor, who provided me continuous encouragement and guidance throughout my doctoral studies. I learned a lot from him both academically and personally, which will become an invaluable asset in my future career life. I am also indebted to the other committee members, Dr. Linkan Bian, Dr. John Usher, and Dr. Mihalis M. Golias (Mike), for their insightful comments and suggestions that helped improving this research. I truly appreciate all of their time and assistance.

There are too many friends to name in the Department of Industrial & Systems Engineering who helped me during the past several years. Especially notable are Dr. Sushil, Sudipta, Dr. Amir, MK, Dr. Mohannad, Badr, Darwesh, Abdulwahab, Hadi, Jack, Dr. Adindu, Ravi, Farjana, and Niamat. They helped me on my research and made the graduate school fun.

Also, I would like to thank my parents, brothers, and sisters. They have always been a tremendous source of encouragement in each day of my life. They taught me how to love unconditionally and be stronger. Then, I will show my deep and earnest thanks to my wife, Nusrat and my daughter, Ruqaiyah. Nusrat was very patient and encouraging me to work

hard during this whole process. She sacrificed a lot for my career development, and she was always there cheering me up and stood by me through the good times and bad.

Finally, and most importantly, I want to thank God (ALLAH). God provided everything I needed to complete this dissertation.

TABLE OF CONTENTS

LIST OF TABLES

LIST OF FIGURES

CHAPTER I

INTRODUCTION

1.1 Introduction

As a result of the growing concern over climate change and dependence on fossil fuels, electric vehicles (EV) have gained considerable attention all over the world in the last few decades. In it's continuation, a tremendous EV sales increase is observed on U.S. market in recent years i.e., approximately, 700% sales increase from 2011 to 2016 [55] where nearly 82% sales increase only in December, 2016 over the same time period in 2015 [35]. Additionally, with a number of incentive policies proposed by both federal and state government, it is anticipated that there will be approximately 2.7 million of EVs on the U.S. road by 2020 [15]. Furthermore, it is expected that EV market share will hit 10% by 2025 [56]. The large EV penetration will bring both challenges and opportunities for the power grid (PG). Running these automobiles on electricity instead of gasoline shifts energy requirements from gas pumps to the power grid. If the charging is unmanaged for such a large number of EVs, the electricity grid can be affected negatively. To support large-scale deployment of EVs and achieve efficient grid operation, there is a urgent need to carefully design and manage electric vehicle charging stations to not only reduce overall system cost, but also provide substantial environmental and social benefits.

As the penetration of electric vehicle widens, the load on the power system is going to increase due to the expansion of the charging infrastructure. A recent study from Washington State's Department of Transportation reveals that a total of 228,725 kWh of energy were supplied to charge electric cars between 2012 and 2015, which is equivalent to displacing 22,397 gallons of gas [125]. Further, projections are made that the load from electric vehicles in the state of Washington will reach around 107 MW by 2029 [24]. Bai et al. [9] demonstrate the effect of daily load curve triggered by electric vehicle under three different charging modes. In another study, Qian et al. [98] show how different percentages of penetration of electric vehicles can add a significant increase to the power consumption. From both studies it has been noticed that electric vehicle has direct impact on the daily load curve. With more EVs in the market, their charging on different time period of the day can add a large load in the electricity grid. This phenomena is generally referred to as *load congestion* to the distributed energy sources which may arise due to various reasons, e.g., very high power consumption during peak hours, concentrated charging of EVs, and excessive power generation from distributed energy sources. If the charging stations are not expanded and managed properly, the resultant load congestion can bring serious distress to the power grid, including directly damaging many key elements of our distribution system such as distribution transformers, feeders, and many others. Moreover, the excessive electricity flow causes line over heating, which in extreme case cause power transmission line failure. To hedge against this projected growth, it may be required to upgrade electric distribution systems, increase capacities, integrate other power sources (i.e., renewable energy sources, vehicle-to-grid, shared energy from commercial buildings), and

introduce dynamic pricing options (i.e., encourage off-peak charging so that the growing loads do not exacerbate peak demand).

This dissertation is divided into three sections. The contribution of each section is mentioned at the chapter corresponding to each section. In the first section (CHAPTER II), we present a novel two-stage stochastic mixed-integer program that incorporates both long term planning decisions and short-term hourly operational decisions to design and manage electric vehicle charging station decisions under stochastic power demand while preventing congestion from occurring. We consider a long-term charging station expansion planning model that features size, location, and timing to open facilities and demand response with a short-term hourly time resolution. The problem is challenging due to the NP-hard nature of location design, uncertainties present in dynamic traffic demands, availability in renewable energy sources, and many other issues which significantly impact hourly power management (e.g., renewable, V2G, grid power usage) and battery charging, discharging, and storage decisions in a charging station. We develop and implement a customized hybrid decomposition algorithm that combines a Constraint Generation algorithm with a Sample Average Approximation algorithm and an enhanced Progressive Hedging algorithm. We introduce a number of algorithmic improvements such as penalty parameter updating techniques, local and global heuristics, and different variants of the rolling horizon heuristic. We construct a real-world case study based on the road network of Washington, D.C. to test the performance of the algorithms and reveal interesting managerial insights. The outcome of this study provides a number of managerial insights on total system cost and optimal system design such as the optimal expansion of charging stations, number of bat-

teries charged, discharged, stored, vehicle-to-grid, renewable, grid power usage decisions under different power demand variability levels and congestion prices. Such results can effectively aid decision makers to investigate the impact of hourly demand management capabilities of a charging station.

In the second section (CHAPTER III), we proposes a novel collaborative energy sharing decision model to study energy sharing among a cluster of commercial buildings and EV charging stations in concert with the PG. The research problem is formulated as a two-stage stochastic mixed-integer linear programming (MILP) model and then solved using an enhanced Sample Average Approximation (SAA) method. The efficiency of the SAA method is enhanced by generating some problem specific valid inequalities. We demonstrate the computational performance of our customized hybrid algorithm relative to its generic version. We Construct a real-world case study to test the performance of the algorithms and reveal interesting managerial insights. We use San Francisco, California as a testing ground to visualize and validate the modeling results. The outcome of this study provides a number of managerial insights, such as the impact of demand variability, grid power disruption, power collaboration limit, and renewable energy cell sizes on overall system performance, which can effectively aid decision makers to design a cost-efficient collaborative system between multiple commercial buildings and EV charging stations.

In the third section (CHAPTER IV) this dissertation we develop and solve a reliable EV charging station planning and managing problem with explicit consideration of random power demand. We model the condition of the line temperature due to the excessive flow of electricity. We develop a novel reliable two-stage stochastic mixed-integer non-linear

programming model that incorporates both long term planning decisions and short-term hourly operational decisions to design and manage reliable electric vehicle charging station decisions under stochastic power demand. We consider a reliable two-stage stochastic program where in the first-stage we determine size, type and timing to open charging stations based on stochastic demand, and in the second-stage we satisfy the charging stations demand and track the operations of demand response with a short-term hourly time resolution. To linearize the model, we employ three linearization techniques based on McCormick relaxation techniques (also known as McCormick envelopes). We propose and implement a customized hybrid decomposition solution approach that combines a Sample Average Approximation algorithm with an enhanced Scenario Decomposition Algorithm to solve our proposed optimization model. The enhanced Scenario Decomposition Algorithm incorporate different variants of the rolling horizon heuristic. We apply the proposed model and algorithm to a realistic scale case study based on the road network of Washington, D.C. The outcome of this study provides a number of interesting managerial insights on total system cost and optimal system design. The decision includes optimal reliable EV charging station expansion, number of batteries charged, discharged, stored, vehicle-to-grid, RES, grid power usage decision under stochastic power demand. These results can effectively help decision makers to investigate the impact of hourly demand management capabilities of a charging station.

CHAPTER II

MANAGING LOAD CONGESTION IN ELECTRIC VEHICLE CHARGING STATIONS-A MULTI-PERIOD STOCHASTIC MODEL

2.1 Introduction

As a result of the growing concern over climate change and dependence on fossil fuels, *electric vehicles* (EV) have gained considerable attention all over the world in the last few decades. In it's continuation, we observe a tremendous EV sales increase on U.S. market in recent years i.e., approximately, 700% sales increase from 2011 to 2016 (shown in Figure 2.1a) [55] where nearly 82% sales increase only in December, 2016 over the same time period in 2015 (shown in Figure 2.1b) [35]. The increasing trend is motivated by a number of initiatives that have been taken by the U.S. government, such as the *EV Everywhere Grand Challenge* which aims to encourage the manufacture of EVs that are as affordable and user friendly as internal combustion vehicles by 2022 [115]. Furthermore, recent developments in battery technologies and the immense on-going research efforts are striving to alleviate the so called "range anxiety" issue for EV [84]. For instance, after a monumental advancement in lithium-ion batteries, Audi e-tron quattro is expected to hit the market in 2018 with a range of more than 310 miles[1]. With this advancement in battery technologies and a number of incentive policies proposed by the government, it is expected that

[1]Available from: `http://www.audi.com/en/innovation/quattro/quattro_IAA2015.html`

there will be approximately 2.7 million EVs on the U.S. road by 2020 [15]. If the charging is unmanaged for such a large number of EVs, the electricity grid can be affected negatively. Furthermore, the proper design and establishment of charging station infrastructure over time would improve the future use and support of EVs. These facts mandate an urgent need to efficiently design and manage charging station to promote widespread use of EVs. To achieve this goal, this study explores the major challenges associated with the establishment and expansion of an EV charging infrastructure and develops an optimization framework that can be used by decision makers to better manage charging stations related activities.

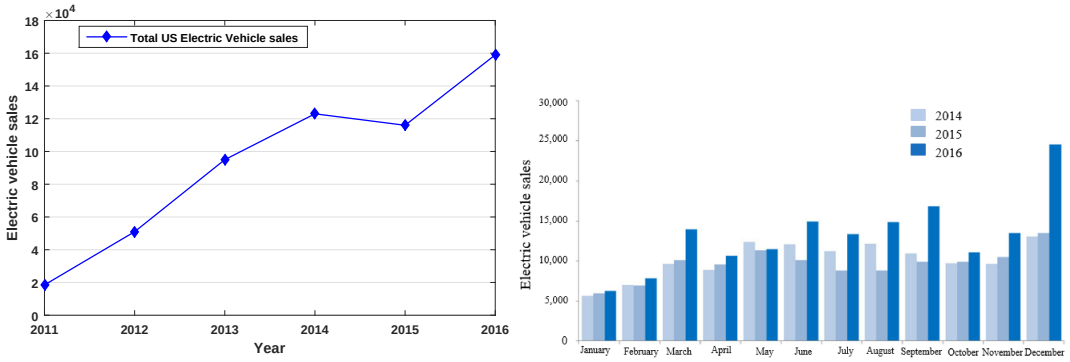

(a) (b)

Figure 2.1: U.S. EV sales by (a) year in between 2011–2016 [55] and (b) year and month distribution in between 2014–2016 [35]

The transition from internal combustion vehicles to EVs is influenced by several non-trivial factors. First, EVs have better fuel economy and lower fuel costs compared to conventional vehicles. For instance, EV fuel costs around 2–3 cents per mile whereas con-

ventional vehicles fuel costs approximately 13 cents per mile[2]. Second, the use of EVs reduces the United States reliance on imported petroleum and eventually increases energy security. These benefits make EVs an important segment of the U.S. automotive industry, which as a whole accounts for more than 3% of U.S. GDP [66]. As the number of EVs on the road increases, the number of charging stations and their capacities will need to be expanded accordingly. A recent study from Washington States Department of Transportation reveals that between 2012 and 2015 a total of 228,725 kWh of energy was utilized for charging electric cars, which is equivalent to displacing 22,397 gallons of gas [125]. In this study, they determined that these charging stations had been used 25,888 times since they were first opened in 2012. They anticipate that the EV load in the State of Washington will reach around 107 MW of electricity energy by 2029 which is an 87% increase from their current usage [24]. The increased use of EVs also increases electrical grid demand, which may increase high-level emission from petroleum-based electrical generation instead of reducing it. Due to the scarcity of fossil fuels and the negative consequences of using them, renewable energy sources are required to be coupled with the power grid as an alternative clean source of electricity. Additionally, the idea of vehicle-2-grid (V2G) is employed for reducing higher EVs charging effects to the grid. In V2G mode, the charging station supplies power to the grid. However, the projected increase of EV usage and integration of renewable energy sources along with V2G technology for EV charging presents opportunities as well as challenges. To hedge against this projected growth, power companies may need to upgrade electric distribution systems, increase capacities, integrate renewable

[2]Available from: `http://www.fueleconomy.gov/feg/findacar.shtml`

energy sources, and introduce dynamic pricing options (i.e., encourage off-peak charging so that the growing loads do not exacerbate peak demand).

The U.S. Energy Information Administration (EIA) reports that the power demand varies significantly throughout the day (see Figure 2.2a) [118] where 10:0 A.M. to 8:0 P.M. are considered as peak hours of a regular day. The EIA further reports that replacing the internal-combustion engine vehicles with EVs will add approximately 1,198 TWh of electricity demand to the grid [119]. This number represents a nearly 29% increase in annual electricity demand in the United States. Figure 2.2b shows the trend of alternative fuel stations in the U.S. by fuel type from 1992 to 2016. Although 2016 experienced the largest growth to support the growing EV population, it is not sufficient to meet the demand for the projected growth of EVs. With more EVs in the market, their charging on different time period of the day can add a large load in the electricity grid. This phenomena is generally referred to as "load congestion" to the distributed energy sources which may arise due to various reasons, e.g., very high power consumption during peak hours, concentrated charging of EVs, and excessive power generation from distributed energy sources. If the charging stations are not expanded and managed properly, the resultant load congestion can bring serious distress to the power grid, including directly damaging many key elements of our distribution system such as distribution transformers, feeders, and many others.

Till now majority of the previous studies have focused on identifying the best locations for refueling stations to maximize traffic flow under deterministic (e.g., [65], [23], [67]) and stochastic settings (e.g., [89], [74], [14], [52]). Further, these studies attempt to extend the single time period flow-refueling location model (FRLM), introduced by Kuby and Lim

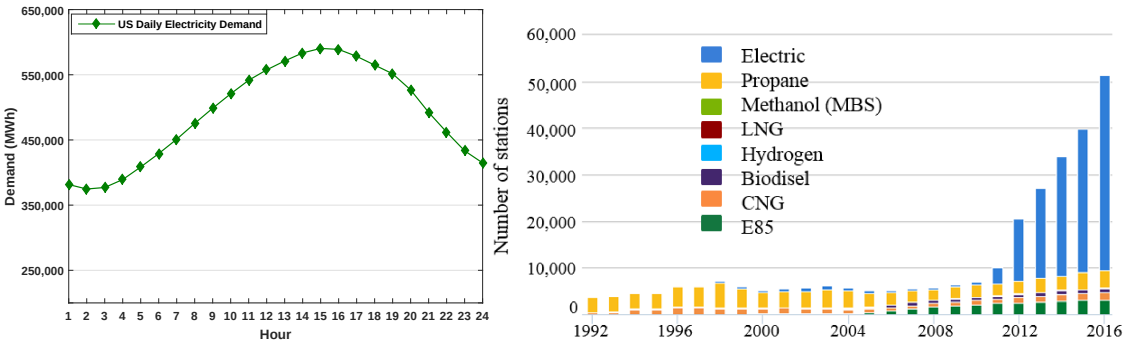

(a) (b)

Figure 2.2: U.S. (a) daily power demand curve [118] and (b) alternative fueling station by fuel type [3]

[65] and later extended by Wang and Lin [124], and MirHassani and Ebrazi [79], to a multi-period charging station location problem (e.g., Chung and Kwon [23] and Li et al. [67]) to gradually expand EV charging stations over time. Although these extensions have practical implications, the authors concentrate on charging station expansion decisions while little or no attention is given towards short-term charging station operational decisions (e.g., hourly management decisions). Further, the prior studies ignored the impact of load congestion to the design and management of charging station expansion decisions.

One possible way to alleviate grid load is to integrate renewable energy with V2G sources while planning for optimal charging schedules for the EVs. We observe a good stream of literatures in this research direction. For instance, Zhang et al. [133] and Su and Chow [110] develop a methodology to manage the charging load for a large number of EVs. The authors consider the travel pattern of EVs and charging characteristics of the EV batteries (e.g., initial state-of-charge (SoC), battery charging time) to determine

an optimal charging schedule for the EVs. Liu et al. [68] introduce the concept of smart charging patterns of EVs while considering coordination of wind energy, thermal units, and V2G sources. Along the same line, Gan et al. [37] formulate the EV charging scheduling problem as an optimal control problem, and propose a decentralized algorithm to solve the problem. Guo et al. [44] plan for the operations of EV parking decks considering the availability of renewable energy sources. The authors develop a tool to decide hourly parking fees and charging prices based upon the forecast values of the available renewable energy. Later, Fathabadi [33] studies the different effects of incorporating V2G and renewable energy in a power network. The goal is to identify the best coordination that is effective in sustaining the system while reducing the cost and loss of power production. Zhang et al. [134] propose a scheduling model to minimize the mean waiting time for charging the EVs at the charging stations equipped with multiple plug outlets and availability of renewable energy sources. Haddadian et al. [46] consider the effects of incorporating V2G and renewable energy as viable sources for the smart grid. The authors further developed in [45] a mixed-integer linear programming (MILP) model to optimize the hourly scheduling of electricity where several key components of the model are considered as hourly load, energy, and outages are generated using a Monte-Carlo simulation. Most of existing studies along this line attempt to manage load congestion for a single facility while little or no attention is given to its impact on the charging station expansion decisions.

Another stream of research in the literature focuses on the application of battery swap stations where EVs can exchange their depleted, or nearly depleted, batteries with full batteries for a fee. Pan et al. [89] develop a two-stage stochastic program that optimally

locates EV battery swapping stations prior to the realization of battery demands, loads, and generation capacity of renewable energies. Worley and Klabjan [129] present a dynamic programming model that determines the number of batteries to purchase and their charging time based on dynamic changes in grid power fees. The authors only consider the transportation system but do not consider V2G or the impact on the power grid. Mak et al. [74] develop two robust optimization models based on incomplete information (e.g., adoption rate of EVs). The first model minimizes costs while the second model maximizes a pre-specified amount of profit associated with optimizing the infrastructure planning for battery swap stations. Two important features of the models are their consideration of the capacity limits at the swapping stations and demand uncertainty. Another study by Zheng et al. [135] develop a framework for optimal design of battery charging/swap stations in distribution systems based on life cycle cost (LCC). Liu et al. [70] propose an optimization model to determine the energy exchange strategies of a battery swap station considering solar energy availability. The authors extend their prior work in [71] to determine the location and capacity of battery swap stations while considering energy demand management decisions (e.g., optimal pricing, number of batteries to charge and discharge). In another study, Avci et al. [8] examine switch stations in comparison to charging stations and conclude that switch stations encourage the adoption of EVs. Both options have advantages and disadvantages when compared to one another. Note that most of existing studies along this line attempt to optimize battery management (e.g., hourly charging, discharging, storing) decisions within the facility while little or no attention is given to the charging station expansion decisions.

To the best of the authors' knowledge, none of the prior studies have investigated the impact of charging station load congestion from a random power demand viewpoint and integrated both the long-term charging station planning decisions (e.g., size, location, and year to open charging stations) and short-term hourly operational decisions (e.g., number of batteries charged, discharged, stored, use of vehicle-to-grid (V2G), renewable, grid power usage) under the same decision making framework. Separate considerations of these factors, as observed in the prior studies, may result in sub-optimal decisions or inaccurate cost estimation. The integration of these factors is motivated by the real cases for which a holistic network design might help developing policies and insights for the potential grow of EVs in the market. To fill this gap in the literature, we have developed a two-stage stochastic mixed-integer non-linear programming model that simultaneously optimizes long-term planning decisions and short-term charging station management decisions over a pre-specified planning horizon and under stochastic power demand while preventing congestion from occurring. The problem is challenging due to the $\mathcal{NP}$-hard nature of location design, uncertainties present in dynamic traffic demands, availability in renewable energy sources, and many other issues which significantly impact hourly power management (e.g., renewable, V2G, grid power usage) and battery charging, discharging, and storage decisions in a charging station. To solve this challenging problem, we propose a highly customized hybrid decomposition algorithm that combines a Constraint Generation algorithm with a Sample Average Approximation algorithm and an enhanced Progressive Hedging algorithm. The enhanced Progressive Hedging algorithm incorporates several algorithmic improvements such as variable fixing techniques, penalty parameter

updating techniques, local and global heuristics, and different variants of the rolling horizon heuristic. It has been verified through multiple experiments that the customized hybrid decomposition algorithm is capable of generating high-quality solutions to large-size problem instances of our model, within a reasonable amount of time.

Besides proposing the general model, another important contribution of this paper is applying this model to a real-world case study based on the road network of Washington, D.C. The outcome of this study provides a number of managerial insights on total system cost and optimal system design such as the optimal expansion of charging stations, number of batteries charged, discharged, stored, vehicle-to-grid, renewable, grid power usage decisions under different power demand variability levels and congestion prices. Such results can effectively aid decision makers to investigate the impact of hourly demand management capabilities of a charging station. Finally, we show how the average unit power charging requirement of a car and the average unit power discharged from a car impact system performance.

The remainder of this paper is organized as follows. Section 2.2 presents the two-stage stochastic programming model formulation for optimal sizing and location of charging stations considering power demand uncertainty. The hybrid solution approach to solve our proposed optimization model is introduced in Section 2.3. Section 2.4 presents a series of numerical experiments to draw managerial insights and verify the algorithmic performances. Lastly, Section 2.5 provides conclusions along with briefly discusses future research directions.

2.2 Problem Description and Model Formulation

This section presents a two-stage stochastic mixed-integer nonlinear programming (MINLP) model that simultaneously addresses long-term electric vehicle charging station expansion decisions (e.g., sizing, location, and timing decisions) and short-term hourly operational decisions (e.g., number of batteries charged, discharged, stored, V2G, renewable, grid power usage) over a pre-specified planning horizon and under power demand uncertainty. Further, the model contains a nonlinear congestion cost function which arises due to overloading the power system of a charging station during the peak charging hours. We then present a modified formulation that linearizes the nonlinear congestion cost function and allow us to solve the proposed optimization model in a reasonable amount of time.

2.2.1 Nonlinar Model Formulation

The problem under investigation divides a transportation network into a set of cells $\mathcal{I} = \{1, 2, ..., I\}$ where each cell can be considered as a candidate location to open a charging station. These charging stations can be constructed over a set of time periods $\mathcal{T} = \{1, 2, ..., T\}$ which is expressed in years. Locating a charging station of capacity $l \in \mathcal{L}$ at cell $i \in \mathcal{I}$ in year $t \in \mathcal{T}$ entails a fixed opening cost Ψ_{lit}. We assume that a budget B_t is available each year $t \in \mathcal{T}$ to open the stations. Let $\mathcal{H} = \{1, 2, ..., H\}$ be the set of hours, and we assume that the number of time-stages are predetermined with equal length (for both hours and years). Let f_{iht} be the expected number of cars that will flow into each cell $i \in \mathcal{I}$ in hour $h \in \mathcal{H}$ of year $t \in \mathcal{T}$. However, there is uncertainty about what percentage of the cars require charging. Let η^{ω}_{ht} be the percentage of cars charging in

hour $h \in \mathcal{H}$ of year $t \in \mathcal{T}$ under scenario $\omega \in \Omega$ where Ω represents the set of scenarios of different realization of electric vehicles and ρ_ω is a probability of a particular realization. We further denote λ^c_{iht} as the average charge required by an EV in cell $i \in \mathcal{I}$ at hour $h \in \mathcal{H}$ of year $t \in \mathcal{T}$ (in kWh). Therefore, the realized power demand for each cell $i \in \mathcal{I}$ at hour $h \in \mathcal{H}$ of year $t \in \mathcal{T}$ can be represented by $\lambda^c_{iht}\eta^\omega_{ht} f_{iht}$.

This model assumes that the electric power consumed in a charging station is provided by one or more of the three energy sources: (i) conventional power generators (CPGs) generally located at power stations, (ii) solar power sources at the charging stations, and (iii) the discharge of EVs into the grid using V2G connection capability. A two-way connection between the power grid and a station is used in the model, i.e., one for power flow from the grid to the stations during the charging process and another for the flow from the stations to the grid during the EV discharging process. Figure 4.1 presents the structure of the power network consisting of one charging station, one power grid, one renewable resource, and one electric car battery. During the EV charging process, a cost results from the charging stations having to buy energy from power grids. However, during an EV's discharging process they can sell power to the grid generating income for the station. We define parameters c^{pg}_{ht}, c^r_{ht}, and c^{v2g}_{ht} to be the cost per kWh for charging EVs to use the grid, solar, and V2G power in hour $h \in \mathcal{H}$ of year $t \in \mathcal{T}$, respectively. We further define c^d_{ht} as the profit per kWh for discharging batteries in hour $h \in \mathcal{H}$ of year $t \in \mathcal{T}$.

Let q^{in}_{lht} and q^{out}_{lht} denote the number of plug-ins of capacity $l \in \mathcal{L}$ available at a station for charging and discharging EVs in hour $h \in \mathcal{H}$ of year $t \in \mathcal{T}$, respectively. We assume a minimum of e^{cs}_{lht} power demand is required to open a charging station while a station

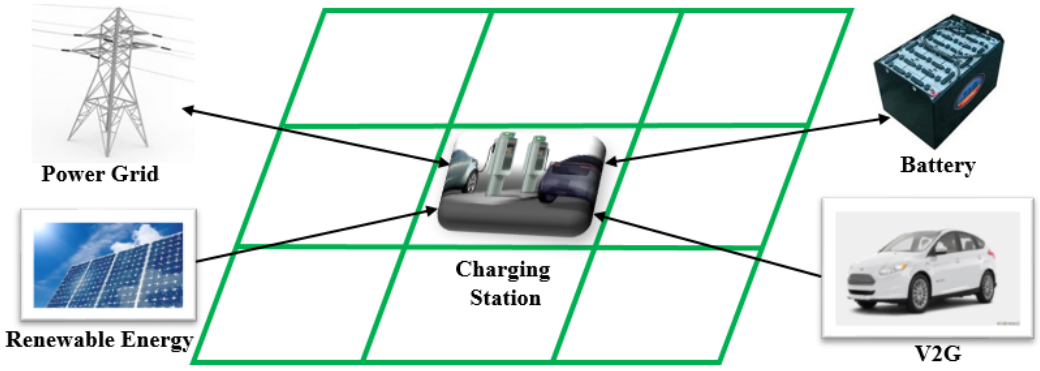

Figure 2.3: Network representation of an electric vehicle charging station with various alternative power sources

of size $l \in \mathcal{L}$ cannot handle more than c_{lht}^{cap} (in kWh) of power demand in a given hour $h \in \mathcal{H}$ of year $t \in \mathcal{T}$. The maximum and minimum power grid electricity availability is denoted by p_{liht}^{+} and p_{liht}^{-}, for each capacity $l \in \mathcal{L}$ in cell $i \in \mathcal{I}$ at hour $h \in \mathcal{H}$ of year $t \in \mathcal{T}$, respectively. We further define r_{ilht} to be the solar power availability of a charging station located in cell $i \in \mathcal{I}$ of capacity $l \in \mathcal{L}$ at hour $h \in \mathcal{H}$ of year $t \in \mathcal{T}$. Apart from grid and renewable sources, charging stations can also obtain power from V2G sources. We approximate this availability by $\lambda_{iht}^{d} \varkappa_{ht} f_{iht}$ where it is assumed that $\varkappa_{ht}$ is the percentage of f_{iht} vehicles that will discharge power to each charging station located in cell $i \in \mathcal{I}$ of capacity $l \in \mathcal{L}$ at hour $h \in \mathcal{H}$ of year $t \in \mathcal{T}$ and λ_{iht}^{d} be the average unit power discharged from an electric vehicle (in kWh). This formulation assumes that if the available energy generation is not sufficient to meet the EVs load demand, then electricity can be imported from other distribution companies for the unmet demand by paying a unit penalty cost, c_{ht}^{u}, per kWh in hour $h \in \mathcal{H}$ of year $t \in \mathcal{T}$. Let ϑ^{c} and ϑ^{d} denote the charging and discharging efficiency and b^{cap} be the rated capacity of an electric

car battery. The *state of charge* (SoC[3]) of each vehicle when it is plugged in for charging and the *depth of discharge* (DoD[4]) of each vehicle when it is plugged in for discharging, are variables. Therefore, electric vehicles coming to the charging stations, whether for charging or discharging, will have different levels of electricity requirements. For each cell $i \in \mathcal{I}$ in hour $h \in \mathcal{H}$ of year $t \in \mathcal{T}$, we assume c^+_{iht}, c^-_{iht} to be the maximum and minimum SoC of the batteries, and similarly, d^+_{iht} and d^-_{iht} represent the maximum and minimum DoD of the batteries, respectively. Note that λ^c_{iht} and λ^d_{iht} denote the unit power charge requirement and discharge capability for each car in hour $h \in \mathcal{H}$ of year $t \in \mathcal{T}$, respectively, which can be obtained as: $\lambda^c_{iht} = b^{cap}(c^+_{iht} - c^-_{iht})$ and $\lambda^d_{iht} = b^{cap}(d^+_{iht} - d^-_{iht})$. Finally, we assume that the charging station has an inventory holding cost for batteries, which is denoted as γ^s_{ht}, and the maximum number of batteries that can be stored at hour $h \in \mathcal{H}$ of year $t \in \mathcal{T}$ is u_{liht}. The following additional assumptions made to simplify our modeling approach are:

Assumption 1 *There is an increasing trend in electric car traffic volume over time. This assumption is consistent with the assumption made by Chung and Kwon [23].*

Assumption 2 *Every charging station that is opened will also have solar energy as an available resource.*

Assumption 3 *Both grid and solar power are available throughout the entire planning horizon without interruptions; i.e., no disruption will occur during the time horizon that causes power failure.*

[3]SoC is the ratio of available energy to maximum storable energy in battery
[4]DoD is used to explain how deeply a battery discharged in electric grid

Assumption 4 *All charging stations will be fast charging DC chargers with battery swapping capability. This assumption is made to ensure the ability to meet the demand.*

Assumption 5 *All charging stations will be open 24 hours a day, 7 days a week.*

Assumption 6 *Charging stations will have V2G technology to encourage electric vehicle owner to sell back power to the grid.*

Assumption 7 *The proposed model assumes an identical type battery that has a specified rated capacity can be recharged or swapped at any charging stations.*

Let us now introduce the following notation for our two-stage stochastic programming model formulation:

Sets:

- $\mathcal{I}$: set of cells
- $\mathcal{T}$: set of years
- $\mathcal{H}$: set of representing hours in a year
- $\mathcal{L}$: set of capacities for charging stations
- Ω: set of scenarios

Parameters:

- Ψ_{lit}: annual cost of constructing a charging station of capacity $l \in \mathcal{L}$ at cell $i \in \mathcal{I}$ in year $t \in \mathcal{T}$
- B_t: budget available for opening charging stations in year $t \in \mathcal{T}$

- f_{iht}: flow of electric vehicles in cell $i \in \mathcal{I}$ at hour $h \in \mathcal{H}$ of year $t \in \mathcal{T}$
- λ^c_{iht}: average charging required of a car in cell $i \in \mathcal{I}$ at hour $h \in \mathcal{H}$ of year $t \in \mathcal{T}$ (in kWh)
- λ^d_{iht}: average power discharged from a car in cell $i \in \mathcal{I}$ at hour $h \in \mathcal{H}$ of year $t \in \mathcal{T}$ (in kWh)
- η^{ω}_{ht}: percentage of cars charging in hour $h \in \mathcal{H}$ of year $t \in \mathcal{T}$ under scenario $\omega \in \Omega$
- $\varkappa_{ht}$: percentage of cars discharging in hour $h \in \mathcal{H}$ of year $t \in \mathcal{T}$
- c^{pg}_{ht}: unit power grid electricity cost consumed by electric vehicles in hour $h \in \mathcal{H}$ of year $t \in \mathcal{T}$ ($/kWh)
- c^{r}_{ht}: unit cost of producing electric power from renewable energy sources in hour $h \in \mathcal{H}$ of year $t \in \mathcal{T}$ ($/kWh)
- c^{v2g}_{ht}: unit V2G electric energy cost in hour $h \in \mathcal{H}$ of year $t \in \mathcal{T}$ ($/kWh)
- r_{liht}: availability of renewable energy at a charging station located in cell $i \in \mathcal{I}$ of capacity $l \in \mathcal{L}$ at hour $h \in \mathcal{H}$ of year $t \in \mathcal{T}$
- p^{+}_{liht}/p^{-}_{liht}: grid power availability (maximum/minimum) at a charging station located in cell $i \in \mathcal{I}$ of capacity $l \in \mathcal{L}$ at hour $h \in \mathcal{H}$ of year $t \in \mathcal{T}$
- c^{u}_{ht}: unit penalty cost for a power shortage in hour $h \in \mathcal{H}$ of year $t \in \mathcal{T}$ ($/kWh)
- e^{cs}_{lht}: minimum power demand required to open a charging station of capacity $l \in \mathcal{L}$ in hour $h \in \mathcal{H}$ of year $t \in \mathcal{T}$
- c^{cap}_{lht}: charging station capacity of size $l \in \mathcal{L}$ in hour $h \in \mathcal{H}$ of year $t \in \mathcal{T}$ (in kWh)
- γ^{s}_{ht}: unit cost of storing a battery in hour $h \in \mathcal{H}$ of year $t \in \mathcal{T}$
- c^{d}_{ht}: unit profit of discharging a battery in hour $h \in \mathcal{H}$ of year $t \in \mathcal{T}$ ($/kWh$)

- q^{in}_{lht}: number of plug-ins available for charging batteries at a charging station of capacity $l \in \mathcal{L}$ in hour $h \in \mathcal{H}$ of year $t \in \mathcal{T}$
- q^{out}_{lht}: number of plug-ins available for discharging batteries at a charging station of capacity $l \in \mathcal{L}$ in hour $h \in \mathcal{H}$ of year $t \in \mathcal{T}$
- u_{liht}: maximum number of batteries that can be stored at a charging station located in cell $i \in \mathcal{I}$ of capacity $l \in \mathcal{L}$ in hour $h \in \mathcal{H}$ of year $t \in \mathcal{T}$
- b^{cap}: rated capacity of a battery
- ϑ^c: charging efficiency of an EV
- ϑ^d: discharging efficiency of an EV
- c^+_{iht}/c^-_{iht}: state of charge of the batteries (maximum/minimum) at cell $i \in \mathcal{I}$ in hour $h \in \mathcal{H}$ of year $t \in \mathcal{T}$
- d^+_{iht}/d^-_{iht}: depth of discharge of the batteries (maximum/minimum) at cell $i \in \mathcal{I}$ in hour $h \in \mathcal{H}$ of year $t \in \mathcal{T}$
- χ^c_{ht}: congestion cost in hour $h \in \mathcal{H}$ of year $t \in \mathcal{T}$
- ρ_ω: probability of scenario $\omega \in \Omega$

Decision variables:

- Y_{lit}: 1 if a charging station of capacity $l \in \mathcal{L}$ is opened in cell $i \in \mathcal{I}$ of year $t \in \mathcal{T}$; 0 otherwise
- G^ω_{iht}: amount of grid power used to satisfy demand at cell $i \in \mathcal{I}$ in hour $h \in \mathcal{H}$ of year $t \in \mathcal{T}$ under scenario $\omega \in \Omega$
- Z^ω_{iht}: amount of renewable energy used to satisfy demand at cell $i \in \mathcal{I}$ in hour $h \in \mathcal{H}$ of year $t \in \mathcal{T}$ under scenario $\omega \in \Omega$

- V_{iht}^{ω}: amount of V2G power used to satisfy demand at cell $i \in \mathcal{I}$ in hour $h \in \mathcal{H}$ of year $t \in \mathcal{T}$ under scenario $\omega \in \Omega$
- U_{iht}^{ω}: amount of power shortage at cell $i \in \mathcal{I}$ in hour $h \in \mathcal{H}$ of year $t \in \mathcal{T}$ under scenario $\omega \in \Omega$
- B_{iht}^{ω}: number of batteries in demand at cell $i \in \mathcal{I}$ in hour $h \in \mathcal{H}$ of year $t \in \mathcal{T}$ under scenario $\omega \in \Omega$
- H_{iht}^{ω}: number of full batteries stored at cell $i \in \mathcal{I}$ in hour $h \in \mathcal{H}$ of year $t \in \mathcal{T}$ under scenario $\omega \in \Omega$
- S_{iht}^{ω}: number of batteries charging at cell $i \in \mathcal{I}$ in hour $h \in \mathcal{H}$ of year $t \in \mathcal{T}$ under scenario $\omega \in \Omega$
- P_{iht}^{ω}: number of batteries discharging at cell $i \in \mathcal{I}$ in hour $h \in \mathcal{H}$ of year $t \in \mathcal{T}$ under scenario $\omega \in \Omega$
- W_{iht}^{ω}: dummy variable for calculating total amount of power used to satisfy demand at cell $i \in \mathcal{I}$ in hour $h \in \mathcal{H}$ of year $t \in \mathcal{T}$ under scenario $\omega \in \Omega$

We now introduce the following first and second-stage decision variables for our two-stage stochastic programming model formulation. The first-stage decision variables $\mathbf{Y} := \{Y_{lit}\}_{l \in \mathcal{L}, i \in \mathcal{I}, t \in \mathcal{T}}$ select the size, location, and time to open a charging station, i.e.,

$$Y_{lit} = \begin{cases} 1 & \text{if a charging station of capacity } l \in \mathcal{L} \text{ is opened at cell } i \in \mathcal{I} \text{ in year } t \in \mathcal{T} \\ 0 & \text{otherwise;} \end{cases}$$

The second-stage decision variables are: $\mathbf{G} := \{G_{iht}^{\omega}\}_{i \in \mathcal{I}, h \in \mathcal{H}, t \in \mathcal{T}, \omega \in \Omega}$ denotes the amount of grid power used to satisfy demand at cell $i \in \mathcal{I}$ in hour $h \in \mathcal{H}$ of year $t \in \mathcal{T}$

under scenario $\omega \in \Omega$; $\mathbf{Z} := \{Z^{\omega}_{iht}\}_{i\in\mathcal{I},h\in\mathcal{H},t\in\mathcal{T},\omega\in\Omega}$ denotes the amount of solar power used to satisfy demand at cell $i \in \mathcal{I}$ in hour $h \in \mathcal{H}$ of year $t \in \mathcal{T}$ under scenario $\omega \in \Omega$; $\mathbf{V} := \{V^{\omega}_{iht}\}_{i\in\mathcal{I},h\in\mathcal{H},t\in\mathcal{T},\omega\in\Omega}$ denotes the amount of V2G power used to satisfy demand at cell $i \in \mathcal{I}$ in hour $h \in \mathcal{H}$ of year $t \in \mathcal{T}$ under scenario $\omega \in \Omega$; $\mathbf{B} := \{B^{\omega}_{iht}\}_{i\in\mathcal{I},h\in\mathcal{H},t\in\mathcal{T},\omega\in\Omega}$ denotes the number of batteries in demand at cell $i \in \mathcal{I}$ in hour $h \in \mathcal{H}$ of year $t \in \mathcal{T}$ under scenario $\omega \in \Omega$; $\mathbf{H} := \{H^{\omega}_{iht}\}_{i\in\mathcal{I},h\in\mathcal{H},t\in\mathcal{T},\omega\in\Omega}$ denotes the number of full batteries available at cell $i \in \mathcal{I}$ in hour $h \in \mathcal{H}$ of year $t \in \mathcal{T}$ under scenario $\omega \in \Omega$; $\mathbf{S} := \{S^{\omega}_{iht}\}_{i\in\mathcal{I},h\in\mathcal{H},t\in\mathcal{T},\omega\in\Omega}$ denotes the number of batteries charging at cell $i \in \mathcal{I}$ in hour $h \in \mathcal{H}$ of year $t \in \mathcal{T}$ under scenario $\omega \in \Omega$; $\mathbf{P} := \{P^{\omega}_{iht}\}_{i\in\mathcal{I},h\in\mathcal{H},t\in\mathcal{T},\omega\in\Omega}$ denotes the number of batteries discharging at cell $i \in \mathcal{I}$ in hour $h \in \mathcal{H}$ of year $t \in \mathcal{T}$ under scenario $\omega \in \Omega$; $\mathbf{W} := \{W^{\omega}_{iht}\}$ denotes a dummy variable for calculating the total amount of power used to satisfy demand at cell $i \in \mathcal{I}$ in hour $h \in \mathcal{H}$ of year $t \in \mathcal{T}$ under scenario $\omega \in \Omega$; and finally $\mathbf{U} := \{U^{\omega}_{iht}\}_{i\in\mathcal{I},h\in\mathcal{H},t\in\mathcal{T},\omega\in\Omega}$ denotes the level of power shortage at cell $i \in \mathcal{I}$ in hour $h \in \mathcal{H}$ of year $t \in \mathcal{T}$ under scenario $\omega \in \Omega$.

With the increase in adoption of EVs in the market, the electricity grid may more likely to be getting congested due to the large load imposed by EVs during the peak charging hours. If the load congestion caused by the EVs are not managed properly, the electricity grid can be seriously impacted due the consequences of such event, examples include but not limited to the direct failure of distribution transformers, feeders, and many others. We assume that when all the available plug-ins (both charging and discharging plug-ins) are occupied by the EVs during a peak operating hour, the power requirement of the EVs, W^{ω}_{iht}, approaches the capacity c^{cap}_{lht} of the charging station $i \in \mathcal{I}$. Under steady-state conditions,

the system-wide average load, considering only the charging station facilities, can be represented as: $\sum_{i\in\mathcal{I}}\sum_{h\in\mathcal{H}}\sum_{t\in\mathcal{T}}\left(\frac{W^{\omega}_{iht}}{\sum_{l\in\mathcal{L}} c^{cap}_{lht}Y_{lit}-W^{\omega}_{iht}}\right)$. For a charging station $i \in \mathcal{I}$, when concentrated charging occurs in the EVs on a specified hour $h \in \mathcal{H}$ of a given year $t \in \mathcal{T}$, the ratio of this equation grows exponentially. Hence, the impact of load congestion can be realistically addressed by the model. Let χ^{c}_{ht} be the load congestion price charged by the charging station at hour $h \in \mathcal{H}$ of year $t \in \mathcal{T}$. The system-wide load congestion cost now becomes: $\sum_{i\in\mathcal{I}}\sum_{h\in\mathcal{H}}\sum_{t\in\mathcal{T}}\chi^{c}_{ht}\left(\frac{W^{\omega}_{iht}}{\sum_{l\in\mathcal{L}} c^{cap}_{lht}Y_{lit}-W^{\omega}_{iht}}\right)$. Taking this factor into consideration, the following two-stage stochastic Mixed-Integer Nonlinear Programming (MINLP) model, referred to as **[NEV]**, can be formulated as follows:

$$\textbf{[NEV]}\ \underset{\mathbf{Y}}{Minimize}\ \sum_{l\in\mathcal{L}}\sum_{i\in\mathcal{I}}\sum_{t\in\mathcal{T}}\Psi_{lit}Y_{lit}+\sum_{\omega\in\Omega}\rho_{\omega}\mathbb{Q}(\mathbf{Y},\omega) \tag{2.1}$$

subject to

$$\sum_{l\in\mathcal{L}}Y_{lit} \leq 1 \qquad \forall i\in\mathcal{I}, t\in\mathcal{T} \tag{2.2}$$

$$Y_{lit-1} \leq Y_{lit} \qquad \forall l\in\mathcal{L}, i\in\mathcal{I}, t\in\mathcal{T} \tag{2.3}$$

$$\sum_{l\in\mathcal{L}}\sum_{i\in\mathcal{I}}\Psi_{lit}Y_{lit} \leq B_t \qquad \forall t\in\mathcal{T} \tag{2.4}$$

$$Y_{lit} \in \{0,1\} \qquad \forall l\in\mathcal{L}, i\in\mathcal{I}, t\in\mathcal{T} \tag{2.5}$$

with $\mathbb{Q}(\mathbf{Y},\omega)$ being the solution of the following second-stage problem:

$$\mathbb{Q}(\mathbf{Y},\omega)=\underset{\textbf{G,Z,B,U,V,W,H,P,S}}{Minimize}\sum_{i\in\mathcal{I}}\sum_{h\in\mathcal{H}}\sum_{t\in\mathcal{T}}\Big\{\Big(\frac{c^{pg}_{ht}}{\vartheta^{c}}\Big)G^{\omega}_{iht}+\Big(\frac{c^{r}_{ht}}{\vartheta^{c}}\Big)Z^{\omega}_{iht}+\Big(\frac{c^{pg}_{ht}\lambda^{c}_{iht}}{\vartheta^{c}}\Big)B^{\omega}_{iht}+$$
$$\Big(\frac{c^{v2g}_{ht}}{\vartheta^{c}}\Big)V^{\omega}_{iht}+\Big(\frac{c^{u}_{ht}}{\vartheta^{c}}\Big)U^{\omega}_{iht}+\gamma^{s}_{ht}H^{\omega}_{iht}+\chi^{c}_{ht}\Big(\frac{W^{\omega}_{iht}}{\sum_{l\in\mathcal{L}}c^{cap}_{lht}Y_{lit}-W^{\omega}_{iht}}\Big)-\Big(\frac{c^{d}_{ht}\lambda^{d}_{iht}}{\vartheta^{d}}\Big)P^{\omega}_{iht}\Big\} \tag{2.6}$$

subject to

$$G^{\omega}_{iht} + Z^{\omega}_{iht} + V^{\omega}_{iht} + \lambda^{c}_{iht} B^{\omega}_{iht} = W^{\omega}_{iht} \ \forall i \in \mathcal{I}, h \in \mathcal{H}, t \in \mathcal{T}, \omega \in \Omega \quad (2.7)$$

$$W^{\omega}_{iht} \geq \sum_{l \in \mathcal{L}} e^{cs}_{lht} Y_{lit} \ \forall i \in \mathcal{I}, h \in \mathcal{H}, t \in \mathcal{T}, \omega \in \Omega \quad (2.8)$$

$$\lambda^{c}_{iht} \eta^{\omega}_{ht} f_{iht} - W^{\omega}_{iht} = U^{\omega}_{iht} \quad \forall i \in \mathcal{I}, h \in \mathcal{H}, t \in \mathcal{T}, \omega \in \Omega \quad (2.9)$$

$$H^{\omega}_{iht} \leq \sum_{l \in \mathcal{L}} u_{liht} Y_{lit} \ \forall i \in \mathcal{I}, h \in \mathcal{H}, t \in \mathcal{T}, \omega \in \Omega \quad (2.10)$$

$$H^{\omega}_{iht} - B^{\omega}_{iht} - P^{\omega}_{iht} + S^{\omega}_{iht} = H^{\omega}_{i,h+1,t} \ \forall i \in \mathcal{I}, h \in \mathcal{H} \backslash |H|, t \in \mathcal{T}, \omega \in \Omega \quad (2.11)$$

$$H^{\omega}_{i|H|t} - B^{\omega}_{i|H|t} - P^{\omega}_{i|H|t} + S^{\omega}_{i|H|t} = H^{\omega}_{i,1,t+1} \ \forall i \in \mathcal{I}, t \in \mathcal{T} \backslash |T|, \omega \in \Omega \quad (2.12)$$

$$S^{\omega}_{i,1,1} = 0 \ \forall i \in \mathcal{I}, \omega \in \Omega \quad (2.13)$$

$$S^{\omega}_{i,h+1,t} = B^{\omega}_{iht} + P^{\omega}_{iht} \ \forall i \in \mathcal{I}, h \in \mathcal{H} \backslash |H|, t \in \mathcal{T}, \omega \in \Omega$$

$$S^{\omega}_{i,1,t+1} = B^{\omega}_{i|H|t} + P^{\omega}_{i|H|t} \ \forall i \in \mathcal{I}, t \in \mathcal{T} \backslash |T|, \omega \in \Omega \quad (2.14)$$

$$S^{\omega}_{iht} \leq \sum_{l \in \mathcal{L}} q^{in}_{lht} Y_{lit} \ \forall i \in \mathcal{I}, h \in \mathcal{H}, t \in \mathcal{T}, \omega \in \Omega \quad (2.15)$$

$$P^{\omega}_{iht} \leq \sum_{l \in \mathcal{L}} q^{out}_{lht} Y_{lit} \ \forall i \in \mathcal{I}, h \in \mathcal{H}, t \in \mathcal{T}, \omega \in \Omega \quad (2.16)$$

$$W^{\omega}_{iht} \leq \sum_{l \in \mathcal{L}} c^{cap}_{lht} Y_{lit} \ \forall i \in \mathcal{I}, h \in \mathcal{H}, t \in \mathcal{T}, \omega \in \Omega \quad (2.17)$$

$$\sum_{l \in \mathcal{L}} p^{-}_{liht} Y_{lit} \leq G^{\omega}_{iht} \leq \sum_{l \in \mathcal{L}} p^{+}_{liht} Y_{lit} \ \forall i \in \mathcal{I}, h \in \mathcal{H}, t \in \mathcal{T}, \omega \in \Omega \quad (2.18)$$

$$V^{\omega}_{iht} \leq \sum_{l \in \mathcal{L}} \lambda^{d}_{iht} \varkappa_{ht} f_{iht} Y_{lit} \ \forall i \in \mathcal{I}, h \in \mathcal{H}, t \in \mathcal{T}, \omega \in \Omega$$

$$Z^{\omega}_{iht} \leq \sum_{l \in \mathcal{L}} r_{liht} Y_{lit} \ \forall i \in \mathcal{I}, h \in \mathcal{H}, t \in \mathcal{T}, \omega \in \Omega \quad (2.19)$$

$$H^{\omega}_{iht}, B^{\omega}_{iht}, S^{\omega}_{iht}, P^{\omega}_{iht} \in Z^{+} \quad \forall i \in \mathcal{I}, h \in \mathcal{H}, t \in \mathcal{T}, \omega \in \Omega \quad (2.20)$$

$$G^{\omega}_{iht}, Z^{\omega}_{iht}, V^{\omega}_{iht}, U^{\omega}_{iht} \geq 0 \quad \forall i \in \mathcal{I}, h \in \mathcal{H}, t \in \mathcal{T}, \omega \in \Omega \quad (2.21)$$

The objective function (2.1) is the sum of the first-stage costs and the expected second-stage costs over all scenarios. The first-stage decisions minimize the charging station open-

ing costs. Constraints (2.2) ensure that at most one charging station of capacity $l \in \mathcal{L}$ is opened in a given cell $i \in \mathcal{I}$ in year $t \in \mathcal{T}$. Constraints (2.3) indicate that if a station is opened in an earlier time period, it will remain open in the subsequent time periods. Constraints (2.4) restrict the number of charging stations that can be opened in a given year $t \in \mathcal{T}$ with a pre-specified budget. Constraints (2.5) set the binary restrictions for the first-stage decision variables.

The objective function (2.6) minimizes the expected value of the second-stage costs. More specifically, the first four terms in (2.6) represent the cost of charging stations due to using grid, renewable, battery, and V2G power sources, respectively. The fifth term represents the expected penalty costs in case of electricity shortage. The next two terms represent the cost associated with not satisfying the electricity demand and storing of batteries in the charging stations. The last two terms of the objective function represent the expected load congestion cost and profit gained due to discharging batteries in the charging stations. Constraints (2.7) calculate the total amount of electricity used (via grid, renewable, battery, and V2G) in a given cell $i \in \mathcal{I}$ at hour $h \in \mathcal{H}$ of year $t \in \mathcal{T}$ under scenario $\omega \in \Omega$. Constraints (2.8) ensure that opening a charging station at a given cell $i \in \mathcal{I}$ mandates a minimum power availability. Constraints (2.9) indicate that the power demand ($\lambda^c_{iht}\eta^\omega_{ht}f_{iht}$) for each cell $i \in \mathcal{I}$ must be satisfied either through the power grid, renewable resources, V2G, swapping batteries, or through the purchase of electricity from other power distribution companies. Constraints (2.10) restrict the number of batteries that can be stored in a charging station. Constraints (2.11) and (2.12) decide the hourly storing, charging, and discharging battery decisions for a charging station located in cell $i \in \mathcal{I}$ of

a given year $t \in \mathcal{T}$ under scenario $\omega \in \Omega$. Constraints (2.13) indicate that the first hour of the planning horizon starts with no charged batteries. Constraints (2.14) indicate that battery charging decisions made on hour $(h+1)$ is dependent on the number of batteries being charged and discharged in hour h. Constraints (2.14) ensure that the number of batteries that should be charged in the first hour of year $(t+1)$ is dependent on the number of batteries being charged and discharged in the last hour of year t. Constraints (2.15) and (2.16) indicate that the number of batteries charged or discharged should be limited by the number of plug-ins available at the charging stations. Constraints (2.17) indicate that the amount of power used (via grid, renewable, battery, and V2G) at a charging station located in cell $i \in \mathcal{I}$ at hour $h \in \mathcal{H}$ of year $t \in \mathcal{T}$ is limited by the capacity (c_{lht}^{cap}) of the station. To ensure power stability, grid power usage at a charging station located in cell $i \in \mathcal{I}$ at hour $h \in \mathcal{H}$ of year $t \in \mathcal{T}$ under scenario $\omega \in \Omega$ should fall between a minimum (p_{ilht}^{-}) and maximum (p_{ilht}^{+}) limit. This is ensured via constraints (2.18). Constraints (2.19) indicate that the availability of V2G power in a given cell $i \in \mathcal{I}$ is limited by the electric vehicles willing to discharge at hour $h \in \mathcal{H}$ of year $t \in \mathcal{T}$ under scenario $\omega \in \Omega$. Constraints (2.19) limit the usage of renewable power in a given cell $i \in \mathcal{I}$ at hour $h \in \mathcal{H}$ of year $t \in \mathcal{T}$ under scenario $\omega \in \Omega$ to its availability (r_{liht}). Constraints (2.20) and (2.21) are the standard integrality and non-negativity constraints, respectively.

2.2.2 Model Linearization

Model **[NEV]** is nonlinear due to the presence of a nonlinear congestion cost function in the objective function. This cost grows exponentially as the load of a charging station

approaches its capacity. To linearize this term, we adopt an approach proposed by Elhedhli and Wu [30]. Let us now introduce a new decision variable $\mathbf{F} := \{F^{\omega}_{iht}\}_{i\in\mathcal{I},h\in\mathcal{H},t\in\mathcal{T},\omega\in\Omega}$ which can be defined as follows:

$$F^{\omega}_{iht} = \frac{W^{\omega}_{iht}}{\sum_{l\in\mathcal{L}} c^{cap}_{lht} Y_{lit} - W^{\omega}_{iht}} \tag{2.22}$$

where equation (2.22) can be further reduced as follows:

$$W^{\omega}_{iht} = \left(\frac{F^{\omega}_{iht}}{1+F^{\omega}_{iht}}\right)\sum_{l\in\mathcal{L}} c^{cap}_{lht} Y_{lit} = \sum_{l\in\mathcal{L}} c^{cap}_{lht}\left(\frac{F^{\omega}_{iht}}{1+F^{\omega}_{iht}}\right) Y_{lit} \quad \forall i \in \mathcal{I}, \; h \in \mathcal{H}, t \in \mathcal{T}, \omega \in \Omega \tag{2.23}$$

Let us introduce another continuous variable $\mathbf{X} := \{X^{\omega}_{liht}\}_{l\in\mathcal{L},i\in\mathcal{I},h\in\mathcal{H},t\in\mathcal{T},\omega\in\Omega}$ which is defined as follows:

$$X^{\omega}_{liht} = \left(\frac{F^{\omega}_{iht}}{1+F^{\omega}_{iht}}\right) Y_{lit} \qquad \forall l \in \mathcal{L}, i \in \mathcal{I}, h \in \mathcal{H}, t \in \mathcal{T}, \omega \in \Omega \tag{2.24}$$

when $\{Y_{lit}\}_{l\in\mathcal{L},i\in\mathcal{I},t\in\mathcal{T}} = 1$, the above equation reduces to the following:

$$\sum_{l\in\mathcal{L}} X^{\omega}_{liht} = \frac{F^{\omega}_{iht}}{1+F^{\omega}_{iht}} \qquad \forall i \in \mathcal{I}, h \in \mathcal{H}, t \in \mathcal{T}, \omega \in \Omega \tag{2.25}$$

It is interesting to note that for the case when $\{Y_{lit}\}_{l\in\mathcal{L},i\in\mathcal{I},t\in\mathcal{T}} = 0$, constraints (2.24) force $\{X^{\omega}_{liht}\}_{l\in\mathcal{L},i\in\mathcal{I},h\in\mathcal{H},t\in\mathcal{T},\omega\in\Omega} = 0$. This condition is enforced via introducing the following additional constraints in the model formulation:

$$0 \leq X^{\omega}_{liht} \leq Y_{lit} \qquad \forall l \in \mathcal{L}, i \in \mathcal{I}, h \in \mathcal{H}, t \in \mathcal{T}, \omega \in \Omega \tag{2.26}$$

Lemma 1 *The function defined by* $X^{\omega}_{liht}(F^{\omega}_{iht}) = \frac{F^{\omega}_{iht}}{1+F^{\omega}_{iht}}$ *is a concave function in* $F^{\omega}_{iht} \in (0, \infty)$.

Proof: The first derivative $w.r.t.$ F^{ω}_{iht} is $\frac{\delta}{\delta F^{\omega}_{iht}}(X^{\omega}_{liht}) = 1/(1+F^{\omega}_{iht})^2 > 0$. Again, taking the second derivative of the previous function provides: $\frac{\delta^2}{\delta {F^{\omega}_{iht}}^2}(X^{\omega}_{liht}) = -2/(1+F^{\omega}_{iht})^3 < 0$. The positive value in the first derivative and negative value in the second derivative proves that the function $X^{\omega}_{liht}(F^{\omega}_{iht})$ is concave in F^{ω}_{iht}. ∎

Lemma 1 implies that the concave function $X^{\omega}_{liht}(F^{\omega}_{iht})$ can be accurately approximated by adding the following set of tangent cutting planes [30]:

$$\frac{F^{\omega}_{iht}}{1+F^{\omega}_{iht}} = Min_{m \in \mathcal{M}} \left[\frac{F^{\omega}_{iht}}{\left(1+F^{\omega,m}_{iht}\right)^2} + \left(\frac{F^{\omega,m}_{iht}}{1+F^{\omega,m}_{iht}} \right)^2 \right] \tag{2.27}$$

which can be represented by:

$$\frac{F^{\omega}_{iht}}{1+F^{\omega}_{iht}} \leq \frac{F^{\omega}_{iht}}{\left(1+F^{\omega,m}_{iht}\right)^2} + \left(\frac{F^{\omega,m}_{iht}}{1+F^{\omega,m}_{iht}} \right)^2 \forall i \in \mathcal{I}, h \in \mathcal{H}, t \in \mathcal{T}, m \in \mathcal{M}, \omega \in \Omega \tag{2.28}$$

where $\{F^{\omega,m}_{iht}\}_{i \in \mathcal{I}, h \in \mathcal{H}, t \in \mathcal{T}, \omega \in \Omega, m \in \mathcal{M}}$ indicate the set of points to approximate equation (2.26). Since the value of $\{Y_{lit}\}_{l \in \mathcal{L}, i \in \mathcal{I}, t \in \mathcal{T}}$ is finite; the value that $\{F^{\omega}_{iht}\}_{i \in \mathcal{I}, h \in \mathcal{H}, t \in \mathcal{T}, \omega \in \Omega}$ provides is also finite. This implies that the set $\mathcal{M}$ should be finite. Then, equation (2.29) can be derived from (2.25) and (2.28) as following:

$$\sum_{l\in\mathcal{L}} X^{\omega}_{liht} \leq \frac{F^{\omega}_{iht}}{\left(1+F^{\omega,m}_{iht}\right)^2} + \left(\frac{F^{\omega,m}_{iht}}{1+F^{\omega,m}_{iht}}\right)^2 \forall i\in\mathcal{I}, h\in\mathcal{H}, t\in\mathcal{T}, m\in\mathcal{M}, \omega\in\Omega \quad (2.29)$$

The approximated linearized objective function of **[NEV]**, referred to as **[LEV]**, is as follows:

$$\textbf{[LEV]} \underset{\textbf{Y,G,Z,B,U,V,W,H,P,S,X,F}}{Minimize} \sum_{i\in\mathcal{I}}\sum_{t\in\mathcal{T}}\left(\sum_{l\in\mathcal{L}}\Psi_{lit}Y_{lit} + \sum_{h\in\mathcal{H}}\sum_{\omega\in\Omega}\rho_{\omega}\left\{\left(\frac{c^{pg}_{ht}}{\vartheta^c}\right)G^{\omega}_{iht} + \left(\frac{c^{r}_{ht}}{\vartheta^c}\right)Z^{\omega}_{iht} + \left(\frac{c^{pg}_{ht}\lambda^{c}_{iht}}{\vartheta^c}\right)B^{\omega}_{iht} + \left(\frac{c^{v2g}_{ht}}{\vartheta^c}\right)V^{\omega}_{iht} + \left(\frac{c^{u}_{ht}}{\vartheta^c}\right)U^{\omega}_{iht} + \gamma^{s}_{ht}H^{\omega}_{iht} + \chi^{c}_{ht}F^{\omega}_{iht} - \left(\frac{c^{d}_{ht}\lambda^{d}_{iht}}{\vartheta^d}\right)P^{\omega}_{iht}\right\}\right) \quad (2.30)$$

subject to (2.2)-(2.5), (2.7)-(2.16), (2.18)-(2.20), and

$$W^{\omega}_{iht} \leq \sum_{l\in\mathcal{L}} c^{cap}_{lht}X^{\omega}_{liht} \qquad \forall i\in\mathcal{I}, h\in\mathcal{H}, t\in\mathcal{T}, \omega\in\Omega \quad (2.31)$$

$$\sum_{l\in\mathcal{L}} X^{\omega}_{liht} \leq \frac{F^{\omega}_{iht}}{\left(1+F^{\omega,m}_{iht}\right)^2} + \left(\frac{F^{\omega,m}_{iht}}{1+F^{\omega}_{iht}}\right)^2 \forall i\in\mathcal{I}, h\in\mathcal{H}, t\in\mathcal{T}, m\in\mathcal{M}, \omega\in\Omega \quad (2.32)$$

$$X^{\omega}_{liht} \leq Y_{lit} \qquad \forall l\in\mathcal{L}, i\in\mathcal{I}, h\in\mathcal{H}, t\in\mathcal{T}, \omega\in\Omega \quad (2.33)$$

$$X^{\omega}_{liht}, F^{\omega}_{iht} \geq 0 \quad \forall l\in\mathcal{L}, i\in\mathcal{I}, h\in\mathcal{H}, t\in\mathcal{T}, \omega\in\Omega \quad (2.34)$$

2.3 Solution Approach

In this section, the solution techniques used to solve model **[LEV]** are discussed. For a single scenario ($|\Omega| = 1$), single year ($|\mathcal{T}| = 1$), and single hour ($|\mathcal{H}| = 1$) case, we can show that model **[LEV]** is actually a special case of a capacitated facility location problem which is known to be an $\mathcal{NP}$-hard problem [73]. Therefore, commercial solvers,

such as CPLEX/GUROBI, fail to solve large-scale instances of this problem. To overcome this computational burden, a hybrid sampling based decomposition algorithm is proposed. The hybrid algorithm nests a sample average approximation algorithm and an enhanced progressive hedging algorithm within a constraint generation algorithmic framework. The aim is to generate a high quality feasible solution for the **[LEV]** problem in a timely fashion.

2.3.1 Constraint Generation Algorithm

In (2.33), model **[LEV]** generates a large number of constraints. This will pose a serious challenge in solving model **[LEV]** efficiently by taking into account all the constraints at once. To remedy this problem, a constraint generation (**[CG]**) algorithm is developed that can efficiently and effectively solve model **[LEV]** despite generating a large number of constraints through (2.33) at once. A few recent studies, such as [128], [95], and [121], support that **[CG]** is capable of solving similar problems efficiently. The algorithm proceeds by solving a series of MILP programs with a subset of the constraints obtained from (2.33) and added thereafter as needed. The algorithm terminates when it finds a solution for the sub-problem which does not violate any constraints within some accepted tolerance in the full problem **[NEV]**. Otherwise, a new set of points $i.e.$, a new set of constraints/cuts, are generated and added to the original model **[LEV]** in the next iteration. The details of the algorithm are discussed below:

Let us define UB^q and LB^q as an upper and lower bound of the original problem at iteration q. We further define $\boldsymbol{\nu}$**[LEV]** as the solution of the objective function value of

[LEV] with

$(\mathbf{Y}^q, \mathbf{G}^q, \mathbf{Z}^q, \mathbf{B}^q, \mathbf{V}^q, \mathbf{U}^q, \mathbf{W}^q, \mathbf{H}^q, \mathbf{P}^q, \mathbf{S}^q)$ as its optimal solution. **Proposition 1** provides the lower bound of the **[CG]** algorithm.

Proposition 1 *Equation* (2.35) *provides the lower bound of the optimal objective function value of* ***[NEV]*** *for any given subset of points* $\{F_{iht}^{\omega,m}\}_{\mathcal{M}^q \subset \mathcal{M}}$.

$$LB = \boldsymbol{\nu}\textbf{[LEV]}(\mathcal{M}^q) = \sum_{i\in\mathcal{I}}\sum_{t\in\mathcal{T}}\left(\sum_{l\in\mathcal{L}}\Psi_{lit}Y_{lit} + \sum_{h\in\mathcal{H}}\sum_{\omega\in\Omega}\rho_\omega\Big\{\Big(\frac{c_{ht}^{pg}}{\vartheta^c}\Big)G_{iht}^{\omega} + \Big(\frac{c_{ht}^{r}}{\vartheta^c}\Big)Z_{iht}^{\omega} + \Big(\frac{c_{ht}^{pg}\lambda_{iht}^{c}}{\vartheta^c}\Big)B_{iht}^{\omega} + \Big(\frac{c_{ht}^{v2g}}{\vartheta^c}\Big)V_{iht}^{\omega} + \Big(\frac{c_{ht}^{u}}{\vartheta^c}\Big)U_{iht}^{\omega} + \gamma_{ht}^{s}H_{iht}^{\omega} + \chi_{ht}^{c}F_{iht}^{\omega} - \Big(\frac{c_{ht}^{d}\lambda_{iht}^{d}}{\vartheta^d}\Big)P_{iht}^{\omega}\Big\}\right) \tag{2.35}$$

Proof: **[LEV]**($\mathcal{M}^q$) is the relaxed version of problem **[LEV]**. Therefore, the optimal objective function value $\boldsymbol{\nu}$**[LEV]**($\mathcal{M}^q$) obtained from equation (2.35) provides the lower bound to the optimal objective value of **[LEV]**. Let $\boldsymbol{\nu}$**[LEV]** and $\boldsymbol{\nu}$**[NEV]** be the optimal objective function values obtained from **[LEV]** and **[NEV]**, respectively. Thus, it can be stated that $\boldsymbol{\nu}$**[LEV]**($\mathcal{M}^q$) $\leq$ $\boldsymbol{\nu}$**[LEV]**. Again, problem **[LEV]** is an approximation for problem **[NEV]**; therefore, the solution $\boldsymbol{\nu}$**[LEV]**($\mathcal{M}^q$) will also provide a valid lower bound for the optimal objective function value of **[NEV]**. Finally, it can be stated that $\boldsymbol{\nu}$**[LEV]**($\mathcal{M}^q$) $\leq$ $\boldsymbol{\nu}$**[LEV]** $\leq$ $\boldsymbol{\nu}$**[NEV]**. ■

The algorithm starts with a subset $\mathcal{M}^q \subset \mathcal{M}$ of the cuts where $\mathcal{M}^1$ can be empty or chosen a priori while the rest are generated as needed. The subset of points $\{F_{iht}^{\omega,m}\}_{\mathcal{M}^q \subset \mathcal{M}}$ are required to obtain the initial subset of cuts and are used to approximate function $X_{liht}^{\omega}(F_{iht}^{\omega})$. The resulting set is then used to obtain $\boldsymbol{\nu}$**[LEV]**($\mathcal{M}^q$) which provides a valid

lower bound for the original **[NEV]** problem (as shown in **Proposition 1**). This solution is then used to obtain an upper bound for the **[CG]** algorithm, as illustrated in the following proposition.

Proposition 2 *Equation* (2.36) *provides an upper bound of the optimal objective function value of* ***[NEV]*** *for any given subset of points* $\{F_{iht}^{\omega,m}\}_{\mathcal{M}^q \subset \mathcal{M}}$.

$$
\begin{aligned}
UB = \sum_{i\in\mathcal{I}}\sum_{t\in\mathcal{T}}\Bigg(\sum_{l\in\mathcal{L}}\Psi_{lit}Y_{lit} + \sum_{h\in\mathcal{H}}\sum_{\omega\in\Omega}\rho_\omega\Big\{\Big(\frac{c_{ht}^{pg}}{\vartheta^c}\Big)G_{iht}^{\omega} + \Big(\frac{c_{ht}^{r}}{\vartheta^c}\Big)Z_{iht}^{\omega} + \\
\Big(\frac{c_{ht}^{pg}\lambda_{iht}^{c}}{\vartheta^c}\Big)B_{iht}^{\omega} + \Big(\frac{c_{ht}^{v2g}}{\vartheta^c}\Big)V_{iht}^{\omega} + \Big(\frac{c_{ht}^{u}}{\vartheta^c}\Big)U_{iht}^{\omega} + \gamma_{ht}^{s}H_{iht}^{\omega} + \\
\chi_{ht}^{c}\Big(\frac{W_{iht}^{\omega}}{\sum_{l\in\mathcal{L}}c_{lht}^{cap}Y_{lit} - W_{iht}^{\omega}}\Big) - \Big(\frac{c_{ht}^{d}\lambda_{iht}^{d}}{\vartheta^d}\Big)P_{iht}^{\omega}\Big\}\Bigg)
\end{aligned}
\tag{2.36}
$$

Proof: All the feasible solutions of **[LEV]**($\mathcal{M}^q$) also provide a feasible solution to **[NEV]** since all the constraints of **[NEV]** are contained in **[LEV]**($\mathcal{M}^q$). Therefore, the objective function value of **[NEV]** evaluated at $(\mathbf{Y}^q, \mathbf{G}^q, \mathbf{Z}^q, \mathbf{B}^q, \mathbf{V}^q, \mathbf{U}^q, \mathbf{W}^q, \mathbf{H}^q, \mathbf{P}^q, \mathbf{S}^q)$, as shown in equation (2.36), provides an upper bound for the optimal objective value of **[NEV]**. ■

The algorithm continues until the gap between the lower and upper bound falls below a tolerance level ϵ; otherwise, a new set of points $\{F_{iht}^{\omega,m_{new}}\}$ are generated using the current solution (shown below) and the process continues.

$$
F_{iht}^{\omega,m_{new}} = \frac{W_{iht}^{\omega,q}}{\sum_{l\in\mathcal{L}}c_{lht}^{cap}Y_{lit}^{q} - W_{iht}^{\omega,q}} \tag{2.37}
$$

A pseudo-code of the **[CG]** algorithm is provided in **Algorithm 1**.

Algorithm 1: Constraint Generation Algorithm

Initialize: $q \leftarrow 1$, ϵ, $UB^q \leftarrow +\infty$, $LB^q \leftarrow -\infty$
terminate $\leftarrow$ **false**
Selecting an initial set of points: $\{F_{iht}^{\omega,m}\}_{\mathcal{M}^q \subset \mathcal{M}}$
while (*terminate* $=$ **false**) **do**
    Solve **[LEV]**($\mathcal{M}^q$) to obtain $\boldsymbol{\nu}$**[LEV]**($\mathcal{M}^q$) and ($\mathbf{Y}^q, \mathbf{G}^q, \mathbf{Z}^q, \mathbf{B}^q, \mathbf{V}^q, \mathbf{U}^q, \mathbf{W}^q, \mathbf{H}^q, \mathbf{P}^q, \mathbf{S}^q$)
    Update the lower bound: $LB^q \leftarrow \boldsymbol{\nu}$**[LEV]**($\mathcal{M}^q$) using (2.35)
    Update the upper bound UB^q using (2.36)
    if $((UB^q - LB^q)/UB^q \leq \epsilon)$ **then**
        terminate $\leftarrow$ **true**
    else
        $F_{iht}^{\omega,m_{new}} = \frac{W_{iht}^{\omega,q}}{\sum_{l \in \mathcal{L}} c_{lht}^{cap} Y_{lit}^q - W_{iht}^{\omega,q}}$
        $F_{iht}^{\omega,h,q+1} = F_{iht}^{\omega,h,q} \cup \{F_{iht}^{\omega,m_{new}}\}$
    end if
    $q \leftarrow q + 1$
end while

2.3.2 Sample Average Approximation

Solving model **[LEV]**($\mathcal{M}^q$) and obtaining a valid lower bound using **[CG]** algorithm is still considered challenging. The actual percentage of electric vehicles η_{ht}^{ω} that require charging in a charging station located at cell $i \in \mathcal{I}$ in hour $h \in \mathcal{H}$ of year $t \in \mathcal{T}$ varies significantly from one hour to the next within a given year. Therefore, it mandates evaluating a large scenario set to provide meaningful insights for the decision makers. However, evaluating such a large scenario set increases the size of the problem and thus poses a significant computational challenge in solving model **[LEV]** in a reasonable amount of time. To remedy this computational burden, a sampling technique, commonly known as the *Sample Average Approximation* (SAA) method, is employed. SAA is used extensively to solve large scale network flow-related problems, such as [120], [101], [105], [106], and many others. Interested readers may refer to the work by Kleywegt et al. [62] for the proof of

convergence properties of SAA, and Norkin et al. [85] and Mark et al. [75] for the evaluation of statistical performance of SAA (e.g., validation and error analysis, stopping rules). In SAA, a sample set $\{\omega^1, \omega^2, ..., \omega^N\}$ of N scenarios are generated from Ω according to a probability distribution $\mathbb{P}$ and they are solved repeatedly until a pre-specified tolerance gap is achieved. The lower bound of the **[CG]** algorithm, defined by equation (2.35) subject to constraints (2.2)-(2.5), (2.7)-(2.16), (2.18)-(2.21), and (2.31)-(2.34), is now approximated by the following SAA problem:

$$LB = \boldsymbol{\nu}\textbf{[LEV]}(\mathcal{M}_N^q) = \sum_{i\in\mathcal{I}}\sum_{t\in\mathcal{T}}\left(\sum_{l\in\mathcal{L}}\Psi_{lit}Y_{lit} + \frac{1}{N}\sum_{h\in\mathcal{H}}\sum_{n=1}^{N}\left\{\left(\frac{c_{ht}^{pg}}{\vartheta^c}\right)G_{iht}^n + \left(\frac{c_{ht}^{r}}{\vartheta^c}\right)Z_{iht}^n + \left(\frac{c_{ht}^{pg}\lambda_{iht}^c}{\vartheta^c}\right)B_{iht}^n + \left(\frac{c_{ht}^{v2g}}{\vartheta^c}\right)V_{iht}^n + \left(\frac{c_{ht}^{u}}{\vartheta^c}\right)U_{iht}^n + \gamma_{ht}^s H_{iht}^n + \chi_{ht}^c F_{iht}^n - \left(\frac{c_{ht}^{d}\lambda_{iht}^d}{\vartheta^d}\right)P_{iht}^n\right\}\right) \tag{2.38}$$

As the sample size increases, the optimal solution of **[LEV]**($\mathcal{M}^q$), i.e., $(\mathbf{Y}^q, \mathbf{G}^q, \mathbf{Z}^q, \mathbf{B}^q, \mathbf{V}^q, \mathbf{U}^q, \mathbf{W}^q, \mathbf{H}^q, \mathbf{P}^q, \mathbf{S}^q)$ and the optimal objective value $\boldsymbol{\nu}$**[LEV]**$(\mathcal{M}^q)$ converge, with a probability of one, to an optimal solution of the original **[EVC]** problem [62]. Assuming that the SAA problem is solved within an absolute optimality gap $\delta \geq 0$, we can estimate the sample size N needed to guarantee an ϵ-optimal solution to the true problem with a probability at least equal to $(1-\alpha)$ as:

$$N \geq \frac{3\sigma_{max}^2}{(\epsilon-\delta)^2}\left(|\mathcal{I}||\mathcal{K}||\mathcal{T}|(log2) - log\alpha\right) \tag{2.39}$$

where $\epsilon > \delta$, $\alpha \in (0,1)$, and σ_{max}^2 is a maximal variance of certain function differences [62]. Estimating the sample size using equation (2.39) is too conservative for practical

applications. Thus, one can choose a sample size N as a trade-off between the solution quality obtained by solving (2.38) to the original problem (2.35) and the computational burden needed to solve it. In each iteration of the algorithmic step, SAA provides a valid statistical lower and upper bound for the original **[EVC]** problem and the process terminates when the gap between the estimators falls below a pre-specified threshold value. The main steps of the SAA approach can be explained as follows:

1. Generate O independent scenarios of size N that have different car recharging percentage scenarios i.e., $\{\eta_o^1(\omega), \eta_o^2(\omega), ..., \eta_o^N(\omega)\}; \forall o = 1, ..., O$, where $\eta = \{\eta_{ht}^{\omega}; \forall h \in \mathcal{H}, t \in \mathcal{T}, \omega \in \Omega\}$ and solve the corresponding SAA (2.35). The lower bound problem for the **[CG]** algorithm, defined by (2.35) and subject to constraints (2.2)-(2.5), (2.7)-(2.16), (2.18)-(2.21), and (2.31)-(2.34), can now be approximated by the following SAA problem. For notation brevity, the mathematical model can be represented as follows:

$$Minimize_{Y \in \mathbf{Y}} \left\{ \hat{g}(Y_N^q) := \sum_{i \in \mathcal{I}} \sum_{t \in \mathcal{T}} \Big(\sum_{l \in \mathcal{L}} \Psi_{lit} Y_{lit} + \frac{1}{N} \sum_{n=1}^{N} \mathbb{Q}(\mathbf{Y}, n) \Big) \right\} \tag{2.40}$$

   where each sample o consists of N realizations of independently and identically distributed $(i.i.d)$ random scenarios. The optimal objective value is denoted by $\mathbf{v}_N^o$ and the optimal solution by $\hat{\mathbf{Y}}_N^o; o = 1, ..., O$.

2. Compute the average of the optimal solutions obtained by solving all SAA problems, $\bar{\mathbf{v}}_O^N$ and variance, $\sigma^2_{\bar{\mathbf{v}}_O^N}$:

$$\bar{\mathbf{v}}_O^N = \frac{1}{O}\sum_{o=1}^{O}\mathbf{v}_N^o \tag{2.41}$$

where $\bar{\mathbf{v}}_O^N$ provides a statistical lower bound on the optimal objective function value for the original problem (2.35), i.e., $\bar{\mathbf{v}}_O^N \leq \mathbf{v}^*$ [86]. Since O samples are generated and $\mathbf{v}_N^1, \mathbf{v}_N^2, ..., \mathbf{v}_N^O$ are independent, the variance of $\bar{\mathbf{v}}_O^N$ is given by:

$$\sigma^2_{\bar{\mathbf{v}}_O^N} = \frac{1}{(O-1)O}\sum_{o=1}^{O}\left(\mathbf{v}_N^o - \bar{\mathbf{v}}_O^N\right)^2 \tag{2.42}$$

3. Pick a feasible first-stage solution $\tilde{Y} \in \mathbf{Y}$ obtained from **Step 1** of the SAA algorithm, i.e., one of the solution from $\hat{\mathbf{Y}}_N^o$ and estimate the objective function value of the original problem using a reference sample N' as follows:

$$\tilde{\mathbf{g}}_{N'}(\tilde{Y}) := \sum_{i\in\mathcal{I}}\sum_{t\in\mathcal{T}}\left(\sum_{l\in\mathcal{L}}\Psi_{lit}Y_{lit} + \frac{1}{N'}\sum_{n=1}^{N'}\mathbb{Q}(\mathbf{Y}, n)\right) \tag{2.43}$$

The estimator $\tilde{\mathbf{g}}_{N'}(\tilde{Y})$ serves as an upper bound for the optimal objective function value of the **[LEV]($\mathcal{M}^q$)** problem which will be updated in each iteration if the value obtained is less than the value of the previous iteration. We now generate a large set of electric vehicle recharging scenarios (N') i.e., $\{\eta^1(\omega), \eta^2(\omega), ..., \eta^{N'}(\omega)\}$; $\forall n = 1, ..., N'$. Typically, the sample size N' is chosen to be much larger than the sample size N in the SAA problems. As discussed by Kleywegt et al. [62], the optimal value of an SAA problem converges to the optimal value of the "true" problem with

a probability of one under the condition of $N \to \infty$. We can estimate the variance of $\tilde{\mathbf{g}}_{N'}(\tilde{Y})$ as follows:

$$\sigma^2_{N'}(\tilde{Y}) = \frac{1}{(N'-1)N'} \sum_{n=1}^{N'} \Big\{ \sum_{i\in\mathcal{I}} \sum_{t\in\mathcal{T}} \Big(\sum_{l\in\mathcal{L}} \Psi_{lit} \tilde{Y}_{lit} + \mathbb{Q}(\mathbf{Y}, n) \Big) - \tilde{\mathbf{g}}_{N'}(\tilde{Y}) \Big\}^2$$

where $\mathbb{Q}(\mathbf{Y}, n)$ represents the solution of the second-stage problem.

4. Compute the optimality gap ($gap_{N,M,N'}(\tilde{Y})$) and its variance (σ^2_{gap}) using the estimators calculated in **Steps 2** and **3**.

$$gap_{N,O,N'}(\tilde{Y}) = \tilde{\mathbf{g}}_{N'}(\tilde{Y}) - \bar{\mathbf{v}}^N_O$$
$$\sigma^2_{gap} = \sigma^2_{N'}(\tilde{Y}) + \sigma^2_{\bar{\mathbf{v}}^N_O}$$

The confidence interval for the optimality gap is then calculated as follows:

$$\tilde{\mathbf{g}}_{N'}(\tilde{Y}) - \bar{\mathbf{v}}^N_O + z_\alpha \Big\{ \sigma^2_{N'}(\tilde{Y}) + \sigma^2_{\bar{\mathbf{v}}^N_O} \Big\}^{1/2}$$

with z_α:= $\Phi^{-1}(1-\alpha)$, where $\Phi(z)$ is the cumulative distribution function of the standard normal distribution.

2.3.3 Progressive Hedging Algorithm

Step 1 in the SAA algorithm involves solving a two-stage stochastic programming model consisting of N scenarios. Depending on the size of $|\mathcal{I}|$, $|\mathcal{H}|$, and $|\mathcal{T}|$, the SAA problem can still be considered challenging from the solution standpoint. To divide the

problem into smaller and more manageable subproblems, a scenario decomposition technique, commonly known as the *Progressive Hedging Algorithm* (PHA), is employed [103]. The PHA utilizes an *augmented Lagrangian relaxation* scheme to solve a number of individual scenario subproblems and finally aggregate the individual scenario solutions. The PHA offers high quality solutions in solving a variety of application-specific problems, such as financial planning [82], fisheries management [49], surgery planning [43], biofuel supply chain network [100, 96], and many others. Interested readers can review the studies by Wallace and Helgason [123] and Watson and Woodruff [126] for a detailed discussion about the theoretical properties and algorithmic implementation of PHA.

Constraints (2.8), (2.10), (2.15)-(2.19), and (2.33) in $\hat{\mathbf{g}}(Y_N^q)$ (shown in **Step 1** on SAA algorithm) link the first-stage decisions with the second-stage decision variables. These constraints will not allow problem $\hat{\mathbf{g}}(Y_N^q)$ to be separable by scenarios. To remedy this problem, we create a new variable $\{Y_{lit}^n\}_{\forall l\in\mathcal{L},i\in\mathcal{I},t\in\mathcal{T},n\in\mathcal{N}} \in \{0,1\}$ that ensures a copy of the first-stage decision variables is created for each scenario $n \in \mathcal{N}$. Problem $\hat{\mathbf{g}}(Y_N^q)$ can now be rewritten as follows:

$$\underset{\mathbf{Y,G,Z,B,U,V,W,H,P,S,X,F}}{Minimize} \frac{1}{N}\sum_{n=1}^{N}\sum_{i\in\mathcal{I}}\sum_{t\in\mathcal{T}}\Bigg(\sum_{l\in\mathcal{L}}\Psi_{lit}Y_{lit}^n + \sum_{h\in\mathcal{H}}\Big\{\Big(\frac{c_{ht}^{pg}}{\vartheta^c}\Big)G_{iht}^n + \Big(\frac{c_{ht}^{r}}{\vartheta^c}\Big)Z_{iht}^n + \tag{2.44}$$
$$\Big(\frac{c_{ht}^{pg}\lambda_{iht}^c}{\vartheta^c}\Big)B_{iht}^n + \Big(\frac{c_{ht}^{v2g}}{\vartheta^c}\Big)V_{iht}^n + \Big(\frac{c_{ht}^{u}}{\vartheta^c}\Big)U_{iht}^n + \gamma_{ht}^s H_{iht}^n + \chi_{ht}^c F_{iht}^n - \Big(\frac{c_{ht}^{d}\lambda_{iht}^d}{\vartheta^d}\Big)P_{iht}^n\Big\}\Bigg)$$

subject to: (2.7), (2.9), (2.11)-(2.14), (2.20), (2.21), (2.31), (2.33), (2.34), and

$$\sum_{l\in\mathcal{L}} Y^n_{lit} \leq 1 \;\forall i \in \mathcal{I}, t \in \mathcal{T}, n \in \mathcal{N} \tag{2.45}$$

$$Y^n_{lit-1} \leq Y^n_{lit} \qquad \forall l \in \mathcal{L}, i \in \mathcal{I}, t \in \mathcal{T}, n \in \mathcal{N} \tag{2.46}$$

$$\sum_{l\in\mathcal{L}}\sum_{i\in\mathcal{I}} \Psi_{lit} Y^n_{lit} \leq B_t \qquad \forall t \in \mathcal{T}, n \in \mathcal{N} \tag{2.47}$$

$$W^n_{iht} \geq \sum_{l\in\mathcal{L}} e^{cs}_{lht} Y^n_{lit} \;\forall i \in \mathcal{I}, h \in \mathcal{H}, t \in \mathcal{T}, n \in \mathcal{N} \tag{2.48}$$

$$H^n_{iht} \leq \sum_{l\in\mathcal{L}} u_{liht} Y^n_{lit} \;\forall i \in \mathcal{I}, h \in \mathcal{H}, t \in \mathcal{T}, n \in \mathcal{N} \tag{2.49}$$

$$S^n_{iht} \leq \sum_{l\in\mathcal{L}} q^{in}_{lht} Y^n_{lit} \;\forall i \in \mathcal{I}, h \in \mathcal{H}, t \in \mathcal{T}, n \in \mathcal{N} \tag{2.50}$$

$$P^n_{iht} \leq \sum_{l\in\mathcal{L}} q^{out}_{lht} Y^n_{lit} \;\forall i \in \mathcal{I}, h \in \mathcal{H}, t \in \mathcal{T}, n \in \mathcal{N} \tag{2.51}$$

$$\sum_{l\in\mathcal{L}} p^-_{liht} Y^n_{lit} \leq G^n_{iht} \leq \sum_{l\in\mathcal{L}} p^+_{liht} Y^n_{lit} \;\forall i \in \mathcal{I}, h \in \mathcal{H}, t \in \mathcal{T}, n \in \mathcal{N} \tag{2.52}$$

$$V^n_{iht} \leq \sum_{l\in\mathcal{L}} \lambda^d_{iht} \varkappa_{ht} f_{iht} Y^n_{lit} \;\forall i \in \mathcal{I}, h \in \mathcal{H}, t \in \mathcal{T}, n \in \mathcal{N} \tag{2.53}$$

$$Z^n_{iht} \leq \sum_{l\in\mathcal{L}} r^+_{liht} Y^n_{lit} \;\forall i \in \mathcal{I}, h \in \mathcal{H}, t \in \mathcal{T}, n \in \mathcal{N} \tag{2.54}$$

$$X^n_{liht} \leq Y^n_{lit} \qquad \forall l \in \mathcal{L}, i \in \mathcal{I}, t \in \mathcal{T}, n \in \mathcal{N} \tag{2.55}$$

$$Y^n_{lit} = Y^k_{lit} \qquad \forall l \in \mathcal{L}, i \in \mathcal{I}, t \in \mathcal{T}, (n,k) \in \mathcal{N}, n \neq k \tag{2.56}$$

$$Y^n_{lit} \in \{0,1\} \qquad \forall l \in \mathcal{L}, i \in \mathcal{I}, t \in \mathcal{T}, n \in \mathcal{N} \tag{2.57}$$

Constraints (2.56) are known to be as *nonanticipativity* constraints, which link the first and second-stage decision variables and force all the scenarios to yield the same first-stage decision variables. This makes the model not separable by scenarios. To make the model separable by scenarios and to apply Lagrangian relaxation, we need to rewrite the *nonanticipativity* constraints. Let $\{\bar{Y}_{lit}\}_{\forall l\in\mathcal{L}, i\in\mathcal{I}, t\in\mathcal{T}} \in \{0,1\}$ be the "overall design vector". The following constraints are equivalent to (2.56):

$$Y_{lit}^{n} = \bar{Y}_{lit} \qquad \forall l \in \mathcal{L}, \forall i \in \mathcal{I}, t \in \mathcal{T}, n \in N \tag{2.58}$$

$$\bar{Y}_{lit} \in \{0,1\} \qquad \forall l \in \mathcal{L}, i \in \mathcal{I}, t \in \mathcal{T} \tag{2.59}$$

We employ the augmented Lagrangian strategy proposed by Rockafellar and Wets [103] to relax constraints (2.58) and obtain the following objective function:

$$\underset{\mathbf{Y,G,Z,B,U,V,W,H,P,S,X,F}}{Minimize} \frac{1}{N}\sum_{n=1}^{N}\sum_{i\in\mathcal{I}}\sum_{t\in\mathcal{T}}\Bigg(\sum_{l\in\mathcal{L}}\Psi_{lit}Y_{lit}^{n} + \sum_{h\in\mathcal{H}}\Big\{\Big(\frac{c_{ht}^{pg}}{\vartheta^{c}}\Big)G_{iht}^{n} + \tag{2.60}$$
$$\Big(\frac{c_{ht}^{r}}{\vartheta^{c}}\Big)Z_{iht}^{n} + \Big(\frac{c_{ht}^{pg}\lambda_{iht}^{c}}{\vartheta^{c}}\Big)B_{iht}^{n} + \Big(\frac{c_{ht}^{v2g}}{\vartheta^{c}}\Big)V_{iht}^{n} + \Big(\frac{c_{ht}^{u}}{\vartheta^{c}}\Big)U_{iht}^{n} + \gamma_{ht}^{s}H_{iht}^{n} + \chi_{ht}^{c}F_{iht}^{n} -$$
$$\Big(\frac{c_{ht}^{d}\lambda_{iht}^{d}}{\vartheta^{d}}\Big)P_{iht}^{n}\Big\} + \sum_{l\in\mathcal{L}}\boldsymbol{\xi}_{lit}^{n}(Y_{lit}^{n} - \overline{Y}_{lit}) + \frac{1}{2}\sum_{l\in\mathcal{L}}\boldsymbol{\pi}(Y_{lit}^{n} - \overline{Y}_{lit})^{2}\Bigg)$$

where $\{\boldsymbol{\xi}_{lit}^{n}\}_{\forall l\in\mathcal{L},i\in\mathcal{I},t\in\mathcal{T},n\in\mathcal{N}}$ defines the Lagrangian multipliers for the relaxed constraints and $\boldsymbol{\pi}$ defines a penalty ratio. Given the binary requirements of variables $\{Y_{lit}^{n}\}_{\forall l\in\mathcal{L},i\in\mathcal{I},t\in\mathcal{T},n\in\mathcal{N}}$ and $\{\bar{Y}_{lit}\}_{\forall l\in\mathcal{L},i\in\mathcal{I},t\in\mathcal{T}}$, the quadratic term $\sum_{l\in\mathcal{L}}\sum_{i\in\mathcal{I}}\sum_{t\in\mathcal{T}}\boldsymbol{\phi}(Y_{lit}^{n} - \bar{Y}_{lit})^{2}$ shown in the above objective function can be reduced as follows:

$$\begin{aligned}\sum_{l\in\mathcal{L}}\sum_{i\in\mathcal{I}}\sum_{t\in\mathcal{T}}\boldsymbol{\pi}(Y_{lit}^{n} - \bar{Y}_{lit})^{2} &= \sum_{l\in\mathcal{L}}\sum_{i\in\mathcal{I}}\sum_{t\in\mathcal{T}}\Big(\boldsymbol{\pi}(Y_{lit}^{n})^{2} - 2\boldsymbol{\pi}Y_{lit}^{n}\bar{Y}_{lit} + \boldsymbol{\pi}(\bar{Y}_{lit})^{2}\Big)\\ &= \sum_{l\in\mathcal{L}}\sum_{i\in\mathcal{I}}\sum_{t\in\mathcal{T}}\Big(\boldsymbol{\pi}Y_{lit}^{n} - 2\boldsymbol{\pi}Y_{lit}^{n}\bar{Y}_{lit} + \boldsymbol{\pi}\bar{Y}_{lit}\Big)\end{aligned}$$

Meanwhile, the objective function can be reduce as follows:

$$\underset{\mathbf{Y,G,Z,B,U,V,W,H,P,S,X,F}}{Minimize} \frac{1}{N}\sum_{n=1}^{N}\sum_{i\in\mathcal{I}}\sum_{t\in\mathcal{T}}\Bigg(\sum_{l\in\mathcal{L}}(\Psi_{lit}+\boldsymbol{\xi}^n_{lit}-\boldsymbol{\pi}\overline{Y}_{lit}+\frac{\boldsymbol{\pi}}{2})Y^n_{lit}+ \tag{2.61}$$

$$\sum_{h\in\mathcal{H}}\Big\{\Big(\frac{c^{pg}_{ht}}{\vartheta^c}\Big)G^n_{iht}+\Big(\frac{c^{r}_{ht}}{\vartheta^c}\Big)Z^n_{iht}+\Big(\frac{c^{pg}_{ht}\lambda^c_{iht}}{\vartheta^c}\Big)B^n_{iht}+\Big(\frac{c^{v2g}_{ht}}{\vartheta^c}\Big)V^n_{iht}+\Big(\frac{c^{u}_{ht}}{\vartheta^c}\Big)U^n_{iht}+\gamma^s_{ht}H^n_{iht}+$$

$$\chi^c_{ht}F^n_{iht}-\Big(\frac{c^d_{ht}\lambda^d_{iht}}{\vartheta^d}\Big)P^n_{iht}\Big\}-\sum_{k\in\mathcal{K}}\boldsymbol{\xi}^n_{lit}\bar{Y}_{lit}+\frac{1}{2}\sum_{l\in\mathcal{L}}\boldsymbol{\pi}\bar{Y}_{lit}\Bigg)$$

When the value of the overall plan $\{\bar{Y}^q_{lit}\}_{\forall l\in\mathcal{L},i\in\mathcal{I},t\in\mathcal{T}}$ is fixed, the last two terms of the above objective function become constant and thus can be eliminated from the formulation. This allow the subproblems to be separable by scenarios, and the overall problem for each scenario $n\in\mathcal{N}$ becomes:

$$\underset{\mathbf{Y,G,Z,B,U,V,W,H,P,S,X,F}}{Minimize} \frac{1}{N}\sum_{n=1}^{N}\sum_{i\in\mathcal{I}}\sum_{t\in\mathcal{T}}\Bigg(\sum_{l\in\mathcal{L}}(\Psi_{lit}+\boldsymbol{\xi}^n_{lit}-\boldsymbol{\pi}\overline{Y}_{lit}+\frac{\boldsymbol{\pi}}{2})Y^n_{lit}+ \tag{2.62}$$

$$\sum_{h\in\mathcal{H}}\Big\{\Big(\frac{c^{pg}_{ht}}{\vartheta^c}\Big)G^n_{iht}+\Big(\frac{c^{r}_{ht}}{\vartheta^c}\Big)Z^n_{iht}+\Big(\frac{c^{pg}_{ht}\lambda^c_{iht}}{\vartheta^c}\Big)B^n_{iht}+\Big(\frac{c^{v2g}_{ht}}{\vartheta^c}\Big)V^n_{iht}+\Big(\frac{c^{u}_{ht}}{\vartheta^c}\Big)U^n_{iht}+$$

$$\gamma^s_{ht}H^n_{iht}+\chi^c_{ht}F^n_{iht}-\Big(\frac{c^d_{ht}\lambda^d_{iht}}{\vartheta^d}\Big)P^n_{iht}\Big\}\Bigg)$$

subject to

$$\sum_{l\in\mathcal{L}}Y^n_{lit} \leq 1\ \forall i\in\mathcal{I},t\in\mathcal{T} \tag{2.63}$$

$$Y^n_{lit-1} \leq Y^n_{lit} \qquad \forall l\in\mathcal{L},i\in\mathcal{I},t\in\mathcal{T} \tag{2.64}$$

$$\sum_{l\in\mathcal{L}}\sum_{i\in\mathcal{I}}\Psi_{lit}Y^n_{lit} \leq B_t \qquad \forall t\in\mathcal{T} \tag{2.65}$$

$$G^n_{iht}+Z^n_{iht}+V^n_{iht}+\lambda^c_{iht}B^n_{iht} = W^n_{iht}\ \forall i\in\mathcal{I},h\in\mathcal{H},t\in\mathcal{T} \tag{2.66}$$

$$W^n_{iht} \geq \sum_{l\in\mathcal{L}}e^{cs}_{lht}Y^n_{lit}\ \forall i\in\mathcal{I},h\in\mathcal{H},t\in\mathcal{T} \tag{2.67}$$

$$\lambda^c_{iht}\eta^n_{ht}f_{iht} - W^n_{iht} = U^n_{iht} \quad \forall i \in \mathcal{I}, h \in \mathcal{H}, t \in \mathcal{T} \tag{2.68}$$

$$H^n_{iht} \leq \sum_{l\in\mathcal{L}} u_{liht}Y^n_{lit} \ \forall i \in \mathcal{I}, h \in \mathcal{H}, t \in \mathcal{T} \tag{2.69}$$

$$H^n_{iht} - B^n_{iht} - P^n_{iht} + S^n_{iht} = H^n_{i,h+1,t} \ \forall i \in \mathcal{I}, h \in \mathcal{H}\backslash|H|, t \in \mathcal{T} \tag{2.70}$$

$$H^n_{i|H|t} - B^n_{i|H|t} - P^n_{i|H|t} + S^n_{i|H|t} = H^n_{i,1,t+1} \ \forall i \in \mathcal{I}, t \in \mathcal{T}\backslash|T| \tag{2.71}$$

$$S^n_{i,1,1} = 0 \ \forall i \in \mathcal{I} \tag{2.72}$$

$$S^n_{i,h+1,t} = B^n_{iht} + P^n_{iht} \ \forall i \in \mathcal{I}, h \in \mathcal{H}\backslash|H|, t \in \mathcal{T} \tag{2.73}$$

$$S^n_{i,1,t+1} = B^n_{i|H|t} + P^n_{i|H|t} \ \forall i \in \mathcal{I}, t \in \mathcal{T}\backslash|T| \tag{2.74}$$

$$S^n_{iht} \leq \sum_{l\in\mathcal{L}} q^{in}_{lht}Y^n_{lit} \ \forall i \in \mathcal{I}, h \in \mathcal{H}, t \in \mathcal{T} \tag{2.75}$$

$$P^n_{iht} \leq \sum_{l\in\mathcal{L}} q^{out}_{lht}Y^n_{lit} \ \forall i \in \mathcal{I}, h \in \mathcal{H}, t \in \mathcal{T} \tag{2.76}$$

$$W^n_{iht} \leq \sum_{l\in\mathcal{L}} c^{cap}_{lht}X^n_{liht} \ \forall i \in \mathcal{I}, h \in \mathcal{H}, t \in \mathcal{T} \tag{2.77}$$

$$\sum_{l\in\mathcal{L}} X^n_{liht} \leq \frac{F^n_{iht}}{\left(1+F^{n,m}_{iht}\right)^2} + \left(\frac{F^{n,m}_{iht}}{1+F^{n,m}_{iht}}\right)^2 \forall i \in \mathcal{I}, h \in \mathcal{H}, t \in \mathcal{T}, m \in \mathcal{M} \tag{2.78}$$

$$X^n_{liht} \leq Y^n_{lit} \quad \forall l \in \mathcal{L}, i \in \mathcal{I}, h \in \mathcal{H}, t \in \mathcal{T} \tag{2.79}$$

$$\sum_{l\in\mathcal{L}} p^-_{liht}Y^n_{lit} \leq G^n_{iht} \leq \sum_{l\in\mathcal{L}} p^+_{liht}Y^n_{lit} \ \forall i \in \mathcal{I}, h \in \mathcal{H}, t \in \mathcal{T} \tag{2.80}$$

$$V^n_{iht} \leq \sum_{l\in\mathcal{L}} \lambda^d_{iht}\varkappa_{ht}f_{iht}Y^n_{lit} \ \forall i \in \mathcal{I}, h \in \mathcal{H}, t \in \mathcal{T} \tag{2.81}$$

$$Z^n_{iht} \leq \sum_{l\in\mathcal{L}} r_{liht}Y^n_{lit} \ \forall i \in \mathcal{I}, h \in \mathcal{H}, t \in \mathcal{T} \tag{2.82}$$

$$Y^n_{lit} \in \{0,1\} \quad \forall l \in \mathcal{L}, i \in \mathcal{I}, t \in \mathcal{T} \tag{2.83}$$

$$H^n_{iht}, B^n_{iht}, S^n_{iht}, P^n_{iht} \in Z^+ \quad \forall i \in \mathcal{I}, h \in \mathcal{H}, t \in \mathcal{T} \tag{2.84}$$

$$G^n_{iht}, Z^n_{iht}, V^n_{iht}, U^n_{iht}, X^n_{liht}, F^n_{iht} \geq 0 \quad \forall i \in \mathcal{I}, h \in \mathcal{H}, t \in \mathcal{T} \tag{2.85}$$

Here, $\{\boldsymbol{\xi}_{lit}^{n,r}\}_{\forall l\in\mathcal{L},i\in\mathcal{I},t\in\mathcal{T},n\in\mathcal{N}}$ and $\boldsymbol{\pi}^r$ denote the lagrangian multipliers and penalty parameter of the PHA, respectively which are updated at each iteration r. The general idea of the basic PHA is to solve N deterministic **[LEV(PHA)]** problems and obtain the consensus parameter $\{\bar{Y}_{lit}^r\}_{\forall l\in\mathcal{L},i\in\mathcal{I},t\in\mathcal{T}}$. If the gap between the binary variable $Y_{lit}^{n,r}$ and the consensus parameter $\bar{Y}_{lit}^r$ falls below a threshold value ϵ ($i.e.$, $\epsilon = 0.001$) for each $l \in \mathcal{L}, i \in \mathcal{I}, t \in \mathcal{T}$, then the algorithm terminates; otherwise, the value of $\boldsymbol{\xi}_{lit}^{n,r}$ and $\boldsymbol{\pi}^r$ are updated using equations (2.86) and (2.87) and the process continues.

$$\boldsymbol{\xi}_{lit}^{n,r} \leftarrow \boldsymbol{\xi}_{lit}^{n,r-1} + \boldsymbol{\pi}^{r-1}(Y_{lit}^{n,r} - \bar{Y}_{lit}^{r-1}) \qquad \forall l \in \mathcal{L}, i \in \mathcal{I}, t \in \mathcal{T} \quad (2.86)$$

$$\boldsymbol{\pi}^r \leftarrow \alpha\boldsymbol{\pi}^{r-1} \quad (2.87)$$

where α is a given constant which we initialize to $\alpha > 1$. We further initialize $\boldsymbol{\xi}_{lit}^{n,0} \leftarrow 0; \forall l \in \mathcal{L}, i \in \mathcal{I}, t \in \mathcal{T}, n \in N$. Finally, $\boldsymbol{\pi}^0$ is set to a fixed positive value to ensure that $\boldsymbol{\pi}^r \rightarrow \infty$ as the number of iterations, r, increases. Pseudo-code of the basic progressive hedging algorithm is provided in **Algorithm 2**.

Termination Criteria: The progressive hedging algorithm terminates when one of the following conditions is satisfied:

- $\frac{1}{N}\sum_{n=1}^{N}\sum_{i\in\mathcal{I}}\sum_{l\in\mathcal{L}}\sum_{t\in\mathcal{T}}|Y_{lit}^{n,r} - \bar{Y}_{lit}^r| \leq \epsilon$; where ϵ is a pre-specified tolerance gap,
- 10 consecutive non-improvement iterations occur,
- Maximum iteration limit is reached (i.e., $iter^{max}$ = 100), or
- Maximum time limit is reached (i.e., $time^{max}$ = 10,800 CPU seconds).

Algorithm 2: Progressive Hedging Algorithm

Initialize, $r \leftarrow 1$, ϵ, $\{\boldsymbol{\xi}_{ikt}^{n,r}\}_{\forall i \in \mathcal{I}, k \in \mathcal{K}, t \in \mathcal{T}, n \in \mathcal{N}} \leftarrow 0$, $\boldsymbol{\pi}^r \leftarrow \boldsymbol{\pi}^0$
terminate $\leftarrow$ **false**
while (*terminate* $=$ **false**) **do**
    for $n = 1$ to N
        Solve **[LEV(PHA)]** and obtain $\{Y_{lit}^{n,r}\}_{\forall l \in \mathcal{L}, i \in \mathcal{I}, t \in \mathcal{T}, n \in \mathcal{N}}$
    end for
    Calculate the consensus parameter:
        $\bar{Y}_{lit}^{r} \leftarrow \frac{1}{N} \sum_{n=1}^{N} Y_{lit}^{n,r}; \forall l \in \mathcal{L}, i \in \mathcal{I}, t \in \mathcal{T}$
    if $(r > 1)$ **then**
        Update the largangian parameter:
            $\boldsymbol{\xi}_{lit}^{n,r} \leftarrow \boldsymbol{\xi}_{lit}^{n,r-1} + \boldsymbol{\pi}^{r-1}(Y_{lit}^{n,r} - \bar{Y}_{lit}^{r-1}); \forall l \in \mathcal{L}, i \in \mathcal{I}, t \in \mathcal{T}$
        Update the penalty parameter:
            $\boldsymbol{\pi}^r \leftarrow \alpha \boldsymbol{\pi}^{r-1}$ and $\alpha > 1$
    end if
    if $((Y_{lit}^{n,r} - \bar{Y}_{lit}^{r-1})_{\forall l \in \mathcal{L}, i \in \mathcal{I}, t \in \mathcal{T}} \leq \epsilon)$ **then**
        terminate $\leftarrow$ **true**
    end if
    $r \leftarrow r + 1$
end while

2.3.4 Enhanced Progressive Hedging Algorithm

The PHA technique demonstrates high computational capability in solving small to medium sized network problems. However, the technique fails to provide a reasonable solution for sufficiently large sized network problems. This motivates us to explore additional enhancement techniques (e.g., local and global heuristics, dynamic penalty parameter updating technique, and different variants of the rolling horizon heuristic) to improve the convergence and stability of the PHA. The following subsection investigates few PHA enhancement techniques in an attempt to solve model **[LEV(PHA)]** faster.

2.3.4.1 Penalty Parameter Updating

Prior studies such as [21, 53] show that the performance of the PHA technique can be significantly improved by choosing an appropriate $\boldsymbol{\pi}$ value. For instance, the algorithm converges faster to a sub-optimal solution for a sufficiently large $\boldsymbol{\pi}$ value. In contrary, the algorithm takes a longer time to converge if a conservative value is chosen for $\boldsymbol{\pi}$. Since there is no way we can estimate the appropriate $\boldsymbol{\pi}$ value for a given optimization problem in advance, we adopt the strategy proposed by Hvattum and Lokketangen [54] to dynamically adjust the value of $\boldsymbol{\pi}$ over iterations based on the computational performance obtained from prior iterations of the PHA algorithm. Let $\boldsymbol{\Delta}_1^r$ and $\boldsymbol{\Delta}_2^r$ define the indicators of the convergence rates in the dual and primal space, respectively. The penalty value can now be updated as follows:

$$\boldsymbol{\Delta}_1^r = \sum_{l\in\mathcal{L}}\sum_{i\in\mathcal{I}}\sum_{t\in\mathcal{T}}\sum_{n\in N}(Y_{lit}^{n,r} - \bar{Y}_{lit}^r)^2 \tag{2.88}$$

$$\boldsymbol{\Delta}_2^r = \sum_{l\in\mathcal{L}}\sum_{i\in\mathcal{I}}\sum_{t\in\mathcal{T}}(\bar{Y}_{lit}^r - \bar{Y}_{lit}^{r-1})^2 \tag{2.89}$$

$$\boldsymbol{\pi}^r = \begin{cases} \varphi\boldsymbol{\pi}^{r-1} & \text{if } \boldsymbol{\Delta}_1^r - \boldsymbol{\Delta}_1^{r-1} > 0 \\ \frac{1}{\varphi}\boldsymbol{\pi}^{r-1} & \text{else if } \boldsymbol{\Delta}_2^r - \boldsymbol{\Delta}_2^{r-1} > 0 \\ \boldsymbol{\pi}^{r-1} & \text{otherwise} \end{cases} \tag{2.90}$$

where φ is a constant parameter which value is set to $\varphi > 1$.

2.3.4.2 Heuristic Strategies

This section utilizes two heuristic strategies, referred to as *local heuristic* and *global heuristic*, to enhance the performance of the PHA technique [28]. These strategies are used to modify the value of Ψ_{lit} in an attempt to solve model **[LEV(PHA)]** faster. The first strategy is referred to as *global heuristic* since this strategy adjusts the value of Ψ_{ikt} at the end of each iteration r. On the other hand, the second strategy, referred to as *local heuristic*, adjusts the value of Ψ_{lit} within the scenario level.

We realize that problem **[LEV(PHA)]** can be decomposed into a series of N deterministic sub-problems. At the end of each iteration r of **Algorithm 2**, we can obtain the values of the consensus parameter $\{\bar{Y}^r_{lit}\}_{\forall l\in\mathcal{L},i\in\mathcal{I},t\in\mathcal{T}}$ which provides an indication of how many times a charging station of capacity $l \in \mathcal{L}$ is opened in cell $i \in \mathcal{I}$ at time period $t \in \mathcal{T}$ in the previous iterations. A higher value of $\bar{Y}^r_{lit}$ indicates that the charging station of a specific size, location, and year was selected many times in the previous iterations. Conversely, a lower value of $\bar{Y}^r_{lit}$ indicates that the charging station of a specific size, location, and year was not a favorable decision in most of the previous iterations. Let $\overline{a}$ and $\underline{a}$ be the two parameters that define an upper and lower threshold value. If the value of $\bar{Y}^r_{lit}$ is greater than the threshold value $\overline{a}$, then lowering the Ψ_{lit} value will attract the subproblems to use that cell more frequently in the coming iterations. Similarly, if the value of $\bar{Y}^r_{lit}$ is lower than the threshold value $\underline{a}$, then increasing the Ψ_{lit} value will discourage the remaining subproblems from using this cell in the coming iterations. This will allow a few of the charging stations to be fixed to value of either one or zero and thus help reduce the size of the problem. The adjustment strategy is given below:

$$\Psi_{lit}^{r} = \begin{cases} \tau \Psi_{lit}^{r-1} & \text{if } \bar{Y}_{lit}^{r-1} < \underline{a} \\ \frac{1}{\tau} \Psi_{lit}^{r-1} & \text{if } \bar{Y}_{lit}^{r-1} > \overline{a} \\ \Psi_{lit}^{r-1} & \text{Otherwise} \end{cases} \tag{2.91}$$

where Ψ_{lit}^{r} represents the modified fixed cost of opening a charging station of capacity $l \in \mathcal{L}$ at cell $i \in \mathcal{I}$ in time period $t \in \mathcal{T}$ and iteration r; τ is a constant parameter whose value is set to $\tau > 1$; and $\underline{a}$ and $\overline{a}$ are the two constant parameters whose values are set to $0 < \underline{a} < 0.3$ and $0.7 < \overline{a} < 1$.

The *global heuristic* strategy can be enhanced further by modifying the selection of Ψ_{lit} locally within the scenario level. This strategy is referred to as a *local heuristic* [28] since the modification of Ψ_{lit} only impacts the current subproblem at scenario n of a particular iteration r. This strategy emphasizes modifying the costs associated with selecting a charging station of capacity $l \in \mathcal{L}$ at cell $i \in \mathcal{I}$ in time period $t \in \mathcal{T}$ under scenario $n \in \mathcal{N}$ at iteration r, if the gap between $Y_{lit}^{n,r}$ and $\bar{Y}_{lit}^{r}$ is sufficiently large. The local adjustment strategy applied to **Algorithm 2** is as follows:

$$\Psi_{lit}^{n,r} = \begin{cases} \tau \Psi_{lit}^{r} & \text{if } |Y_{lit}^{n,r-1} - \bar{Y}_{lit}^{r}| \geq a^{far} \text{ and } Y_{lit}^{n,r-1} = 1 \\ \frac{1}{\tau} \Psi_{lit}^{r} & \text{if } |Y_{lit}^{n,r-1} - \bar{Y}_{lit}^{r}| \geq a^{far} \text{ and } Y_{lit}^{n,r-1} = 0 \\ \psi_{lit}^{r} & \text{Otherwise} \end{cases} \tag{2.92}$$

where $\Psi_{lit}^{n,r}$ represents the modified Ψ_{lit} of selecting a charging station of capacity $l \in \mathcal{L}$ at location $i \in \mathcal{I}$ in time period $t \in \mathcal{T}$ under scenario $n \in \mathcal{N}$ and at iteration r; τ is a constant parameter whose value is set to $\tau > 1$; and a^{far} is a threshold value at which a local adjustment to the Ψ_{lit} is made and is set to $0.5 < a^{far} < 1$.

2.3.4.3 Rolling Horizon Heuristic Strategy

Algorithm 2 requires solving a deterministic, multi-time period problem **[LEV(PHA)]** N times. This evaluation may be considered challenging from a solution standpoint. One way to tackle this problem is to split the planning horizon (i.e., years and hours) into multiple slices and solve them sequentially until all the slices are investigated. To serve this purpose, this study employs a *Rolling Horizon* heuristic (**[CG]**) that decomposes problem **[LEV(PHA)]** into a series of smaller subproblems comprising a few consecutive hour-year combinations from the overall planning horizon. The algorithm terminates when all the hour-year combinations of the planning horizon are investigated. Interested readers can review the studies by Balasubramanian and Grossman [11], Poudel et al. [94], and Kostina et al. [63] to learn more about the rolling horizon heuristic. In this section, we present three different variants of the rolling horizon heuristic. The aim is to identify which variant of the rolling horizon heuristic provides a quality solution in solving problem **[LEV(PHA)]** in a reasonable amount of time. The first variant of the rolling horizon heuristic, referred to as **[RH1]**, decomposes problem **[LEV(PHA)]** on yearly basis. The second and third variants of the rolling horizon heuristic, referred to as **[RH2]** and **[RH3]**, decompose problem **[LEV(PHA)]** on hourly, and the combination of hourly and yearly

basis, respectively. A pseudo-code of the basic *Rolling Horizon* heuristic is provided in **Algorithm 3**.

Let **[LEV(PHA(*r*))]** be an approximate subproblem of the rolling horizon algorithm at iteration r. We further let t_0^r, h_0^r, M^r, and Q^r be the starting time period for years, hours, and number of time periods for years and hours for each subproblem r, respectively. In the rolling horizon heuristic, one can either set a fixed value of M^r and Q^r or vary them across the different iterations of the algorithm. For each scenario $n \in \mathcal{N}$, the approximate subproblems **[LEV(PHA(*r*))]** are solved by setting the variables as: (i) $\left\{Y_{lit}^n\right\}_{\forall l\in\mathcal{L},i\in\mathcal{I},t\in\mathcal{T}}\in \{0,1\}$ and $\left\{B_{iht}^n, H_{iht}^n, S_{iht}^n, P_{iht}^n\right\}_{\forall i\in\mathcal{I},h\in\mathcal{H},t\in\mathcal{T}}\in \mathbb{Z}^+$ for $t_0^r \leq t \leq t_0^r + M^r$ and $h_0^r \leq h \leq h_0^r + Q^r$, (ii) $0 \leq \left\{Y_{lit}^n\right\}_{\forall l\in\mathcal{L},i\in\mathcal{I},t\in\mathcal{T}} \leq 1$ and $\left\{B_{iht}^n, H_{iht}^n, S_{iht}^n, P_{iht}^n\right\}_{\forall i\in\mathcal{I},h\in\mathcal{H},t\in\mathcal{T}}\in \mathbb{R}^+$ for $t > t_0^r + M^r$ and $h > h_0^r + Q^r$. After solving a subproblem, we fix the values of $Y_{lit}^{n,r} = Y_{lit}^{n,r-1}, \forall l \in \mathcal{L}, i \in \mathcal{I}, t \in \mathcal{T}$; $B_{iht}^{n,r} = B_{iht}^{n,r-1}, \forall i \in \mathcal{I}, h \in \mathcal{H}, t \in \mathcal{T}$; $H_{iht}^{n,r} = H_{iht}^{n,r-1}, \forall i \in \mathcal{I}, h \in \mathcal{H}, t \in \mathcal{T}$; $S_{iht}^{n,r} = S_{iht}^{n,r-1}, \forall i \in \mathcal{I}, h \in \mathcal{H}, t \in \mathcal{T}$; and $P_{iht}^{n,r} = P_{iht}^{n,r-1}, \forall i \in \mathcal{I}, h \in \mathcal{H}, t \in \mathcal{T}$ for $t < t_0^r$ and $h < h_0^r$ and update the step size r. Note that by varying parameters t_0^r, h_0^r, M^r, and Q^r a number of different variants of the rolling horizon algorithm can be developed. Figures 2.4-2.6 provide an illustration of solving a three year and four hour time period problem using three different variants of the rolling horizon heuristic (**[RH1]**-**[RH3]**). Later in Section 2.4.2, we analyze the settings at which a particular variant of the rolling horizon heuristic solves problem **[LEV(PHA(*r*))]** efficiently.

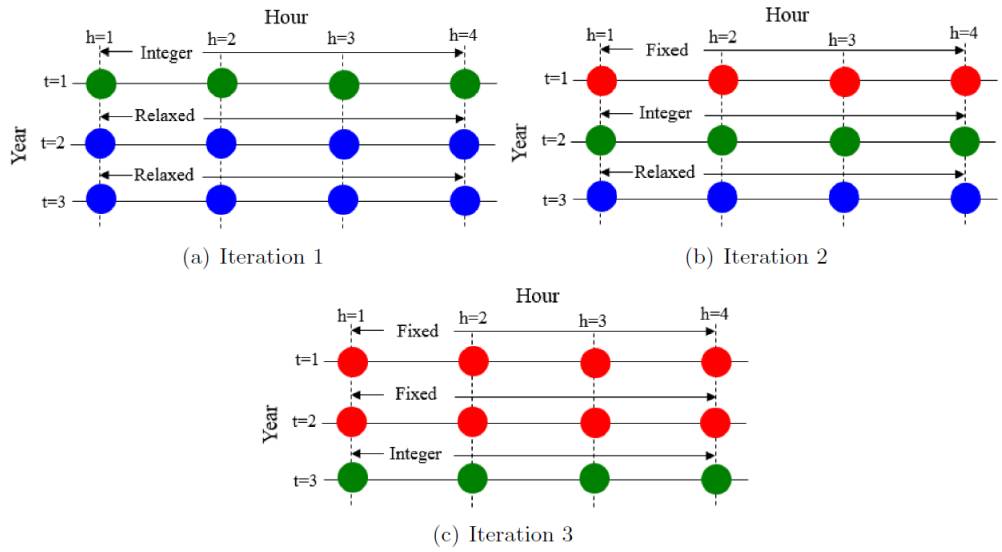

Figure 2.4: Illustration of a rolling horizon strategy for **[RH1]**

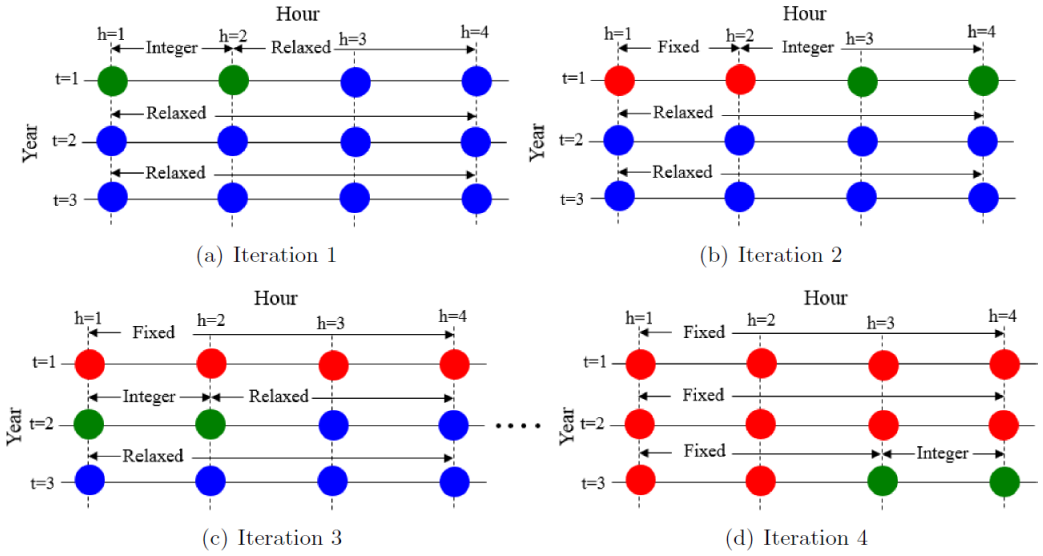

Figure 2.5: Illustration of a rolling horizon strategy for **[RH2]**

Algorithm 3: Rolling Horizon Heuristic

$r \leftarrow 1$, $t_0^r \leftarrow 0$, $h_0^r \leftarrow 0$, M^r, Q^r, *terminate* $\leftarrow$ **false**

while (*terminate* = **false**) **do**

Set:

- $\{Y_{lit}^n\}_{\forall l \in \mathcal{L}, i \in \mathcal{I}, t \in \mathcal{T}} \in \{0,1\}$ and $\{B_{iht}^n, H_{iht}^n, S_{iht}^n, P_{iht}^n\}_{\forall i \in \mathcal{I}, h \in \mathcal{H}, t \in \mathcal{T}} \in \mathbb{Z}^+$ for $t_0^r \leq t \leq t_0^r + M^r$ and $h_0^r \leq h \leq h_0^r + Q^r$
- $0 \leq \{Y_{lit}^n\}_{\forall l \in \mathcal{L}, i \in \mathcal{I}, t \in \mathcal{T}} \leq 1$ and $\{B_{iht}^n, H_{iht}^n, S_{iht}^n, P_{iht}^n\}_{\forall i \in \mathcal{I}, h \in \mathcal{H}, t \in \mathcal{T}} \in \mathbb{R}^+$ for $t > t_0^r + M^r$ and $h > h_0^r + Q^r$

Solve the approximate sub-problem **[EVC(PHA(*r*))]** using CPLEX

if($t_0 > |\mathcal{T}|$) **then**

terminate $\leftarrow$ **true**

else

Fixing the values of $\{Y_{lit}^n\}_{\forall l \in \mathcal{L}, i \in \mathcal{I}, t \in \mathcal{T}}$, $\{B_{iht}^n, H_{iht}^n, S_{iht}^n, P_{iht}^n\}_{\forall i \in \mathcal{I}, h \in \mathcal{H}, t \in \mathcal{T}}$ for $t < t_0^r$ and $h < h_0^r$

end if

$r \leftarrow r + 1$

end while

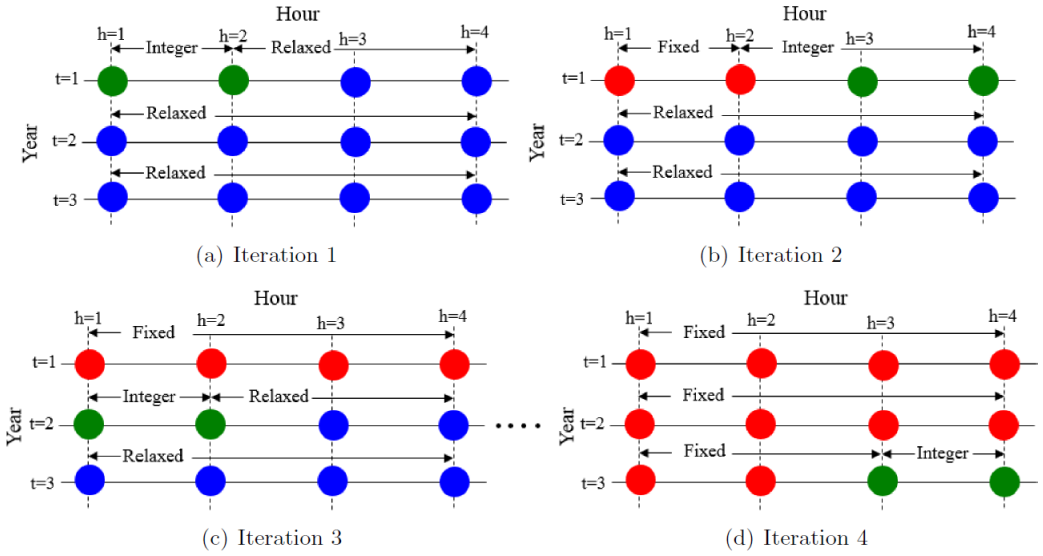

Figure 2.6: Illustration of a rolling horizon strategy for **[RH3]**

2.4 Computational Study and Managerial Insights

This section summarizes our computational experiences in solving model **[LEV]** using the nested algorithms proposed in Section 2.3 and offers managerial insights derived from

a real life case study. All the algorithms are coded in GAMS 24.2.1 [39] and executed on a desktop computer with an Intel Core i7 3.50 GHz processor with 16.0 GB RAM. We use ILOG CPLEX 12.6[5] as an optimization solver.

2.4.1 Input Parameters

This study considers Washington, DC as a testing ground to visualize and validate the modeling results. A network representation and demand distribution for Washington, DC is shown in Figure 2.7. The main reason behind choosing Washington, DC is that the area has a strong growing electric vehicle population over other major metropolitan cities in US. We divide the entire map into grids of size 306 cells (i.e., $|\mathcal{I}| = 306$) where each cell corresponds to an area of approximately 1.0 $mile^2$. The data for cell-specific parameters are obtained only for those that have a road passing through them; otherwise, the values for the cells are set to zero. We have considered a 5-year planning horizon starting in 2018 and ending in 2022 ($|\mathcal{T}| = 5$). Further, we have drawn a representative 24 hour period from each year of the planning horizon to account for the short term operational decisions ($|\mathcal{H}| = 24$). Note that all cost components are calculated based on 2017 dollars and are adjusted based on inflation. The cost of opening an electric vehicle charging station that includes a battery swap station (Ψ_{ikt}) at cell $i \in \mathcal{I}$ is set to be \$500,000 [40]. We consider three different electric vehicle charging station capacities (l = 400 kWh, 500 kWh, and 600 kWh). We assume that we are given an annual budget (B_t = \$5M, \$6M, \$7M, \$8M, and \$9M) to build infrastructure for EV charging stations (which include battery swapping

[5] https://www-01.ibm.com/software/commerce/optimization/cplex-optimizer/

capabilities) for our test region in years 2018–2022. The hourly electricity pricing plan for power grid (c^{pg}_{ht}), renewable resources (c^{r}_{ht}), and V2G (c^{v2g}_{ht}) are obtained from [104, 108, 91]. The projected flow of cars f_{iht} at each cell $i \in \mathcal{I}$ of hour $h \in \mathcal{H}$ in year $t \in \mathcal{T}$ is made based upon the number of EVs available in Washington, DC in 2014 [92]. Factors such as density of population, hospitals, and colleges located near major roads are considered to project f_{iht}. We set car charging percentage $\eta^{\omega}_{ht} = 40\%$ and car discharging percentage $\beta_{ht} = 5\%$ for our base case experimentations. The availability of grid power (g_{iht}) and renewable resources (r_{iht}) are adopted from [31] and [97], respectively. The charging and discharging efficiencies of EV's are both set to be ϑ^c = ϑ^d = 90%. The maximum and minimum SoC and DoD are set to be $c^{+}_{iht} = d^{+}_{iht} = 0.90$ and $c^{-}_{iht} = d^{-}_{iht} = 0.20$, respectively. Finally, we set unit profit associated with battery discharging $c^{d}_{ht} =$ \$0.03/hr, battery storing cost $\gamma^{s}_{ht} =$ \$0.02/hr, and rated EV battery capacity $b^{cap} = 35$ kWh for our base case experiments.

2.4.2 Analyzing the Performance of Solution Algorithms

This section presents our computational experiences in solving model **[LEV]** using the algorithms proposed in Section 2.3. To help the readers follow our solution approaches, we introduce the following notations to represent the algorithms:

- **[CG]**: represents the Constraint Generation (**[CG]**) algorithm (described in Section 2.3.1)

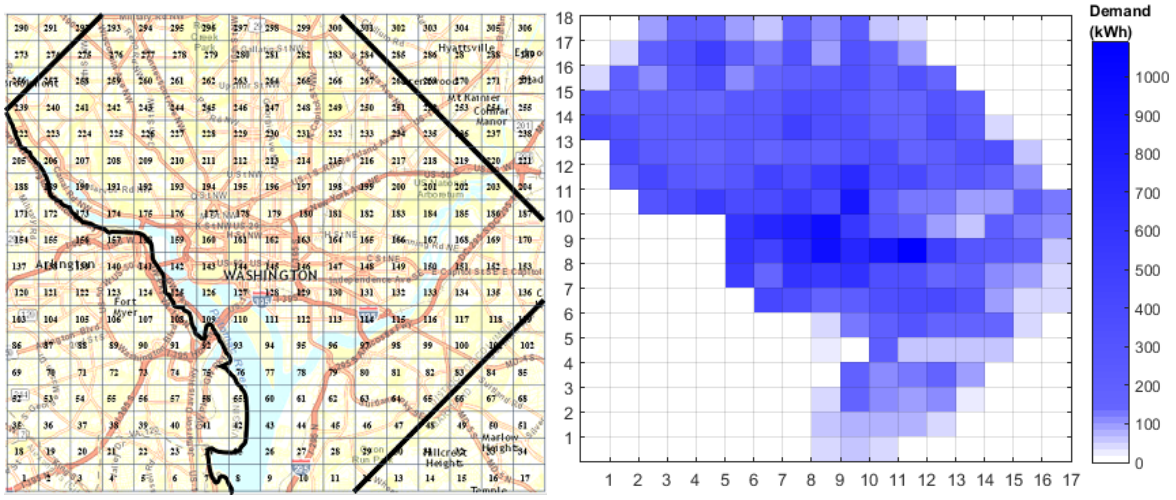

(a) (b)

Figure 2.7: (a) Network representation (original map obtained from [6]) and (b) geographical demand distribution of Washington DC

- **[CG+SAA]**: represents a **[CG]** algorithm where the subproblems of the **[CG]** are solved using a Sample Average Approximation (**[SAA]**) algorithm (described in Section 2.3.2)
- **[CG+SAA+PHA]**: represents a **[CG]** algorithm where the subproblems of the **[CG]** are solved using an integration of **[SAA]** and a Progressive Hedging (**[PHA]**) algorithm (described in Section 2.3.3)
- **[CG+SAA+PHA+HR]**: represents a **[CG]** algorithm where the subproblems of the **[CG]** are solved using an integration of **[SAA]** and an enhanced **[PHA]** algorithm that uses the enhancement techniques described in Section 2.3.4.1
- **[CG+SAA+PHA+HR+RH]**: represents a **[CG]** algorithm where the subproblems of the **[CG]** are solved using an integration of **[SAA]** and an enhanced **[PHA]** algorithm

that uses the enhancement techniques described in Section 2.3.4.1, 2.3.4.1, 2.3.4.2, and 2.3.4.3

The algorithms presented above are terminated when at least one of the following criteria is met: (a) the optimality gap (i.e., $\epsilon = |UB - LB|/UB$) falls below a threshold value ϵ = 0.01, (b) the maximum time limit $time^{max}$ = 36,000 (in CPU seconds) is reached, or (c) the maximum number of iteration $iter^{max}$ = 100 is reached. Additionally, to terminate the progressive heading algorithm, some additional stopping criteria are used (described at the end of Section 2.3.3). Table 2.1 presents the size of the deterministic equivalent problem of the **[LEV]** model. Note that the twelve problem instances, reported in Table 2.1, are produced by varying the size of $|\mathcal{I}|$, $|\mathcal{H}|$, and $|\mathcal{T}|$.

Table 2.1: Problem size of the test instances

Case	$\|\mathcal{L}\|$	$\|\mathcal{I}\|$	$\|\mathcal{H}\|$	$\|\mathcal{T}\|$	Binary variables	Integer variables	Continuous variables	Total variables	Total constraints
1	3	100	24	5	1,500	48,000	48,000	97,500	135,505
2	3	100	24	10	3,000	96,000	96,000	195,000	271,010
3	3	100	48	5	1,500	96,000	96,000	193,500	267,505
4	3	100	48	10	3,000	192,000	192,000	387,000	535,010
5	3	200	24	5	3,000	96,000	96,000	195,000	271,005
6	3	200	24	10	6,000	192,000	192,000	390,000	542,010
7	3	200	48	5	3,000	192,000	192,000	387,000	535,005
8	3	200	48	10	6,000	384,000	384,000	774,000	1,070,010
9	3	306	24	5	4,590	146,880	146,880	298,350	414,635
10	3	306	24	10	9,180	293,760	293,760	596,700	829,270
11	3	306	48	5	4,590	293,760	293,760	592,110	818,555
12	3	306	48	10	9,180	587,520	587,520	1,184,220	1,637,110

The first set of experiments (reported in Table 2.2) provide a computational comparison between CPLEX and three different variants of the rolling horizon heuristic (e.g.,

[RH1], **[RH2]**, and **[RH3]**). Note that the subproblems of the rolling horizon heuristic are solved using CPLEX where we set a maximum time limit of 10,800 CPU seconds for each of the subproblems. Results in Table 2.2 indicate that all three variants of the rolling horizon heuristic demonstrate improvements over CPLEX, particularly as the problem size increases. On average, algorithm **[RH3]** provides a 17.78% and 19.07% faster solution over algorithms **[RH1]** and **[RH2]**, respectively while dropping the average optimality gap from 1.24% and 1.20% to 0.91%. Note that rolling horizon heuristic only provides an upper bound for model **[LEV]**. Therefore, we use the lower bound from CPLEX to compute the optimality gap (Gap (%)) for the rolling horizon heuristics i.e., $100 \times (UB_{\textbf{[RH]}} - LB_{CPLEX})/UB_{\textbf{[RH]}}\%$. In summary, the **[RH3]** seems to offer high quality solutions consistently within the experimental range.

Table 2.2: Comparison between different variants of the rolling horizon heuristic over CPLEX

Case	CPLEX		[RH1]		[RH2]		[RH3]	
	Gap (%)	CPU (sec)	Gap (%)	CPU (sec)	Gap (%)	CPU (sec)	Gap (%)	CPU (sec)
1	0.36	2569.8	0.79	**1,265.2**	0.74	1,892.5	0.68	1,412.6
2	0.64	3,468.3	0.61	**1,564.7**	0.65	2,045.2	0.64	1,626.8
3	0.73	3,125.4	0.87	1,896.8	0.87	**1,481.6**	0.89	1,587.9
4	0.72	15,486.3	0.66	5,385.6	0.71	5,014.4	0.72	**4,359.4**
5	0.87	3,589.9	0.59	1,626.8	0.88	2,154.7	0.74	**1,512.8**
6	0.89	18,642.5	0.67	5,696.3	0.82	5,926.9	0.85	**4,796.5**
7	0.92	14,957.8	0.84	5,486.3	0.69	5,164.5	0.67	**4,282.9**
8	4.18	36,000.0	0.69	9,856.7	0.92	10,247.8	0.75	**7,985.6**
9	0.58	13,562.4	0.86	4,892.5	0.84	4,789.5	0.78	**3,756.4**
10	2.56	36,000.0	0.94	8,786.3	0.84	9,245.1	0.67	**8,175.4**
11	5.16	36,000.0	0.81	8,254.6	0.79	7,684.5	0.82	**7,354.2**
12	12.63	36,000.0	6.12[a]	19,682.5	5.15[a]	20,542.5	**2.45**[a]	14,687.2
Average	2.72	19,712.1	1.24	6,648.1	1.20	6,754.2	0.91	**5,465.9**

[a]Unable to solve the first subproblem within 10,800 CPU seconds

The second set of experiments analyze how using different accelerated techniques (described in Section 2.3.4.1 and 2.3.4.2) along with three different variants of the rolling horizon heuristic (i.e., **[RH1]**, **[RH2]**, and **[RH3]**) speed up the convergence and improve the quality of the progressive hedging algorithm (**[PHA]**). We set the scenario size $N = \{25, 50\}$ to test the performance of the algorithms. Table 2.3 summarizes the computational benefits obtained by implementing different enhancement techniques inside the **[PHA]** algorithm. Results indicate that implementing different variants of the rolling horizon heuristic substantially improve the performance of the **[PHA]** algorithm. Clearly, algorithm **[PHA+HR+RH3]** outperforms the remaining algorithms (e.g., **[PHA]**, **[PHA+HR]**, **[PHA+HR+RH1]**, and **[PHA+HR+RH2]**) by solving 22 out of the 24 problem instances by obeying the pre-specified termination criteria. On average, algorithm **[PHA+HR+RH3]** provides a 71.5%, 40.2%, 8.5%, and 9.9% faster solution over algorithms **[PHA]**, **[PHA+HR]**, **[PHA+HR+RH1]**, and **[PHA+HR+RH2]**, respectively, while maintaining an average optimality gap below 1.0%. In summary, algorithm **[PHA+HR+RH3]** seems to offer high quality solutions consistently within the experimental range. Note that the results of algorithms **[RH1]** and **[RH2]** are not presented in the next two set of experiments, since algorithm **[RH3]** consistently produces high quality feasible solutions.

Table 2.3: Performance of the enhancement techniques used in **[PHA]** algorithm

Case	N	[PHA]		[PHA+HR]		[PHA+HR+RH1]		[PHA+HR+RH2]		[PHA+HR+RH3]	
		Gap (%) (%)	CPU (sec) (sec)	Gap (%) (%)	CPU (sec) (sec)	Gap (%) (%)	CPU (sec) (sec)	Gap (%) (%)	CPU (sec) (sec)	Gap (%) (%)	CPU (sec) (sec)
1	25	0.91	2,087.6	0.88	1,825.4	0.84	815.3	0.69	**712.5**	0.72	782.5
	50	0.78	4,587.4	0.97	3,412.5	0.89	1,826.5	0.72	1,952.4	0.68	**1,268.7**
2	25	0.84	12,160.3	0.87	2,561.4	0.61	**1,242.8**	0.75	1,345.1	0.58	1,298.9
	50	4.18	36,000.0	0.64	8,674.3	0.73	4,852.4	0.81	5,042.8	0.67	**4,153.6**
3	25	0.91	11,965.4	0.76	2,396.5	0.84	1,193.9	0.86	1,127.1	0.58	**1,085.3**
	50	5.95	36,000.0	0.56	8,168.6	0.67	4,358.6	0.85	4,136.8	0.84	**3,965.8**
4	25	6.13	36,000.0	0.81	9,247.6	0.54	6,327.8	0.57	6,524.7	0.63	**5,976.8**
	50	8.27	36,000.0	0.68	10,467.8	0.67	8,475.6	0.81	8,045.6	0.78	**6,457.4**
5	25	0.67	13,863.6	0.84	3,162.1	0.44	1,354.1	0.65	1,563.4	0.61	**1,204.9**
	50	5.78	36,000.0	0.79	9,063.4	0.81	4,867.8	0.81	5,175.1	0.51	**4,328.4**
6	25	7.54	36,000.0	0.64	9,681.1	0.84	6,821.3	0.93	7,124.5	0.88	**6,371.9**
	50	9.98	36,000.0	0.96	11,460.1	0.62	9,471.8	0.86	10,545.8	0.65	**8,850.7**
7	25	6.87	36,000.0	0.78	9,478.1	0.72	6,435.7	0.56	6,024.1	0.51	**5,876.4**
	50	9.13	36,000.0	0.68	10,578.7	0.87	8,745.7	0.89	8,954.6	0.64	**6,684.1**
8	25	12.65	36,000.0	5.54	36,000.0	0.68	10,682.5	0.88	10,358.4	0.81	**9,524.6**
	50	16.54	36,000.0	7.57	36,000.0	0.92	12,452.6	0.68	11,982.4	0.64	**10,824.9**
9	25	3.27	36,000.0	0.87	7,884.2	0.84	5,628.9	0.76	5,876.8	0.57	**5,012.4**
	50	4.56	36,000.0	0.68	9,665.8	0.71	7,477.2	0.68	7,654.2	0.72	**5,782.8**
10	25	4.15	36,000.0	0.92	19,214.4	0.67	12,456.0	0.82	13,652.8	0.59	**11,364.5**
	50	5.42	36,000.0	0.85	24,653.7	0.84	14,857.6	0.85	15,742.3	0.75	**12,547.6**
11	25	4.15	36,000.0	0.81	18,985.1	0.54	11,551.5	0.67	12,051.8	0.81	**10,660.1**
	50	5.42	36,000.0	0.77	22,650.1	0.82	12,887.1	0.91	12,742.8	0.41	**11,500.4**
12	25	19.63	36,000.0	14.56	36,000.0	4.63	36,000.0	5.12	36,000.0	**3.41**	36,000.0
	50	25.84	36,000.0	18.65	36,000.0	14.74	36,000.0	9.64	36,000.0	**2.24**	36,000.0
Average		7.07	30,361.0	2.59	14,468.0	1.48	9,449.3	1.32	9,597.3	0.84	**8,646.8**

To see the benefits of using different enhancement techniques in each replication of the **[SAA]** algorithm, a third set of experiments is introduced. Figure 2.8 compares the average runtime spend solving each replication of the **[SAA]** algorithm using algorithms **[SAA+PHA]**, **[SAA+PHA+HR]**, and **[SAA+PHA+HR+RH3]**. For this experiment, a small problem instance with a problem size $|\mathcal{L}| = 3$, $|\mathcal{I}| = 100$, $|\mathcal{H}| = 24$, $|\mathcal{T}| = 5$, $N = 10$, and $M = 40$ is considered. From figure 2.8 it is evident that incorporating different enhancement techniques improves the runtime in each replication of the **[SAA]** algorithm. More specifically, use of algorithm **[SAA+PHA+HR]** reduces runtime significantly over algorithm **[SAA+PHA]**. Notice that further reduction in computational time is achieved by employing the rolling horizon heuristic (**[SAA+PHA+HR+RH3]**) inside algorithm **[SAA+PHA+HR]**. Finally, on average, algorithm **[SAA+PHA+HR+RH3]** generates a solution 1.2 and 1.6 times faster than the algorithms **[SAA+PHA+HR]** and **[SAA+PHA]**, respectively.

The last set of experiments presents the results from solving model **[LEV]** using the algorithms proposed in Section 2.3 (shown in Table 2.4). To test the performance of the accelerated algorithms, we use *Cases 9-12* (the largest test cases from Table 2.1) and vary the sample size N and replication number M in the **[SAA]** algorithm to obtain 24 different problem instances. A large scenario size, $N' = 500$, is used to evaluate the **[SAA]** gap. We do not present the results obtained from CPLEX since CPLEX runs out of memory while solving all the problem instances reported in Table 2.4. Results indicate that **[CG]** is able to solve only 6 out of 24 problem instances by obeying the pre-specified termination criterions. The performance improved slightly by incorporating **[SAA]** inside

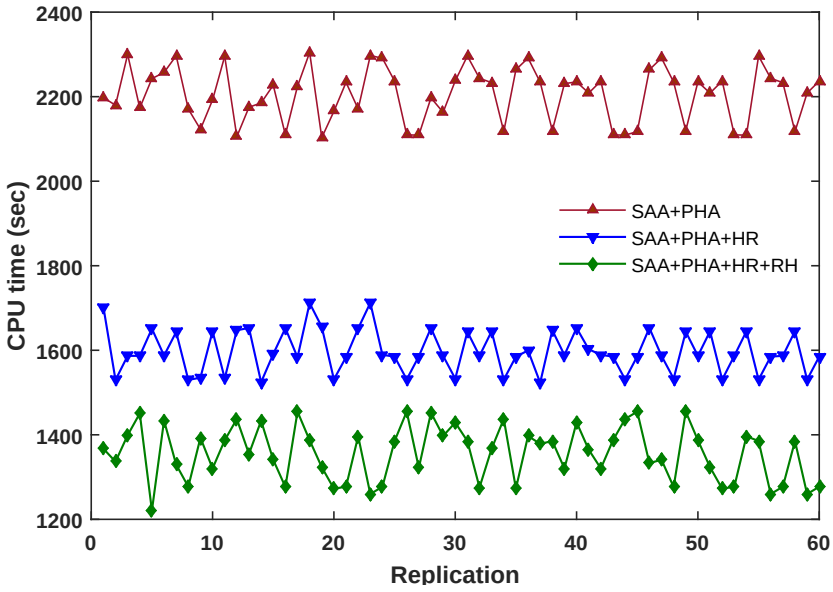

Figure 2.8: Comparison of solution time in each replication of the **[SAA]** algorithm

the subproblems of the **[CG]** framework, referred as the **[CG+SAA]** algorithm, with an ability to now solve 14 out of 24 problem instances as reported in Table 2.4. The performance of the **[CG+SAA]** algorithm can be enhanced further by solving the subproblems of this algorithm using the **[PHA]** algorithm, referred to as the **[CG+SAA+PHA]** algorithm. With this enhancement, algorithm **[CG+SAA+PHA]** is now able to solve 20 out of 24 problem instances while resulting in less than a 1% optimality gap within the specified time limit. The benefits of using the algorithms become even more obvious when the heuristic enhancement strategies are incorporated in the **[CG+SAA+PHA]** algorithm, referred to as the **[CG+SAA+PHA+HR]** algorithm. It is observed that with these enhancement strategies, the average optimality gap of the **[CG+SAA+PHA+HR]** algorithm drops to 0.54% from 0.74% as reported for the **[CG+SAA+PHA]** algorithm. Furthermore, the results in Table 2.4 indicate that algorithm **[CG+SAA+PHA+HR]** is now capable of

solving 22 out of 24 problem instances by obeying the pre-specified termination criteria. Finally, we observe a significant improvement in computational efficiency when the rolling horizon heuristic is incorporated in the **[CG+SAA+PHA+HR]** algorithm, referred to as the **[CG+SAA+PHA+HR+RH3]** algorithm. As is found in Tables 2.2 and 2.3, the rolling horizon heuristic variant **[RH3]** provides superior computational performance over the other two variants (e.g., **[RH1]** and **[RH2]**). Thus, the **[RH3]** algorithm is utilized inside the **[CG+SAA+PHA+HR+RH3]** algorithmic framework. With this enhancement, **[SAA]** is now able to solve 23 out of 24 problem instances by obeying the pre-specified termination criteria. We further observe that algorithm **[CG+SAA+PHA+HR+RH3]** on average saves 50% in computation time over algorithm **[CG+SAA+PHA+HR]** in reporting the optimality gaps presented in Table 2.4. In summary, algorithm **[CG+SAA+PHA+HR+RH3]** seems to offer high quality solutions consistently within the experimental range.

Table 2.4: Comparison between different solution approaches

Case	N	M	[CG]			[CG+SAA]			[CG+SAA+PHA]			[CG+SAA+PHA+HR]			[CG+SAA+PHA+HR+RH3]		
			Gap (%)	CPU (sec)	iter	Gap (%)	CPU (sec)	iter	Gap (%)	CPU (sec)	iter	Gap (%)	CPU (sec)	iter	Gap (%)	CPU (sec)	iter
9	20	5	0.48	4,252.3	1	0.64	2,685.6	1	0.16	**886.5**	1	0.38	1,856.4	2	0.27	1,084.3	1
		10	0.27	6,747.4	3	0.43	4,124.7	1	0.14	2,286.1	1	0.45	**1,025.6**	1	0.33	1,196.2	2
	40	5	0.52	8,452.6	2	0.13	3,251.4	2	0.25	1,985.6	2	0.34	**1,265.3**	1	0.61	1,412.7	2
		10	0.52	11,258.9	1	0.39	4,896.8	2	0.62	2,984.4	1	0.61	3,254.2	1	0.61	**865.4**	1
	60	5	0.38	14,257.3	2	0.27	2,473.5	1	0.47	1,783.7	2	0.58	1,453.6	1	0.43	**917.5**	1
		10	0.46	18,524.8	3	0.49	3,365.4	1	0.74	4,125.4	1	0.48	2,789.5	2	0.29	**1,178.3**	1
10	20	5	7.25	36,000.0	1	0.25	4,256.8	2	0.23	4,753.6	2	0.44	3,352.4	1	0.51	**1,526.3**	1
		10	12.52	36,000.0	1	0.51	4,841.3	2	0.43	3,842.5	1	0.32	5,423.6	2	0.28	**1,842.7**	2
	40	5	mem^a	-	-	0.78	10,253.6	1	0.36	11,542.6	1	0.82	10,584.1	1	0.75	**5,654.9**	1
		10	mem	-	-	0.26	19,236.4	2	0.18	18,632.2	2	0.25	12,578.9	1	0.24	**6,875.1**	1
	60	5	mem	-	-	2.56	36,000.0	1	0.26	21,546.6	1	0.19	16,875.2	2	0.29	**7,128.5**	2
		10	mem	-	-	3.45	36,000.0	1	0.39	26,365.8	2	0.63	18,524.6	1	0.36	**7,985.6**	1
11	20	5	7.25	36,000.0	1	0.47	4,352.2	1	0.34	4,895.1	1	0.52	4,152.3	1	0.51	**1,485.5**	2
		10	12.52	36,000.0	1	0.51	4,542.8	2	0.69	4,152.7	2	0.66	4,532.1	1	0.45	**1,785.9**	1
	40	5	mem	-	-	0.78	9,854.7	1	0.51	10,685.4	2	0.61	11,452.8	1	0.53	**5,239.9**	1
		10	mem	-	-	0.26	14,592.3	1	0.27	13,789.5	2	0.54	11,542.6	1	0.48	**5,643.5**	2
	60	5	mem	-	-	2.35	36,000.0	2	0.26	18,541.2	2	0.71	14,872.5	2	0.61	**6,358.4**	1
		10	mem	-	-	4.14	36,000.0	1	0.39	21,568.4	1	0.41	15,863.9	1	0.48	**6,985.1**	2
12	20	5	mem	-	-	mem	-	-	0.65	15,988.9	2	0.85	11,587.4	1	0.59	**8,254.3**	1
		10	mem	-	-	mem	-	-	0.71	18,475.8	2	0.62	14,523.1	1	0.18	**9,954.2**	1
	40	5	mem	-	-	mem	-	-	2.61	36,000.0	1	0.65	18,524.6	1	0.58	**10,856.4**	2
		10	mem	-	-	mem	-	-	5.64	36,000.0	1	0.89	28,693.4	2	0.65	**12,452.2**	1
	60	5	mem	-	-	mem	-	-	mem	-	-	mem	-	-	0.85	**13,458.6**	1
		10	mem	-	-	mem	-	-	mem	-	-	mem	-	-	**1.25**	36,000.0	1
Average			4.22^b	20,749.3	1.6	1.04^b	13,151.5	1.4	0.74^b	12,765.1	1.5	0.54^b	9,760.4	1.4	0.51	**6,505.9**	1.3

[a] Out of Memory

[b] Instances where (a) did not contribute to the average calculation

2.4.3 Experimental Results

2.4.3.1 Impact of Load Congestion Cost χ^c_{ht} on System Performance

The first set of experiments analyzes the impact of load congestion cost χ^c_{ht} on system performance. For the base case, load congestion cost is set at \$10 per hour. Figure 2.9 portrays a relationship between the load congestion cost and the number of charging stations opened, $|\mathbf{Y}|$. Clearly, the decision to open a station is highly impacted by this cost. It is observed that as the value of χ^c_{ht} increases the number of charging station opened decreases. Moreover, it is important to notice that after a certain threshold value of χ^c_{ht} the line becomes a flat. This is the critical point after which the model does not open any additional charging stations and thus the EVs' demand is satisfied via other distribution companies by incurring a higher penalty cost.

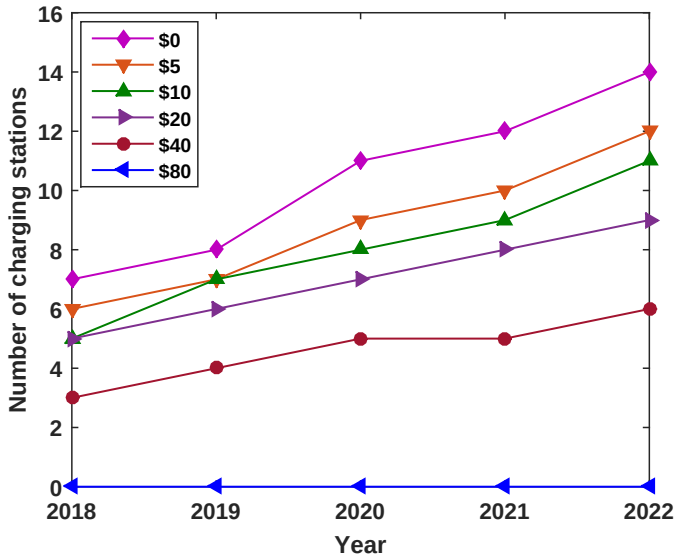

Figure 2.9: Impact of χ^c_{ht} on opening charging station decisions

We now evaluate the optimal planning decisions for charging stations while considering a low (i.e., χ^c_{ht} = \$5/hour) and a high congestion cost (i.e., χ^c_{ht} = \$20/hour) into account. Figures 2.10 and 2.11 demonstrate the network under low and high load congestion cost. Results indicate the number of cells with charging station $|\mathbf{Y}|$ decreases with an increase in load congestion cost. For instance, in year 2018, a total of six charging stations are selected for a low load congestion cost compared with five stations when a higher load congestion cost is in place. Among the six charging stations, three are selected with a small size capacity, two of medium size capacity, and the remaining one with large size capacity. On the contrary, for the high load congestion cost case, among the five charging stations, two are selected with small size capacity, one of medium size capacity, and the remaining two with large size capacity. It is important to state that although with the increase in load congestion cost, the number of charging stations opened decreases; however, the tendency to select the charging station with higher load capacity increases. This implies that the load congestion cost directly impacts both the number and size of charging stations.

2.4.3.2 Impact of Electric Vehicle Charging Percentage (η^{ω}_{ht}) Variability on System Performance

The second set of experiments investigates how different level of car charging percentage η^{ω}_{ht} impact system performance. To serve this purpose, we construct three different realistic scenarios. In the first scenario (base case), we solve the **[LEV]** model using the input parameters discussed in Section 2.4.1. The second and third scenarios are created by setting ϵ to 5% and 50% to represent the low and high car charging percentage levels. We employ Monte Carlo simulation to generate these scenarios where the car charging

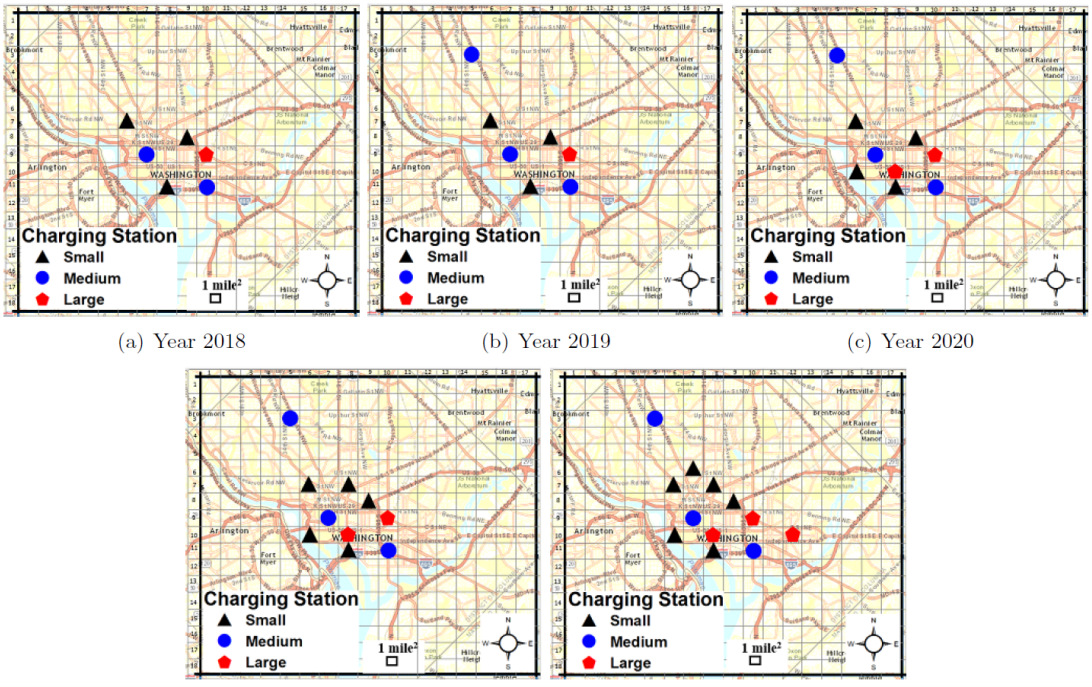

(a) Year 2018 (b) Year 2019 (c) Year 2020

(d) Year 2021 (e) Year 2022

Figure 2.10: Electric vehicle charging station location under a low load congestion cost scenario

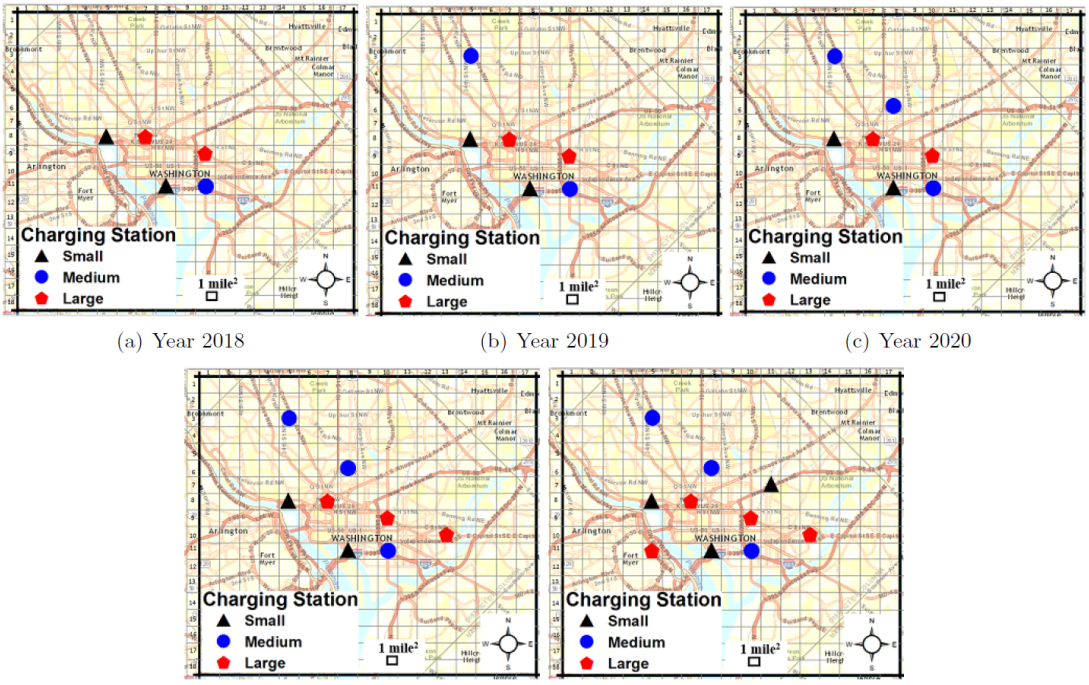

(a) Year 2018 (b) Year 2019 (c) Year 2020

(d) Year 2021 (e) Year 2022

Figure 2.11: Electric vehicle charging station location under a high load congestion cost scenario

percentage for each period is independent and varies in the range $[\overline{\boldsymbol{\eta}}_{ht}(1-\epsilon), \overline{\boldsymbol{\eta}}_{ht}(1+\epsilon)]$ for each hour $h \in \mathcal{H}$ in year $t \in \mathcal{T}$. Note that $\overline{\boldsymbol{\eta}}_{ht}$ represents the mean car charging percentage scenario for each hour $h \in \mathcal{H}$ in year $t \in \mathcal{T}$. Furthermore, we assume that the car charging percentage follows a uniform distribution. Figures 2.12 and 2.13 show the deployment of charging stations $\mathbf{Y}$ (symbol "△" represents *small* size charging station, "◯" represents *medium* size charging station, and "⬠" represents *large* size charging station) for the second and third case scenarios. Results indicate that the number of charging stations increases with the increase in variability of the car charging percentage under a specific budget limit. More specifically, the model decides to open an additional 26.83% charging stations to counter high car charging percentage variability over the low car charging percentage variability. It is important to note that for the high variability case of car charging percentage, the charging stations are distributing their capacities to minimize the overall system costs (shown in Figure 2.13).

Figure 2.14 illustrates the impact of car charging percentage variability η^{ω}_{ht} on system performance. It is evident from the results that, with increasing the level of car charging percentage variability the amount of power utilized to satisfy the electricity demand from diversified power sources (e.g., grid, solar, V2G) increases as well. Clearly, model **[LEV]** is highly responsive to a number of time-dependent parameters such as solar power availability, electricity prices, vehicle flows, which severely impact the hourly operational decisions of a charging station located in cell $i \in \mathcal{I}$ of a given year $t \in \mathcal{T}$. For example, Figures 2.14(a) and 2.14(c) illustrate that the EV power demand is satisfied primarily via the grid and V2G sources during low cost operating hours and solar power unavailability

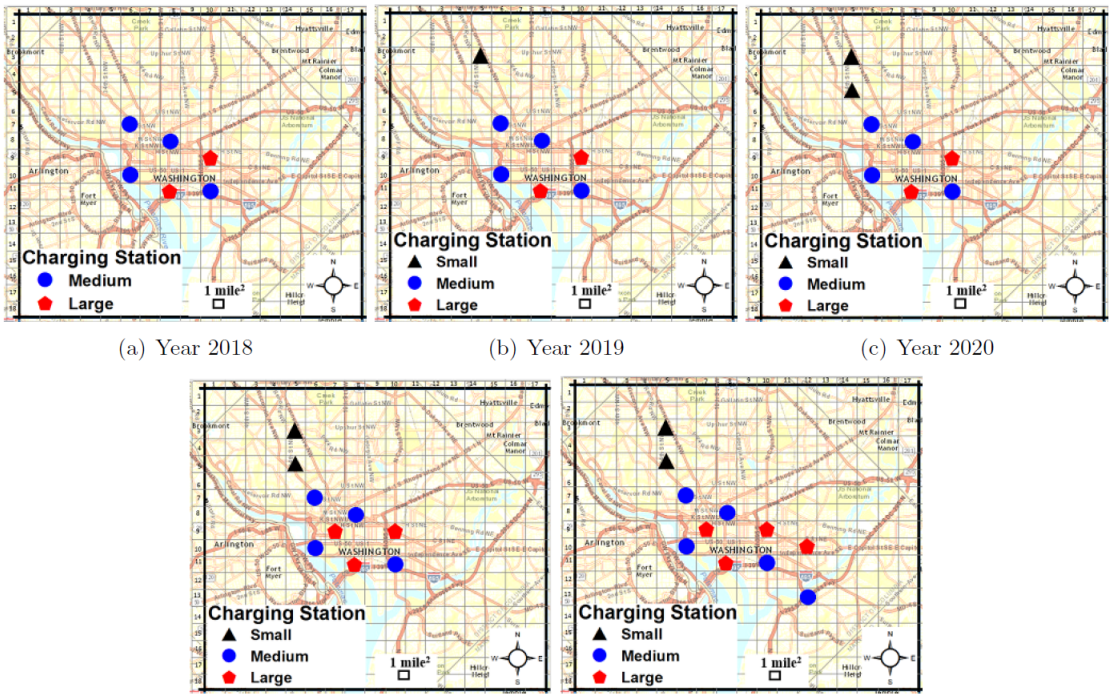

(a) Year 2018 (b) Year 2019 (c) Year 2020

(d) Year 2021 (e) Year 2022

Figure 2.12: Impact of low electric vehicle charging percentage (η_{ht}^{ω}) variability on system performance

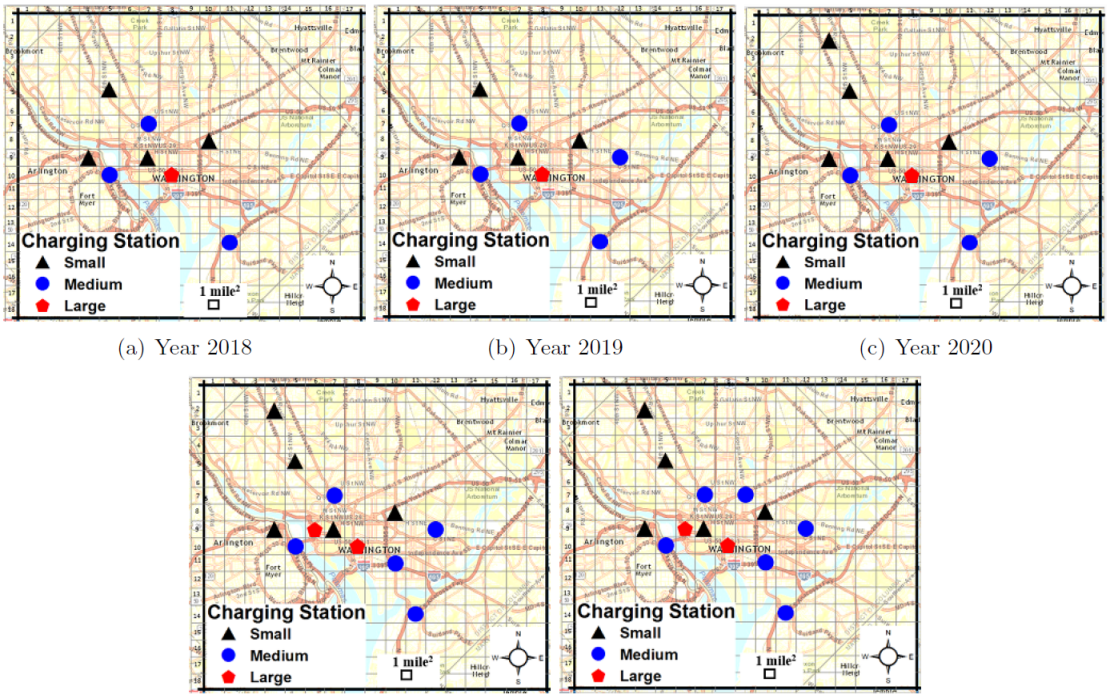

(a) Year 2018 (b) Year 2019 (c) Year 2020

(d) Year 2021 (e) Year 2022

Figure 2.13: Impact of high electric vehicle charging percentage (η_{ht}^{ω}) variability on system performance

(i.e., from 8:0 P.M. to 8:0 A.M.). On the contrary, as shown in Figure 2.14(b), the demand is satisfied first via solar and then via grid and V2G during peak operating hours (i.e., from 10:0 A.M. to 2:0 P.M.). Figure 2.15 signifies the impact of car charging percentage variability on the battery-related decisions when the **[LEV]** model fulfills demand by swapping batteries in the tested region. It is observed that to cope with high power demand variability, the charging stations decide to charge more batteries during off peak hours (shown in Figure 2.15(c)) which they then discharge during peak hours (shown in Figure 2.15(d)). Since more batteries are charged during off peak hours, more batteries are required to be stored in the charging stations during those operating hours as illustrated in Figure 2.15(b). Note that in Figures 2.14 and 2.15, and the figures introduced later in this manuscript, we denote $\overline{G}^{\omega}_{iht} = \sum_{i\in\mathcal{I},h\in\mathcal{H},t\in\mathcal{T},\omega\in\Omega} \rho_{\omega} G^{\omega}_{iht}/|\mathbf{Y}^*|$; $\overline{Z}^{\omega}_{iht} = \sum_{i\in\mathcal{I},h\in\mathcal{H},t\in\mathcal{T},\omega\in\Omega} \rho_{\omega} Z^{\omega}_{iht}/|\mathbf{Y}^*|$; $\overline{V}^{\omega}_{iht} = \sum_{i\in\mathcal{I},h\in\mathcal{H},t\in\mathcal{T},\omega\in\Omega} \rho_{\omega} V^{\omega}_{iht}/|\mathbf{Y}^*|$; $\overline{B}^{\omega}_{iht} = \sum_{i\in\mathcal{I},h\in\mathcal{H},t\in\mathcal{T},\omega\in\Omega} \rho_{\omega} B^{\omega}_{iht}/|\mathbf{Y}^*|$; $\overline{H}^{\omega}_{iht} = \sum_{i\in\mathcal{I},h\in\mathcal{H},t\in\mathcal{T},\omega\in\Omega} \rho_{\omega} H^{\omega}_{iht}/|\mathbf{Y}^*|$; $\overline{S}^{\omega}_{iht} = \sum_{i\in\mathcal{I},h\in\mathcal{H},t\in\mathcal{T},\omega\in\Omega} \rho_{\omega} S^{\omega}_{iht}/|\mathbf{S}^*|$; and $\overline{P}^{\omega}_{iht} = \sum_{i\in\mathcal{I},h\in\mathcal{H},t\in\mathcal{T},\omega\in\Omega} \rho_{\omega} P^{\omega}_{iht}/|\mathbf{Y}^*|$ be the average consumption of grid, solar, and V2G power and the number of batteries demand, stored, charged, and discharged in a charging station located in cell $i \in \mathcal{I}$ on hour $h \in \mathcal{H}$ of year $t \in \mathcal{T}$. Moreover, we denote $|\mathbf{Y}^*|$ as the number of charging stations opened in cell $i \in \mathcal{I}$ of year $t \in \mathcal{T}$. Overall, we observe that the car charging percentage variability levels highly impact the operational decisions in the electric vehicle charging stations.

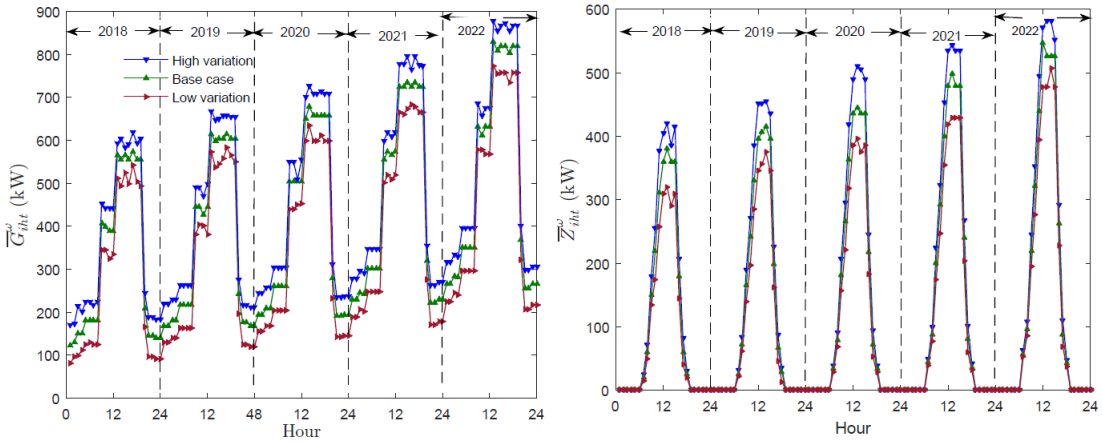

(a) G^{ω}_{iht} vs. time (hr)

(b) Z^{ω}_{iht} vs. time (hr)

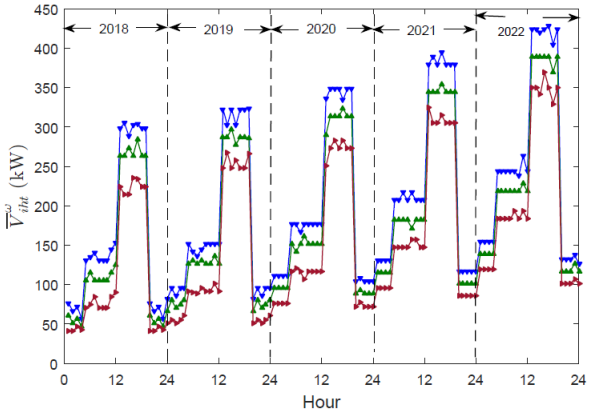

(c) V^{ω}_{iht} vs. time (hr)

Figure 2.14: Impact of car charging percentage (η^{ω}_{ht}) variability on utilizing resources

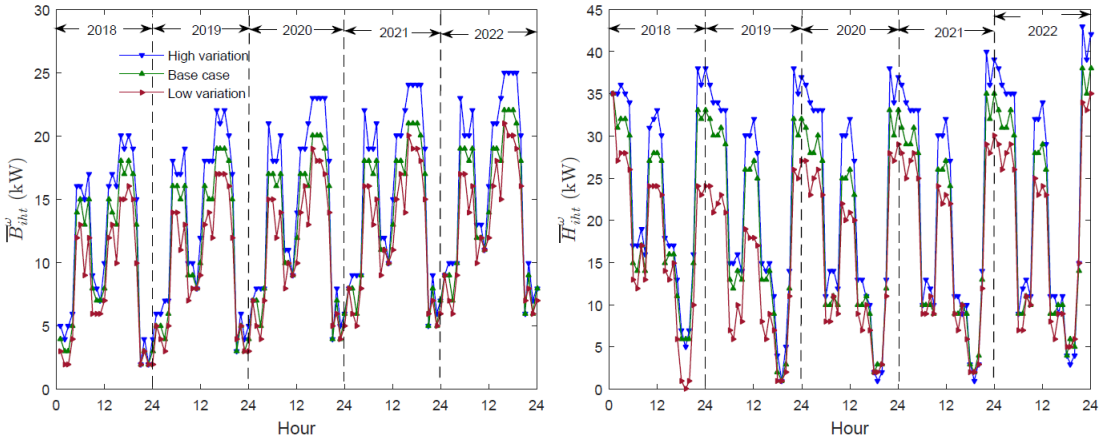

(a) B^{ω}_{iht} vs. time (hr)

(b) H^{ω}_{iht} vs. time (hr)

(c) S^{ω}_{iht} vs. time (hr)

(d) P^{ω}_{iht} vs. time (hr)

Figure 2.15: Impact of car charging percentage (η^{ω}_{ht}) variability on real-time demand response

2.4.3.3 Impact of λ^c_{iht} and λ^d_{iht} on System Performance

The third set of experiments analyzes the impact of average unit power charging requirement for a car λ^c_{iht} and average unit power discharged from a car λ^d_{iht} on system performance. The average unit power charging requirement for each car at cell $i \in \mathcal{I}$ in hour $h \in \mathcal{H}$ of year $t \in \mathcal{T}$ is calculated based on the SoC of the electric vehicles coming to the stations for charging. Similarly, the average unit power discharged from a car at cell $i \in \mathcal{I}$ in hour $h \in \mathcal{H}$ of year $t \in \mathcal{T}$ is calculated based on the DoD of the electric vehicles discharging at the station. Realizing that the electric vehicles coming to a station, whether for charging or discharging, will have different levels of remaining power ((c^+_{iht}, c^-_{iht}), (d^+_{iht}, d^-_{iht})) in their batteries. To incorporate these scenarios, we construct two cases: (i) average unit power charging requirement for each car is considered to be stochastic $\lambda^c_{iht\omega}$ (where $\lambda^c_{iht\omega}$ is generated using a uniform distribution between [$\lambda^c_{iht}(1-\epsilon)$, $\lambda^c_{iht}(1+\epsilon)$]), and (ii) the average unit power discharged from a car is considered as stochastic $\lambda^d_{iht\omega}$ (where $\lambda^d_{iht\omega}$ is generated using a uniform distribution between [$\lambda^d_{iht}(1-\epsilon)$, $\lambda^d_{iht}(1+\epsilon)$]). We set $\epsilon = 10\%$ to account for the variations in generating scenarios. It is observed from the results in Figures 2.16 and 2.17 that considering both $\lambda^c_{iht\omega}$ and $\lambda^d_{iht\omega}$ as stochastic increases the number of charging stations to be opened. For instance, uncertainty in $\lambda^c_{iht\omega}$ increases the average number of charging station opened decisions by 18.18%. A network representation for this instance is shown in Figure 2.16. However, we observe that the stochastic parameter $\lambda^d_{iht\omega}$ provides less sensitivity in the decision to open charging stations compared to $\lambda^c_{iht\omega}$. For example, experiments with the stochastic parameter $\lambda^d_{iht\omega}$ result in an increase in

the average number of charging station opened by 9.09%. Figure 2.17 portrays the network representation for this instance.

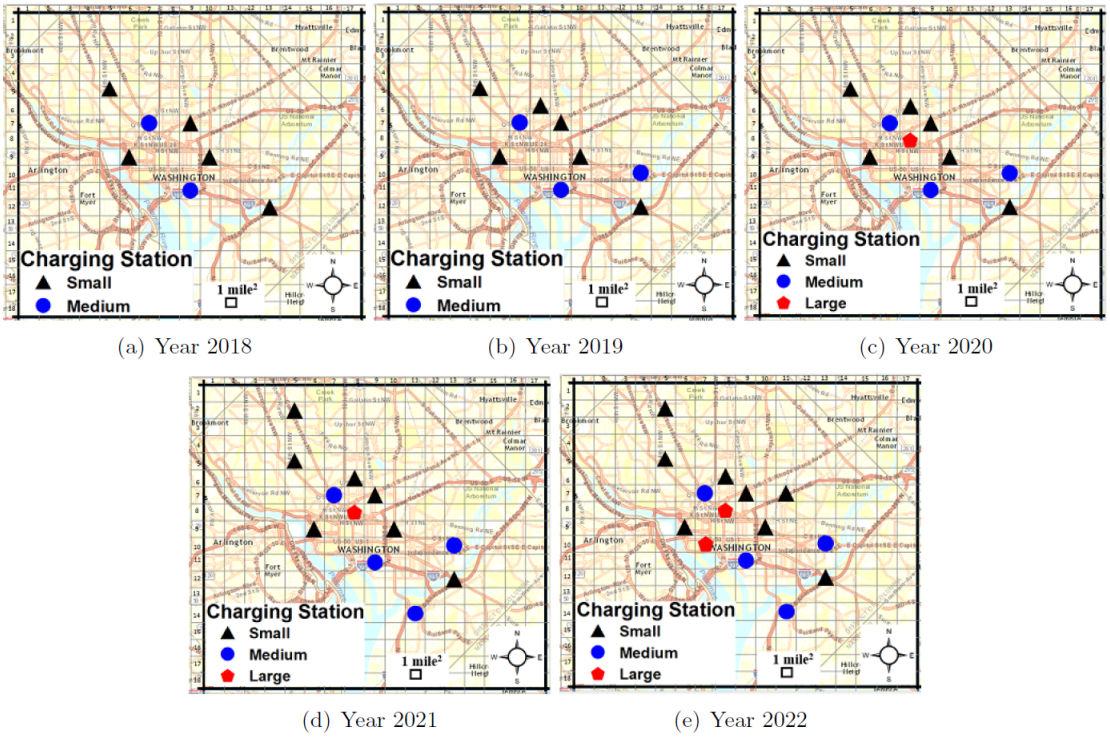

(a) Year 2018 (b) Year 2019 (c) Year 2020

(d) Year 2021 (e) Year 2022

Figure 2.16: Impact of $\lambda^{c}_{iht\omega}$ on system performance

2.5 Conclusion

This paper proposes a novel optimization framework that integrates both long-term multi-period investment decisions and short-term hourly operational decisions to design and manage charging stations operating under power demand uncertainty. A two-stage stochastic mixed-integer programming model **[LEV]** is developed that not only decides the optimal size, location, and timing for opening charging stations over a long-term plan-

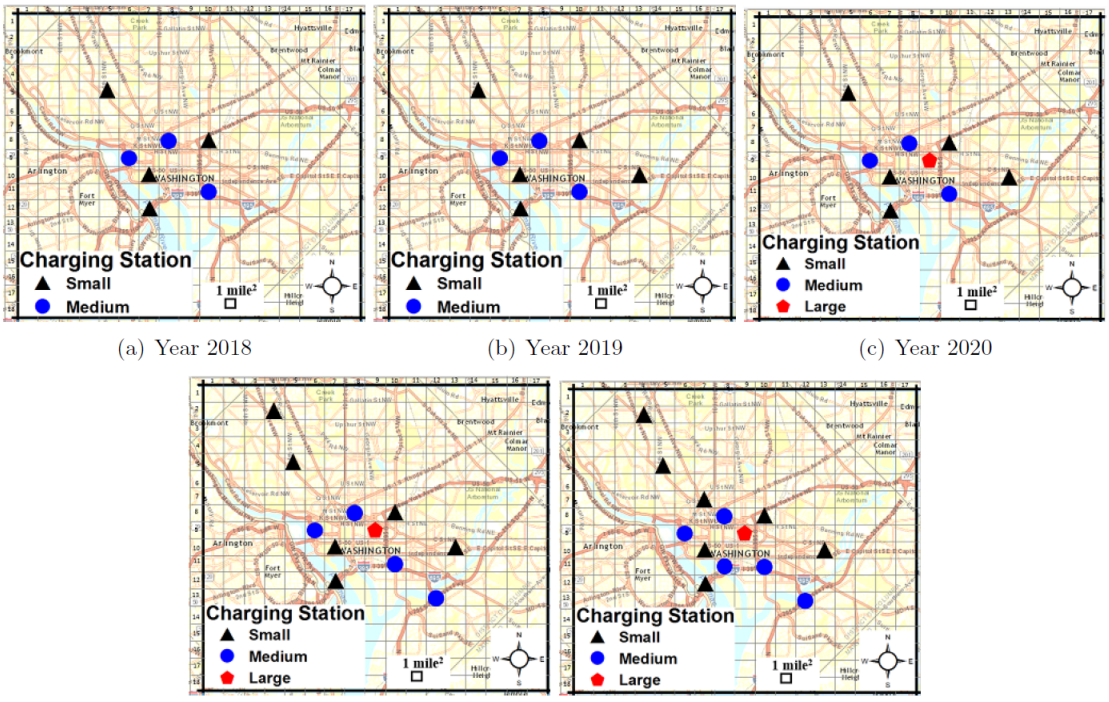

(a) Year 2018 (b) Year 2019 (c) Year 2020

(d) Year 2021 (e) Year 2022

Figure 2.17: Impact of $\lambda^{d}_{iht\omega}$ on system performance

ning horizon, but it also helps with the short-term hourly operational decisions (number of batteries charged, discharged, and stored, along with usage of V2G, renewable, and grid power) while simultaneously managing load congestion and supporting the stochastic power demands at the charging stations. To solve this challenging problem, a highly customized hybrid decomposition algorithm is proposed. The hybrid algorithm combines constraint generation and sample average approximation method with an enhanced progressive hedging algorithm. Moreover, the hybrid algorithm incorporates several algorithmic improvements such as a penalty parameter updating technique, local and global heuristics, and different variants of the rolling horizon heuristic. Computational experiments reveal that the enhanced variant of the hybrid algorithm **[CG+SAA+PHA+HR+RH3]** is capable of producing consistently high-quality solutions to realistic large-sized problem instances within a reasonable amount of time.

We use Washington, DC as a testing ground to evaluate the performance of the modeling results. The numerical experiments reveal some managerial insights about the impact of load congestion on the design and management of charging stations. It is observed that as the load congestion cost increases, the number of charging stations decreases, but there is a tendency to open larger capacity charging stations, which reveals that the congestion cost has a substantial impact in charging station investment decisions. Through investigation it has been also found that the system is highly sensitive towards car charging percentage variability which results in selection of different location of charging stations. This ultimately affects the short-term hourly operational decisions of the charging stations. Furthermore, a sensitivity analysis is carried out considering the impact of uncertainty in

the average unit power charging requirement (λ^c_{iht}) and the average unit power discharged (λ^d_{iht}) from each car on the decision to open charging stations. Results indicate that the model recommended increasing the number of charging stations opened by 18.18% and 9.09% for the uncertainty in λ^c_{iht} and λ^d_{iht}, respectively. The proposed model and results can help decision makers to develop a future sustainable transportation system that will add value not only to the economy, but also positively impact the environment we live in.

This work can be extended in several research directions. This study only considers load congestion; however, in reality congestion may arise in serving EV's on the charging stations. Furthermore, this work assumes that the power network is robust and will never fail. However, power network is frequently impacted by a number of weather-related extreme events (e.g., ice storms, hurricanes, tornados) and/or human-induced events (e.g., cyber-attacks). It will be interesting to see how congestion at charging stations can be managed under facility disruptions. These issues will be investigated in future studies.

CHAPTER III

AN ENERGY SHARING STOCHASTIC MODEL AMONG ELECTRIC VEHICLE CHARGING STATIONS AND COMMERCIAL BUILDINGS, AND POWER GRID

3.1 Introduction

Commercial buildings and road transportation sectors utilize a significant portion of energy which causes global challenges like climate change and resource scarcity. According to the U.S. Energy Information Administration [116], buildings and road transportation sectors consume approximately 43.35% and 28.79% of total energy generated in the United States, respectively. Regarding indirect emissions, both sectors causes approximately 78.9% of greenhouse gas (GHG) emissions, of which the building and transportation sectors are responsible for 44.6% and 34.3%, respectively [117]. Recently, the growing concerns of energy efficiency, dependence on fossil fuels, and environmental impacts have attracted increasing attention on smart buildings and electric vehicles (EVs) in relation to commercial building and road transportation sectors, respectively.

A smart building is a structure utilizing automated processes to control the building's operations including heating, ventilation, air conditioning, lighting, security, and other systems. According to [114] an undeniable fact about smart building management is the need to accurately coordinate its electrical and thermal loads. To achieve greater economic performance and environmental sustainability, an efficient energy management system is

needed which can optimally coordinate the generation, consumption, and storage of energy across the available resources.

Electric vehicle sales in the U.S. increased by 22% from 2015 to 2016 and it is anticipated that there will be approximately 2.7 million EVs on the U.S. road by 2020 [56]. Furthermore, it is expected that the EV market share will hit 10% by 2025 [56]. Higher EV market penetration brings both challenges and opportunities in the area of power grid (PG) management. Unmanaged charging of EVs might trigger an extreme swell in electricity demand at peak hours and, consequently, negatively affect the stability and security of the PG. This being the case, there is an urgent need to manage EV charging activity efficiently to promote widespread adoption of EVs. Towards this goal, this study investigates optimal operational strategies in relation to smart commercial buildings and electric vehicle charging stations to optimize individual and integrated operations under systems uncertainty.

The PG is faced with a variety of challenges from the viewpoint of sustainable development of advanced technologies. Therefore, the future power grid, known as the smart grid, together with smart commercial buildings defines the next-generation of electrical power generation and consumption systems, respectively, which are characterized by increased utilization of real time communications, information technology, and control and management in the production, distribution, and consumption of electrical energy. The aim of employing an upgraded smart grid together with smart commercial buildings is to allow two-way electricity and information flow between them so that they are capable of monitoring and responding to demand changes.

One possible way to alleviate excessive loads on the PG is to design EV charging stations that integrate renewable energy resources (RES) with vehicle-to-grid (V2G) resources, while planning optimal charging schedules for EVs. A stream of studies have addressed the integration of the RES with V2G. Liu et al. [68] and Marmaras et al. [77] study the effects of EV smart charging patterns on power system scheduling, while considering coordination of wind energy, thermal units, and V2G. Likewise, He et al. [48] present a global and local scheduling model that is able to make charging and discharging decisions for EVs with the goal of minimizing overall system cost. Another study proposed by Ortega et al. [88] integrates V2G with power systems in order to achieve better efficiency along with security while operating under an existing power infrastructure. Along the same line, Haddadian et al. [46, 45] study the effects of considering V2G and RES as viable resources for the smart grid. Similarly, Fathabadi [33] studies the different effects of incorporating V2G and RES with a power network. The goal is to identify the best coordination that is effective in sustaining the system while reducing cost and loss of power production. Jin et al. [59] and Hong et al. [51] propose a stochastic optimization model to minimize the average cost of utilizing RES under system uncertainty. Another study addressed by Zhang et al. [134] introduced a scheduling model to minimize the mean waiting time for charging electric vehicles at EV charging stations equipped with multiple plug outlets and the availability of RES. The authors consider arrival time of EVs, fluctuation in grid power prices, and the RES generation level using a markov decision process (MDP). The existing studies provided along this line attempt to manage operational decisions for a

single charging station while there is no considerable attention given to cluster-based EV charging stations.

Some studies investigate battery related activities at battery swapping stations where an EV can quickly exchange its depleted battery with a fully-charged battery. Pan et al. [89] present a two-stage stochastic programming model to determine the optimal location of battery swapping stations and then make appropriate operational decisions (e.g., the number of charged and discharged batteries) based upon realized battery demands, EV loads, and production of RES energies. Discharging batteries to the PG during peak hours is an important feature of the proposed model. Similarly, Worley and Klabjan [129] present a dynamic programming model to determine the number of purchased batteries and their charging time based on dynamic changes in the PG pricing rate. Along the same line, Mak et al. [74] propose various models that aid the planning process for establishing battery swapping infrastructure based on a robust optimization framework that considers uncertainty in demand. The authors have determined the potential impact of battery standardization and others technology advancements on the optimal infrastructure establishment strategy. Nurre et al. [87] develop an integer programming model to determine the optimal operational decisions (e.g., the number of charged, discharged, and exchanged batteries) of a battery swapping station over a pre-specified time horizon. Liu et al. [70, 71] propose an optimization model to determine energy exchange strategies of a battery swapping station considering solar energy availability and demand management decisions (e.g., optimal pricing, and the number of charging and discharging batteries). Recently, Widrick et al. [127] demonstrates optimal policies for battery swapping station management, integrated

with V2G capability, to control charging and discharging operations under a non-stationary stochastic demand for battery swap, non-stationary prices for charging depleted batteries, and non-stationary prices for discharging fully-charged batteries. Note that most of the existing studies provided along this line attempt to optimize battery management decisions (e.g., hourly charging, discharging, storing, and exchanging) within a battery facility, while there is no considerable attention given to the management of cluster-based charging stations that include capabilities for both battery swapping and EV charging.

In addition to PG load reduction and EV charging station management, another possible way to reduce the energy consumption from the two main sectors (i.e., commercial buildings and road transportation) is through vehicle-to-building (V2B) connection capability. In the V2B integration mode, a smart commercial building can cooperate with an EV charging station(s) to achieve higher energy efficiency and lower network costs. This being the case, two-way electricity flow among related buildings and charging stations can help manage demand fluctuation. Flores et al. [36] show that network costs can be reduced by integrating a charging station with a commercial or industrial building using a coordinated operation strategy. Karan et al. [60] investigate possible CO_2 emission reduction and the effectiveness of GHG mitigation strategies based on the current trend of energy usage in transportation and building sectors. In another study, Clarke et al. [25] and Stadler et al. [109] demonstrate how the design of distributed energy systems can be improved by increasing participation of EVs battery storage, which enhances system flexibility and facilitates integration of further distributed energy resources such as solar and wind energy. Pang et al. [90] and Su et al. [111] demonstrate that V2B connections provide some

benefits including backup power, high power quality for buildings, and peak shaving in the PG. Additionally, the authors also state that V2B integration can significantly improve demand side management and power outage. Gough et al. [41] find that participating in both the peak power and the ancillary services market may prove the most profitable for V2B connections. Sehar et al. [107] and Liu et al. [69] propose a heuristic operation strategy for a commercial building microgrid equipped with EVs and a photovoltaic (PV) system to improve self-consumption capability of PV energy. Erdinc [32] considers both pricing scheme and peak power limiting on demand response, which can further improve the economic advantage of the home energy management structure by increasing flexibility.

To the best of the author's knowledge, none of the prior studies have investigated the effects that integrated cluster-based smart commercial buildings and EV charging stations will have on operational decisions under uncertainty. To fill this gap in the literature, this study proposes a novel collaborative energy sharing decision model to study energy sharing among a cluster of commercial buildings and EV charging stations in concert with the PG. The research problem is formulated as a two-stage stochastic mixed-integer linear programming (MILP) model and then solved using an enhanced Sample Average Approximation (SAA) method. The efficiency of the SAA method is enhanced by generating some problem specific valid inequalities. Another contribution is the application of the proposed MILP model to a real life case study constructed based upon the road network of San Francisco, California. Additionally, an extensive analysis is performed to investigate the energy network cost and design under different operating conditions pertaining

to demand variability and power transaction among network entities. From these results relevant managerial insights are provided.

An outline of this paper is as follows. Section 3.2 introduces the network structure, the problem description, and the model formulation, which is followed by problem specific valid inequalities. The proposed solution approach to solve the mathematical problem is then discussed in Section 3.3. The first part of Section 3.4 describes the data used to generate problem instances along with a scenario generation mechanism. The second and third parts of this section represent, respectively, the performance of the proposed solution approach and sensitivity analysis results, obtained by varying a number of factors of our proposed optimization model. Finally, Section 3.5 concludes our study by summarizing the key managerial insights obtained from this study and offers possible future research directions.

3.2 Problem Description and Model Formulation

This section determines the energy sharing among all entities at a energy network including EV charging stations, commercial buildings, and power grid along with collaborative decision scheme inside each entity. The network structure and the problem description are provided which are followed by a mixed-integer linear programming (MILP) model to solve the research problem optimally. The purpose is to minimize the overall network cost of energy sharing with respect to energy demand of entities, which allows decision makers for serving demands in an efficient way. In addition, valid inequalities are proposed to accelerate the solution of the problem.

3.2.1 Network Structure

The electricity, cooling, and heating demands of commercial buildings along with the electricity demand of EV charging stations are supplied with respect to limited energy resources at both inside and outside of network entities. Inside energy resources of a commercial building include the RES, a thermal energy storage (TES), a combined cooling, heating, and power (CCHP) system (consisting of a power generation unit (PGU), a heat recovery subsystem (HRS), an absorption chiller, and a heating exchanger), a battery storage called commercial-grade battery, and an auxiliary boiler. Likewise, inside energy resources of an EV charging station include the RES, vehicle-to-grid (V2G), and swappable batteries. Finally, outside energy resources of commercial buildings and EV charging stations are the PG and transnational energy among related commercial buildings and EV charging stations. Each building might be connected to more than one EV charging station and vice versa, while both are connected to only one PG. Figure 3.1 demonstrates the structure of energy network consisting of a PG, a commercial building, and an EV charging station.

In relation to a commercial building, the PGU provides a portion of the electricity energy required for the building, while its surplus electricity is stored at commercial-grade battery. Required thermal energy of commercial buildings might not be satisfied only through an auxiliary boiler due to its limited capacity. In addition, the PGU is capable of supplying thermal energy to fulfill thermal demand. Therefore, there is a need to consider thermal load requirement of commercial buildings into energy network since thermal en-

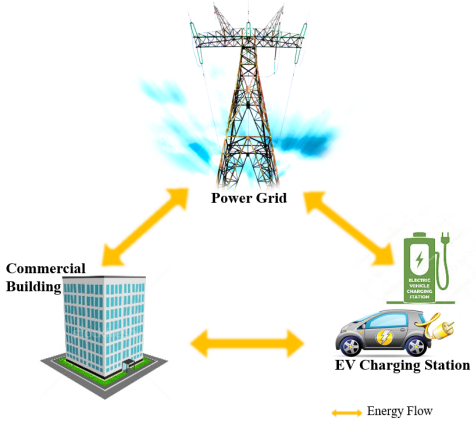

Figure 3.1: Energy network illustration of two-way energy flow among network entities

ergy generated by the PGU is the outcome of the PGU electricity generation. The thermal load requirement of the building is fulfilled from the waste heat of the PGU recovered through the HRS in the CCHP system and/or a auxiliary boiler. The auxiliary boiler converts fuel into heat to compensate the possible shortage of thermal load on the building. An absorption chiller and a heating exchanger are used as the cooling and heating components (the CC and HC, respectively) in the CCHP system, while surplus thermal energy of both the PGU and the auxiliary boiler is stored at the TES. Therefore, commercial-grade battery and the TES control any fluctuation as a result of the stochasticity in prime mover of the electricity and thermal energies, respectively. In relation to an EV charging station, some vehicles swap their battery, while the others are charged through charging stations.

In relation to transnational energy, each commercial building/EV charging station can cooperate with an EV charging station(s)/ a commercial building(s) to send its surplus energy, i.e., V2B integration. This cooperation leads to more energy efficiency in energy network. Thus, the PG supplies the electric load requirements of commercial buildings and

EV charging stations if their self-supplied electricity can not satisfy the electric demands of both; otherwise, their surplus electric energy is sent back to the PG. On the other hand, if the self-supplied electricity of commercial buildings and EV charging stations along with the electricity supplied by the PG are not sufficient to satisfy electric load required for commercial buildings and EV charging stations, then electricity shortage might be imported from outside of the network and, consequently, a penalty cost is considered. As a result, the electric load of a commercial building is supplied by the PGU, a commercial-grade battery, the RES, the PG, and V2B connection, while the electric load of an EV charging station is supplied by the RES, the PG, swapped batteries, and a transnational energy sent by a commercial building(s). Figure 4.1 demonstrates the structure and energy flow among network entities along with components of each entity.

3.2.2 Problem description

The research problem is to determine the optimal energy flow through a set of time periods $\mathcal{T}$ among a set of commercial buildings $\mathcal{B}$, a set of EV charging stations $\mathcal{I}$, and a PG. In addition, optimal operation strategies and collaborative decision scheme among components of each entity in energy network are determined in each time period. Those strategies and decisions determine the amount of energy flow through the CCHP system, the RES, the TES, the boiler, and the commercial-grade battery of each commercial building, along with the amount of energy flow through V2G and the RES as well as the number of stored, charged, discharged, and exchanged EV batteries of each EV charging station.

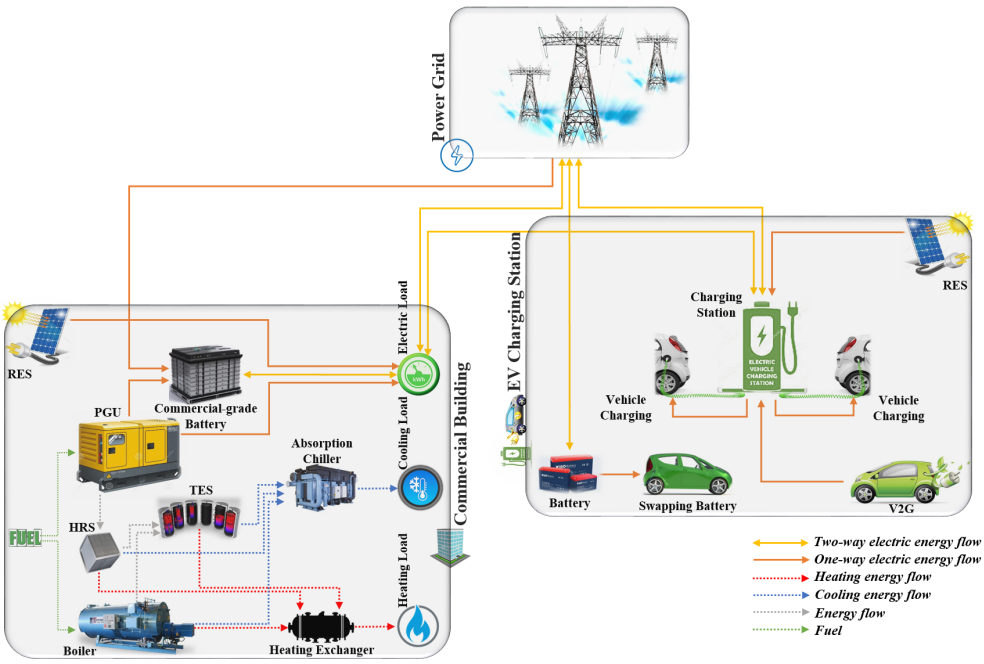

Figure 3.2: Energy network illustration of energy flow among network entities and components

Each commercial building is associated to a subset of EV charging stations $\mathcal{I}_b \ \forall b \in \mathcal{B}$, while each EV charging station is associated to a subset of commercial building $\mathcal{B}_i \ \forall i \in \mathcal{I}$.

The demand of commercial buildings and EV charging stations are modeled as a random variable of which probability distribution might not be known in advance. Accurate prediction, even for small-scale network, is difficult due to the stochastic nature of network entities and components along with the uncertainty in available resources. This being the case, a set of scenarios Ω is determined, where each scenario is associated with a positive probability. Then, the total load including electric, cooling, and heating loads of each commercial building is determined in each time period under each scenario. In addition, the total electric load of each EV charging station is determined in terms of the expected

number of electric vehicles traversed through the charging station in each time period and, consequently, the percentage of those that requires to be charged under each scenario. Likewise, expected V2G power availability is determined in terms of the percentage of electric vehicles required to be discharged in each time period under each scenario. The assumptions of the research problem are summarized as follows:

- limited fuel consumption capacity of PGU/boiler
- fixed-size RES for commercial buildings/EV charging stations
- maximum and minimum rate of charging/discharging of commercial-grade battery/TES
- initial, maximum, and minimum SoC[1] level of commercial-grade battery/the TES
- limited capacity of commercial-grade battery/TES
- limited energy flow from PG to all network entities
- limited energy flow from PG to commercial buildings/EV charging stations
- limited energy flow to PG from commercial buildings/EV charging stations
- limited transnational energy among related commercial buildings and EV charging stations
- limited number of batteries stored in an EV charging station
- limited number of plug-ins for charging/discharging of batteries in an EV charging station
- limited solar radiation
- electricity-/fuel-to-carbon emission

[1]SoC stands for state of charge which is the ratio of available energy to the maximum storage energy in commercial-grade battery/TES

3.2.3 Model Fomulation

Since electricity demand is stochastic, a two-stage stochastic MILP model is proposed to determine energy flow among network entities as well as operation strategies and collaborative decisions related to commercial buildings and EV charging stations, under uncertain electricity demand. In the first-stage, energy network is designed in terms of the state of components of network entities, while energy flow among network entities and inside components of each entity is determined in each time period under each scenario in the second-stage of the MILP model. The first-stage decision variables determine the state of the following entities and components in energy network:

- the state of PGU and boiler in each commercial building
- the state of charging/discharging of commercial-grade battery/TES in each commercial building
- the state of charging/discharging of batteries in each EV charging station
- the state of electricity transaction among commercial buildings, EV charging stations, and the PG

while the second-stage decision variables determine energy flow among the following entities and components in each time period under each scenario:

- electricity transaction among PG, commercial buildings, and EV charging stations
- electricity generation by PGU in each commercial building
- electricity transaction from PGU to commercial-grade battery and building demand
- electricity shortage in each building/EV charging station

- electricity storage in commercial-grade battery of each commercial building
- V2G electricity flow in each EV charging station
- fuel consumption by PGU/boiler in each commercial building
- thermal energy consumption by CC/HC and storage by TES in each commercial building
- charging/discharging batteries in each EV charging station
- full-charged battery storage in each EV charging station
- RES electricity utilization rate by each commercial building/EV charging station
- electricity utilization for charging/discharging commercial-grade battery in each commercial building
- HRS/boiler thermal energy flow to CC/HC/TES in each commercial building

In the following, the sets and indices, subsets, parameters, and decision variables are briefly explained and followed by the mathematical formulation. Parameters are introduced by lowercase and Greek letters, while variables are introduced by uppercase letters. Additionally, the superscript of parameters and variables represent their brief descriptions, while their subscripts represent their indices.

Sets and Indices:

$\mathcal{B}$ set of commercial buildings, indexed by b
$\mathcal{I}$ set of EV charging stations, indexed by i
$\mathcal{T}$ set of time periods, indexed by t
Ω set of scenarios, indexed by ω

Subsets:

$\mathcal{I}_b$	subset of EV charging stations associated to commercial building b	$\mathcal{I}_b \subset \mathcal{I}$
$\mathcal{B}_i$	subset of commercial buildings associated to EV charging station i	$\mathcal{B}_i \subset \mathcal{B}$

For the sake of simplicity in parameters and decision variables definitions, commercial buildings and EV charging stations are summarized as buildings and charging stations, respectively.

Commercial Building Parameters:

ψ_b^{pgu}/ψ_b^{bo}	PGU/boiler startup cost in building b
s_b^{pgu}/s_b^{bo}	PGU/boiler fuel consumption capacity in building b
η^{pgu}/η^{bo}	PGU/boiler system efficiency
c^f	unit fuel price for PGU/boiler ($/gl)
a^{pgu}, b^{pgu}	PGU electricity generation efficiency
a_b	RES size in building b
$d_{bt\omega}$	total demand load in building b in time period t under scenario ω
π_t^e	percentage of total demand load for electric demand in time period t
π_t^c	percentage of total demand load for cooling demand in time period t
π_t^h	percentage of total demand load for heating demand in time period t
η^{cb}/η^{db}	commercial-grade battery charging/discharging efficiency
η^{ce}/η^{de}	TES charging/discharging efficiency
η^{cc}/η^{hc}	CC/HC efficiency
b_{bt}^{bp}	grid power available for building b in time period t
b_{bt}^{bn}	maximum power flow to PG from building b in time period t
$\overline{q}^{b+}/\underline{q}^{b+}$	maximum/minimum percentage of commercial-grade battery charging capacity
$\overline{q}^{b-}/\underline{q}^{b-}$	maximum/minimum percentage of commercial-grade battery discharging capacity
$\overline{q}^{e+}/\underline{q}^{e+}$	maximum/minimum percentage of TES charging capacity
$\overline{q}^{e-}/\underline{q}^{e-}$	maximum/minimum percentage of TES discharging capacity
s_b^{bs}/s_b^{tes}	commercial-grade battery/TES capacity in building b
$s_{bt}^{bs+}/s_{bt}^{bs-}$	maximum/minimum SoC of commercial-grade battery in building b in time period t
$s_{bt}^{tes+}/s_{bt}^{tes-}$	maximum/minimum SoC of TES in building b in time period t
s_{b0}^{bs}	initial SoC of commercial-grade battery in building b
s_{b0}^{tes}	initial SoC of TES in building b

EV Charging Station Parameters:

f_{it} electric vehicle flow around charging station i in time period t

$\delta_{t\omega}$ percentage of electric vehicles charged at an EV charging station in time period t under scenario ω

β_t percentage of electric vehicles discharged at an EV charging station in time period t

c_t^{v2g} unit V2G electricity energy cost in time period t ($/kWh)

c_t^s unit storage cost per battery in time period t

a_i RES size in charging station i

u_i maximum number of available batteries in charging station i

b_{it}^{cp} grid power available for charging station i in time period t

b_{bt}^{bn} maximum power flow to PG from charging station i in time period t

λ average unit power required to charge each electric vehicle (kWh)

γ average unit power obtained from discharge each electric vehicle (kWh)

q_i^{in} number of plug-ins available for charging batteries in charging station i

q_i^{out} number of plug-ins available for discharging batteries in charging station i

Other Parameters:

g_t^{pg} grid power available in time period t

g_t^{bp} grid power available for all buildings in time period t

g_t^{cp} grid power available for all charging stations in time period t

χ_{bit}^{bc} maximum power flow to charging station i from building b in time period t

χ_{ibt}^{cb} maximum power flow to building b from charging station i in time period t

c_t^+ unit electricity purchasing price from PG in time period t ($/kWh)

c_t^- unit electricity selling price to PG in time period t ($/kWh)

c_t^t unit electricity transaction price among any pair of building & charging station in time period t ($/kWh)

c_t^{us} unit penalty cost for a power shortage in time period t ($/kWh)

γ^c carbon emission tax ($/ton)

ν^{etc} electricity-to-carbon conversion factor

ν^{ftc} fuel-to-carbon conversion factor

μ_t solar radiation available in time period t

η^{rr} RES electricity generation efficiency

τ energy conversion factor (kWh to Btu)

ρ_ω probability of scenario ω

In the following, the first- and second-stage decision variables of two-stage stochastic MILP model divided in terms of commercial buildings and EV charging stations are briefly explained.

Commercial Building Decision Variables:

First-stage Decision Variables:

Z_{bt}^{p} 1 if PGU state is on in building b in time period t; 0 otherwise

Z_{bt}^{b} 1 if boiler state is on in building b in time period t; 0 otherwise

S_{bt}^{e+} 1 if TES charging state is on in building b in time period t; 0 otherwise

S_{bt}^{e-} 1 if TES discharging state is on in building b in time period t; 0 otherwise

S_{bt}^{b+} 1 if commercial-grade battery charging state is on in building b in time period t; 0 otherwise

S_{bt}^{b-} 1 if commercial-grade battery discharging state is on at building b in time period t; 0 otherwise

Y_{bt}^{p+} 1 if electricity transaction state from PG is on in building b in on in time period t; 0 otherwise

Y_{bt}^{p-} 1 if electricity transaction state to PG is on in building b in on in time period t; 0 otherwise

Y_{bit}^{s+} 1 if electricity transaction state to charging station i is on in building b in time period t; 0 otherwise

Second-stage Decision Variables:

$H_{bt\omega}^{+}$ electricity flow from PG to building b in time period t under scenario ω

$H_{bt\omega}^{-}$ electricity flow from building b to PG in time period t under scenario ω

$X_{bt\omega}^{pb}$ electricity flow from PGU to commercial-grade battery in building b in time period t under scenario ω

$X_{bt\omega}^{gb}$ electricity flow from PG to commercial-grade battery in building b in time period t under scenario ω

$M_{bit\omega}^{+}$ electricity flow from building b to charging station i in time period t under scenario ω

$Z_{bt\omega}^{brr}$ RES generated electricity in building b in time period t under scenario ω

$X_{bt\omega}^{pgu}$ PGU generated electricity in building b in time period t under scenario ω

$U_{bt\omega}^{bd}$ power shortage in building b in time period t under scenario ω

$B_{bt\omega}^{bd}$ PGU fuel consumed in building b in time period t under scenario ω

$B_{bt\omega}^{bo}$ boiler fuel consumed in building b in time period t under scenario ω

$X_{bt\omega}^{cb}$ electricity flow from building b to its commercial-grade battery in time period t under scenario ω

$X_{bt\omega}^{db}$ electricity flow to building b from its commercial-grade battery in time period t under scenario ω

$X_{bt\omega}^{b}$ commercial-grade battery stored electricity in building b in time period t under scenario ω

$X_{bt\omega}^{e}$ TES stored thermal energy in building b in time period t under scenario ω

$X^{ce}_{bt\omega}$ thermal energy charged in building b in time period t under scenario ω
$X^{de}_{bt\omega}$ thermal energy discharged in building b in time period t under scenario ω
$Q^{cc}_{bt\omega}$ thermal energy flow from HRS and boiler to CC in building b in time period t under scenario ω
$Q^{sc}_{bt\omega}$ thermal energy flow from TES to CC in building b in time period t under scenario ω
$Q^{ch}_{bt\omega}$ thermal energy flow from HRS and boiler to HC in building b in time period t under scenario ω
$Q^{sh}_{bt\omega}$ thermal energy flow from TES to HC in building b in time period t under scenario ω
$Q^{cs}_{bt\omega}$ thermal energy flow from HRS and boiler to TES in building b in time period t under scenario ω

EV Charging Station Decision Variables:
First-stage Decision Variables:
Y^{c+}_{it} 1 if battery charging state is on in charging station i in time period t; 0 otherwise
Y^{c-}_{it} 1 if battery discharging state is on in charging station i in time period t; 0 otherwise
Y^{p+}_{it} 1 if electricity transaction state from PG is on in charging station i in time period t; 0 otherwise
Y^{p-}_{it} 1 if electricity transaction state to PG is on in charging station i in time period t; 0 otherwise
Y^{s-}_{ibt} 1 if electricity transaction state to building b is on in charging station i in time period t; 0 otherwise

Second-stage Decision Variables:
$G^{+}_{it\omega}$ electricity flow from PG to charging station i in time period t under scenario ω
$G^{-}_{it\omega}$ electricity flow from charging station i to PG in time period t under scenario ω
$V_{it\omega}$ electricity flow from V2G to charging station i in time period $t \in \mathcal{T}$ under scenario ω
$M^{-}_{ibt\omega}$ electricity flow from charging station i to building b in time period t under scenario ω
$U^{cs}_{it\omega}$ power shortage in charging station i in time period t under scenario ω
$Z^{crr}_{it\omega}$ RES generated electricity in charging station i in time period t under scenario ω
$B_{it\omega}$ swapped batteries in charging station i in time period t under scenario ω
$W_{it\omega}$ full-charged available batteries in charging station i in time period t under scenario ω
$S_{it\omega}$ charging batteries in charging station i in time period t under scenario ω

$P_{it\omega}$ discharging batteries in charging station i in time period t under scenario ω

Mathematical Model

The objective function minimizes energy flow costs through available energy resources to satisfy the demands of network entities. The first-stage decisions made prior to realizing any stochastic event (e.g., entity demand) correspond to the state of planning and scheduling of network entities and components in each time period, while the second-stage decisions include determining the energy generation resources under each scenario in terms of the first-stage planning and scheduling made in each time period. The resource decisions include the amount of power dispatched from energy generation resources in each time period. The aim is to minimize the first-stage costs and the expected value of the random second-stage costs across all possible entity demand scenarios. The objective function of the two-stage stochastic MILP model **[BEV]** is proposed as follows:

$$\textbf{[BEV]}\ Min \underbrace{\sum_{t\in\mathcal{T}}\Bigg(\sum_{b\in\mathcal{B}}(\psi_b^{pgu}Z_{bt}^{p}+\psi_b^{bo}Z_{bt}^{b})\Bigg)}_{\text{First-stage startup cost}}-$$

$$\underbrace{\sum_{t\in\mathcal{T}}\sum_{\omega\in\Omega}\rho_w\Bigg(\sum_{b\in\mathcal{B}}c_t^{-}H_{bt\omega}^{-}+\sum_{i\in\mathcal{I}}\left(c_t^{-}G_{it\omega}^{-}+\gamma c_t^{-}P_{it\omega}\right)\Bigg)}_{\text{Second-stage building and charging station benefit}}+$$

$$\underbrace{\begin{array}{c}\sum_{t\in\mathcal{T}}\sum_{\omega\in\Omega}\rho_w\Bigg(\sum_{b\in\mathcal{B}}\Big(c_t^{+}H_{bt\omega}^{+}+\gamma^{c}\nu^{etc}H_{bt\omega}^{+}+c_t^{us}U_{bt\omega}^{bd}+c_t^{+}X_{bt\omega}^{gb}+\\ c_t^{t}\sum_{i\in\mathcal{I}_b}M_{ibt\omega}^{-}\Big)\Bigg)\end{array}}_{\text{Second-stage commercial building electricity cost}}+$$

$$\underbrace{\sum_{t\in\mathcal{T}}\sum_{\omega\in\Omega}\rho_w\Bigg(\sum_{b\in\mathcal{B}}\left(c^{f}B_{bt\omega}^{bd}+\gamma^{c}\nu^{ftc}B_{bt\omega}^{bd}+c^{f}B_{bt\omega}^{bo}+\gamma^{c}\nu^{ftc}B_{bt\omega}^{bo}\right)\Bigg)}_{\text{Second-stage commercial building thermal energy cost}}+$$

$$\underbrace{\begin{array}{c}\sum_{t\in\mathcal{T}}\sum_{\omega\in\Omega}\rho_w\Bigg(\sum_{i\in\mathcal{I}}\Big(c_t^{+}G_{it\omega}^{+}+\gamma^{c}\nu^{etc}G_{it\omega}^{+}+\gamma^{c}\nu^{etc}S_{it\omega}+c_t^{v2g}V_{it\omega}+\\ c_t^{us}U_{it\omega}^{cs}+c_t^{t}\sum_{b\in\mathcal{B}_i}M_{bit\omega}^{+}\Big)\Bigg)\end{array}}_{\text{Second-stage EV charging station electricity cost}}+$$

$$\underbrace{\sum_{t\in\mathcal{T}}\sum_{\omega\in\Omega}\rho_w\Bigg(\sum_{i\in\mathcal{I}}\left(\lambda c_t^{+}S_{it\omega}+c_t^{s}W_{it\omega}\right)\Bigg)}_{\text{Second-stage EV charging station battery cost}}$$

In **[BEV]**, the first-stage objective function represents the cost associated with the PGU and boiler startup, while the second-stage objective function represents the cost associated with the PG, commercial buildings, and EV charging stations, i.e., the energy network cost. Electricity flow to the PG from commercial buildings and EV charging stations determine the PG cost, i.e., commercial buildings and EV charging stations benefit. Electricity flow to a particular commercial building from the PG, related EV charging station(s), the RES, commercial-grade battery, and the PGU is considered as the electricity cost of the commercial building. In addition, thermal flow to the CC and HP from the HRS, boiler, and the

TES determines the thermal energy cost of the commercial building. Also, the PGU and boiler fuel consumption are considered as part of the commercial building cost. Electricity flow to a particular EV charging station from the RES, V2G, and the PG is considered as the electricity cost of the EV charging station. In addition, electricity flow to available discharged batteries from the PG is considered as the electricity cost of the EV charging station. The cost of electricity carbon emission and power shortage account for each commercial building and EV charging station.

Constraints Associated with Commercial Buildings

Constraints for Electric Load Balance: Constraints (3.2) guarantee electricity supply for uncertain electric demand of each commercial building. As mentioned, electricity resources include the RES, commercial-grade battery, the PGU, related EV charging stations, the PG, and an external resource(s) as power shortage compensation. Extra supplied electricity is considered as power storage on commercial-grade battery as well as power flow to the PG and related EV charging stations.

$$H^{+}_{bt\omega} + Z^{brr}_{bt\omega} + X^{pgu}_{bt\omega} + \eta^{db} X^{db}_{bt\omega} + \sum_{i \in \mathcal{I}_b} M^{-}_{ibt\omega} + U^{bd}_{bt\omega} = \pi^{e}_{t} d_{bt\omega} + H^{-}_{bt\omega} + \frac{X^{cb}_{bt\omega}}{\eta^{cb}} + \sum_{i \in \mathcal{I}_b} M^{+}_{bit\omega} \; \forall b \in \mathcal{B}, t \in \mathcal{T}, \omega \in \Omega \quad (3.1)$$

Constraints (3.2) restrict electricity flow to an EV charging station from a related commercial building. Constraints (3.3) indicate there is one-way electricity flow among a related pair of commercial building and EV charging station in a particular time period.

$$M^{+}_{bit\omega} \leq \chi^{bc}_{bit} Y^{s+}_{bit} \quad \forall b \in \mathcal{B}, i \in \mathcal{I}, t \in \mathcal{T}, \omega \in \Omega \tag{3.2}$$

$$Y^{s+}_{bit} + Y^{s-}_{ibt} \leq 1 \quad \forall b \in \mathcal{B}, i \in \mathcal{I}, t \in \mathcal{T}, \tag{3.3}$$

Constraints for Thermal Energy Load Balance: Constraints (3.4) and (3.5) guarantee cooling and heating supply for cooling and heating loads of each building based upon thermal energy flow from the HRS, boiler, and the TES.

$$\eta^{cc}(Q^{cc}_{bt\omega} + Q^{sc}_{bt\omega}) = \tau \pi^{c}_{t} d_{bt\omega} \quad \forall b \in \mathcal{B}, t \in \mathcal{T}, \omega \in \Omega \tag{3.4}$$

$$\eta^{hc}(Q^{ch}_{bt\omega} + Q^{sh}_{bt\omega}) = \tau \pi^{h}_{t} d_{bt\omega} \quad \forall b \in \mathcal{B}, t \in \mathcal{T}, \omega \in \Omega \tag{3.5}$$

Constraints for the RES: Constraints (3.6) restrict the utilization of renewable energy to the RES size, electricity generation efficiency, and the amount of solar radiation absorbed by the RES.

$$Z^{brr}_{bt\omega} \leq a_b \mu_t \eta^{rr} \quad \forall b \in \mathcal{B}, t \in \mathcal{T}, \omega \in \Omega \tag{3.6}$$

Constraints for Commercial-grade Battery: Constraints (3.7) through (3.13) determine the state of commercial-grade battery in each time period under each scenario. Constraints (3.7) indicate that a commercial-grade battery cannot be charged and discharged simultaneously in a particular time period. Constraints (3.8) restrict the electricity storage in a commercial-grade battery, while constraints (3.9) and (3.10) determine stored battery electricity based on its previous storage along with the amount of charged or discharged

battery electricity in terms of battery charging and discharging rates. Constraints (3.11) and (3.12) restrict the amount of charged and discharged battery electricity. Finally, constraints (3.13) determine the amount of stored battery electricity in terms of electricity flow obtained from the PGU, the PG, and its related building.

$$S_{bt}^{b+} + S_{bt}^{b-} \leq 1 \quad \forall b \in \mathcal{B}, t \in \mathcal{T} \tag{3.7}$$

$$s_b^{bs} s_{bt}^{bs-} \leq X_{bt\omega}^{b} \leq s_b^{bs} s_{bt}^{bs+} \quad \forall b \in \mathcal{B}, t \in \mathcal{T}, \omega \in \Omega \tag{3.8}$$

$$X_{b1\omega}^{b} - s_b^{bs} s_{b0}^{bs} = \frac{X_{b1\omega}^{cb}}{\eta^{cb}} - \frac{X_{b1\omega}^{db}}{\eta^{db}} \quad \forall b \in \mathcal{B}, \omega \in \Omega \tag{3.9}$$

$$X_{bt\omega}^{b} - X_{bt-1\omega}^{b} = \frac{X_{bt\omega}^{cb}}{\eta^{cb}} - \frac{X_{bt\omega}^{db}}{\eta^{db}} \quad \forall b \in \mathcal{B}, t \geq 2, t \in \mathcal{T}, \omega \in \Omega \tag{3.10}$$

$$s_b^{bs} \underline{q}^{b+} S_{bt}^{b+} \leq \frac{X_{bt\omega}^{cb}}{\eta^{cb}} \leq s_b^{bs} \overline{q}^{b+} S_{bt}^{b+} \quad \forall b \in \mathcal{B}, t \in \mathcal{T}, \omega \in \Omega \tag{3.11}$$

$$s_b^{bs} \underline{q}^{b-} S_{bt}^{b-} \leq \frac{X_{bt\omega}^{db}}{\eta^{db}} \leq s_b^{bs} \overline{q}^{b-} S_{bt}^{b-} \quad \forall b \in \mathcal{B}, t \in \mathcal{T}, \omega \in \Omega \tag{3.12}$$

$$X_{bt\omega}^{b} = X_{bt\omega}^{pb} + X_{bt\omega}^{gb} + \frac{X_{bt\omega}^{cb}}{\eta^{cb}} \quad \forall b \in \mathcal{B}, t \in \mathcal{T}, \omega \in \Omega \tag{3.13}$$

Constraints for the PGU and Boiler: Constraints (3.14) and (3.15) restrict the PGU and boiler fuel consumption with respect to their maximum capacity. Constraints (3.16) restrict electricity flow to commercial-grade battery and corresponding building in terms of the PGU fuel consumption and electricity generation efficiency. Constraints (3.17) restrict thermal energy flow generated by the PGU and boiler to the CC, HC, and TES. It is worth noting that extra thermal energy is stored at the TES.

$$B^{bd}_{bt\omega} \leq s^{pgu}_{b} Z^{p}_{bt} \quad \forall b \in \mathcal{B}, t \in \mathcal{T}, \omega \in \Omega \tag{3.14}$$

$$B^{bo}_{bt\omega} \leq s^{bo}_{b} Z^{b}_{bt} \quad \forall b \in \mathcal{B}, t \in \mathcal{T}, \omega \in \Omega \tag{3.15}$$

$$X^{pb}_{bt\omega} + X^{pgu}_{bt\omega} = (B^{bd}_{bt\omega} - b^{pgu} Z^{p}_{bt})/a^{pgu} \quad \forall b \in \mathcal{B}, t \in \mathcal{T}, \omega \in \Omega \tag{3.16}$$

$$Q^{cs}_{bt\omega} + Q^{cc}_{bt\omega} + Q^{ch}_{bt\omega} \leq \eta^{pgu} B^{bd}_{bt\omega} + \eta^{bo} B^{bo}_{bt\omega} \quad \forall b \in \mathcal{B}, t \in \mathcal{T}, \omega \in \Omega \tag{3.17}$$

Constraints for the TES: Constraints (3.18) through (3.25) determine the TES state in each time period under each scenario. Constraints (3.18) indicate that the TES cannot be charged and discharged simultaneously in a particular time period. Constraints (3.19) restrict the thermal energy storage in the TES, while constraints (3.20) and (3.21) determine thermal energy storage based on its previous storage along with the amount of charged or discharged TES thermal energy in terms of the TES charging and discharging rates. Constraints (3.22) and (3.23) restrict the amount of charged and discharged TES thermal energy. Constraints (3.24) indicate that the thermal energy flow provided by the TES to the CC and HC is restricted by its discharging rate. Finally, constraints (3.25) indicate that thermal energy flow from the HRS and boiler to the TES is restricted by its charging rate.

$$S^{e+}_{bt} + S^{e-}_{bt} \leq 1 \quad \forall b \in \mathcal{B}, t \in \mathcal{T} \tag{3.18}$$

$$s^{tes}_{b} s^{tes-}_{bt} \leq X^{e}_{bt\omega} \leq s^{tes}_{b} s^{tes+}_{bt} \quad \forall b \in \mathcal{B}, t \in \mathcal{T}, \omega \in \Omega \tag{3.19}$$

$$X^{e}_{b1\omega} - s^{tes}_{b} s^{tes}_{b0} = \frac{X^{ce}_{b1\omega}}{\eta^{ce}} - \frac{X^{de}_{b1\omega}}{\eta^{de}} \quad \forall b \in \mathcal{B}, \omega \in \Omega \tag{3.20}$$

$$X^{e}_{bt\omega} - X^{e}_{bt-1\omega} = \frac{X^{ce}_{bt\omega}}{\eta^{ce}} - \frac{X^{de}_{bt\omega}}{\eta^{de}} \quad \forall b \in \mathcal{B}, t \geq 2, t \in \mathcal{T}, \omega \in \Omega \tag{3.21}$$

$$s^{tes}_{b}\underline{q}^{e+}S^{e+}_{bt} \leq \frac{X^{ce}_{bt\omega}}{\eta^{ce}} \leq s^{tes}_{b}\overline{q}^{e+}S^{e+}_{bt} \quad \forall b \in \mathcal{B}, t \in \mathcal{T}, \omega \in \Omega \tag{3.22}$$

$$s^{tes}_{b}\underline{q}^{e-}S^{e-}_{bt} \leq \frac{X^{de}_{bt\omega}}{\eta^{de}} \leq s^{tes}_{b}\overline{q}^{e-}S^{e-}_{bt} \quad \forall b \in \mathcal{B}, t \in \mathcal{T}, \omega \in \Omega \tag{3.23}$$

$$Q^{sc}_{bt\omega} + Q^{sh}_{bt\omega} = \frac{X^{de}_{bt\omega}}{\eta^{de}} \quad \forall b \in \mathcal{B}, t \in \mathcal{T}, \omega \in \Omega \tag{3.24}$$

$$\frac{X^{ce}_{bt\omega}}{\eta^{ce}} = Q^{cs}_{bt\omega} \quad \forall b \in \mathcal{B}, t \in \mathcal{T}, \omega \in \Omega \tag{3.25}$$

Constraints Associated with EV Charging Stations

Constraints for Electric Load Balance: Constraints (3.27) guarantee electricity supply for uncertain electric demand of each EV charging station. As mentioned, electricity resources include the RES, full-charged batteries, related commercial buildings, the PG, V2G, and an external resource(s) as power shortage compensation. Total electricity demand in a given time period under a particular scenario is determined in terms of electric vehicle flow, percentage of charged vehicles, and average unit power required to charge each vehicle. Extra supplied electricity is considered as power flow to the PG and related commercial buildings.

$$G^{+}_{it\omega} + Z^{crr}_{it\omega} + \sum_{b\in\mathcal{B}_i} M^{+}_{bit\omega} + V_{it\omega} + \lambda B_{it\omega} + U^{cs}_{it\omega} = \lambda\delta_{t\omega}f_{it} + \sum_{b\in\mathcal{B}_i} M^{-}_{ibt\omega} + G^{-}_{it\omega} \quad \forall i \in \mathcal{I}, t \in \mathcal{T}, \omega \in \Omega \tag{3.26}$$

Constraints (3.27) restrict electricity flow to a commercial building from a related EV charging station. Constraints (3.28) restricts electricity flow of V2G at an EV charging

station. Total electricity supplied by V2G in a given time period under a particular scenario is determined in terms of electric vehicle flow, percentage of discharged vehicles, and average unit power required to discharge each vehicle.

$$M^{-}_{ibt\omega} \leq \chi^{cb}_{ibt} Y^{s-}_{ibt} \quad \forall i \in \mathcal{I}, b \in \mathcal{B}, t \in \mathcal{T}, \omega \in \Omega \tag{3.27}$$

$$V_{it\omega} \leq \gamma \beta_t f_{it} \quad \forall i \in \mathcal{I}, t \in \mathcal{T}, \omega \in \Omega \tag{3.28}$$

Constraints for the RES: Constraints (3.29) restrict the utilization of renewable energy to the RES size, electricity generation efficiency, and the amount of solar radiation absorbed by the RES.

$$Z^{crr}_{it\omega} \leq a_i \mu_t \eta^{rr} \quad \forall i \in \mathcal{I}, t \in \mathcal{T}, \omega \in \Omega \tag{3.29}$$

Constraints for EV Charging Station Batteries: Constraints (3.30) through (3.37) determine the state of utilized batteries in each time period under each scenario. Constraints (3.30) represents a restricted set of full-charged batteries at each EV charging station at the beginning of the planning horizon. Constraints (3.31) indicate that batteries cannot be charged and discharged simultaneously in a particular time period. Constraints (3.32) and (3.33) restrict the number of charging and discharging batteries by the number of plug-ins available at each EV charging station. Constraints (3.34) determine the number of available full-charged batteries in terms of previous inventory along with the number of charging/discharging batteries and battery demand. Constraints (3.35) indicate that no battery is charged during the first hour of the planning horizon since constraints (3.30) guarantee full-charged batteries at the first time period. Constraints (3.36) restrict the number

of charging batteries to the number of depleted batteries. Finally, constraints (3.37) restrict the number of discharging batteries and battery demand to available full-charged batteries.

$$W_{i,1,\omega} = u_i \quad \forall i \in \mathcal{I}, \omega \in \Omega \tag{3.30}$$

$$Y_{it}^{c+} + Y_{it}^{c-} \leq 1 \quad \forall i \in \mathcal{I}, t \in \mathcal{T} \tag{3.31}$$

$$S_{it\omega} \leq q_i^{in} Y_{it}^{c+} \quad \forall i \in \mathcal{I}, t \in \mathcal{T}, \omega \in \Omega \tag{3.32}$$

$$P_{it\omega} \leq q_i^{out} Y_{it}^{c-} \quad \forall i \in \mathcal{I}, t \in \mathcal{T}, \omega \in \Omega \tag{3.33}$$

$$W_{it\omega} - B_{it\omega} - P_{it\omega} + S_{it\omega} = W_{i,t+1,\omega} \quad \forall i \in \mathcal{I}, t \in \mathcal{T} \backslash |T|, \omega \in \Omega \tag{3.34}$$

$$S_{i,1,\omega} = 0 \quad \forall i \in \mathcal{I}, \omega \in \Omega \tag{3.35}$$

$$S_{it\omega} \leq u_i - W_{it\omega} \quad \forall i \in \mathcal{I}, t \geq 2, t \in \mathcal{T}, \omega \in \Omega \tag{3.36}$$

$$B_{it\omega} + P_{it\omega} \leq W_{it\omega} \quad \forall i \in \mathcal{I}, t \in \mathcal{T}, \omega \in \Omega \tag{3.37}$$

Constraints Associated with Power Grid

Constraints (3.38) through (3.46) determine the PG state in each time period under each scenario. Constraints (3.38) restrict the available grid power utilized for all commercial buildings and EV charging stations, while constraints (3.39) and (3.40) restrict the available grid power utilized only for all commercial buildings and EV charging stations, respectively. Constraints (3.41) indicate that there is one-way electricity flow among the PG and a commercial building in each time period, while constraints (3.42) and (3.43) restrict electricity flow among the PG and a commercial building under each scenario. Likewise, constraints (3.44) indicate that there is one-way electricity flow among the PG and an EV

charging station in each time period, while constraints (3.45) and (3.46) restrict electricity flow among the PG and an EV charging station under each scenario.

$$\sum_{i\in\mathcal{I}} G^{+}_{it\omega} + \sum_{b\in\mathcal{B}} H^{+}_{bt\omega} \leq g^{pg}_{t} \quad \forall t \in \mathcal{T}, \omega \in \Omega \tag{3.38}$$

$$\sum_{b\in\mathcal{B}} H^{+}_{bt\omega} \leq g^{bp}_{t} \quad \forall t \in \mathcal{T}, \omega \in \Omega \tag{3.39}$$

$$\sum_{i\in\mathcal{I}} G^{+}_{it\omega} \leq g^{cp}_{t} \quad \forall t \in \mathcal{T}, \omega \in \Omega \tag{3.40}$$

$$Y^{p+}_{bt} + Y^{p-}_{bt} \leq 1 \quad \forall b \in \mathcal{B}, t \in \mathcal{T} \tag{3.41}$$

$$H^{+}_{bt\omega} \leq b^{bp}_{bt} Y^{p+}_{bt} \quad \forall b \in \mathcal{B}, t \in \mathcal{T}, \omega \in \Omega \tag{3.42}$$

$$H^{-}_{bt\omega} \leq b^{bn}_{bt} Y^{p-}_{bt} \quad \forall b \in \mathcal{B}, t \in \mathcal{T}, \omega \in \Omega \tag{3.43}$$

$$Y^{p+}_{it} + Y^{p-}_{it} \leq 1 \quad \forall i \in \mathcal{I}, t \in \mathcal{T} \tag{3.44}$$

$$G^{+}_{it\omega} \leq b^{cp}_{it} Y^{p+}_{it} \quad \forall i \in \mathcal{I}, t \in \mathcal{T}, \omega \in \Omega \tag{3.45}$$

$$G^{-}_{it\omega} \leq b^{cn}_{it} Y^{p-}_{it} \quad \forall i \in \mathcal{I}, t \in \mathcal{T}, \omega \in \Omega \tag{3.46}$$

Binary and Non-negativity Constraints

Constraints (3.47) define binary restriction for the first-stage decision variables. Likewise, constraints (3.48) and (3.49) define standard integrality and non-negativity constraints for the second-stage decision variables, respectively.

$$
\begin{aligned}
Z^{p}_{bt}, Z^{b}_{bt}, S^{e+}_{bt}, S^{e-}_{bt}, S^{b+}_{bt}, S^{b-}_{bt}, Y^{p+}_{bt}, Y^{p-}_{bt}, \\
Y^{c+}_{it}, Y^{c-}_{it}, Y^{p+}_{it}, Y^{p-}_{it}, Y^{s+}_{bit}, Y^{s-}_{ibt}, &\in \{0,1\} \\
\forall b \in \mathcal{B}, i \in \mathcal{I}, t \in \mathcal{T} & \qquad (3.47) \\
W_{it\omega}, B_{it\omega}, S_{it\omega}, P_{it\omega} &\in \mathbb{Z}_{\geq 0} \\
\forall i \in \mathcal{I}, t \in \mathcal{T}, \omega \in \Omega & \qquad (3.48) \\
G^{+}_{it\omega}, G^{-}_{it\omega}, H^{+}_{bt\omega}, H^{-}_{bt\omega}, M^{+}_{bit\omega}, M^{-}_{ibt\omega}, V_{it\omega}, Z^{crr}_{it\omega}, Z^{brr}_{bt\omega}, X^{pgu}_{bt\omega}, \\
B^{bd}_{bt\omega}, B^{b0}_{bt\omega}, X^{cb}_{bt\omega}, X^{db}_{bt\omega}, X^{pb}_{bt\omega}, X^{gb}_{bt\omega}, X^{b}_{bt\omega}, X^{ce}_{bt\omega}, X^{de}_{bt\omega}, \\
X^{e}_{bt\omega}, U^{bd}_{bt\omega}, U^{cs}_{it\omega}, Q^{cc}_{bt\omega}, Q^{sc}_{bt\omega}, Q^{ch}_{bt\omega}, Q^{sh}_{bt\omega}, Q^{cs}_{bt\omega} &\geq 0 \\
\forall i \in \mathcal{I}, b \in \mathcal{B}, t \in \mathcal{T}, \omega \in \Omega & \qquad (3.49)
\end{aligned}
$$

3.2.4 Valid Inequalities

Regarding valid inequalities, we attempt to accelerate the solution of the problem using both model **[BEV]** and an optimization algorithm proposed in Section 3.3. Valid inequalities are able to enhance a linear programming relaxation of the problem. Readers are referred to the studies [26] discussed in detail about valid inequalities. Inspired from those studies, the following valid inequalities are developed.

- A commercial-grade battery at building b is not capable of discharging electricity energy in a given time period t if no charging is made up to time period $(t-1)$.

$$
\sum_{j \leq (t-1)} S^{e+}_{bj} \geq S^{e-}_{bt} \qquad \forall b \in \mathcal{B}, t \in \mathcal{T} \qquad (3.50)
$$

- The TES at building b is not capable of discharging thermal energy in a given time period t if no charging is made up to time period $(t-1)$.

$$\sum_{j \leq (t-1)} S_{bj}^{b+} \geq S_{bt}^{b-} \quad \forall b \in \mathcal{B}, t \in \mathcal{T} \tag{3.51}$$

- A battery(es) at EV charging station b is not capable of charging electricity energy in a given time period t if no discharging is made up to time period $(t-1)$.

$$\sum_{j \leq (t-1)} Y_{ij}^{c-} \geq Y_{it}^{c+} \quad \forall i \in \mathcal{I}, t \in \mathcal{T} \tag{3.52}$$

- There is no thermal energy flow to the TES, HC, and CC if the PGU and/or boiler state is not switched to *on* at building b in a given time period t under a particular scenario ω.

$$Q_{bt\omega}^{cs} + Q_{bt\omega}^{cc} + Q_{bt\omega}^{ch} \leq \eta^{pgu} s_b^{pgu} Z_{bt}^{p} + \eta^{bo} s_b^{bo} Z_{bt}^{b} \quad \forall b \in \mathcal{B}, t \in \mathcal{T}, \omega \in \Omega \tag{3.53}$$

3.3 Solution Methodology

Since model **[BEV]** contains binary decision variables in the first-stage as well as integer and continues decision variables in the second-stage, it is very challenging to solve using commercial solvers such as CPLEX. In other words, model **[BEV]** is not capable of obtaining optimal solutions for industry-size problems and, consequently, there is a need to propose an optimization algorithm to obtain the optimal/near optimal solutions in reasonable computational times. This being the case, an efficient Sample Average Approximation (SAA) method is proposed to generate high-quality solutions for model **[BEV]** effectively. The performance of the SAA method is also enhanced by considering proposed valid inequalities.

3.3.1 Sample Average Approximation

Electricity and thermal demands of commercial buildings, $d_{bt\omega}$, differ significantly due to different timetable of working hours, usage intensity of equipment and lighting facilities, and air conditioning system data. Likewise, the percentage of electric vehicles charged in EV charging stations, $\delta_{t\omega}$, differs significantly due to variable electric vehicle flows at EV charging stations. Therefore, an extremely large number of scenarios is required to investigate variations in demand. Since the research problem is NP-hard, computational time increases significantly when a large set of scenarios is considered. To remedy this problem, the SAA method is proposed so that the expected energy network cost of the stochastic problem is approximated by a corresponding sample average function. The problem is solved by deterministic optimization techniques under the sample average approximation. The procedure is repeated with different samples until a stopping criterion (a pre-determined optimality gap) is satisfied. The SAA method has been successfully implemented for solving large-scale supply chain network flow related problems ([105], [76], [99], and [120]). In relation to the convergence properties and statistical performance of the SAA method, readers are referred to Kleywegt et al. [62], Mak et al. [75], as well as Norkin et al. [85] and [86].

Electricity demand of commercial buildings, $d_{bt\omega}$, follows a normal distribution for each commercial building b at time period t. Likewise, the percentage of electric vehicles charged in EV charging stations, $\delta_{t\omega}$, follows a normal distribution for each time period t. The SAA method generates set N of random samples n with realizations of uncertain

parameters ($n \in N$ and $|N| < |\Omega|$) to approximate the objective function value of the second-stage problem as follows:

$$\mathbb{E}[Q(\mathbf{Z}, \omega)] := \frac{1}{N} \sum_{n \in N} Q(\mathbf{Z}, \omega^n)$$

where $Q(\mathbf{Z}, \omega^n)$ is a solution of the second-stage problem for a given value of $\mathbf{Z}$ under scenario ω^n. Problem **[BEV]** is now approximated by the following SAA problem:

$$Minimize \left\{ \mathrm{Z}_N^m = \sum_{t \in \mathcal{T}} \sum_{b \in \mathcal{B}} \left(\psi_b^{pgu} Z_{bt}^p + \psi_b^{bo} Z_{bt}^b \right) + \frac{1}{N} \sum_{n \in N} Q(\mathbf{Z}, \omega^n) \right\}$$

As the sample size increases, the optimal solution approximated by the above equation converges with probability one to an optimal solution of the original problem **[BEV]** [62]. By solving the SAA problem within an absolute optimality gap $\delta \geq 0$, the sample size $|N|$ is estimated to guarantee an ϵ-optimal solution to the true problem with probability at least equal to $(1 - \alpha)$ as follows:

$$|N| \quad \geq \quad \frac{3\sigma_{max}^2}{(\epsilon - \delta)^2} \left(|\mathcal{B}||\mathcal{T}|(log2) - log\alpha \right)$$

where $\epsilon > \delta$, $\alpha \in (0, 1)$, and σ_{max}^2 is a maximal variance of certain function differences [62]. It is worth noting that choosing sample size $|N|$ is a trade-off between the solution quality and required computational time. The above equation provides a conservative sample size estimation for practical applications. In each iteration of the SAA method, valid statistical lower and upper bounds are provided for the original problem **[BEV]** and

the process terminates when the gap between aforementioned bounds falls below a pre-determined threshold value. The following steps briefly summarize the SAA method to solve problem **[BEV]**.

Step 1: Generate set M of independent commercial building load scenarios, each of size $|N|$, i.e., $\{d_{bt\boldsymbol{\omega}_m^1}, d_{bt\boldsymbol{\omega}_m^2}, ..., d_{bt\boldsymbol{\omega}_m^{|N|}}\}$, $\forall m \in M, b \in \mathcal{B}, t \in \mathcal{T}$. Likewise, generate set M of independent percentage scenarios of electric vehicles charged in EV charging station, each of size $|N|$, i.e., $\{\delta_{t\boldsymbol{\omega}_m^1}, \delta_{t\boldsymbol{\omega}_m^2}, ..., \delta_{t\boldsymbol{\omega}_m^{|N|}}\}$, $\forall m \in M, t \in \mathcal{T}$. Then, solve the corresponding SAA for each generated sample consisting of $|N|$ realizations of independently and identically distributed $(i.i.d.)$ random scenarios. The optimal objective function value and the optimal solution are denoted by $\mathtt{Z}_N^m$ and $\hat{\mathtt{Z}}_M$, respectively. The optimal objective function value of the m^{th} replication is obtained as follows:

$$\mathtt{Z}_N^m = \sum_{b\in\mathcal{B}}\sum_{t\in\mathcal{T}}\left(\psi_b^{pgu} Z_{bt}^p + \psi_b^{bo} Z_{bt}^b\right) + \frac{1}{N}\sum_{n\in N} Q(\mathbf{Z}, \omega^n)$$

Step 2: Compute the average of all optimal objective function values obtained from the SAA problems, $\bar{\mathtt{Z}}_N^M$ as follows:

$$\bar{\mathtt{Z}}_N^M = \frac{1}{|M|}\sum_{m\in M} \mathtt{Z}_N^m$$

where, $\bar{\mathrm{Z}}_N^M$ provides a statistical lower bound on the optimal objective function value for the original problem **[BEV]** [86]. Since $\mathrm{Z}_N^1, \mathrm{Z}_N^2, ..., \mathrm{Z}_N^M$ generated samples are independent, the corresponding variance of $\bar{\mathrm{Z}}_N^M$, i.e., $\sigma^2_{\bar{\mathrm{Z}}_N^M}$, is given by:

$$\sigma^2_{\bar{\mathrm{Z}}_N^M} = \frac{1}{(|M|-1)(|M|)} \sum_{m \in M} \left(\mathrm{Z}_N^M - \bar{\mathrm{Z}}_N^M \right)^2$$

Step 3: Generate set N' including larger sample size ($|N'| \gg |N|$) to compute the estimated optimal objective solution of the SAA method [62]. This estimator, which is the upper bound of the optimal solution on the generated sample size $|N'|$, is obtained by one of the solutions of $\hat{\mathrm{Z}}_M$ as follows:

$$\mathrm{Z}_{N'}(\hat{\mathrm{Z}}_M) = \sum_{b \in \mathcal{B}} \sum_{t \in \mathcal{T}} \left(\psi_b^{pgu} Z_{bt}^p + \psi_b^{bo} Z_{bt}^b \right) + \frac{1}{N'} \sum_{n \in N'} Q(\mathbf{Z}, \omega^n)$$

In each iteration, the estimator upper bound $\mathrm{Z}_{N'}(\hat{\mathrm{Z}}_M)$ is updated. The variance of this estimator upper bound is calculated as follows:

$$\sigma^2_{N'}(\hat{\mathrm{Z}}_M) = \frac{1}{(|N'-1|)(|N'|)} \sum_{n \in N'} \Big\{ \sum_{b \in \mathcal{B}} \sum_{t \in \mathcal{T}} \left(\psi_b^{pgu} Z_{bt}^p + \psi_b^{bo} Z_{bt}^b \right) + Q(\hat{\mathrm{Z}}_M, \omega^n) - \mathrm{Z}_{N'}(\hat{\mathrm{Z}}_M) \Big\}^2$$

Step 4: Compute the SAA gap, $Gap_{(N,N')}$, and the variance of this gap, $\sigma^2_{Gap_{(N,N')}}$, using the estimators determined in **Steps 2** and **3**.

$$Gap_{(N,N')}(\tilde{Z}) = \mathtt{Z}_{N'}(\hat{\mathtt{Z}}_M) - \bar{\mathtt{Z}}_N^M$$

$$\sigma^2_{Gap_{(N,N')}} = \sigma^2_{N'}(\hat{\mathtt{Z}}_M) + \sigma^2_{\bar{\mathtt{Z}}_N^M}$$

The confidence interval for the optimality gap is then calculated as follows:

$$\mathtt{Z}_{N'}(\hat{\mathtt{Z}}_M) - \bar{\mathtt{Z}}_N^M + z_\alpha \left\{ \sigma^2_{N'}(\hat{\mathtt{Z}}_M) + \sigma^2_{\bar{\mathtt{Z}}_N^M} \right\}^{1/2}$$

with z_α:= $\Phi^{-1}(1-\alpha)$, where $\Phi(z)$ is the cumulative distribution function of the standard normal distribution.

Step 5: Define the best solution among the solutions of $\hat{\mathtt{Z}}_M(\forall m \in M)$ that represents the lowest upper bound $\mathtt{Z}_{N'}(\hat{\mathtt{Z}}_M)$.

3.4 Computational Study and Managerial Insights

This section focuses on solving model **[BEV]** using the SAA method to draw managerial insights derived from a real life case study. This section is composed of three sub-sections. First, a brief description of the data used to generate problem instances along with scenario generation are provided. Second, the efficiency and effectiveness of the MILP model and proposed SAA method are evaluated for the energy network problem with respect to valid inequalities. Finally, a case study, using the city of San Francisco, explores aspects of energy management that makes use of the connections between limited energy resources to satisfy network demand. In addition, the study analyzes the impact of demand variability, power transaction limit, power grid disruption, and the renewable

resource size on the overall energy network design and cost. Managerial insights are derived from this case study in the form of perspective and understanding. All numerical experiments are coded in GAMS 24.2.1 [39] on a desktop computer equipped with an Intel Core i7 - 3.50 GHz processor with 32 GB of RAM. The optimization solver used is ILOG CPLEX 12.6.

3.4.1 Data Description

Since San Francisco has a strong-growing electric vehicle population, it was chosen as a testing ground to visualize and validate the modeling results. In addition, it has a reputation as being one of the nation's most environmentally conscious cities. Several factors contribute to this status, not the least of which San Francisco also happens to be one of the wealthiest cities in the country. Furthermore, San Francisco offers some of the most electric vehicle-friendly incentives for EV owners at both the state and local levels. For example, under the *Bay Area Air Quality Management District's EV Rebate Program* public agencies can receive an additional $2,500 toward the purchase of an electric vehicle and $1,000 for a plug-in hybrid electric vehicle.

Surplus electricity from one or more commercial buildings might be sent to a nearby EV charging station(s) and an EV charging station might share its surplus electricity with nearby commercial buildings, as well for higher energy efficiency. This being the case, within San Francisco, 11 fast EV charging stations ($|\mathcal{I}| = 11$) and 43 commercial buildings ($|\mathcal{B}| = 43$) located near those charging stations were selected for the real life case study [93]. The goal is to determine the impact of parameter changes on the overall energy

network cost. Figure 3.3 demonstrates the distribution of fast EV charging station locations along with their nearby commercial buildings.

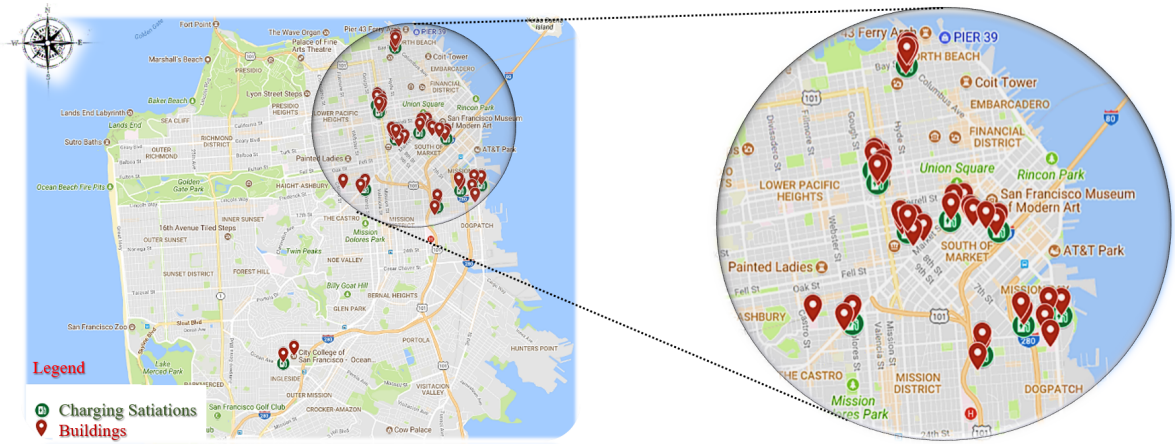

Figure 3.3: EV Charging station distribution with nearby commercial buildings in San Francisco

Information from a 2010 report on uses of solar radiation in San Francisco is used as input for determining available electricity obtained from solar panels during a day [83]. In addition, the size of the solar panels used for commercial buildings (a_b) and EV charging stations (a_i) are assumed to be 100 m^2 and 75 m^2, respectively. Commercial and industrial time-of-use (TOU) rates are adopted from [104] to determine unit electricity transaction price among network entities (c_t^+, c_t^-, and c_t^t). Based on the TOU rate, 1:00 P.M. through 8:00 P.M. are the peak hours of electricity usage where the electricity transaction price is high, while 5:00 A.M. through 12:00 P.M. along with 9:00 P.M. through 11:00 P.M. are the sub-peak hours of electricity usage where the electricity transaction price is lower

compared to peak hours. All other hours throughout a day are off-peak hours with the lowest price. Figure 3.4 represents different electricity usage hours. The hourly electricity pricing plan for V2G (c_t^{v2g}) is obtained from [91].

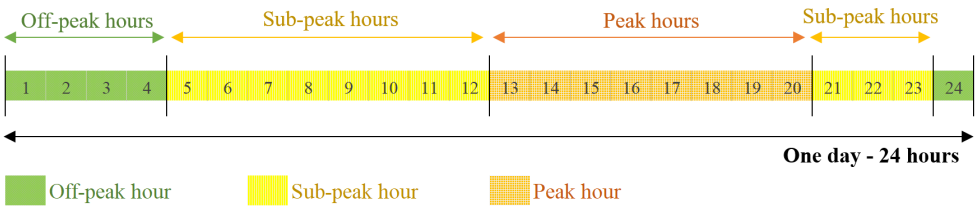

Figure 3.4: Electricity usage hours

The hourly projected commercial building demands ($d_{bt\omega}$) are determined in terms of the TOU rate, while the hourly projected flow of electric vehicles around each charging station (f_{it}) is determined based on the number of electric vehicles that were available in San Francisco in 2016 [92]. Other factors such as population density along with the number of hospitals and colleges located near major roads are considered to project EV flow (f_{it}). Then, in terms of electric vehicle flow around EV charging stations, in this study the percentage of electric vehicles charged in a particular time period ($\delta_{t\omega}$) is set to 40% for the base case, while the discharging rate (β_t) is set to 5%. The average unit power requirement for charging each car (λ) is set to 25.7 kWh. Similarly, average unit power discharged from each car (γ) is also set to 25.7 kWh. The daily fuel consumption capacity of the PGU is set to 200 gl. The grid power available for each commercial building (b_{bt}^{bp}) and EV charging station (b_{it}^{cp}) is set to 200 kWh and 250 kWh, respectively. The

commercial-grade battery capacity (s_b^{bs}) is set to 100 kW. The maximum power transaction between related commercial buildings and EV charging stations (i.e., χ_{bit}^{bc} and χ_{ibt}^{cb}) are set to 100 kWh. For simplification purposes, the minimum and maximum percentages of SoC/charging capacity/discharging capacity of a commercial-grade battery/TES are set to 20% and 90%, respectively, while their charging and discharging efficiencies (η) are both set to 90%. Unit penalty cost of power shortage (c_t^{us}) is determined in terms of the unit production power of other resources, i.e., $c_t^{us} > max\{c_t^+, c_t^t, c^f\}$. Finally, the unit storage cost of a battery in an EV charging station (c_t^s) is set to 0.02 \$/hr.

3.4.2 Computational Performance of the Proposed Algorithms

The efficiency and effectiveness of the SAA method proposed in Section 3.3 is evaluated by solving model **[BEV]**. To simplify the definition of the proposed solution approaches and obtained results, the following notations are provided.

- **[CPLEX]**: Model **[BEV]** solved by CPLEX
- **[CPLEX-VI]**: Model **[BEV]** accompanied by valid inequalities and solved by CPLEX
- **[SAA]**: The SAA method
- **[SAA-VI]**: The SAA method accompanied by valid inequalities for samples with small-size scenario

In relation to the research problem, there are no benchmark instances available in the literature. Hence, a new set of problem instances are generated with respect to a real life case study and problem size, impacting the computational time of **[CPLEX-VI]**. For the purpose of comparison, three sets of problem instances have been generated: small-,

medium-, and large-sized instances, where the case study proposed for San Francisco is considered a medium-size problem. The ratio of the number of commercial buildings to the number of EV charging stations is set to four for all problem sizes, i.e., $\frac{|\mathcal{B}|}{|\mathcal{I}|} = 4$. In other words, each commercial building is connected to four EV charging stations on average. So, for example in the case of a small size problem ratios of 8 buildings to 2 charging stations, 12 to 3, 16 to 4, 20 to 5 and 24 to 6 are used for the various instances in that set. In addition, the time period spans used are 12 and 24 hours (around one day) for small-size instances, 24 and 72 hours (1 and 3 days) for medium-size instances, and 168 and 360 hours (7 and 15 days) for large-size instances. Table 3.1 represents generated instances for each set of problem sizes in terms of $|\mathcal{I}|$, $|\mathcal{B}|$, and $|\mathcal{T}|$, where the deterministic equivalent for model **[BEV]** is indicated based on the number of variables and constraints for each generated case.

Table 3.1: Problem size of the deterministic equivalent of the model based on the number of variables and constraints

Sizes	Instances	$\|\mathcal{I}\|$	$\|\mathcal{B}\|$	$\|\mathcal{T}\|$	Variables				Total constraints
					Binary	Integer	Continuous	Total	
Small	1	2	8	12	480	96	2,520	3,096	5,754
	2	2	8	24	960	192	5,040	6,192	11,526
	3	3	12	12	720	144	4,068	4,932	8,901
	4	3	12	24	1,440	288	8,136	9,864	17,829
	5	4	16	12	960	192	5,808	6,960	12,240
	6	4	16	24	1,920	384	11,616	13,920	24,516
	7	5	20	12	1,200	240	7,740	9,180	15,771
	8	5	20	24	2,400	480	15,480	18,360	31,587
	9	6	24	12	1,440	288	9,864	11,592	19,494
	10	6	24	24	2,880	576	19,728	23,184	39,042
Medium	1	8	32	24	3,840	768	29,376	33,984	55,104
	2	8	32	72	11,520	2,304	88,128	101,952	165,456
	3	9	36	24	4,320	864	34,776	39,960	63,711
	4	9	36	72	12,960	2,592	104,328	119,880	191,295
	5	10	40	24	4,800	960	40,560	46,320	72,702
	6	10	40	72	14,400	2,880	121,680	138,960	218,286
	7	11	43	24	5,160	1,056	45,696	51,912	80,351
	8	11	43	72	15,480	3,168	137,088	155,736	241,247
	9	12	48	24	5,760	1,152	53,280	60,192	91,836
	10	12	48	72	17,280	3,456	159,840	180,576	275,724
Large	1	15	60	168	50,400	10,080	526,680	587,160	864,729
	2	15	60	360	108,000	21,600	1,128,600	1,258,200	1,853,145
	3	17	68	168	57,120	11,424	642,600	711,144	1,025,655
	4	17	68	360	122,400	24,480	1,377,000	1,523,880	2,198,007
	5	20	80	168	67,200	13,440	836,640	917,280	1,287,204
	6	20	80	360	144,000	28,800	1,792,800	1,965,600	2,758,500
	7	22	88	168	73,920	14,784	979,440	1,068,144	1,475,010
	8	22	88	360	158,400	31,680	2,098,800	2,288,880	3,160,962
	9	25	100	168	84,000	16,800	1,213,800	1,314,600	1,776,879
	10	25	100	360	180,000	36,000	2,601,000	2,817,000	3,807,855

A proposed solution approach is evaluated based upon the best lower bound obtained from all solution approaches. In other words, the percentage deviation (gap) between the upper bound and lower bound of the i^{th} solution approach, UB_i and LB_i, respectively, is determined as $\Delta f_i(\%) = (\frac{UB_i - LB_{Best}}{LB_{Best}}) \times 100\% \ \ \forall i \in \mathcal{S}$, where $\mathcal{S} = \{$**[CPLEX]**, **[CPLEX-VI]**, **[SAA]**, **[SAA-VI]**$\}$. LB_{Best} stands for the best lower bound obtained from all solution approaches, i.e., $LB_{Best} = Max\{LB_i\} \ \ \forall i \in \mathcal{S}$. All solution approaches are terminated when at least one of the following criteria is satisfied: (a) the gap falls below a threshold value ε, i.e., $\Delta f_i(\%) \leq \varepsilon$ or (b) the maximum computational time limit, CT^{max}, is reached. In this study, the stopping criteria are set as $\varepsilon = 1\%$ and $CT^{max} = 3600\ s$.

Table 3.2 shows the comparative results obtained for the proposed solution approaches in terms of the gap and computational time. Scenario size is set to $N = 1,000$ for **[CPLEX]** and **[CPLEX-VI]**, while for **[SAA]** and **[SAA-VI]**, sizes of $N = 20$ and $N' = 1,000$ are used for small- and large-size scenarios, respectively. The boldface values under the $T(s)$ columns indicate the best computational time obtained across the proposed solution approaches, while the boldface values under the $\Delta f(\%)$ column indicate the best gap developed by solution approaches when $T(s) = CT^{max}$. The following results are obtained from Table 3.2 under restricted computational time and pre-determined gap:

- Results indicate that all proposed solution approaches outperform **[CPLEX]**, particularly as the problem size increases.
- Although **[CPLEX]** is able to solve all small-size instances optimally, its performance is increase by incorporating valid inequalities to model **[BEV]**, i.e., **[CPLEX-VI]**, in relation to medium-size instances.

- **[CPLEX-VI]** reduces the overall gap reported by **[CPLEX]**.
- **[SAA]** improves the overall performance of **[CPLEX-VI]** by solving all small- and medium-size instances optimally.
- **[SAA-VI]** is capable of solving all problems optimally, except three large-size instances. The gap reported by **[SAA-VI]** is $\frac{1}{5}$ of the gap reported by **[SAA]** on average. This gap is improved significantly in relation to large-size instances.
- **[SAA-VI]** reduces computational time in 50% on average compared to **[SAA]**.
- **[SAA-VI]** outperforms all proposed solution approaches and presents high-quality solutions with respect to both required computational time and the developed gap, particularly for large-size instances.

Table 3.2: Comparison of the results obtained from **[CPLEX]**, **[CPLEX-VI]**, **[SAA]**, and **[SAA-VI]**

Size		**[CPLEX]**		**[CPLEX-VI]**		**[SAA]**		**[SAA-VI]**	
	Case	$\Delta f\,(\%)$	$T(s)$	$\Delta f\,(\%)$	$T(s)$	$\Delta f\,(\%)$	$T(s)$	$\Delta f\,(\%)$	$T(s)$
Small	1	0.09	**6.63**	0.16	7.04	0.08	8.61	0.11	8.91
	2	0.13	**11.24**	0.17	13.47	0.14	15.66	0.19	13.87
	3	0.14	9.57	0.15	**8.25**	0.23	11.47	0.34	12.62
	4	0.23	19.79	0.33	**12.98**	0.29	22.64	0.27	20.74
	5	0.16	**11.78**	0..64	14.82	0.18	16.85	0.42	14.97
	6	0.28	27.02	0.49	**19.88**	0.44	32.87	0.16	29.14
	7	0.34	17.64	0.67	**10.24**	0.36	19.64	0.27	18.35
	8	0.46	38.06	0.34	**24.38**	0.28	42.05	0.25	33.64
	9	0.35	22.09	0.75	**15.09**	0.74	25.67	0.55	23.78
	10	0.24	49.87	0.41	38.54	0.68	**30.41**	0.28	35.64
Average		0.24	21.37	0.39	**16.47**	0.34	22.59	0.28	21.17
Medium	1	0.51	865.06	0.38	425.08	0.25	**171.73**	0.77	188.69
	2	12.95	CT^{max}	7.63	CT^{max}	0.76	1,336.87	0.39	**589.67**
	3	0.85	2,912.59	0.73	3,152.67	0.37	1,187.63	0.14	**468.97**
	4	14.25	CT^{max}	9.49	CT^{max}	0.84	1,763.87	0.64	**785.41**
	5	7.12	CT^{max}	4.97	CT^{max}	0.53	1,587.09	0.26	**597.28**
	6	15.63	CT^{max}	10.23	CT^{max}	0.84	2,364.43	0.72	**987.68**
	7	8.02	CT^{max}	5.34	CT^{max}	0.65	1,873.04	0.38	**653.41**
	8	16.52	CT^{max}	11.41	CT^{max}	0.84	3,174.58	0.12	**1,009.34**
	9	9.12	CT^{max}	6.58	CT^{max}	0.58	2,141.78	0.62	**763.14**
	10	18.71	CT^{max}	12.54	CT^{max}	0.46	3,374.21	0.44	**1,143.81**
Average		10.37	3,257.77	6.93	3,237.78	0.61	1,897.52	0.45	**718.74**
Large	1	22.88	CT^{max}	17.54	CT^{max}	1.89	CT^{max}	0.63	**1,244.35**
	2	OM	-	OM	-	2.24	CT^{max}	0.41	**1,465.38**
	3	OM	-	OM	-	3.14	CT^{max}	0.83	**1,301.41**
	4	OM	-	OM	-	5.73	CT^{max}	0.67	**2,354.25**
	5	OM	-	OM	-	2.12	CT^{max}	0.29	**1,423.12**
	6	OM	-	OM	-	8.67	CT^{max}	**1.09**	CT^{max}
	7	OM	-	OM	-	3.54	CT^{max}	0.38	**1,478.63**
	8	OM	-	OM	-	15.96	CT^{max}	**1.27**	CT^{max}
	9	OM	-	OM	-	4.63	CT^{max}	0.89	**1,396.54**
	10	OM	-	OM	-	18.54	CT^{max}	**1.64**	CT^{max}
Average		22.88	CT^{max}	17.54	CT^{max}	6.65	CT^{max}	0.81	**2,146.37**
Total average		6.14	1,732.92	4.52	1,721.07	2.53	1,840.04	0.51	**962.09**

CT^{max} stands for maximum computational time, i.e., 3600(s).
OM stands for out of memory.

A hypothesis test is applied to compare the median gap generated by **[SAA]** with that by **[SAA-VI]**. The result of implementing the Wilcox signed-rank test for $H_0 : \mu_d = 0$ vs. $H_a : \mu_d \neq 0$ indicates that there is a statistically significant difference between the performances of the two aforementioned solution approaches ($P_{value} < 0.05$), where μ_d represents the difference between the gap generated by **[SAA]** and **[SAA-VI]**. Thus, the median gap generated by **[SAA-VI]** is significantly less from the median gap generated by **[SAA]**, endorsing the fact that **[SAA-VI]** is superior to **[SAA]**.

3.4.3 Experimental Results

How to best utilize power resources during each time period of a day determines energy network design. For a given set of assumptions, a sensitivity analysis is performed to determine how different values of demand variability, power transaction limit, power grid disruption, and the renewable resource size impact overall energy network cost.

All sensitivity analyses are performed with respect to a real life case study developed for San Francisco (base case study). Figure 3.5(a) and 3.5(b) show the average utilization of the various power sources used to satisfy electricity demand of a commercial building and EV charging station, respectively, while Figure 3.5(c) shows the number of batteries in each of the various states of swapped, charged, charging, and discharging.

Figures 3.5(a) and 3.5(b) clearly supports that the electricity demand of commercial buildings and EV charging stations is primarily satisfied through the PG during the period of 5:00 P.M. to 8:00 A.M.$^+$ (almost at the end of peak hours, whole off-peak hours, and at the beginning of the first sub-peak hours). This is due to the low electricity transac-

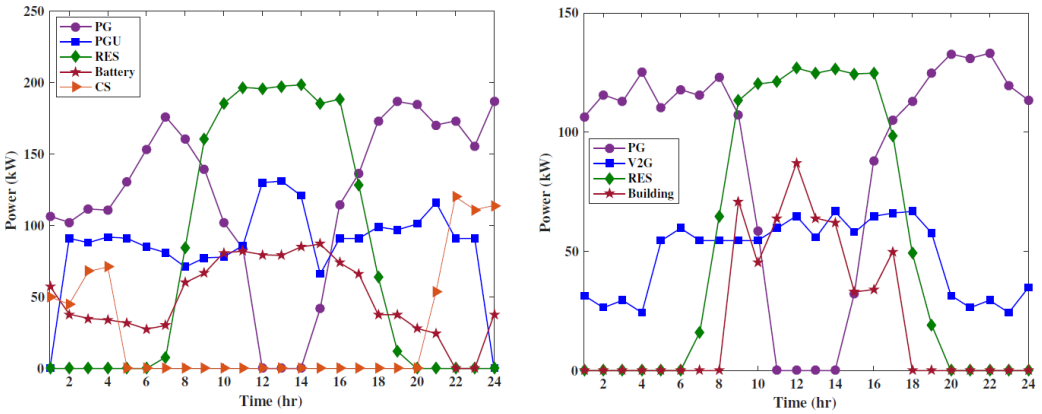

(a) Commercial building

(b) EV charging station

(c) Swapping batteries at EV charging station

Figure 3.5: Average resource power utilization in a typical day for a building and charging station in the base case study

tion price during this period. In addition, electricity flow to commercial buildings and EV charging stations from the PG reaches its minimum, $G^{+}_{it\omega} \simeq 0$ and $H^{+}_{it\omega} \simeq 0$, in the period of 11:00 A.M. to 2:00 P.M. due to the high electricity transaction price during these times. Furthermore, other power sources, particularly RES, have a significant impact on the reducing the demand on the PG during the mid-day time period and, consequently, reducing overall network cost. It is worth noting that a flow of surplus electricity between EV charging stations and commercial buildings shifts electricity demand with buildings providing energy to charging stations during peak hours with the reverse occurring during off-peak hours. Figure 3.5(c) supports that more batteries are charged and stored in the middle time periods at EV charging stations. Also, the electricity stored in the batteries at a station is discharged to the PG after fulfilling the electricity demand at the station. In the following sections, the impact of critical parameters on the energy network cost is determined.

3.4.3.1 Impact of Demand Variability

We first investigate the impact of *demand variability* on utilization of diversified power resources and, consequently, energy network cost. Let $\overline{d}_{bt}$ and σ^2_{bt} be the *mean* and *variance* of demand related to commercial building b at time period t, respectively. Three different demand variation levels are considered: low ($\sigma^2_{bt} = 5\%\overline{d}_{bt}$), medium ($\sigma^2_{bt} = 15\%\overline{d}_{bt}$ - set as base case), and high ($\sigma^2_{bt} = 50\%\overline{d}_{bt}$). Let $\overline{\delta}_t$ and σ^2_b be the *mean* and *variance* of the percentage of charged electric vehicles at time period t, respectively. Likewise, three different variation levels are generated: low ($\sigma^2_t = 5\%\overline{\delta}_t$), medium ($\sigma^2_t = 15\%\overline{\delta}_t$ set as base case), and high ($\sigma^2_t = 50\%\overline{\delta}_t$). We then implement Monte Carlo simulation tech-

niques to generate the scenarios for those different variation levels. Figures 3.6a and 3.6b represent electricity flow to the PG from commercial buildings and EV charging stations, respectively, at low, medium (base case study), and high demand variation levels.

As shown in Figure 3.6a, as demand variability is reduced, electricity flow from a commercial building to the PG increases. The reason lies in the fact that demand fluctuations in electricity and thermal energy are controlled via a commercial grade battery system, and the TES, respectively. In other words, a high level of demand variation leads to more storage in the commercial-grade battery and TES, along with less electricity flow to the PG and associated EV charging stations. Similarly, low demand variation level leads to less storage in the buffers and more electricity flow to the PG and associated EV charging stations. This indicates that demand variation has a significant impact on electricity and thermal energy management in a building.

Likewise, high demand fluctuation leads to more electricity storage as stored batteries at a charging station, which is shown by Figure 3.6b. In this regard, Figures 3.7a and 3.7b represent the number of charging and discharging batteries at each demand variation level, respectively. As shown in Figure 3.7, the number of charging batteries has a direct relationship with demand variation levels, while the number of discharged batteries has an indirect relationship with demand variation levels. The reason lies in the fact that the number of charged, discharged, exchanged batteries and, consequently, the number of stored batteries at an EV charging station changes based on the variation in the percentage of electric vehicles that need to be charged, i.e., demand fluctuation. Therefore, a high level of demand variation leads to less electricity flow to the PG and related commercial buildings and more

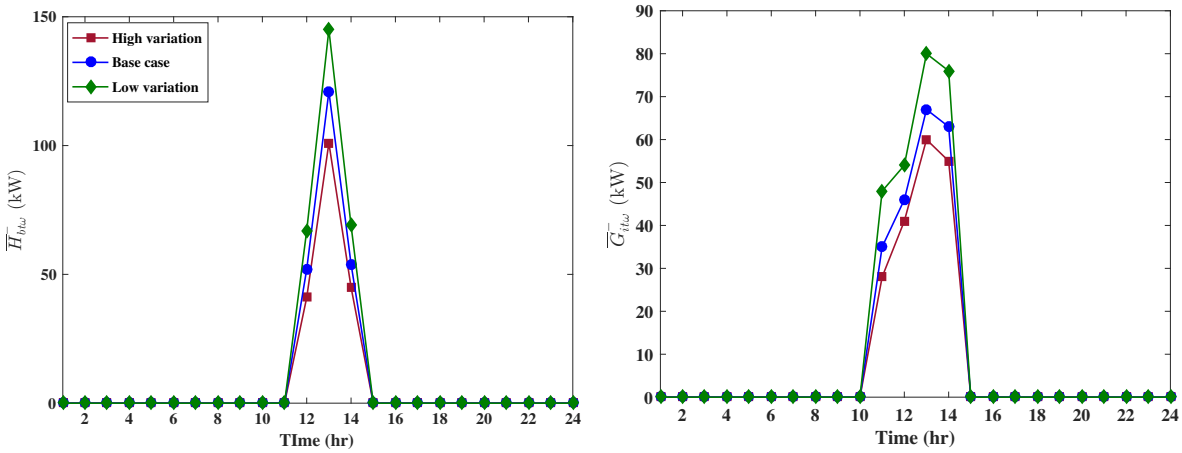

(a) Commercial building to PG

(b) EV charging station to PG

Figure 3.6: Impact of buildings and charging stations demand variability on electricity flow to the PG

stored batteries at an EV charging station, while low demand variation leads to more electricity flow to the PG and related commercial buildings and less inventory of fully-charged batteries.

In summary, the level of demand variation has a direct relationship with the electricity and thermal energy that are stored in the buffers of the commercial buildings and the number of fully-charged batteries stored at EV charging stations. In addition, the level of demand variation has an indirect relationship with power transaction between commercial buildings and EV charging stations, as well as electricity flow to the PG.

3.4.3.2 Impact of Power Transaction Limit

This set of experiments studies the impact of *power transaction*, between related commercial buildings and EV charging stations, i.e., χ^{bc}_{bit} and χ^{cb}_{ibt}, has on overall energy net-

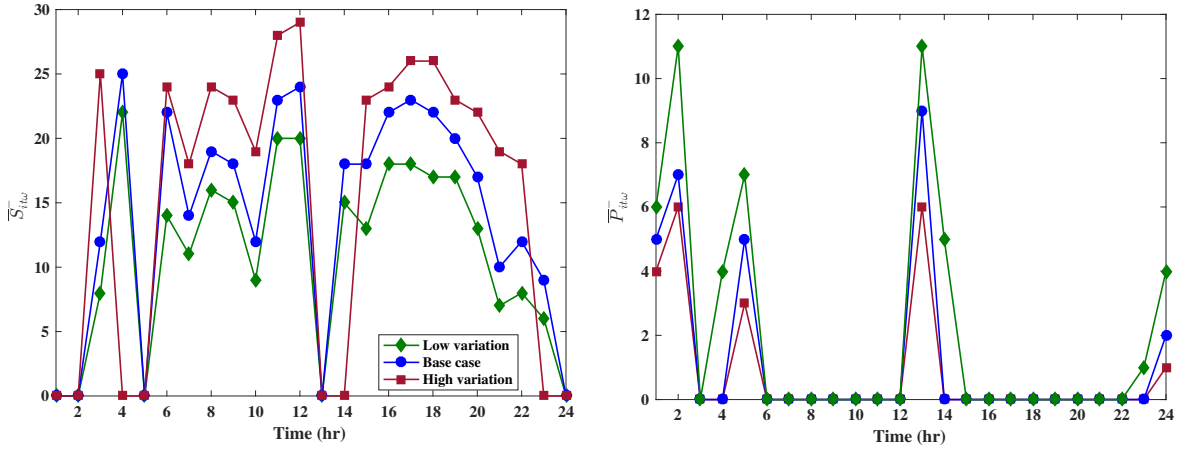

(a) Charging electric vehicle batteries

(b) Discharging electric vehicle batteries

Figure 3.7: Impact of charging station demand variability on charging and discharging electric vehicle batteries

work cost. To study this effect, the maximum amount of power transferred is increased and decreased by both 10% and 20%. Table 3.3 shows the operation costs of commercial buildings, EV charging stations, and overall network costs based on changes in the power transaction limit. As shown in Table 3.3, it is clear that there is an indirect relationship between the power transaction limit and network cost. In other words, the overall energy network cost is reduced more by increasing the upper bound of power transaction.

To realize more the impact of power transaction between related commercial buildings and EV charging stations on the overall energy network cost, power transaction is disregarded by setting $\chi^{bc}_{bit} = 0$ & $\chi^{cb}_{ibt} = 0 \ \ \forall i \in \mathcal{I}, b \in \mathcal{B}, t \in \mathcal{T}$. Regarding power transaction, i.e., $\chi^{bc}_{bit} > 0$ & $\chi^{cb}_{ibt} > 0$, network cost is decreased by 14.24% due to surplus electricity flow between the commercial buildings and EV charging stations and, consequently, elec-

tricity demand is shifted from peak hours to off-peak hours. Overall, we observe that the power transaction limit has a considerable effect on the overall energy network cost.

Table 3.3: System performance under different amount of electricity transaction between building and CS

Percent change in $\chi^{bc}_{bit}/\chi^{cb}_{ibt}$	Costs			Cost saving (%)
	Buildings	Charging stations	Overall network costs	
-20%	15,813.12	1,095.73	16,908.85	-6.88
-10%	15,326.35	1,023.51	16,349.86	-3.35
0%(Base case)	14,878.49	941.54	15,820.03	0.00
10%	14,464.63	873.78	15,338.41	3.04
20%	13,941.09	816.21	14,757.30	6.72
No power transaction	16,896.68	1,176.43	18,073.11	-14.24

3.4.3.3 Impact of Power Grid disruption

Transmission line failure might occur due to excessive power flow between the PG and a commercial building or EV charging station, or by a man-made/natural disaster. While the occurrence of a disaster is not under our control, excess power flow can be controlled by limiting power flow over consecutive time periods. A power shortage might occur in an energy network due to a disruption and, consequently, a penalty cost is imposed on the network due to either there being unmet demand or demand satisfied by an external source(s). Since the PG has an important effect on the utilization of the different power resources, the impact of a *power grid disruption* on energy network cost is investigated. A commercial building or EV charging station is selected randomly and its connection with the PG is terminated for several consecutive time periods. The disruption time period is set to the last three peak hours, i.e., 5:00 P.M. to 8:00 P.M., when more power flow exists on the transmission lines of the PG.

Figure 3.8 shows the utilization of power resources in relation to a particular commercial building, under both normal (Figure 3.8a) and disruption 3.8b) conditions. Figure 3.8b demonstrates that part of power shortage created by a power grid disruption (during the last three peak hours) is satisfied by other power resources including the PGU and commercial-grid battery with respect to their capacities. There is no significant change in the RES utilization since it is utilized near to its maximum capacity under normal conditions. In addition, there is no power transaction to the commercial building from the EV charging stations during the aforementioned peak hours. Therefore, the remaining power shortage is satisfied by one or more external resources, which is considered a penalty cost. In addition, there are no changes in RES use after the disruption since it is utilized based on its maximum capacity.

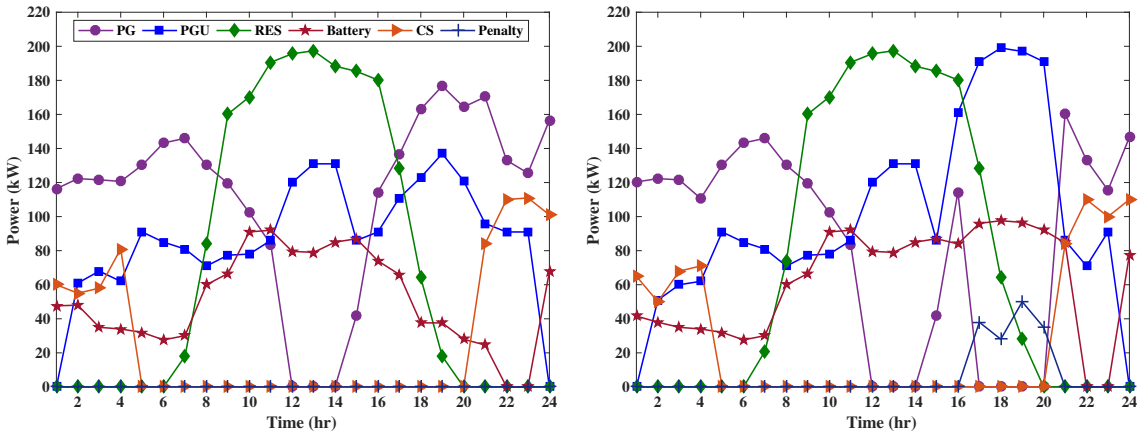

(a) Normal condition

(b) Disruption condition

Figure 3.8: Utilization of a commercial building's resources in a typical day under normal and disruption conditions

Likewise, Figure 3.9 shows the utilization of power resources in relation to a particular EV charging station, under both normal and disruption conditions. Figure 3.9b demonstrates that part of the power shortage created by a power grid disruption (during the last three peak hours) is satisfied by V2G and commercial buildings sources with respect to their capacities. There is not much change in RES utilization since it is already utilized near to its maximum capacity under normal conditions. Thus, the remaining power shortage is satisfied by one or more external resources, which is considered a penalty cost. Some demands are satisfied by swapping batteries in the range [154.2kW, 450.3kW]. Since the upper bound of the electricity range of swapping batteries is 450.3kW, it is not shown in Figure 3.9. It is worth noting that the overall energy network cost is increased by disruption, particularly due to penalty cost.

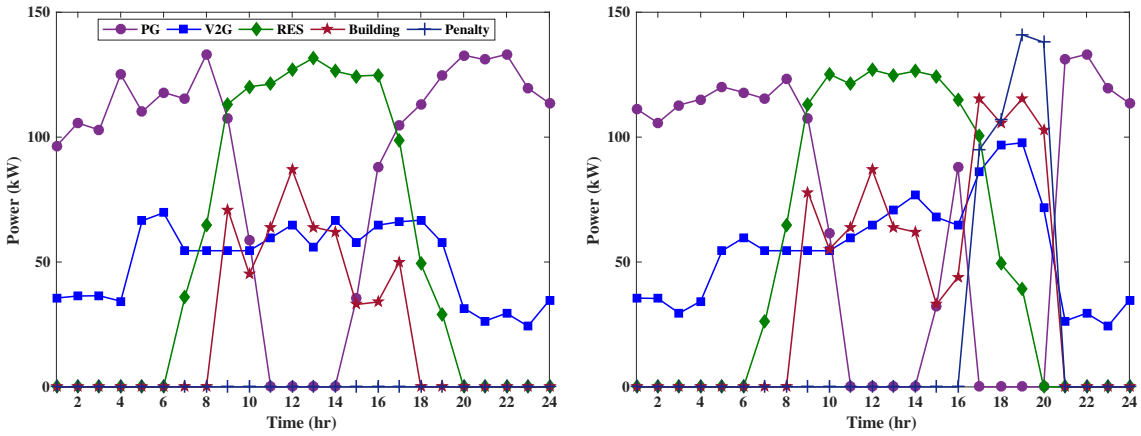

(a) Normal condition

(b) Disruption consition

Figure 3.9: Utilization of a EV charging station resources in a typical day under normal and disruption conditions

3.4.3.4 Impact of the Renewable Resource Size

Depending on the level of demand of the commercial buildings and EV charging stations, the RES size is determined. The availability and amount of energy that can be drawn from a RES, μ_t, can vary during a day. The amount of electricity generated by the RES is dependent on its size within commercial building b, a_b, or within EV charging station i, a_i. Since RES size has an important effect on the utilization of other resources, particularly during the first sup-peak hours and peak hours, the impact of the r*renewable resource size* on the overall energy network cost is investigated.

Since the RES size has an effect on power transaction between commercial buildings and EV charging stations, as well as electricity flow to the PG, its effect is investigated at four different levels of RES size in addition to the base case. These settings change the RES size by $\pm 25\%$ and $\pm 50\%$. As shown in Table 3.4, it is clear that there is an indirect relationship between RES size and network cost with the overall energy network cost being reduced as RES size increases. In addition, the impact of the RES size on network cost is greater with respect to power transaction. Therefore, RES size has a considerable effect on the energy network design (power transaction and electricity flow to the PG) and, consequently, the overall energy network cost. This being the case, when power transaction is considered, network cost is reduced by 23.72% when the RES size is increased by 50%.

3.5 Conclusion

This paper proposes a novel collaborative energy sharing optimization framework, which considers two-way electricity flow among the PG, commercial buildings, and EV

Table 3.4: System performance under different size of RES for building and CS

Percent change in a_b/a_i	Power Transaction (PT)						CS^1 (%)	CS^2 (%)	CS^3 (%)
	Operation cost with PT			Operation cost without PT					
	Building	CS	Total	Building	CS	Total			
-50%	16,954.36	1,215.73	18,170.09	17,865.13	1,347.89	19,213.02	-14.85	-6.31	5.74
-25%	15,581.74	1,135.38	16,717.12	17,123.44	1,203.57	18,327.01	-5.67	-1.40	9.63
0% (Base case)	14,878.49	941.54	15,820.03	16,896.68	1,176.43	18,073.11	0.00	0.00	14.24
25%	14,123.47	836.56	14,960.03	16,763.84	1,104.51	17,868.35	5.44	1.13	19.44
50%	13,563.24	781.68	14,344.92	16,684.58	1,062.71	17,747.29	9.32	1.80	23.72

[1]Cost savings obtained comparing the altered RES size to its base case when PT is considered
[2]Cost savings obtained comparing the altered RES size to its base case when there is no PT
[3]Cost savings obtained at a given level comparing the use of PT against and not using of PT

charging stations. A two-stage stochastic MILP model **[BEV]** is formulated to determine the key operational factors with the aim of network cost minimization under energy demand uncertainty (thermal and electric energy). The operational decisions of buildings include hourly power management decisions consisting of defining the startup/shutdown time of the PGU and boiler, RES usage, charging/discharging state of a commercial-grade battery and the TES, amount of electricity flow from/to the PG and related charging stations, and the amount of electricity and thermal energy charged, discharged, stored, and transmitted from any of the components of the system. Likewise, the hourly operational decisions of the charging stations include electricity flow from/to the PG and related buildings, RES usage, V2G power usage, and the number of batteries charged, discharged, swapped, and stored. The model is computationally very challenging depending on the number of buildings, charging stations, time periods, and potential number of scenarios defined by a decision maker. To alleviate these challenges and to solve industry-size instances, we develop an enhanced Sample Average Approximation (SAA) method. The performance of the SAA method is improved with respect to generated valid inequalities. Computational results indicate that the enhanced SAA method is capable of producing con-

sistently high-quality solutions to realistic large-size problem instances within reasonable computational times.

Sensitivity analysis performed on a case study based on the road network in San Francisco provides insightful results about the impact of demand variability, power transaction limit, power grid disruption, and renewable resource size on the overall energy network cost and design. In addition, computational experiments reveal numerous managerial insights for managers to make operational decisions at the optimum network cost. The following outcomes of our data-driven analysis can help decision makers to develop a sustainable power management decision system related to commercial buildings and road transportation sectors. Demand variability can be controlled by the buffer capacity. A buffer with larger capacity is capable of reducing the amount of fluctuation on electricity demand and electricity flow on a network entity. In addition, the overall energy network cost is reduced more by increasing the permissible amount of power transferred between related buildings and charging stations due to electricity demand shifting from peak hours to off-peak hours. Also, availability of larger-scale RES has a considerable effect on power transaction and electricity flow to the PG and, consequently, reduces the overall energy network cost and design. Finally, the amount of power flow from the PG to a building or charging station should be controlled so that PG utilization does not exceed a pre-specified upper bound for electricity flow over several consecutive time periods. In summary, overall energy network cost is considerably affected by any change in the permissible power transaction between buildings and charging stations, the buffer capacity of buildings, and the RES size.

There are several possible extensions of this research. A first would be to include consideration of the impact of EV congestion at charging stations on a driver charging decision. Apart from this, a more realistic approach can track drivers' behaviors in relation to the congestion at EV charging stations. Prevention and disruption models can be surveyed with respect to limited power grid utilization. Furthermore, it would be interesting to consider the stochastic nature of other parameters in the model such as the RES availability, the SoC of commercial-grade batteries and the TES, and the SoC of EV batteries.

CHAPTER IV

DESIGNING A RELIABLE ELECTRIC VEHICLE CHARGING STATION EXPANSION UNDER UNCERTAINTY

4.1 Introduction

As a result of the growing concern over global warming, weather changes, and dependence on fossil fuels, electric vehicles (EV) have gained tremendous attention all over the world in the last few decades. In it's continuation, we observe a tremendous EV sales increase on U.S. market in recent years i.e., approximately, 700% sales increase from 2011 to 2016 [55] where nearly 82% sales increase only in December, 2016 over the same time period in 2015 [35]. Additionally, with a number of incentive policies proposed by both federal and state government, it is anticipated that there will be approximately 2.7 million of EVs on the U.S. road by 2020. Furthermore, it is expected that EV market share will hit 10% by 2025 [56].

However, the large EV penetration will bring both challenges and opportunities for the power grid (PG). Running these automobiles on electricity instead of gasoline shifts energy requirements from gas pumps to the power grid. For instance, recent report reveal that the high penetration of EVs have a significant impact on the existing power network systems [72]. With another study by Qian et al. [98] state that a 10% market penetration of EVs would increase the daily peak electricity demand up to 17.9%, whereas 20% level of EV

penetration would lead to a 35.8% increase in peak electricity load. The Excessive power flow through a transmission line leads to the line overheating and, consequently, cause the transmission line failure. Thus, if the charging is unmanaged for such a large number of EVs, the power grid can be affected negatively. These facts mandates an urgent need to efficiently design and manage EV charging station to support large-scale deployment of EVs and achieve efficient grid operation and true environmental protection.

The U.S. Energy Information Administration (EIA) reports that the power demand varies significantly throughout the day [118] and from 10:0 A.M. to 8:0 P.M. are considered as peak hours of a regular day. The EIA further reports that replacing the internal-combustion engine vehicles with EVs will add approximately 1,198 TWh of electricity demand to the grid [119]. This number represents a nearly 29% increase in annual electricity demand in the United States. With more EVs in the market, their charging on different time period of the day can add a large load in the electricity grid. The excessive electricity flow causes line over heating, which in extreme case cause power transmission line failure. Thus, if the charging stations are not expanded and managed properly, the resultant excessive load can bring serious disruption effect to the power grid system. To hedge against this projected growth, power companies may need to upgrade electric distribution systems, increase capacities, integrate other forms of energies (e.g., renewable energy sources (RES),vehicle-to-grid (V2G) system), introduce dynamic segment-wise pricing options, and encourage off-peak charging so that the growing loads do not exacerbate peak demand.

To alleviate of excessive load on the PG one possible way is to integrate renewable energy sources (RES) with vehicle-to-grid (V2G) sources while planning for optimal charg-

ing schedules for EVs. We observe a stream of research that address the integration of renewable energy with V2G sources while planning for charging schedules of the electric vehicles. For instance, Liu et al. [68] study how the smart charging patterns of electric vehicles affect the power system scheduling while considering coordination of wind energy, thermal units, and V2G sources. With another study by Ortega et al. [88] and Haddadian et al. [46] investigate how the integration of V2G with power systems can be made to achieve better efficiency and security. Results show that this coordination will allow to operate efficiently under the existing power infrastructure. Likewise, Fathabadi [33] studies the different effects of incorporating V2G and renewable energy with a power network. The goal is to identify the best coordination that is effective in sustaining the system while reducing the cost and loss of power production. Another study by He et al. [48] present a global and a local scheduling model to decide on charging and discharging decisions for electric vehicles with an aim of minimizing the overall system cost. Haddadian et al. [45] consider electric vehicles as distributed storage devices and study their coordination with renewable energy to make the power supply more stable. The authors propose a mixed-integer programming (MIP) model to optimize the hourly scheduling of electricity where several key components of the model such as hourly load, energy, and outages are generated using a Monte-Carlo simulation. Guo et al. [44] plan for the operations of electric vehicle parking decks considering the availability of renewable energy sources. The goal is to develop a tool to decide on hourly parking fees and charging prices based upon the forecast values of the available renewable energy. Zhang et al. [134] introduce a scheduling model to minimize the mean waiting time for charging the electric vehicles at the charging

stations equipped with multiple plug outlets and availability of renewable energy sources. Electric vehicle arrival, fluctuation in grid power prices, and level of production of renewable energy are modeled using a markov decision process. Hong et al. [51] and Jin et al. [59] propose a stochastic optimization model model to determine charging strategies for electric vehicles by taking into account overnight charging, peak-load discharging, and availability of renewable energy. Although these studies have practical implications, they attempt to manage EV charging activities for a single charging station while no attention is given for charging station expansion decisions.

Another stream of research is dedicated to integration of microgrid system in electric vehicle charging to pacify the electricity load on power grid. For example, Beer et al. [16] analyze the possibility of extending the life-cycle of EV batteries to a secondary, stationary application. The important finding from the study that battery usage can be optimized by installing used battery packs in buildings' micro-grids. Likewise, Momber et al. [80] investigate the EVs' integration into a building's energy management system. The authors model the relation by the distributed energy resources customer adoption model (DER-CAM), which can able to find optimal equipment combinations for meeting microgrid requirements at minimum cost and carbon footprint. With another study by Kriett and Salani [64] consider a generic mixed integer linear programming model to nd the minimum cost operating schedule of both electrical and thermal supply and demand in a residential microgrid system. Along in the same line, Kavousi-Fard and Khodaei [61] investigate the viability of the re-configurable microgrids (RMGs) in facilitating the integration of electric vehicles (EVs). The goal of the proposed optimal scheduling problem is to minimize the

total cost of power supply by distributed energy resources (DERs) and upstream network energy exchange, battery degradation cost in PEVs, cost of switching during the reconfiguration, and expected customer interruption costs as a reliability index. Deilami et al. [29] in another study, develop a novel load management solution for coordinating the charging of multiple EVs in a smart grid system. The authors employ a real-time smart load management algorithm based on maximum sensitivities selection optimizations to improve smart grid performance with high penetration of EVs. Honarmand et al. [50] propose a new energy resources scheduling for a microgrid consisting of renewable generation and EVs. The authors shows that the intelligent scheduling and control of charging and discharging of EVs introduces a great opportunity for evolving a sustainable integration of electrical and transportation system. Note that most of the existing studies along this line attempt to optimize EV charging (e.g., hourly charging, discharging, storing) and microgird operations decisions within the facility while little or no attention is given to the design and expansions of charging stations.

Another theme found in the literature focuses on locating refueling stations to maximize traffic flow. For instacne, some stuides attempt to extend the single time period flow-refueling location model (FRLM), introduced by Kuby and Lim [65], to multi-time period expansion models. Chung and Kwon [23] extend the FRLM to a multi-period charging station location model where the comparison between the single-time and multi-time period expansion model are made by constructing a case study using real traffic flow data obtained from the Korean Expressway network. Zhang et al. [132] further extend FRLM to determine an expansion plan (both location and capacity expansion) for the charging

stations and charging modules over a pre-defined planning horizon. Another study by Li et al. [67] propose a dynamic multi-period, multi-path refueling-location model that captures the dynamics of topological structures of a network. The authors formulate the model as a mixed-integer linear program which is later solved by using a GA approach. The objective of this model is to minimize the total cost of installing new stations and relocating existing stations for the electric vehicles that can be used for intercity trips. Sweda and Klabjan [112] identify the patterns in residential electric vehicle ownership and driving activities by developing an agent-based decision support system to allow strategic deployment of new charging stations. Chen et al. [22] perform regression analysis on parking survey data to predict parking demand variables, local jobs and population densities, trip attributes, and other variables to determine where to locate charging stations in a parking location. Jia et al. [58] optimize the sizing and siting of electric vehicle charging stations and minimize the cost of charging stations. Bouche et al. [12] use trip based origin-destination (OD) data to evaluate the energy consumption of the electric vehicles that is used as an input to optimally locate charging stations. Ge et al. [38] partition the planning area and then evaluate the best location and sizing of charging stations for each partition using a GA approach. The main goal is to minimize the cost of travel for an EV user. Hosseini and MirHassani [52] introduce a two-stage stochastic refueling station location model, where the first-stage locates permanent stations while the second locates portable station. A two-step heuristic algorithm is used to solve the problem, where the first step reduces the size of the problem by solving a relaxed version of the original model while the second step applies a greedy algorithm to locate the charging stations. He et al. [47] use an equilibrium framework

to capture the interactions between electricity prices, traffic flow, and availability of public charging opportunities. The information obtained is used to determine the optimal location of the electric vehicle charging stations. A mathematical program model is presented and solved using an active-set decomposition algorithm. Ip et al. [57] use a clustering technique that compile data points that contain quantified road information of electric vehicle charging demand in an urban setting to inform the location plans for the electric vehicle charging stations. Xi et al. [130] use a simulation-optimization model that determines where to locate electric vehicle chargers and the best combinations of power levels to be used at each location. Bhatti et al. [17] study a two-stage optimal location decision problem, where the demand information is learned over time. A key feature of the model is to provide a solution for whether to actively learn the market through a greater initial investment in the alternative fuel stations network or to deter the commitment since an overly aggressive investment often results in sub-optimal alternative fuel stations' locations. With another study, Arslan and Karasan [7] study the charging station location problem with plug-in hybrid electric vehicles as a generalization of the flow refueling location problem (FRLM). Furthermore, the authors propose a Benders decomposition approach to solve this problem. Recently, Vries and Duijzer [122] prove FRLM as strongly NP-hard, and propose a novel mixed-integer linear programming formulation for the FRLM. The authors also demonstrate how this model can be extended to the case for which the driving range varies during a trip. Though these extensions are practical, the authors only concentrate on charging station expansion decisions and little or almost no attention is paid on how to manage them. However, in reality, both long-term ($e.g.$, location decisions) and short-term

charging station decisions ($e.g.$, hourly management decisions) need to be optimized simultaneously in order to benefit the development of this future sustainable transportation system. Although these studies have some implications, however, they give little attentions to short-term EV charging station operational decisions. Further, they ignore the reliability of power network due to the over flowing of electricity.

After surveying the literature we found that till now no prior studies have investigated the reliability of EV charging station with uncertain power demand and integrated long-term charging station planning decisions with short-term operational decisions in a same decision making framework. We notice from the existing body of literature that there are models that captures either long-term charging station planning decisions or short-term operational charging stations managing decisions. To fill this gap in the literature, we develop and solve a reliable EV charging station planning and managing problem with explicit consideration of random power demand. We model the condition of the line temperature due to the excessive flow of electricity. The contributions of this paer are summarized as follows:

1. We develop a novel reliable two-stage stochastic mixed-integer non-linear programming model that incorporates both long term planning decisions and short-term hourly operational decisions to design and manage reliable electric vehicle charging station decisions under stochastic power demand. The proposed model differs from existing studies in that:

    (a) We consider a reliable two-stage stochastic program where in the first-stage we determine size, type and timing to open charging stations based on stochastic

demand, and in the second-stage we satisfy the charging stations demand and track the operations of demand response with a short-term hourly time resolution.

(b) To lienarized the model, we employ three linearization techniques based on McCormick relaxation techniques (also known as McCormick envelopes).

2. We propose and implement a customized hybrid decomposition solution approach that combines a Sample Average Approximation algorithm with an enhanced Scenario Decomposition Algorithm to solve our proposed optimization model. The enhanced Scenario Decomposition Algorithm incorporate different variants of the rolling horizon heuristic.

3. We apply the proposed model and algorithm to a realistic scale case study based on the road network of Washington, D.C. The outcome of this study provides a number of interesting managerial insights on total system cost and optimal system design. The decision includes optimal reliable EV charging station expansion, number of batteries charged, discharged, stored, vehicle-to-grid, RES, grid power usage decision under stochastic power demand. These results can effectively help decision makers to investigate the impact of hourly demand management capabilities of a charging station. Further, we demonstrate the computational performance of our customized hybrid algorithm relative to its generic version. It is worth mentioning that that algorithm **[SAA**$_{SD/LD}$**]** provides an 44.3% and 57.5% faster solution than algorithms **[SAA**$_{SD}$**]** and **[SAA**$_{basic}$**]**, respectively while dropping the average

optimality gap from 2.33% and 2.05% to 0.66%, respectively. By conducting a comprehensive computational study, we show that the enhanced variant of the hybrid decomposition algorithm is capable of producing high-quality solutions consistently to solve realistic large-size problem instances in a reasonable amount of time.

The remainder of this paper is organized as follows. Section 4.2 presents the two-stage stochastic programming model formulation for optimal sizing and locating of charging station considering power demand uncertainty. The hybrid solution approach to solve our optimization model is introduced in Section 4.3. Section 4.4 presents a series of numerical experiments to draw managerial insights and verify the algorithmic performances. Lastly, Section 4.5 provides conclusions and also briefly discusses future research directions.

4.2 Problem Description and Model Formulation

The electricity supply for electric vehicle charging stations at a transportation network is known as an electricity supply network. The problem description is provided in this section, which is followed by two-stage stochastic mixed-integer nonlinear programming (MINLP) model to solve the research problem optimally. The model determines the design of the electricity supply network in terms of the type, location, and time of established charging stations along with electricity flow from limited resources to established charging stations. The purpose of the model is to minimize the overall electricity supply network cost with respect to network design, which allows decision makers for serving electricity demands in an efficient way. In addition, three linearization techniques are proposed in terms of basic McCromick linearization technique to relax bilinear variables of the model.

4.2.1 Problem Description

The problem addressed in this study considers an electricity supply network including multiple charging stations with different electric supply capacities to satisfy electricity demand under demand uncertainty. In order to make strategic and operational decisions for satisfying uncertain demands, the transportation network is divided into a set of cells $\mathcal{I}$, where each cell can be considered as a potential location to establish a charging station over a set of time periods including a set of hours $\mathcal{H}$ and a set of years $\mathcal{T}$. Charging stations are established at different cells with respect to a set of electric supply capacities $\mathcal{K}$. In this research, two types of charging stations are considered with respect to set $\mathcal{K}$: *type 1* charging stations which include the PG, the RES, and V2G usage as power resources; and *type 2* charging stations which include swappable batteries as the main power resource in addition to power resources available for *type 1* charging stations.

Electricity demand of charging stations are satisfied by limited electricity supplied through three different resources: (i) *conventional power generators*, which are generally located in power stations and send electricity through power grids; (ii) solar power as *renewable energy sources*; and (iii) discharge of electric vehicles into the grid through *vehicle-to-grid* connection capabilities. If the self-supplied electricity of a charging station, i.e., the RES, along with the electricity supplied by the PG and V2G are not sufficient to satisfy electricity demand of the charging station, penalty cost is imposed to the network in relation to unsatisfied demands due to power shortage and/or satisfied demands due to imported power from resources outside of the network. Figure (4.1) demonstrates

the electricity supply network including several network cells and two types of established charging stations along with electric energy flow of different electricity resources.

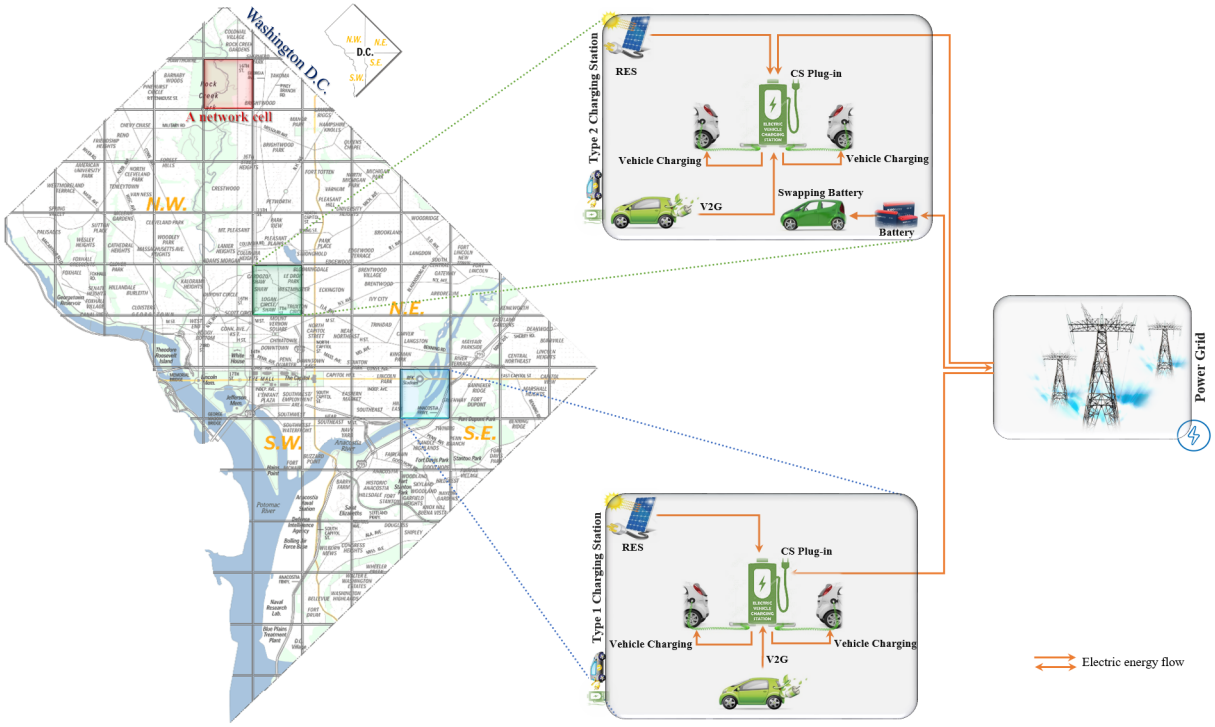

Figure 4.1: Illustration of integration of different electricity supply resources with two types of charging stations established at different network cells

The demand of each cell is modeled as a random variable of which probability distribution might not be known in advance. Accurate prediction, even for small-scale network, is difficult due to the stochastic nature of network along with the uncertainty in available resources. Therefore, a set of scenarios Ω is determined, where each scenario is associated with a positive probability. Electricity demand of each cell is determined in terms of the expected number of electric vehicles traversed through the cell in each time period

and, consequently, the percentage of those that requires to be charged under each scenario. Likewise, expected V2G electricity availability is determined in terms of the percentage of electric vehicles required to be discharged in each time period under each scenario. Since electricity usage cost is dependent on the amount of electricity usage so that it is exponentially increased by electricity usage increment, a pricing mechanism is determined based on a set of segments $\mathcal{R}$ in such a way that each segment is related to a different range of electricity usage with a particular price per unit consumption.

Excessive power flow through a transmission line leads to the line overheating and, consequently, the transmission line failure. To describe this effect, the evolution of the line temperature is monitored based on power flow in the line. Then, the failure of a transmission line is determined based on power flow loading over the line transmission capacity. Thus, a prevention model is proposed to prevent electricity supply network disruption. Regarding strategic and operational decisions, the research problem is to design an electricity supply network over a pre-specified planning horizon and under electricity demand uncertainty. Optimal strategic decisions include long-term electric vehicle charging station expansion decisions consisting of establishment time, location, and type for charging stations in each year. Optimal operational decisions include short-term power management decisions to not only satisfy demands, but also prevent network disruption. Operational decisions determine the number of charged, discharged, exchanged, and stored batteries as well as the amount of V2G, renewable, power grid usage in each hour.

The other assumptions considered for the research problem are summarized as follows:

- annual establishment and development costs of charging stations
- annual dynamic size of RES at each charging station
- annually limited number of available batteries at each charging station
- annually limited number of plug-ins for charging/discharging of batteries at each charging station
- minimum annual demand to establish charging stations
- limited solar radiation and V2G energy
- maximum amount of hourly electricity flow to network cells from PG
- no power transaction among charging stations
- power flow restriction through the transmission lines
- pre-determined equally time periods in terms of hours and years

4.2.2 Model Formulation

Since electricity demand is stochastic, a two-stage stochastic MINLP model is proposed to simultaneously determine yearly strategic decisions and hourly operational decisions through a set of time periods over a pre-specified planning horizon. In the first-stage, an electricity supply network is designed in terms of annual establishment location and type of charging stations at different cells of a transportation network, while hourly electricity flow from power resources is determined with respect to disruption prevention under each scenario in the second-stage of the MINLP model. The first-stage decision variable determines the electricity supply network design in each year, while the second-stage decision variables determine hourly electricity flow as follows:

- electricity flow from PG to charging stations under disruption prevention

- electricity flow from V2G and RES to charging stations
- number of charged, discharged, stored. and exchanged batteries at type 2 charging stations
- power shortage in each charging station

In the following, the sets and indices, subsets, parameters, and decision variables are briefly explained and followed by the mathematical formulation. Parameters are introduced by lowercase and Greek letters, while variables are introduced by uppercase letters. Additionally, the superscript of parameters represent their brief descriptions, while their subscripts represent their indices.

Sets and Indices

$\mathcal{I}$ set of cells, indexed by i

$\mathcal{K}$ set of charging station types, indexed by k

$\mathcal{R}$ set of segments of charging price, indexed by r

Ω set of scenarios, indexed by ω

$\mathcal{H}$ set of hours, indexed by h

$\mathcal{T}$ set of years, indexed by t

Parameters

- ψ_{ikt}: annual establishment and development cost of charging station of type k at cell i in year t
- f_{iht}: electric vehicle flow at cell i in hour h of year t

- λ: average unit power required for charging each electric vehicle (kWh)
- γ: average unit power obtained from discharging each electric vehicle (kWh)
- $\eta_{ht\omega}$: percentage of electric vehicle charged in hour h of year t under scenario ω
- β_{ht}: percentage of electric vehicle discharged in hour h of year t
- c^{+}_{rht}: unit PG electricity cost for segment r of charging price in hour h of year t ($/kWh)
- c^{v2g}_{ht}: unit V2G electricity cost in hour h of year t ($/kWh)
- a^{r}_{it}: RES size of a charging station established at cell i in year t
- η^{r}: RES electricity generation efficiency
- b^{r}_{iht}: solar radiation available at cell i in hour h of year t
- c^{u}_{ht}: unit penalty cost for power shortage in hour h of year t ($/kWh)
- p^{cs}_{kt}: minimum power requirement to establish a charging station of type k in year t
- c^{s}_{ht}: unit storage cost per battery in hour h of year t
- c^{-}_{ht}: unit electricity selling price to PG in hour h of year t ($/kWh)
- q^{in}_{t}: number of plug-ins available for charging batteries in year t
- q^{out}_{t}: number of plug-ins available for discharging batteries in year t
- u_t: maximum number of available batteries at each *type 2* charging station in year t
- w^{a}_{iht}: outside temperature at cell i in hour h of year t
- u^{a}_{iht}: air velocity at cell i in hour h of year t
- t^{d}: duration of time period (hr)
- φ^{max}_{iht}: maximum limit of power line temperature before disruption at cell i in hour h of year t

- g_{iht}^{max}: maximum limit of power line electricity before disruption at cell i in hour h of year t
- g_r: maximum electricity availability in segment r of charging price
- π: percentage of the risk aversion degree
- ν^{etc}: electricity-to-carbon conversion factor
- c^c: carbon emission tax ($/ton)
- a_{iht}^{max}: maximum power available for charging electric vehicles[1] at cell i in hour h of year t
- ρ_ω: probability of scenario ω

In the following, the first- and second-stage decision variables of two-stage stochastic MINLP model are briefly explained.

Decision Variables First-stage Decision Variable

- Y_{ikt}: 1 if a charging station of type k is established at cell i in year t; 0 otherwise

Second-stage Decision variables

- $G_{riht\omega}$: electricity flow from PG to cell i in hour h of year t under segment r and scenario ω
- $E_{riht\omega}$: electricity flow from PG to cell i to charge electric vehicles in hour h of year t under segment r and scenario ω
- $Z_{iht\omega}$: electricity flow from RES to cell i in hour h of year t under scenario ω
- $V_{iht\omega}$: electricity flow from V2G to cell i in hour h of year t under scenario ω

[1]Calculated based on the number of plug-in available and average charging time of electric vehicles

- $R_{iht\omega}$: power shortage at cell i in hour h of year t under scenario ω
- $H_{iht\omega}$: number of full-charged batteries available at cell i in hour h of year t under scenario ω
- $B_{iht\omega}$: number of swapped batteries at cell i in hour h of year t under scenario ω
- $S_{riht\omega}$: number of charging batteries at cell i in hour h of year t under segment r and scenario ω
- $P_{iht\omega}$: number of discharging batteries at cell i in hour h of year t under scenario ω
- $X_{riht\omega}$: 1 if a charging price of a charging station established at cell i in year t is in segment r in hour h under scenario ω; 0 otherwise

Before going through the proposed model, the operational decision in relation to the prevention and control of the transmission line failure is explained. The behavior of customers, i.e., charging stations owners, determines risk aversion π, when exposed to uncertainty, in attempting to lower that uncertainty. It is a trade-off between a situation with an unknown payoff and another situation with a more predictable payoff but possibly lower expected payoff. Transmission lines are assumed to be so thin such that the temperature is the same at all points of their cross-section. A transmission line is considered with a constant area of cross-section ω, perimeter p, thermal conductivity K, electrical conductivity σ, density ρ, and specific heat c. The heat flux across the surface of the line is proportional to the temperature difference between the surface and the surrounding medium (air). It is given by $H(T - T^{'})$, where T and $T^{'}$ denote the surface and surrounding temperatures of a line, respectively, and H signifies the surface conductance. In order to estimate H, it is assumed that the loss of heat across the surface of the line is due to forced convec-

tion. In addition, H depends on the velocity and the nature of the surrounding medium along with the transmission line shape [5]. The surface conductance is represented as $H = 8 \times 10^{-5}(u^a_{iht}/d)^{1/2}\ cal/(cm^2 s\, K)$, where u^a_{iht} and d represent turbulent flow of air velocity and transmission line diameter, respectively.

The power flow fluctuation through transmission lines propagates much faster than any heat flow transient. In addition, the spatial variation in temperature through the line is neglected since the heat source is equally distributed through a line. Therefore, the impact of time evolution in the line temperature in term of the power flowing through the line, i.e., $T_{iht\omega}(t_d, G_{riht\omega})$, is described as follows:

$$T_{iht\omega}(t_d, G_{riht\omega}) = e^{-\nu_{iht} t_d}\Big(\underbrace{T_{i(h-1)t\omega}(G_{ri(h-1)t\omega}) - T_{iht\omega}(G_{riht\omega})}_{\text{Temp. difference between two consecutive periods}}\Big) + T_{iht\omega}(G_{riht\omega})$$

and

$$T_{iht\omega}(G_{riht\omega}) = \frac{\alpha}{\nu_{iht}}\frac{(G_{riht\omega})^2}{V^2} + w^a_{iht}$$

where t_d is time evolution for each time period $h,\ \forall h \in \mathcal{H}$; $G_{riht\omega}$ is the amount of power flowing through the line; and $T_{iht\omega}(G_{riht\omega})$ and $T_{iht\omega}(t_d, G_{riht\omega})$ are the surface temperature of the line in time period h and during time evolution t_d, respectively. The voltage of the line is obtained by $V = G_{riht\omega}/I_{iht}$, while w^a_{iht} is the surrounding temperature of the line. Furthermore, $\nu_{iht} = Hp/(\rho c\omega)$ and $\alpha = 0.239/(\rho c\omega^2\sigma)$. By substituting α, ν_{iht}, and H in $T_{iht\omega}(G_{riht\omega})$, the surface line temperature in time period h is obtained as follows:

$$T_{iht\omega}(G_{riht\omega}) = c^a\frac{(G_{riht\omega})^2}{(u^a_{iht})^{\frac{1}{2}}} + w^a_{iht}$$

where c^a is a constant value as $c^a = (0.239d^{\frac{1}{2}})/(8 \times 10^{-5}\omega\sigma pV^2)$. As a result, the surface line temperature has an indirect relationship with air velocity. Following the same procedure, ν_{iht} is calculated based on air velocity as follows:

$$\nu_{iht} = c^b(u^a_{iht})^{\frac{1}{2}}$$

where c^b is a constant value as $c^b = (8 \times 10^{-5}p)/(\rho c\omega d^{\frac{1}{2}})$. Generally, the surface line temperature during time evolution depends on the surrounding line temperature, power flow through the line, and air velocity in a particular time period. Therefore, the surface line temperature during time evolution is recalculated with the help of $T_{iht\omega}(G_{riht\omega})$ and ν_{iht} which are represented by $G_{riht\omega}$, u^a_{iht}, and w^a_{iht} as follows:

$$\begin{aligned} T_{iht\omega}(t_d, G_{riht\omega}) &= e^{-c^b(u^a_{i(h+1)t})^{\frac{1}{2}}t_d}\Bigg(c^a\Big(\big((u^a_{iht})^{-\frac{1}{2}}(G_{riht\omega})^2\big) - \big((u^a_{i(h+1)t})^{-\frac{1}{2}}(G_{ri(h+1)t\omega})^2\big)\Big) \\ &\quad + \big(w^a_{iht} - w^a_{i(h+1)t}\big)\Bigg) + c^a(u^a_{i(h+1)t})^{-\frac{1}{2}}(G_{ri(h+1)t\omega})^2 + w^a_{i(h+1)t} \end{aligned}$$

where the surface line temperature during a particular time evolution is set as $T_{iht\omega}(t_d, G_{riht\omega}) \leq \varphi^{max}_{iht}$ in order to prevent and control the transmission line failure. It is clear that φ^{max}_{iht} restricts g^{max}_{iht} also. In addition, the maximum limit of power line electricity is not permissible for electricity flow from the PG to a charging station for each two consecutive time periods, since it leads to power disruption. In the following, two-stage stochastic MINLP model refereed as **[NEV]** is presented.

Mathematical Model

The objective function minimizes annual establishment and development costs of established charging stations along with power flow costs through available energy resources to satisfy electricity demand of network cells. The first-stage decisions made prior to realizing any stochastic event (e.g., electricity demand) correspond to the state of establishing and developing charging stations in each time period, while the second-stage decisions include determining electricity flow from the PG, RES, and V2G to established charging stations as well as battery inventory management at established charging stations of type 2. The aim is to minimize the first-stage costs and the expected value of the random second-stage costs across all possible electricity demand scenarios. The objective function of model **[NEV]** is proposed as follows:

$$\textbf{[NEV]}\ \underset{\mathbf{Y}}{Minimize}\ \underbrace{\sum_{i\in\mathcal{I}}\sum_{k\in\mathcal{K}}\sum_{t\in\mathcal{T}}\psi_{ikt}Y_{ikt}}_{\text{Establishment cost}}+\mathbb{E}[Q(\mathbf{Y},\omega)] \tag{4.1}$$

In **[NEV]**, the first-stage objective function represented by the first term of Eq. (4.1) determines the cost associated with annual establishment and development costs of different types of charging stations established on different cells of an electricity supply network. The following constraints (4.2) through (4.4) are related to the first-stage problem.

$$\sum_{k\in\mathcal{K}} Y_{ikt} \leq 1 \qquad \forall i\in\mathcal{I}, t\in\mathcal{T} \tag{4.2}$$

$$Y_{ik(t-1)} \leq Y_{ikt} \qquad \forall i\in\mathcal{I}, k\in\mathcal{K}, t\in\mathcal{T} \tag{4.3}$$

$$Y_{ikt} \in \{0,1\} \qquad \forall i\in\mathcal{I}, k\in\mathcal{K}, t\in\mathcal{T} \tag{4.4}$$

Constraints (4.2) ensure that at most one charging station of all types is established in a given cell of network, while constraints (4.3) indicate that if a charging station is established in a particular year, it remains active for the subsequent years. Constraints (4.4) set the binary restrictions for the first-stage decision variables.

In **[NEV]**, $\mathbb{E}[Q(\mathbf{Y},\omega)] = \sum_{\omega\in\Omega}\rho_\omega Q(\mathbf{Y},\omega)$ and $Q(\mathbf{Y},\omega)$ is the objective function of the following second-stage problem:

$$Q(\mathbf{Y},\omega) = \underset{\mathbf{G,S,V,R,H,P}}{Minimize} \sum_{i\in\mathcal{I}}\sum_{h\in\mathcal{H}}\sum_{t\in\mathcal{T}} \Bigg(\underbrace{\sum_{r\in\mathcal{R}} c^{+}_{rht} G_{rihtw} + c^{v2g}_{ht} V_{ihtw}}_{\text{Electricity flow cost}} + \underbrace{c^{c}\nu^{etc}\sum_{r\in\mathcal{R}} G_{rihtw}}_{\text{Carbon emission cost}} + \underbrace{c^{u}_{ht} R_{ihtw}}_{\text{Power shortage cost}} + \underbrace{c^{s}_{ht} H_{ihtw}}_{\text{Battery storage cost}} - \underbrace{c^{-}_{ht}\gamma P_{ihtw}}_{\text{Battery discharging benefit}} \Bigg) \quad (4.5)$$

In **[NEV]**, the second-stage objective function represented by the second term of Eq. (4.1) determines the expected cost associated with electricity flow, carbon emission, and power shortage at established charging stations of each type along with the expected cost associated with battery storage and the expected benefit of battery discharging at established charging stations of type 2. With respect to charge loading of electric vehicles and batteries, optimal electricity flow is determined from the PG to charging stations in terms of a particular charging price. In addition, electricity flow from the PG imposes carbon emission cost to the model. Restricted capacities of power resources and charging price strategy along with predicting power disruption determine power shortage cost (unsatisfied demands), while battery inventory management determines battery storage cost. Finally, the surplus electricity of type 2 charging stations is sent to the PG in order to reduce op-

erational costs. The following constraints (4.6) through (4.31) related to the second-stage problem determine operational decisions.

$$\sum_{r\in\mathcal{R}} E_{rih t\omega} + Z_{iht\omega} + V_{iht\omega} + \lambda B_{iht\omega} \geq \sum_{k\in\mathcal{K}} p^{cs}_{kt} Y_{ikt} \ \forall i \in \mathcal{I} \quad (4.6)$$
$$h \in \mathcal{H}, t \in \mathcal{T}, \omega \in \Omega$$

$$\Big(\lambda \eta_{ht\omega} f_{iht} - (\sum_{r\in\mathcal{R}} E_{rih t\omega} + Z_{iht\omega} + V_{iht\omega} + \lambda B_{iht\omega})\Big) = R_{iht\omega} \quad \forall i \in \mathcal{I}, \quad (4.7)$$
$$h \in \mathcal{H}, t \in \mathcal{T}, \omega \in \Omega$$

$$max\Big\{ \Big\lfloor \frac{\lambda \eta_{ht\omega} f_{iht} - (a^{max}_{iht} + a^{r}_{it} b^{r}_{iht} \eta^{r} + \gamma \beta_{ht} f_{iht})}{\lambda} \Big\rfloor, 0 \Big\} Y_{i2t} \geq B_{iht\omega} \quad \forall i \in \mathcal{I}, \quad (4.8)$$
$$h \in \mathcal{H}, t \in \mathcal{T}, \omega \in \Omega$$

Constraints (4.6) guarantee to satisfy a set of minimum power requirement to establish charging stations in different time periods. Constraints (4.7) guarantee electricity supply for uncertain electric demand of each charging station where electricity resources include the RES, full-charged batteries, the PG, V2G, and an external resource(s) as power shortage compensation. Constraints (4.8) restrict the number of swapped batteries at type 2 charging station with respect to the difference between electricity demand and electricity supplied by resources. The following constraints (4.9) through (4.18) correspond to battery storage management at type 2 charging stations.

$$H_{i11\omega} = u_1 Y_{i21} \quad \forall i \in \mathcal{I}, \omega \in \Omega \tag{4.9}$$

$$\sum_{r \in \mathcal{R}} S_{ri11\omega} = 0 \quad \forall i \in \mathcal{I}, \omega \in \Omega \tag{4.10}$$

$$\sum_{r \in \mathcal{R}} S_{rih1\omega} \leq u_1 - H_{ih1\omega} \quad \forall i \in \mathcal{I}, h \geq 2, \omega \in \Omega \tag{4.11}$$

$$\sum_{r \in \mathcal{R}} S_{riht\omega} \leq u_t - H_{iht\omega} \quad \forall i \in \mathcal{I}, h \in \mathcal{H}, t \geq 2, \omega \in \Omega \tag{4.12}$$

$$\sum_{r \in \mathcal{R}} S_{riht\omega} \leq q_t^{in} Y_{i2t} \quad \forall i \in \mathcal{I}, h \in \mathcal{H}, t \in \mathcal{T}, \omega \in \Omega \tag{4.13}$$

$$P_{iht\omega} \leq q_t^{out} Y_{i2t} \quad \forall i \in \mathcal{I}, h \in \mathcal{H}, t \in \mathcal{T}, \omega \in \Omega \tag{4.14}$$

$$B_{iht\omega} + P_{iht\omega} \leq H_{iht\omega} \quad \forall i \in \mathcal{I}, h \in \mathcal{H}, t \in \mathcal{T}, \omega \in \Omega \tag{4.15}$$

$$H_{iht\omega} - B_{iht\omega} - P_{iht\omega} + \tag{4.16}$$

$$\sum_{r \in \mathcal{R}} S_{riht\omega} = H_{i(h+1)t\omega} \quad \forall i \in \mathcal{I}, h \in \mathcal{H} \backslash |H|, t \in \mathcal{T}, \omega \in \Omega$$

$$H_{i|H|t\omega} - B_{i|H|t\omega} - P_{i|H|t\omega} + \tag{4.17}$$

$$\sum_{r \in \mathcal{R}} S_{ri|H|t\omega} = H_{i1(t+1)\omega} \quad \forall i \in \mathcal{I}, t \in \mathcal{T} \backslash |T|, \omega \in \Omega$$

At the beginning of the planning horizon, a restricted number of full-charged batteries is considered at type 2 charging stations. In addition, since all available batteries are charged, the number of charging batteries is set to zero. Therefore, constraints (4.9) and (4.10) are added into the model. Constraints (4.11) and (4.12) restrict the number of charging batteries based upon battery availability and inventory. Constraints (4.13) and (4.14) restrict the number of charging and discharging batteries by the number of plug-ins available at each type 2 charging station, respectively. Constraints (4.15) restrict the number of discharging batteries and battery demand to available full-charged batteries. Finally, con-

straints (4.17) and (4.18) determine the number of available full-charged batteries in terms of previous inventory along with the number of charging/discharging batteries and battery demand.

$$\sum_{r\in\mathcal{R}} X_{riht\omega} = \sum_{k\in\mathcal{K}} Y_{ikt} \quad \forall i\in\mathcal{I}, h\in\mathcal{H}, t\in\mathcal{T}, \omega\in\Omega \tag{4.18}$$

$$X_{riht\omega} g_{r-1} \leq G_{riht\omega} \leq X_{riht\omega} g_r \quad \forall r\in\mathcal{R}, i\in\mathcal{I}, h\in\mathcal{H}, t\in\mathcal{T}, \omega\in\Omega \tag{4.19}$$

$$G_{riht\omega} = E_{riht\omega} + \lambda S_{riht\omega} \quad \forall r\in\mathcal{R}, i\in\mathcal{I}, h\in\mathcal{H}, t\in\mathcal{T}, \omega\in\Omega \tag{4.20}$$

Constraints (4.18) consider a segment of charging price at each time period for each charging station and, consequently, constraints (4.19) and (4.20) restrict electricity flow from the PG to each charging station based on selected charging price in relation to charge electric vehicles and/or batteries.

$$\sum_{r\in\mathcal{R}} (G_{riht\omega} + G_{ri(h+1)t\omega}) \leq \sum_{k\in\mathcal{K}} Y_{ikt} \left(g_{iht}^{max} + g_{i(h+1)t}^{max}\right)(1-\pi) \quad \forall i\in\mathcal{I}, h\in\mathcal{H}\backslash|H|, t\in\mathcal{T}, \omega\in\Omega \tag{4.21}$$

$$\sum_{r\in\mathcal{R}} (G_{ri|H|t\omega} + G_{ri1(t+1)\omega}) \leq \sum_{k\in\mathcal{K}} Y_{ikt} \left(g_{i|H|t}^{max} + g_{i1(t+1)}^{max}\right)(1-\pi) \quad \forall i\in\mathcal{I}, t\in\mathcal{T}\backslash|T|, \omega\in\Omega \tag{4.22}$$

Constraints (4.21) indicate that electricity flow from the PG to each charging station is not beyond the maximum limit of power line electricity for each two consecutive time period in order to prevent power disruption. The maximum limit of power line electricity is

dependent on risk aversion degree, i.e., π, of decision makers. Likewise, constraints (4.22) create a connection between the last and first time periods of each of two consecutive years.

$$e^{-c^b\{u^a_{i1t}\}^{\frac{1}{2}}t_d}\Big[-c^a\Big((u^a_{i1t})^{-\frac{1}{2}}\sum_{r\in\mathcal{R}}(G_{ri1t\omega})^2\Big)+\big(w^a_{i0t}-w^a_{i1t}\big)\Big]+ \tag{4.23}$$
$$c^a\{u^a_{i1t}\}^{-\frac{1}{2}}\sum_{r\in\mathcal{R}}(G_{ri1t\omega})^2+w^a_{i1t}\leq\varphi^{max}_{i1t}\forall i\in\mathcal{I},t\in\mathcal{T},\omega\in\Omega$$

$$e^{-c^b\{u^a_{i(h+1)t}\}^{\frac{1}{2}}t_d}\Big[c^a\Big(\big((u^a_{iht})^{-\frac{1}{2}}\sum_{r\in\mathcal{R}}(G_{rihtw})^2\big)-\big((u^a_{i(h+1)t})^{-\frac{1}{2}}\sum_{r\in\mathcal{R}}(G_{ri(h+1)tw})^2\big)\Big) \tag{4.24}$$
$$+\big(w^a_{iht}-w^a_{i(h+1)t}\big)\Big]+c^a\{u^a_{i(h+1)t}\}^{-\frac{1}{2}}\sum_{r\in\mathcal{R}}(G_{ri(h+1)t\omega})^2+w^a_{i(h+1)t}\leq\varphi^{max}_{i(h+1)t}$$
$$\forall i\in\mathcal{I},h\in\mathcal{H}\backslash|H|,t\in\mathcal{T},\omega\in\Omega$$

$$e^{-c^b(u^a_{i1(t+1)})^{\frac{1}{2}}t_d}\Big[c^a\Big(\big((u^a_{i|H|t})^{-\frac{1}{2}}\sum_{r\in\mathcal{R}}(G_{ri|H|t\omega})^2\big)-\big((u^a_{i1(t+1)})^{-\frac{1}{2}}\sum_{r\in\mathcal{R}}(G_{ri1(t+1)\omega})^2\big)\Big) \tag{4.25}$$
$$+\big(w^a_{i|H|t}-w^a_{i1(t+1)}\big)\Big]+c^a(u^a_{i1(t+1)})^{-\frac{1}{2}}\sum_{r\in\mathcal{R}}(G_{ri1(t+1)\omega})^2+w^a_{i1(t+1)}\leq\varphi^{max}_{i1(t+1)}$$
$$\forall i\in\mathcal{I},t\in\mathcal{T}\backslash|T|,\omega\in\Omega$$

Constraints (4.23) through (4.25) restrict the surface line temperature to the maximum limit of power line temperature in order to prevent power disruption during each time period. As mentioned, the current surface line temperature depends on the electricity flow from the PG in relation to the current and previous time periods (G_{rihtw} and $G_{ri(h+1)tw}$), duration of each time period (t_d), outside temperature (w^a_{iht}), and air velocity (u^a_{iht}). Constraints (4.23) and (4.25) control the transmission line failure at the beginning of each year, while constraints (4.24) control it during time periods within each year.

$$V_{iht\omega} \leq \sum_{k\in\mathcal{K}} \gamma\beta_{ht} f_{iht} Y_{ikt} \quad \forall i \in \mathcal{I}, h \in \mathcal{H}, t \in \mathcal{T}, \omega \in \Omega \tag{4.26}$$

$$Z_{iht\omega} \leq \sum_{k\in\mathcal{K}} a^r_{it} b^r_{iht} \eta^r Y_{ikt} \quad \forall i \in \mathcal{I}, h \in \mathcal{H}, t \in \mathcal{T}, \omega \in \Omega \tag{4.27}$$

Constraints (4.26) restrict the availability of V2G electricity flow based on electric vehicles inclined to be discharged at each cell of the network, while constraints (4.27) restrict the RES electricity flow based on RES size and electricity generation efficiency as well as the solar radiation availability.

$$X_{rih t\omega} \in \{0,1\} \quad \forall r \in \mathcal{R}, i \in \mathcal{I}, h \in \mathcal{H}, t \in \mathcal{T}, \omega \in \Omega \tag{4.28}$$

$$B_{iht\omega}, H_{iht\omega}, S_{rih t\omega}, P_{iht\omega} \in Z^+ \quad \forall r \in \mathcal{R}, i \in \mathcal{I}, h \in \mathcal{H}, t \in \mathcal{T}, \omega \in \Omega \tag{4.29}$$

$$G_{rih t\omega}, E_{rih t\omega}, Z_{iht\omega}, \tag{4.30}$$

$$V_{iht\omega}, R_{iht\omega} \geq 0 \quad \forall r \in \mathcal{R}, i \in \mathcal{I}, h \in \mathcal{H}, t \in \mathcal{T}, \omega \in \Omega$$

Constraints (4.28) define the binary restriction for the second-stage decision variables, while constraints (4.29) through (4.31) define standard integrality and non-negativity constraints.

4.2.3 Model Linearization

McCormick Envelopes are a type of convex relaxation used to define the convex envelopes of the bilinear function/term on the rectangular domain. Since solving non convex problems, which lead to multiple local solutions, is a complicated task, the non convex

function is transformed into a convex function by relaxing the parameters on the problem. Relaxing the bounds through a convex relaxation decreases the computational burden. Having a tighter relaxation that is still convex will provide a lower bound that is closer to the solution. The McCormick Envelope is one particular kind of relaxation that guarantees convexity and tight bounds simultanously. McCormick relaxation is a widely used approach to linearize bi-linear terms when the lower bound and an upper bound of each bi-linear variable are known [78].

Based upon McCormick relaxation method, also known as McCormick envelopes, three linearization techniques are used to solve model **[NEV]**. The first technique, referred to **[LEV1]**, is based on the standard McCormick relaxation. The second technique, referred to **[LEV2]**, divides the domain of bi-linear variables into a set of uniform partitions. In addition to uniform partition of the domain of bi-linear variables, a new set of binary variables are introduced into the third technique, referred to **[LEV3]**. Recognizing a new decision variable $\mathbf{Q} := \{Q_{rihto}\}_{r\in\mathcal{R},i\in\mathcal{I},h\in\mathcal{H},t\in\mathcal{T},\omega\in\Omega}$ as $Q_{rihto} = (G_{rihto})^2$, the following bi-linear set is determined:

$$\mathbf{Q} := \Big((Q_{rihto}, G_{rihto}) \in \mathbb{R}_+ : Q_{rihto} = (G_{rihto})^2, g^L_{iht} \leq G_{rihto} \leq g^U_{iht} \forall r \in \mathcal{R}, \quad i \in \mathcal{I}, h \in \mathcal{H}, t \in \mathcal{T}, \omega \in \Omega\Big) \tag{4.31}$$

where g^L_{iht} and g^U_{iht} are, respectively, the lower bound and upper bound of the amount of power flow from the PG to network cell i in time period h of year t, i.e., $G_{rihto} \in [0, g^{max}_{iht}]$, under different demand scenarios and segments of charging prices. Model **[ELV1]** replaces

all squared instances of variable $G_{riht\omega}$, i.e., $(G_{riht\omega})^2$, with a new variable denoted as $Q_{riht\omega}$ in constraints (4.23) through (4.25). In addition, the following constraints are added into model **[ELV1]**:

$$\sum_{r\in\mathcal{R}} Q_{riht\omega} \geq \sum_{r\in\mathcal{R}} 2g^L_{iht}G_{riht\omega} - (g^L_{iht})^2 \quad \forall i\in\mathcal{I}, h\in\mathcal{H}, t\in\mathcal{T}, \omega\in\Omega \tag{4.32}$$

$$\sum_{r\in\mathcal{R}} Q_{riht\omega} \geq \sum_{r\in\mathcal{R}} 2g^U_{iht}G_{riht\omega} - (g^U_{iht})^2 \quad \forall i\in\mathcal{I}, h\in\mathcal{H}, t\in\mathcal{T}, \omega\in\Omega \tag{4.33}$$

$$\sum_{r\in\mathcal{R}} Q_{riht\omega} \leq \sum_{r\in\mathcal{R}} g^L_{iht}G_{riht\omega} + \sum_{r\in\mathcal{R}} g^U_{iht}G_{riht\omega} - g^L_{iht}g^U_{iht} \quad \forall i\in\mathcal{I}, h\in\mathcal{H}, \tag{4.34}$$
$$t\in\mathcal{T}, \omega\in\Omega$$

Based on previous studies [10, 102], the accuracy of the standard McCormick relaxation is enhanced by dividing the domain of bi-linear variables into a set of uniform partitions. Model **[LEV2]** divides the domain of $G_{riht\omega}$ into set $\mathcal{L}$ of uniforms partitions as follows:

$$g^L_{ihtl} = g^L_{iht} + (g^U_{iht} - g^L_{iht})\frac{l-1}{|\mathcal{L}|} \quad \forall i\in\mathcal{I}, h\in\mathcal{H}, t\in\mathcal{T}, l\in\mathcal{L}$$

$$g^U_{ihtl} = g^L_{iht} + (g^U_{iht} - g^L_{iht})\frac{l}{|\mathcal{L}|} \quad \forall i\in\mathcal{I}, h\in\mathcal{H}, t\in\mathcal{T}, l\in\mathcal{L}$$

where g^L_{ihtl} and g^U_{ihtl} are the lower bound and the upper bound of partition l, $\forall l\in\mathcal{L}$, respectively. It is clear that the lower bound and the upper bound of the first and last partitions of $G_{riht\omega}$, respectively, are its original lower bound and the upper bound, i.e., $g^L_{iht1} = 0$ and $g^U_{iht(|\mathcal{L}|)} = g^{max}_{iht}$. Model **[ELV2]** replaces all squared instances of variable $G_{riht\omega}$ with $Q_{riht\omega}$ in constraints (4.23) through (4.25) and, consequently, the following constraints are added into model **[ELV2]**:

$$\sum_{r\in\mathcal{R}} Q_{rihtw} \geq \sum_{r\in\mathcal{R}} g^{L}_{ihtl} G_{rihtw} + \sum_{r\in\mathcal{R}} g^{L}_{iht} G_{rihtw} - g^{L}_{iht} g^{L}_{ihtl} \quad \forall i \in \mathcal{I}, h \in \mathcal{H}, \quad (4.35)$$
$$t \in \mathcal{T}, \omega \in \Omega, l \in \mathcal{L}$$

$$\sum_{r\in\mathcal{R}} Q_{rihtw} \geq \sum_{r\in\mathcal{R}} g^{U}_{ihtl} G_{rihtw} + \sum_{r\in\mathcal{R}} g^{U}_{iht} G_{rihtw} - g^{U}_{iht} g^{U}_{ihtl} \quad \forall i \in \mathcal{I}, h \in \mathcal{H}, \quad (4.36)$$
$$t \in \mathcal{T}, \omega \in \Omega, l \in \mathcal{L}$$

$$\sum_{r\in\mathcal{R}} Q_{rihtw} \leq \sum_{r\in\mathcal{R}} g^{L}_{ihtl} G_{rihtw} + \sum_{r\in\mathcal{R}} g^{U}_{iht} G_{rihtw} - g^{U}_{iht} g^{L}_{ihtl} \quad \forall i \in \mathcal{I}, h \in \mathcal{H}, \quad (4.37)$$
$$t \in \mathcal{T}, \omega \in \Omega, l \in \mathcal{L}$$

$$\sum_{r\in\mathcal{R}} Q_{rihtw} \leq \sum_{r\in\mathcal{R}} g^{U}_{ihtl} G_{rihtw} + \sum_{r\in\mathcal{R}} g^{L}_{iht} G_{rihtw} - g^{L}_{iht} g^{U}_{ihtl} \quad \forall i \in \mathcal{I}, h \in \mathcal{H}, \quad (4.38)$$
$$t \in \mathcal{T}, \omega \in \Omega, l \in \mathcal{L}$$

$$g^{L}_{ihtl} \leq G_{rihtw} \leq g^{U}_{ihtl} \quad \forall r \in \mathcal{R}, i \in \mathcal{I}, h \in \mathcal{H}, t \in \mathcal{T}, \omega \in \Omega, l \in \mathcal{L} \quad (4.39)$$

$$g^{L}_{iht} \leq G_{rihtw} \leq g^{U}_{iht} \quad \forall r \in \mathcal{R}, \in \mathcal{I}, h \in \mathcal{H}, t \in \mathcal{T}, \omega \in \Omega, l \in \mathcal{L} \quad (4.40)$$

To further increase the accuracy of the standard McCormick relaxation, i.e., better bounds and, consequently, lower gap between bounds, a new set of binary variables U_{rihtlw} is introduced into model **[LEV2]**. These binary variables are generated for activating/deactivating generated partitions/search regions. In other words, They guarantee the activation of only one generated serach region at any time. This techniques was first introduced by Castro [19], which is known as piecewise McCormick relaxation. Model **[ELV3]** replaces all basic and squared instances of bi-linear variable G_{rihtw} with new variables denoted as G_{rihtlw} and Q_{rihtw}, respectively, through the whole model. In addition, the following constraints are added into model **[ELV3]**:

$$G_{rihtω} = \sum_{l\in\mathcal{L}} G_{rihtlω} \quad \forall r \in \mathcal{R}, i \in \mathcal{I}, h \in \mathcal{H}, t \in \mathcal{T}, \omega \in \Omega \tag{4.41}$$

$$\sum_{l\in\mathcal{L}} U_{rihtlω} = 1 \quad \forall r \in \mathcal{R}, i \in \mathcal{I}, h \in \mathcal{H}, t \in \mathcal{T}, \omega \in \Omega \tag{4.42}$$

$$U_{rihtlω} g^L_{ihtl} \leq G_{rihtlω} \leq U_{rihtlω} g^U_{ihtl} \forall r \in \mathcal{R}, i \in \mathcal{I}, h \in \mathcal{H}, t \in \mathcal{T}, l \in \mathcal{L}, \omega \in \Omega \tag{4.43}$$

$$U_{rihtlω} g^L_{iht} \leq G_{rihtlω} \leq U_{rihtlω} g^U_{iht} \forall r \in \mathcal{R}, i \in \mathcal{I}, h \in \mathcal{H}, t \in \mathcal{T}, l \in \mathcal{L}, \omega \in \Omega \tag{4.44}$$

$$\sum_{r\in\mathcal{R}} Q_{rihtω} \geq \sum_{r\in\mathcal{R}} \sum_{l\in\mathcal{L}} \left(g^L_{ihtl} G_{rihtlω} + g^L_{iht} G_{rihtlω} - g^L_{ihtl} g^L_{iht} U_{rihtlω} \right) \forall i \in \mathcal{I}, \quad h \in \mathcal{H}, t \in \mathcal{T}, \omega \in \Omega \tag{4.45}$$

$$\sum_{r\in\mathcal{R}} Q_{rihtω} \geq \sum_{r\in\mathcal{R}} \sum_{l\in\mathcal{L}} \left(g^U_{ihtl} G_{rihtlω} + g^U_{iht} G_{rihtlω} - g^U_{ihtl} g^U_{iht} U_{rihtlω} \right) \forall i \in \mathcal{I}, \quad h \in \mathcal{H}, t \in \mathcal{T}, \omega \in \Omega \tag{4.46}$$

$$\sum_{r\in\mathcal{R}} Q_{rihtω} \leq \sum_{r\in\mathcal{R}} \sum_{l\in\mathcal{L}} \left(g^U_{ihtl} G_{rihtlω} + g^L_{iht} G_{rihtlω} - g^U_{ihtl} g^L_{iht} U_{rihtlω} \right) \forall i \in \mathcal{I}, \quad h \in \mathcal{H}, t \in \mathcal{T}, \omega \in \Omega \tag{4.47}$$

$$\sum_{r\in\mathcal{R}} Q_{rihtω} \leq \sum_{r\in\mathcal{R}} \sum_{l\in\mathcal{L}} \left(g^L_{ihtl} G_{rihtlω} + g^U_{iht} G_{rihtlω} - g^L_{ihtl} g^U_{iht} U_{rihtlω} \right) \forall i \in \mathcal{I}, \quad h \in \mathcal{H}, t \in \mathcal{T}, \omega \in \Omega \tag{4.48}$$

$$G_{rihtlω} \geq 0 \qquad \forall r \in \mathcal{R}, i \in \mathcal{I}, h \in \mathcal{H}, t \in \mathcal{T}, \omega \in \Omega, l \in \mathcal{L} \tag{4.49}$$

$$U_{rihtlω} \in \{0, 1\} \qquad \forall r \in \mathcal{R}, i \in \mathcal{I}, h \in \mathcal{H}, t \in \mathcal{T}, \omega \in \Omega, l \in \mathcal{L} \tag{4.50}$$

It is worth noting that there is no method to estimate $|\mathcal{L}|$ as a function of problem complexity. On the other hand, there is a need to provide a fair comparison with commercial solver. The following proposed formula guarantees the minimum of two partitions to take the benefits from piecewise relaxation scheme:

$$|\mathcal{L}| = 1 + \lceil \frac{\alpha}{(v_i + v_j)} \rceil$$

where $\alpha = 1.8E4$. In addition, v_i and v_j indicate the number of non-partitioned and partitioned variables, respectively. Since preliminary investigations indicate that model **[LEV3]** is capable of providing superior relaxation with lower gap compared to model **[LEV1]** and model **[LEV2]**, model **[LEV3]** is utilized to linearize model **[NEV]**.

4.3 Solution Approach

Minimizing uncapacitated facility location problem has been shown to be a strongly NP-Hard problem [27]. The problem addressed in this research can easily be displayed as a reduced version of the problem under the following conditions:

- only one time period is considered, i.e., $|\mathcal{H}| = 1$ and $|\mathcal{T}| = 1$;
- there is only one demand scenario, i.e., $|\Omega| = 1$;
- electricity demand is fulfilled primarily by the PG ($Z_{iht\omega}$ & $V_{iht\omega} = 0 \; \forall i \in \mathcal{I}, h \in \mathcal{H}, t \in \mathcal{T}, \omega \in \Omega$);
- there is no restriction on PG consumption and, consequently, no power shortage;
- charging price is not dependent on power usage in each time period ($|\mathcal{R}| = 1$); and,
- only type 1 charging station is considered, i.e., $|\mathcal{K}| = 1$. Then, no battery activities are considered at charging stations, i.e., $H_{iht\omega}, S_{iht\omega}, P_{iht\omega}$ & $B_{iht\omega} = 0 \; \forall i \in \mathcal{I}, h \in \mathcal{H}, t \in \mathcal{T}, \omega \in \Omega$.

Therefore, it can be concluded that the problem investigated in this research is also strongly NP-hard, and there is no guarantee of solving this problem optimally in polyno-

mial time. This being the case, we focus on developing a Sample Average Approximation (SAA) method enhanced with a Scenario Decomposition (SD) algorithm which is accompanied by a Rolling Horizon (RH) strategy.

4.3.1 Sample Average Approximation

Electricity demand of network cells ($d_{iht\omega}$) differ significantly due to variable electric vehicle flows at different cells on different time periods (f_{iht}) as well as variable percentages of electric vehicles charged under different scenarios on different time periods ($\eta_{ht\omega}$), i.e., $d_{iht\omega} = \eta_{ht\omega} f_{iht}\ \forall i \in \mathcal{I}, h \in \mathcal{H}, t \in \mathcal{T}, \omega \in \Omega$. Therefore, an extremely large number of scenarios is required to investigate variations in demand. Since the research problem is NP-hard, computational time increases significantly when a large set of scenarios is considered. To remedy this computational challenge, the SAA method is proposed so that the expected electricity supply network cost of the stochastic problem is approximated by a corresponding sample average function. The problem is solved by deterministic optimization techniques under the sample average approximation. The procedure is repeated with different samples until a stopping criterion (a pre-determined optimality gap) is satisfied. The SAA method has been implemented extensively to solve large-scale supply chain network flow related problems including [20], [105], [106], [120], and others. Interested readers are reffered to the studies performed by Kleywegt et al. [62] in relation to the proof of convergence properties of SAA and Norkin et al. [86], [85], and Mak et al. [75] in relation to the evaluation of developed statistical inference of SAA (e.g., validation and error analysis, stopping rules).

Electricity demand of network cells, $d_{iht\omega}$, follows a normal distribution for each network cell i at each time period h of year t. The SAA method generates set $\mathcal{N}$ of random samples n with realizations of uncertain parameters ($n \in \mathcal{N}$ and $|\mathcal{N}| < |\Omega|$) to approximate the objective function value of the second-stage problem as follows:

$$\mathbb{E}[Q(\mathbf{Y}, \omega)] := \frac{1}{|\mathcal{N}|} \sum_{n \in \mathcal{N}} Q(\mathbf{Y}, \omega^n)$$

where $Q(\mathbf{Y}, \omega^n)$ is a solution of the second-stage problem for a given value of $\mathbf{Y}$ under scenario ω^n. Problem **[LEV3]** is now approximated by the following SAA problem:

$$Minimize \left\{ \mathrm{Y}_{\mathcal{N}}^{m} = \sum_{i \in \mathcal{I}} \sum_{k \in \mathcal{K}} \sum_{t \in \mathcal{T}} \left(\psi_{ikt} Y_{ikt} \right) + \frac{1}{|\mathcal{N}|} \sum_{n \in \mathcal{N}} Q(\mathbf{Y}, \omega^n) \right\}$$

As the sample size increases, the optimal solution approximated by the above equation converges with probability one to an optimal solution of the original problem **[LEV3]** [62]. By solving the SAA problem within an absolute optimality gap $\delta \geq 0$, the sample size $|\mathcal{N}|$ is estimated to guarantee an ϵ-optimal solution to the true problem with probability at least equal to $(1 - \alpha)$ as follows:

$$|\mathcal{N}| \quad \geq \quad \frac{3\sigma_{max}^2}{(\epsilon - \delta)^2} \left(|\mathcal{I}||\mathcal{K}||\mathcal{T}|(log2) - log\alpha \right)$$

where $\epsilon > \delta$, $\alpha \in (0, 1)$, and σ_{max}^2 is a maximal variance of certain function differences [62]. It is worth noting that choosing sample size $|\mathcal{N}|$ is a trade-off between the solution quality and required computational time. The above equation provides a conservative sample size estimation for practical applications. In each iteration of the SAA method,

valid statistical lower and upper bounds are provided for the original problem **[LEV3]** and the process terminates when the gap between aforementioned bounds falls below a pre-determined threshold value. The following steps briefly summarize the SAA method to solve problem **[LEV3]**.

Step 1: Generate set M of independent percentage scenarios of electric vehicles charged in network cells, each of size $|\mathcal{N}|$, i.e., $\{\eta_{ht\boldsymbol{\omega}_m^1}, \eta_{ht\boldsymbol{\omega}_m^2}, ..., \eta_{ht\boldsymbol{\omega}_m^{|\mathcal{N}|}}\}$, $\forall m \in M, h \in \mathcal{H}, t \in \mathcal{T}$. Then, solve the corresponding SAA for each generated sample consisting of $|\mathcal{N}|$ realizations of independently and identically distributed $(i.i.d.)$ random scenarios. The optimal objective function value and the optimal solution are denoted by $\mathrm{Y}_{\mathcal{N}}^m$ and $\hat{\mathrm{Y}}_M$, respectively. The optimal objective function value of the m^{th} replication is obtained as follows:

$$\mathrm{Y}_{\mathcal{N}}^m = \sum_{i\in\mathcal{I}}\sum_{k\in\mathcal{K}}\sum_{t\in\mathcal{T}}\left(\psi_{ikt}Y_{ikt}\right) + \frac{1}{|\mathcal{N}|}\sum_{n\in N} Q(\mathbf{Y}, \omega^n)$$

Step 2: Compute the average of all optimal objective function values obtained from the SAA problems, $\bar{\mathrm{Y}}_{\mathcal{N}}^M$ as follows:

$$\bar{\mathrm{Y}}_{\mathcal{N}}^M = \frac{1}{|M|}\sum_{m\in M} \mathrm{Y}_{\mathcal{N}}^m$$

where, $\bar{\mathrm{Y}}_{\mathcal{N}}^M$ provides a statistical lower bound on the optimal objective function value for the original problem **[LEV3]** [86]. Since $\mathrm{Y}_{\mathcal{N}}^1, \mathrm{Y}_{\mathcal{N}}^2, ..., \mathrm{Y}_{\mathcal{N}}^M$ generated samples are independent, the corresponding variance of $\bar{\mathrm{Y}}_{\mathcal{N}}^M$, i.e., $\sigma^2_{\bar{\mathrm{Y}}_{\mathcal{N}}^M}$, is given by:

$$\sigma^2_{\bar{\mathtt{Y}}^M_{\mathcal{N}}} = \frac{1}{(|M|-1)(|M|)} \sum_{m \in M} \left(\mathtt{Y}^M_{\mathcal{N}} - \bar{\mathtt{Y}}^M_{\mathcal{N}} \right)^2$$

Step 3: Generate set $\mathcal{N}'$ including larger sample size ($|\mathcal{N}'| \gg |\mathcal{N}|$) to compute the estimated optimal objective solution of the SAA method [62]. This estimator, which is the upper bound of the optimal solution on the generated sample size $|\mathcal{N}'|$, is obtained by one of the solutions of $\hat{\mathtt{Y}}_M$ as follows:

$$\mathtt{Y}_{\mathcal{N}'}(\hat{\mathtt{Y}}_M) = \sum_{i \in \mathcal{I}} \sum_{k \in \mathcal{K}} \sum_{t \in \mathcal{T}} \left(\psi_{ikt} Y_{ikt} \right) + \frac{1}{|\mathcal{N}'|} \sum_{n \in \mathcal{N}'} Q(\mathbf{Y}, \omega^n)$$

In each iteration, the estimator upper bound $\mathtt{Y}_{\mathcal{N}'}(\hat{\mathtt{Y}}_M)$ is updated. The variance of this estimator upper bound is calculated as follows:

$$\sigma^2_{\mathcal{N}'}(\hat{\mathtt{Y}}_M) = \frac{1}{(|\mathcal{N}'-1|)(|\mathcal{N}'|)} \sum_{n \in \mathcal{N}'} \left\{ \sum_{i \in \mathcal{I}} \sum_{k \in \mathcal{K}} \sum_{t \in \mathcal{T}} \left(\psi_{ikt} Y_{ikt} \right) + Q(\hat{\mathtt{Y}}_M, \omega^n) - \mathtt{Y}_{\mathcal{N}'}(\hat{\mathtt{Y}}_M) \right\}^2$$

Step 4: Compute the SAA gap, $Gap_{(\mathcal{N},\mathcal{N}')}$, and the variance of this gap, $\sigma^2_{Gap_{(\mathcal{N},\mathcal{N}')}}$, using the estimators determined in **Steps 2** and **3**.

$$Gap_{(\mathcal{N},\mathcal{N}')}(\tilde{Y}) = \mathtt{Y}_{\mathcal{N}'}(\hat{\mathtt{Y}}_M) - \bar{\mathtt{Y}}^M_{\mathcal{N}}$$

$$\sigma^2_{Gap_{(\mathcal{N},\mathcal{N}')}} = \sigma^2_{\mathcal{N}'}(\hat{\mathtt{Y}}_M) + \sigma^2_{\bar{\mathtt{Y}}^M_{\mathcal{N}}}$$

The confidence interval for the optimality gap is then calculated as follows:

$$\mathtt{Y}_{\mathcal{N}'}(\hat{\mathtt{Y}}_M) - \bar{\mathtt{Y}}^M_{\mathcal{N}} + z_\alpha \left\{ \sigma^2_{\mathcal{N}'}(\hat{\mathtt{Y}}_M) + \sigma^2_{\bar{\mathtt{Y}}^M_{\mathcal{N}}} \right\}^{1/2}$$

with z_α:= $\Phi^{-1}(1-\alpha)$, where $\Phi(z)$ is the cumulative distribution function of the standard normal distribution.

Step 5: Define the best solution among the solutions of $\hat{\Upsilon}_M(\forall m \in M)$ that represents the lowest upper bound $\Upsilon_{\mathcal{N}'}(\hat{\Upsilon}_M)$.

4.3.2 Scenario Decomposition Algorithm

The SAA method requires to solve a two-stage stochastic programming model of $|N|$ scenarios. Depending upon the size of $|\mathcal{I}|$, $|\mathcal{H}|$, and $|\mathcal{T}|$, the problem might still be considered computationally expensive to solve by SAA due to memory limit for solving N scenarios of the problem. Since decomposition-based methods are used to divide a mster problem into smaller and more manageable sub-problems [81, 2], each problem scenario of SAA is solved with the help of a Scenario Decomposition (SD) algorithm accompanied by the Lagrangian Decomposition (LD) scheme on the bases of novel Lagrangian multiplier updating strategy. As the first rigorous algorithmic procedure, the SD algorithm has been successfully applied for various application fields including production planning [131], maintenance and operations sceheduling [13], cargo loading [113], and many mores. In the following, the algorithmic steps of SD accompanied by LD are explained in detail.

The brevity of notation contributed in the **[NEV]** model is represented as follows:

$$z = \underset{\mathbf{x,y}}{Minimize} \left(cx + \sum_{n \in \mathcal{N}} \rho^n (q y^n) \right) \tag{4.51}$$

subject to;

$$Ax \leq b \tag{4.52}$$

$$Ux + Vy^n \leq f^n \qquad \forall n \in \mathcal{N} \tag{4.53}$$

$$y^n \in Y \qquad \forall n \in \mathcal{N} \tag{4.54}$$

$$x \in \{0,1\}^n \tag{4.55}$$

$$y^n \geq 0 \qquad \forall n \in \mathcal{N} \tag{4.56}$$

where *c* and *q* on the objective function are *n*- and *ρ-dimensional* vectors, respectively; *b* and f on the set of constraints (4.52) and (4.53) are *m*- and *q-dimensional* vectors, respectively; and A, U, and V are matrices of *m*×*n*, *q*×*n*, and *q*×*ρ* dimensions, respectively. cx represents the establishment and development costs of charging stations (i.e., first-stage costs), while $\sum_{n\in\mathcal{N}} \rho^n(qy^n)$ represents the hourly operational costs (i.e., second-stage costs). The set of constraints $Ax \leq b$ represents constraints (4.2)-(4.4) in **[NEV]** model, while the set of constraints $Ux + Vy^n \leq f^n$ represents constraints (4.6)-(4.9), (4.13), (4.14), (4.18), (4.21), (4.22), (4.26), and (4.27). Finally, set Y denotes the rest of constraints in **[NEV]** model, i.e., (4.7), (4.10)-(4.12), (4.15)-(4.18), (4.19), (4.20), and (4.23)-(4.25). Constraints (4.55) and (4.56) define binary restrictions and non-negativity constraints domain, respectively.

It is worth noting that this problem has a special block-angular structure which can be decomposed to a mster problem and several independent sub-problems. In relation to multi-stage stochastic optimization problems, one of the most commonly techniques implemented is LD [34, 18], which decomposes the problem based on time-stage. In the

first step of the SD algorithm, a set of copies of the first-stage decision variable, i.e., $\{x^1, x^2, ..., x^{|\mathcal{N}|}\}$ is generated and, consequently, part of the problem is re-written as follows:

$$z = \underset{\mathbf{x,y}}{Minimize} \sum_{n \in \mathcal{N}} \rho^n (cx^n + qy^n) \tag{4.57}$$

subject to;

$$Ax^n \leq b \qquad \forall n \in \mathcal{N} \tag{4.58}$$

$$Ux^n + Vy^n \leq f^n \qquad \forall n \in \mathcal{N} \tag{4.59}$$

$$y^n \in Y \qquad \forall n \in \mathcal{N} \tag{4.60}$$

$$x^n = x^{n+1} \qquad \forall n \in \mathcal{N} \backslash |\mathcal{N}| \tag{4.61}$$

Regarding relaxed constraints (4.61), Lagrangian relaxation is the problem of finding x^n and y^n $\forall n \in \mathcal{N}$ as follows:

$$\textbf{[SDEV]}\ D(\lambda) = \underset{\mathbf{x,y}}{Minimize} \sum_{n \in \mathcal{N}} \rho^n (cx^n + qy^n) + \sum_{n \in \mathcal{N}} \lambda^n \theta^n \tag{4.62}$$

subject to;

$$Ax^n \leq b \qquad \forall n \in \mathcal{N} \tag{4.63}$$

$$U_n x^n + V_n y^n \leq f^n \qquad \forall n \in \mathcal{N} \tag{4.64}$$

$$y^n \in Y \qquad \forall n \in \mathcal{N} \tag{4.65}$$

where $\theta^n = (x^n - x^{n+1})$ $\forall n \in \mathcal{N} \backslash |\mathcal{N}|$ and λ is $(|\mathcal{N}| - 1)$-*dimensional* vector. In addition, Lagrangian dual is to find λ as follows:

$$z_{LD} \quad = \quad \underset{\lambda}{Maximize}\ D(\lambda) \tag{4.66}$$

Based on duality theory, $z \geq z_{LD}$ [42], particularly for non-convex cases, $z > z_{LD}$, which implies the existance of a duality gap [18]. One important property of Lagrangian dual problem (4.66) is that it is a convex non-smooth program, which splits into independent sub-problems based on each scenario n. Each scenario sub-problem is presented as follows:

$$D^n(\lambda) \quad = \quad \underset{\mathbf{x,y}}{Minimize} \sum_{n \in \mathcal{N}} \rho^n(cx^n + qy^n) + h^n(\lambda)x^n \tag{4.67}$$

subject to;

$$Ax^n \quad \leq \quad b \tag{4.68}$$

$$U_n x^n + V_n y^n \quad \leq \quad f^n \tag{4.69}$$

$$y^n \quad \in \quad Y \tag{4.70}$$

where $D(\lambda) = \sum_{n \in \mathcal{N}} D^n(\lambda)$ and $h^n(\lambda)$ is given as follows:

$$h^n(\lambda) = \begin{cases} \lambda^1 & if\ n = 1 \\ -\lambda^{|\mathcal{N}|} & if\ n = |\mathcal{N}| \\ \lambda^n - \lambda^{n-1} & \text{otherwise} \end{cases} \tag{4.71}$$

Although it is computationally convenient to solve, the decomposition framework is not capable of solving the original full-space problem. However, it is widely known that Lagrangian dual represents a relaxation of the original problem for any given set of Lagrange multipliers [42]. This being the case, it is focused on finding better multiplier sets, i.e., multipliers yielding tighter relaxation to the original problem, that approximate the solution of Lagrangian dual to the solution of the full-space problem.

In this study, we use the most common technique called sub-gradient for updating the Lagrangian multipliers. This technique consists of an iterative method in which at a given iteration r, with a current set of Lagrangian multipliers λ^r, a step is taken along the sub-gradient of $D(\lambda)$. Let consider d^r the sub-gradient vector of dimension $(|\Omega| - 1)$ with components given as $d^{nr} = x^{nr} - x^{n+1,r} \quad \forall n \in \mathcal{N} \backslash |\mathcal{N}|$, where $x^{nr} \quad \forall n \in \mathcal{N}$ is the solution of Lagrangian dual given λ^r. The Lagrange multipliers are updated using the sub-gradient information as follows:

$$\lambda^{n,r+1} = \lambda^{nr} + \sigma^r \frac{UB - LB^r}{\sum_{n \in \mathcal{N}} (d^{nr})^2} d^{nr} \quad \forall n \in \mathcal{N} \tag{4.72}$$

where UB is an approximation to the optimal value for z and $LB^r = D(\lambda^r)$. The term $\sigma^r \in (0, 2)$ is used to correct the error in the estimation of the true optimal value. The updating procedure continues until any stopping criteria is met.

One possible feature of the proposed algorithm is the particular heuristic that uses information derived from the solution of the Lagrangean dual problem to derive a feasible solution and a valid upper bound to the full-space problem. It should be noted that it is not

computationally demanding to calculate an upper bound for the full-space problem, once a first-stage solution is available. This is mainly due to the fact that for a fixed first-stage solution, the full-space problem becomes decomposable in scenarios.

The heuristic is based in the following formation rule. Consider a given iteration r. First, we calculate τ^r as follows:

$$\tau^r = \sum_{n \in \mathcal{N}} P^n x^{n,r} - \sum_{n \in \mathcal{N}} P^n (1 - x^{n,r}) \tag{4.73}$$

If $\tau^r > 0$, the investment is selected to compose feasible solution. The time period for the selected investment will be the earliest among the scenarios where the investment was decided. We choose the earliest time period as the one to be implemented based on the observation that the costs incurred by recourse actions are typically larger than the increase in first-stage costs due to investing earlier in a given project. In addition to that, one might notice that the existence of more logistic options allows the system to possibly reach more efficient and less costly logistics, which yields economics of scale.

Since we are using a heuristic to generating solutions based on information that comes from scenarios individually, it might be the case that the solution generated is not feasible for the full-space problem. If this is the case, then we use integer cut to remove this infeasible solution from the search space of the relaxed dual. Let $X_1 = \{j | x_j = 1\}$ and $X_1 = \{j | x_j = 0\}$. Then, we can write the integer cut as:

$$\sum_{j \in \mathcal{X}_0} x_j + \sum_{j \in \mathcal{X}_1} (1 - x_j) \geq 1 \tag{4.74}$$

and add it to every scenario subproblem. We then solve again the Lagrangean relaxation and proceed with algorithm execution. Pseudo-code of the basic Scenario Decomposition Algorithm is provided in **Algorithm 1**.

Algorithm 1: Scenario Decomposition

Input: Termination criteria: $iter_{max}$, $time_{max}$, and ϵ;
Output: Upper bound $z(x^r)$;
Step 1: Initialize: $r \leftarrow 1$, $UB \leftarrow +\infty$, $LB \leftarrow -\infty$, $\lambda^{n,r}$;
$Terminate \leftarrow false$;
while $(Terminate = false)$ **do**
  Step 2: Solve Lagrangian dual problem:
  for *(i=1 to N)* **do**
    Solve each subproblem (4.62)-(4.67);
    Combine subproblem solutions and calculate lower bound $LB^r = \sum_{n \in \mathcal{N}} D^n(\lambda^r)$;
    if $LB^r > LB$) **then**
      $LB = LB^r$;
      Store solution for generating cuts later;
    end
  end
  Step 3: Generate first-stage solution and derive UB:
  Apply the proposed heuristics for generating a first-stage solution x^r;
  Obtain $z(x^r)$ evaluating x^r in (4.51)-(4.56). If x^r is not feasible, add the integer cut (4.74) and return to *Step 2*;
  if $z(x^r) < UB$ **then**
    $UB = z(x^r)$;
  end
  Step 4: Lagrangian multiplier update:
  Update Lagrangean multipliers using (4.47);
  Return to *Step 2*;
  Step 5: Terminate:
  if $UB - LB < \epsilon$ *or any other termination criteria* **then**
    Return x^r, UB ;
    terminate $\leftarrow$ true;
  else
    $r \leftarrow r + 1$;
  end
end
return $z(x^r)$

4.3.3 Rolling Horizon Heuristic Strategy

The SD algorithm demonstrates high-computational capability in solving small- to medium-size problems. However, SD is not capable of providing a reasonable solution

for large-size problems. This motivates us to explore additional enhancement techniques with different variants of Rolling Horizon Heuristic Strategy in order to improve the convergence and stability of the SD algorithm, i.e., solving sub-problems faster.

It is worth noting that **Algorithm 1** requires solving a deterministic and multi-time period problem **[SDEV]** for $|\mathcal{N}|$ times, which is still considered as a challenging problem from a solution standpoint. One way to tackle this problem is to split the planning horizon (i.e., years and hours) into multiple parts and solve those parts sequentially until all are investigated. This being the case, this study implements a *Rolling Horizon* (RH) heuristic that decomposes problem **[SDEV]** into a series of smaller sub-problems comprising a few consecutive hour-year combinations from the overall planning horizon. The algorithm terminates when all hour-year combinations of the planning horizon are investigated. This approach shows efficiency and good converging properties in solving problem instances with relatively a long time horizon. Interested readers are referred to the studies performed by Balasubramanian and Grossman [11], and Kostina et al. [63] to learn more about the RH heuristic.

Three different variants of the RH heuristic are proposed in an attempt to find high-quality solutions from solving problem **[SDEV]** in a reasonable amount of time. The first variant of the RH heuristic, i.e., **[RH1]**, decomposes problem **[SDEV]** on yearly basis, while the second and third variants of the RH heuristic, i.e., **[RH2]** and **[RH3]**, respectively, decompose problem **[SDEV]** on hourly and a combination of hourly and yearly basis, respectively. A pseudo-code of the basic *Rolling Horizon* heuristic is provided in **Algorithm 2**.

Algorithm 2: Rolling Horizon Heuristic

Input: Termination criteria: $iter_{max}$, $time_{max}$, and ϵ;
Output: Upper bound $z(x^r)$;
Step 1: Initialize: $r \leftarrow 1$, $t_0^r \leftarrow 0$, $h_0^r \leftarrow 0$, M^r, Q^r ;
$terminate \leftarrow false$;
while $(terminate = false)$ **do**
  Set:
    • $x^n \in \{0,1\}$ and $y^n \in \mathbb{Z}^+$ for $t_0^r \leq t \leq t_0^r + M^r$ and $h_0^r \leq h \leq h_0^r + Q^r$
    • $0 \leq x^n \leq 1$ and $y^n \in \mathbb{R}^+$ for $t > t_0^r + M^r$ and $h > h_0^r + Q^r$
  Solve the approximate subproblem **[SDEV(*r*)]** using CPLEX
  if $(t_0 > |\mathcal{T}|)$ **then**
    terminate $\leftarrow$ true;
  else
    Fixing the value x^n, y^n for $t < t_0^r$ and $h < h_0^r$;
  end
  $r \leftarrow r + 1$;
end
return $z(x^r)$

Let **[SDEV(*r*)]** be an approximate sub-problem of the RH algorithm at iteration r. Define t_0^r and h_0^r as the starting time period for years and hours, respectively, while M^r and Q^r are the number of time periods of years and hours, respectively, for each sub-problem r. In the RH heuristic, either a set of fixed or different values of M^r and Q^r is considered across different iterations of the algorithm. For a particular scenario n, an approximate sub-problem **[SDEV(*r*)]** is solved by setting the variables as follows:

$$\begin{cases} x^n \in \{0,1\} \;\&\; y^n \in \mathbb{Z}^+ \quad for \quad t_0^r \leq t \leq t_0^r + M^r \;\&\; h_0^r \leq h \leq h_0^r + Q^r \\ 0 \leq x^n \leq 1 \;\&\; y^n \in \mathbb{R}^+ \quad for \quad t > t_0^r + M^r \;\&\; h > h_0^r + Q^r \end{cases}$$

After solving the sub-problem, the values of variables are fixed as $x^{n,r} = x^{n,r-1}$ & $y^{n,r} = y^{n,r-1}$ for $t < t_0^r$ & $h < h_0^r$ and step size r is updated. It is worth noting that by varying parameters t_0^r, h_0^r, M^r, and Q^r, a number of different variants of the RH algorithm

might be developed. Figures 4.2 through 4.4 provide an illustration of solving a three-year and four-hour time period problem using three different variants of the RH heuristic. In terms of preliminary experiments, **[RH3]** provides better computational results to solve problem **[SDEV(r)]** efficiently.

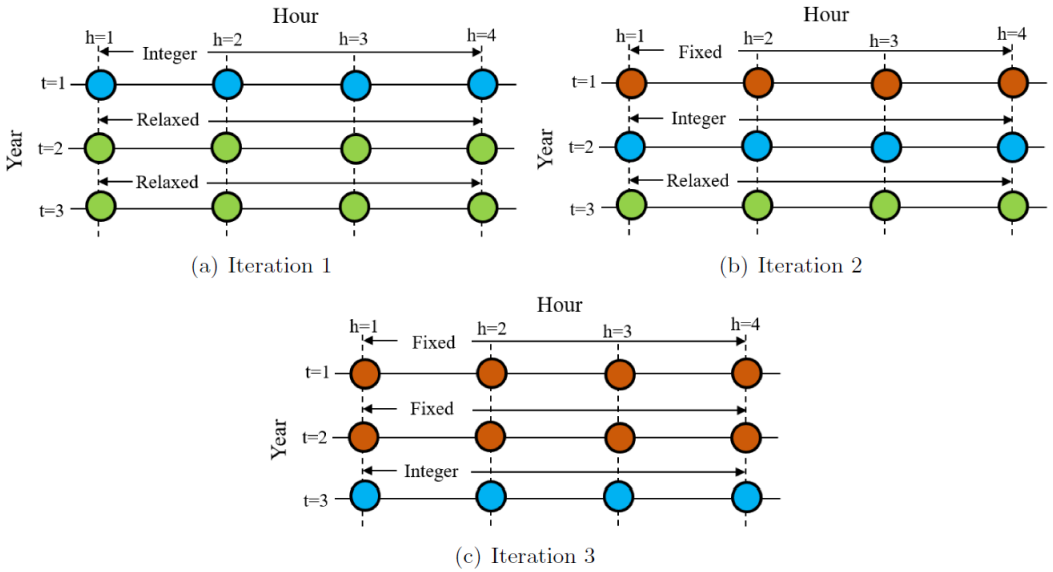

Figure 4.2: Illustration of a rolling horizon strategy for **[RH1]**

4.4 Computational Study

This section focuses on solving model **[LEV3]** using hybrid Sample Average Approximation based Scenario Decomposition algorithm to draw managerial insights obtained from a real-life case study. This section is composed of three sub-sections. First, a brief description of the data used to generate instances along with scenario generation are provided. Second, the efficiency and effectiveness of model **[LEV3]** and proposed algorithms

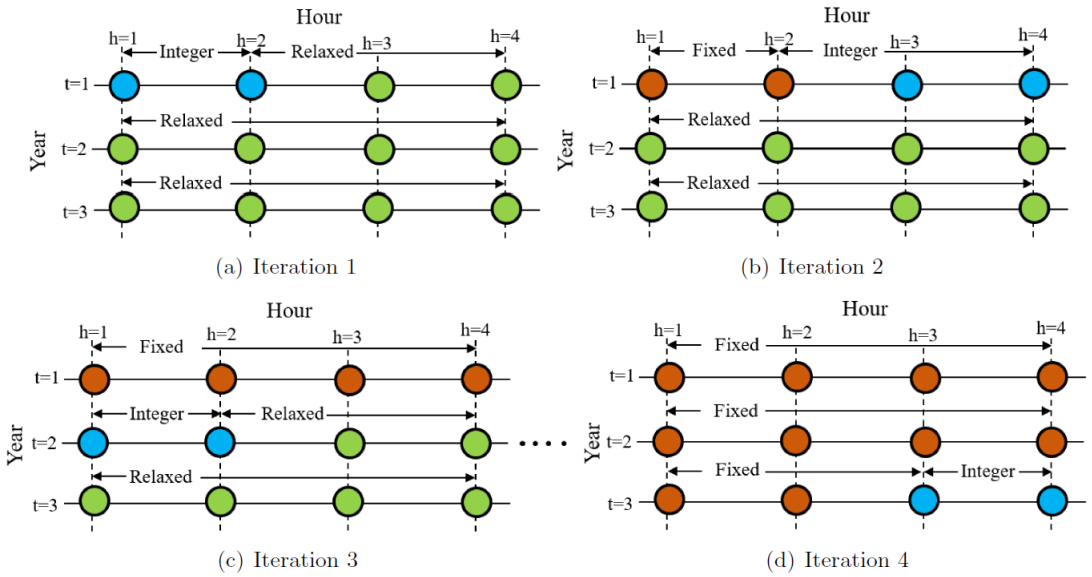

Figure 4.3: Illustration of a rolling horizon strategy for **[RH2]**

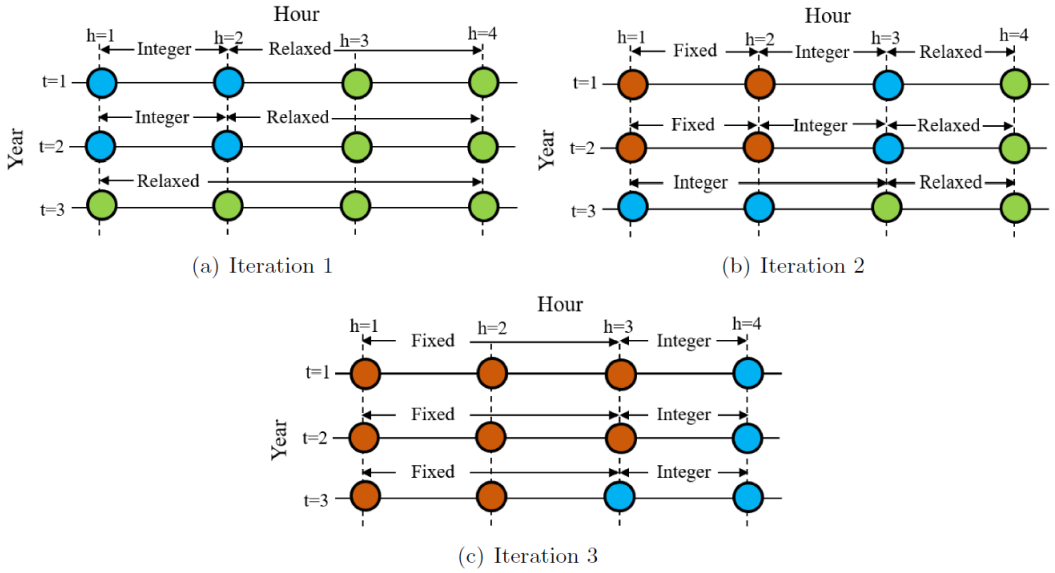

Figure 4.4: Illustration of a rolling horizon strategy for **[RH3]**

are evaluated in the electricity supply network problem. Finally, a case study, provided for Washington, DC as a testing ground for the analysis, explores the potential connections of limited power resources in power management to satisfy network demand. In addition, the impact of demand variation, power grid disruption, and minimum power requirement to establish charging stations on the overall electricity supply network design and cost are analyzed. Managerial insights will be derived from this case study in the form of perspective and understanding. The All numerical experiments are coded in GAMS 24.2.1 [39] on a desktop computer equipped with an Intel Core i7 processor 3.50 GHz with 32 GB RAM. The optimization solver used is ILOG CPLEX 12.6.

4.4.1 Data Description

Density of electricity demand in a network cell at a particular time period is determined based on the number of major roads and, consequently, hourly projected flow of electric vehicles on the network cell (f_{iht}) [92] as well as the percentage of electric vehicles that require to be charged under a demand scenario ($\eta_{ht\omega}$). Other factors including the density of population, hospitals, commercial buildings, and colleges located nearby major roads have a significant effect on projecting electric vehicle flow. The percentage of electric vehicles charged in a particular time period ($\eta_{ht\omega}$) is set to 40%, while the discharging rate (β_{ht}) is set to 5%.

The network, known as a grid network, is divided into $n \times m$ network cells, i.e., $|\mathcal{I}| = n \times m$, where each cell contributes an area of approximately 1.0 mi^2. The data related to cell-specific parameters are generated only for those cells that include a passing road(s);

otherwise, the values of parameters related to a cell without road passing are set to zero. Therefore, a network cell with a passing road(s) is considered as a candidate location to establish a charging station. Long term investment decisions are made up to 10 years, i.e., $|\mathcal{T}| = [2, 10]$, while short term operational decisions are made up to 360 hours (15 days) as a representative of each year, i.e., $|\mathcal{H}| = [12, 360]$.

The maximum limit of power line temperature before disruption (φ_{iht}^{max}) is set to 200^0F [4]. Since the power flow through transmission lines has a considerable impact on line temperature, the maximum limit of power line electricity before disruption (g_{iht}^{max}), which is adopted from [31], is restricted in terms of φ_{iht}^{max}. With respect to commercial and industrial time-of-use (TOU) rate as well as the amount of electricity usage, unit electricity price of charging stations is determined based on five segments of charging price, i.e., $|\mathcal{R}| = 5$. Each segment r represents a particular range of power availability with its own charging price. Although a double exponential hazard function can plot utilized powers and charging prices, for simplicity sake, an step function determines charging prices for pre-determined segments of utilized power. Subsequently, hourly electricity price plan for the PG (c_{rht}^{+}) is determined. In addition, hourly electricity price plan for V2G power (c_{ht}^{v2g}) is determined with respect to [91, 104]. It is clear that the upper bound of the last segment of charging price, i.e., $UB_{|\mathcal{R}|}$, is equal to the maximum limit of power line electricity, i.e., $UB_{|\mathcal{R}|} = g_{iht}^{max}$.

Two types of fast electric vehicle charging stations are considered to establish on network cells, i.e., $|\mathcal{K}| = 2$. The construction cost of establisning type 1 and type 2 charging stations is set to \$50,000 [1] and \$500,000 [40], respectively. Therefore, the annual estab-

lishment cost of a charging station, which is established on year t, is determined in terms of the ratio of the investment on planning horizon ($|\mathcal{T}|-t+1$) to lifetime of the established charging station of type k ($\mathcal{LT}_k$), i.e., $(\frac{|\mathcal{T}|-t+1}{\mathcal{LT}_1})\times 50,000$ and $(\frac{|\mathcal{T}|-t+1}{\mathcal{LT}_2})\times 500,000$. In addition, development cost is a percentage of annual investment cost, which is incurred mainly from growing a current service and/or introducing a new service along with marketing analysis, developmental engineering, and customer surveying.

The information on uses of solar radiation for target city is used to determine available electricity obtained from solar panels during a day in each cell (b^r_{iht}). In addition, the size of utilized solar panels for charging stations (a^r_{it}) is assumed to be 100 m^2. The minimum power requirement to establish a charging station of type 1 (p^{cs}_{1t})/type 2 (p^{cs}_{2t}) in a network cell is 5/10 MW. The unit storage cost of a battery in a type 2 charging station (c^s_{ht}) is set to 0.02 \$/hr. The average unit power required to charge/obtained from discharge each electric vehicle (λ/γ) is set to 35.6 kWh. Finally, we set the maximum available batteries as well as the number of plug-in and plug-out at charging stations as $u_t = 40$, $q^{in}_t = 10$, and $q^{out}_t = 10$, respectively. It is worth noting that all costs and benefits are calculated and then adjusted for inflation.

There is uncertainty on $\eta_{ht\omega}$ so that it varies significantly from hour to hour due to different levels of remaining charge on electric vehicle batteries, car owner's willingness to stay at a charging station, and charging/discharging time. This requires a large set of scenarios for the estimation of hourly electricity demand. Based on a historical data of target city, Monte Carlo simulation is implemented to generate a large number of scenarios with

equal probabilities $1/|\mathcal{N}|$ for $\eta_{ht\omega}$, where $\mathcal{N}$ is a set of sample scenarios. The generated samples are independent and identically distributed (*iid*) random variables.

4.4.2 Experimental Results

Since Washington, DC is considered as one of strong-growing electric vehicle populations over other major metropolitan cities in US [92], it is chosen as a testing ground to visualize and validate the modeling results. In addition, it has reputation as one of the nation's most environmentally conscious cities. The electricity supply network representation along with demand distribution for Washington, DC is shown in Figure 4.5. The network as a grid of size 12×11 is divided into 132 network cells, i.e., $|\mathcal{I}| = 132$. Five-year as long term investment decisions along with 24-hour in each year as a representative of short term operational decisions are considered, i.e., $|\mathcal{T}| = 5$ and $|\mathcal{H}| = 24$. The information on uses of solar radiation for Washington, DC in year 2010 is used to determine available electricity obtained from solar panels during a day [83]. A historical data of Washington, DC is considered into account that helps in predicting the future electric vehicle charging/discharging percentage. Finally, Monte Carlo simulation is implemented to generate a large number of scenarios.

A sensitivity analysis is performed to determine how different values of an independent parameter impact a particular dependent variable(s) as well as the overall electricity supply network cost and design, under a given set of assumptions. Yearly decisions on established charging stations determine the electricity supply network design. Therefore, a considerable changes on critical factors definitely result in changes on network design.

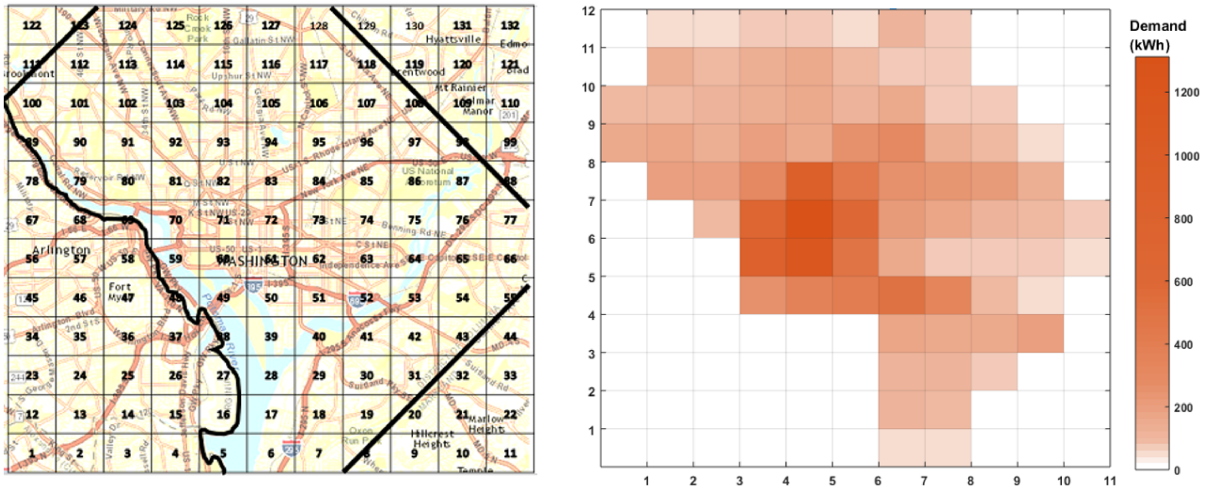

Figure 4.5: Network representation and geographical demand distribution of Washington DC [6]

In particular, the impact of demand variation, power grid disruption, and minimum power requirement to establish a charging station on the overall electricity supply network design and cost are analyzed.

All sensitivity analyses are performed with respect to real life case study developed for Washington, DC (base case study). Figure (4.6) shows five-year network design of long term investment decisions in relation to the base case study. A noticeable expansion of charging stations in Washington, DC is observed from year 2018-2022. Moving forward, the number of established charging stations is increased due to increase in demand so that the number of charging stations of each type is increased around 50% after five years. In addition, the results indicate that most charging stations are established on the cells located on downtown area of Washington, DC due to high density flow of electric vehicles on those cells.

In the following, the impact of critical parameters on the electricity supply network cost and design are determined. We denote $\overline{E}_{rih t\omega} = \big(\sum_{(r\in\mathcal{R}, i\in\mathcal{I}, h\in\mathcal{H}, \omega\in\Omega)} \rho_\omega E_{rih t\omega}\big)/|\mathbf{Y}_t|$ as a representative of the average electricity flow from the PG to charge electric vehicles (not including batteries) at any type of charging stations established at cell $i \in \mathcal{I}$ on hour $h \in \mathcal{H}$ of year $t \in \mathcal{T}$ under segment $r \in \mathcal{R}$ of charging price and demand scenario ω. Moreover, $|\mathbf{Y}_t|$ is considered as the number of charging stations of any type established at the electricity supply network in a particular year t. Likewise, $\overline{Z}_{iht\omega}$ and $\overline{V}_{iht\omega}$ are representatives of an average of hourly electricity power supplied by solar power and V2G power, respectively, related to any type of charging stations established at any network cell. In addition, $\overline{B}_{iht\omega} = \big(\sum_{(i\in\mathcal{I}, h\in\mathcal{H}, \omega\in\Omega)} B_{iht\omega}\big)/|\mathbf{Y}'_t|$ is considered as a representative of the average number of batteries, which are hourly utilized at a type 2 charging station established at any network cell. Likewise, $\overline{H}_{iht\omega}$, $\overline{S}_{rih t\omega}$, and $\overline{P}_{iht\omega}$ are considered as representatives of the average number of batteries, which are hourly stored, charged, and discharged at a type 2 charging station established at any network cell, respectively. In addition, $|\mathbf{Y}'_t|$ is considered as the number of type 2 charging stations established at the electricity supply network in a particular year t.

4.4.2.1 Impact of Demand Variation

We first investigate the impact of *demand variation* or equivalently electric vehicle charging percentage variation ($\eta_{ht\omega}$) and/or electric vehicle flow variation (f_{iht}) on utilization of diversified power resources and, consequently, electricity supply network design and cost. Since variations on $\eta_{ht\omega}$ and f_{iht} are on the same direction, the impact of demand

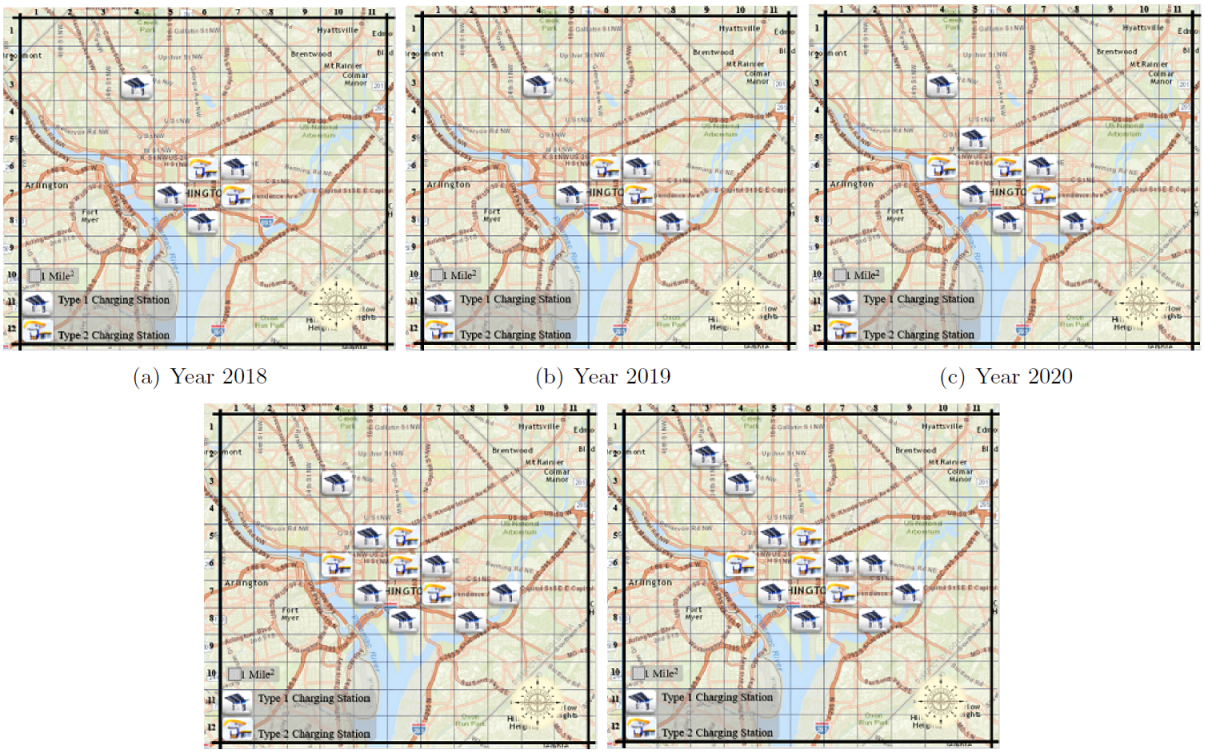

(a) Year 2018 (b) Year 2019 (c) Year 2020

(d) Year 2021 (e) Year 2022

Figure 4.6: Electric vehicle charging station locations under base case scenario

variations on different time periods are determined only by $\eta_{ht\omega}$ with respect to the *mean* ($\overline{\eta}_{ht}$) and *variance* (σ^2_{ht}) of $\eta_{ht\omega}$ in time period h of year t under different scenarios ω. In this experiment, three different variation levels are generated for σ^2_{ht} with respect to the same $\overline{\eta}_{ht}$: (a) $\sigma^2_{ht} = 5\%\overline{\eta}_{ht}$ as low demand variation level; (b) $\sigma^2_{ht} = 15\%\overline{\eta}_{ht}$ as medium demand variation level set to base case study; and (c) $\sigma^2_{ht} = 50\%\overline{\eta}_{ht}$ as high demand variation level. With respect to normality assumptions for $\eta_{ht\omega}$, Monte Carlo simulation techniques are implemented to generate the scenarios for those different variation levels in which $\overline{\eta}_{ht}$ is independent for each time period and varies in the range $(\overline{\eta}_{ht} \pm \sigma^2_{ht})$ $\forall h \in \mathcal{H}, t \in \mathcal{T}$.

Figure 4.7 demonstrates the impact of $\eta_{ht\omega}$ on utilization of diversified power resources on a charging station. As evidenced from the results, demand variation has a direct relationship with utilized power resources so that any increase in $\eta_{ht\omega}$ results in an increase on utilization of a power resource(s), i.e., $E_{rht\omega}, Z_{iht\omega}, V_{iht\omega}$, and $\lambda B_{iht\omega}$. In addition, a set of time-dependent parameters including solar radiation availability, charging prices, and electric vehicle flows critically affects the hourly operational decisions of utilized power resources, particularly for high demand variation level. As shown by Figure 4.7(d), full-charged batteries, i.e., $\lambda B_{iht\omega}$, satisfy main portion of electricity demands related to type 2 charging stations so that $\lambda B_{iht\omega} \leq (G_{rht\omega} - E_{rht\omega})$, $\forall r \in \mathcal{R}, i \in \mathcal{I}, h \in \mathcal{H}, t \in \mathcal{T}.\omega \in \Omega \mid Y_{i2t} = 1$. Irrespective of battery demand of type 2 charging stations, electricity demands are primarily satisfied through the PG ($\overline{E}_{rht\omega}$) and V2G power ($\overline{V}_{iht\omega}$), shown by sub-figures 4.7(a) and 4.7(b) of Figure 4.7, respectively, during solar radiation unavailability, low-charging price hours, and low electric vehicle flows, i.e., 1.00 AM - 4.00 AM, 9.00 AM - 12.00 PM, and 9.00 PM - 12.00 AM. Alternatively, major part of

electricity demands is satisfied first through solar energy ($\overline{Z}_{iht\omega}$), shown by Figure 4.7(c) and, then primarily through V2G power ($\overline{V}_{iht\omega}$) and the PG ($\overline{E}_{riht\omega}$) during solar radiation availability, high-charging prices, and more electric vehicle flows, i.e., 10:00 AM - 2:00 PM.

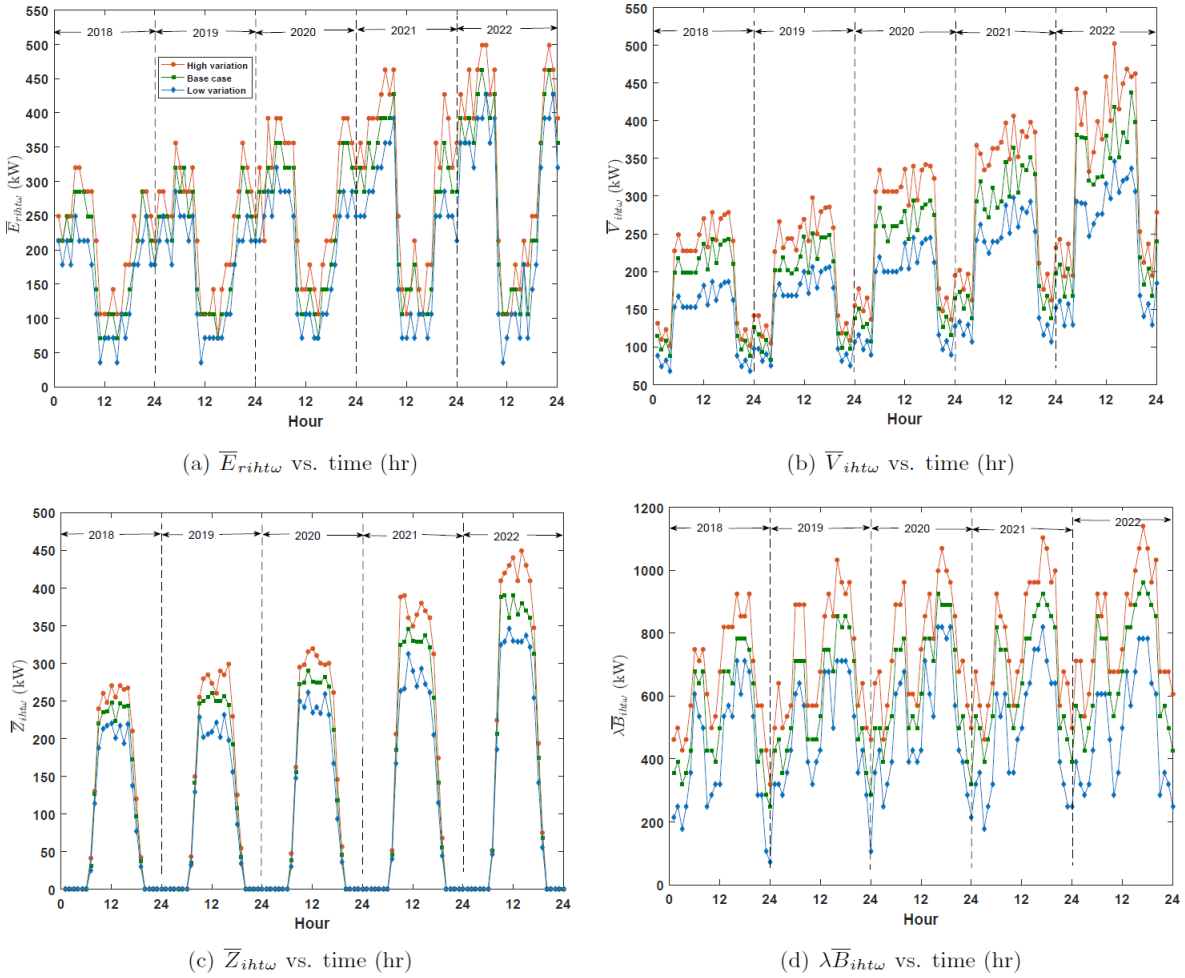

(a) $\overline{E}_{riht\omega}$ vs. time (hr)

(b) $\overline{V}_{iht\omega}$ vs. time (hr)

(c) $\overline{Z}_{iht\omega}$ vs. time (hr)

(d) $\lambda\overline{B}_{iht\omega}$ vs. time (hr)

Figure 4.7: Impact of electric vehicle charging percentage variations on utilization of power resources

Demand variations have significant impact on battery activities of type 2 charging stations, i.e., the number of charged, discharged, and swapped batteries and, consequently, the number of stored batteries at type 2 charging stations. Figure 4.8 demonstrates the impact of $\eta_{ht\omega}$ on battery related activities of a type 2 charging station on average. High demand variation level leads to less discharged batteries, i.e., $\overline{P}_{iht\omega}$, more charged batteries, i.e., $\overline{S}_{riht\omega}$, more utilized batteries to satisfy demands, $\overline{B}_{iht\omega}$, and subsequently, more stored batteries at type 2 charging stations, i.e., $\overline{H}_{iht\omega}$. Contrary, low demand variation level leads to more electricity flow to the PG to discharge batteries, $\gamma\overline{P}_{iht\omega}$, less electricity flow from the PG to charge batteries, $\lambda\overline{S}_{riht\omega}$, less utilized batteries to satisfy demands and, consequently, less inventory for full-charged batteries. It is worth noting that the rate of changes on $S_{riht\omega}$ and $P_{iht\omega}$ depends on charging prices as well as the peak/sub-peak hours of electricity demands.

In summary, variation on $\eta_{ht\omega}$ highly impacts power resource utilization and, consequently, the network design and cost. There are direct relationship between demand variation levels, the network design, and the network cost. Finally, the number of established charging stations is either increased or not changed by high demand variation level and vice versa.

4.4.2.2 Impact of Power Grid Disruption

A transmission line failure is occurred due to the line overheating as a result of power flow loading over the line transmission capacity between the PG and a charging station. Therefore, power shortage might occur to electricity supply network and, consequently,

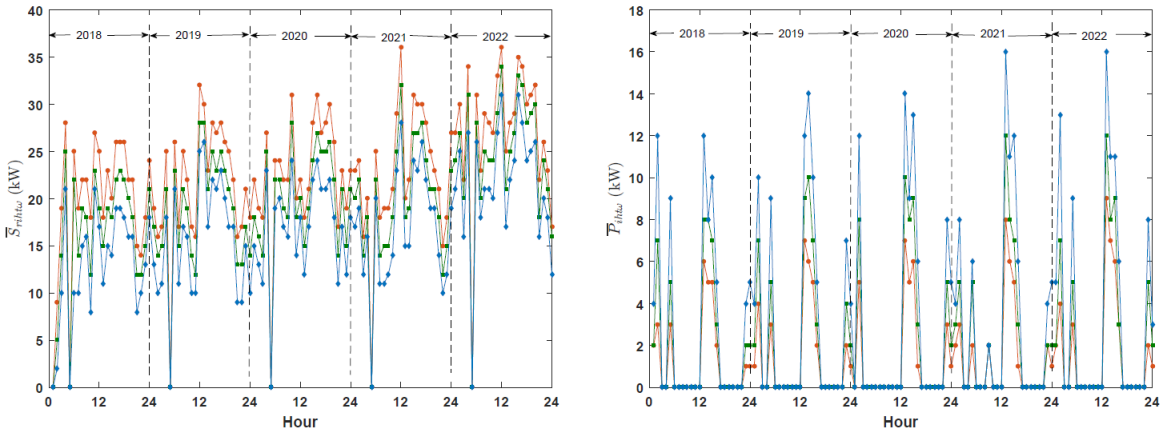

(a) $\overline{S}_{rihtw}$ vs. time (hr)

(b) $\overline{P}_{ihtw}$ vs. time (hr)

(c) $\overline{B}_{ihtw}$ vs. time (hr)

(d) $\overline{H}_{ihtw}$ vs. time (hr)

Figure 4.8: Impact of electric vehicle charging percentage variations on battery activities

penalty cost is imposed to the network in spite of utilizing the maximum available capacity of other resources. Penalty cost is considered due to either unmet demands or demands satisfied by an external resource(s). Since the PG capacity, as the main electricity resource of charging stations, has a critical effect on the amount of utilization of diversified power resources in different time periods, the impact of *power grid disruption* for n consecutive time periods ($G_{rih t\omega} = 0 \ \forall h, (h+1), ..., (h+n-1) \in \mathcal{H}$) on the electricity supply network cost is investigated.

In order to show the impact of power grid disruption on utilized resources and the network cost, model **[NEV]** is solved irrespective of power disruption constraints, i.e., model **[NEV]** without constraints (4.21) through (4.25), which is known as model **[EV]**. Then, after accounting risk aversion, power grid disruption is simulated for a particular cell i as follows: power flow from the PG is set to zero during three consecutive time periods $(h+1)$, $(h+2)$, and $(h+3)$ at model **[EV]**, i.e., $G_{ri(h+1)t\omega} = G_{ri(h+2)t\omega} = G_{ri(h+3)t\omega} = 0$, when utilized PG power is greater than the maximum allowable power in network cell i at time period h of year t, i.e., $G_{rih t\omega}(1-\pi) > g_{iht}^{max}$, or utilized PG powers are equal to the maximum allowable powers in network cell i for two consecutive time periods $(h-1)$ and h, i.e., $G_{ri(h-1)t\omega}(1-\pi) = g_{i(h-1)t}^{max}$ & $G_{rih t\omega}(1-\pi) = g_{iht}^{max}$.

Figure 4.9(a) shows the utilization of power resources with respect to power disruption management (disruption prevention model), while Figure 4.9(b) shows the utilization of power resources irrespective of power disruption management (disrupted model). Part of power shortage in the disrupted model is satisfied by other power resources including V2G power and the RES. During power disruption, the utilization of V2G power reaches to its

maximum availability compared to the disruption prevention model. In addition, there is no sensible changes on the RES utilization at both models since it is utilized nearby to its maximum capacity at the disruption prevention model. The remaining power shortage is satisfied by an external resource(s), which is considered as penalty cost.

Since the PG is the main resource of charging stations, Figure 4.9(c) shows the utilization of PG power and, consequently, power shortage at both disruption prevention and disrupted models in order to follow the changes on annual network costs, shown by Figure 4.10. Although the PG utilization almost overlaps each other at both models, power disruption occurs frequently at the disrupted model, which leads to increase in power shortage, while power shortage is remained on its reasonable level at the disruption prevention model due to power disruption management. As a result, annual network costs are improved from 8% up to 16% when power disruption prevention strategy is used in electricity supply network. In addition, total electricity supply network cost is reduced by 12% under power disruption management, while even 1% improvement in the network cost of electricity supply network is significant.

4.4.2.3 Impact of Minimum Power Requirement to Establish a Charging Station

This set of experiments study the impact of *minimum power requirement to establish a charging station* (p^{cs}_{kt}) on the overall network design and cost. Figure 4.11 illustrates the impact of the percentage of change in p^{cs}_{kt} on the number of established charging stations in a particular year of planning horizon, i.e., $\sum_{i\in\mathcal{I},k\in\mathcal{K}} Y_{ikt},\ \forall t \in \mathcal{T}$. Decrease in p^{cs}_{kt}, i.e, a percentage change with negative number, is shown by dash-line, while increase in p^{cs}_{kt},

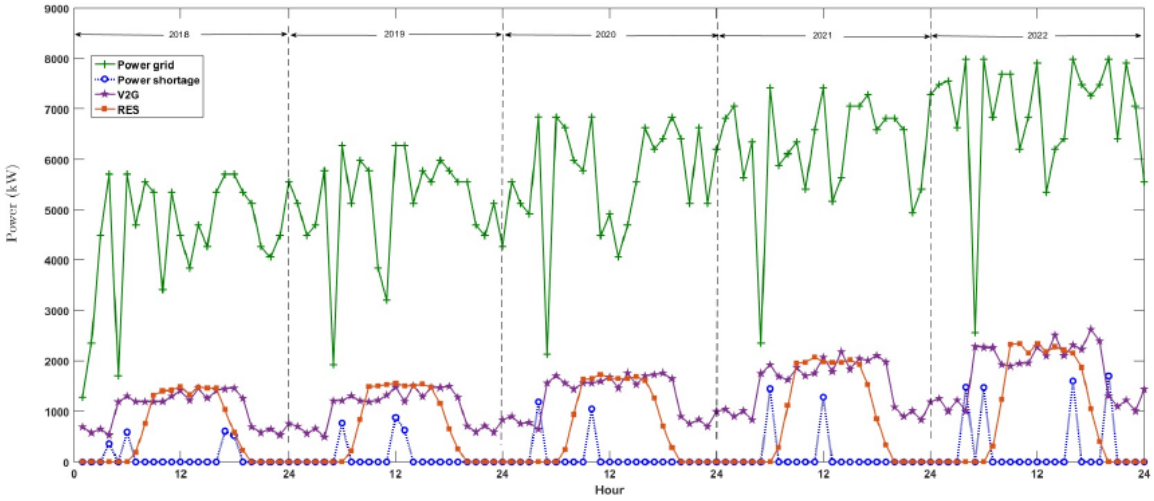

(a) Power disruption prevention model

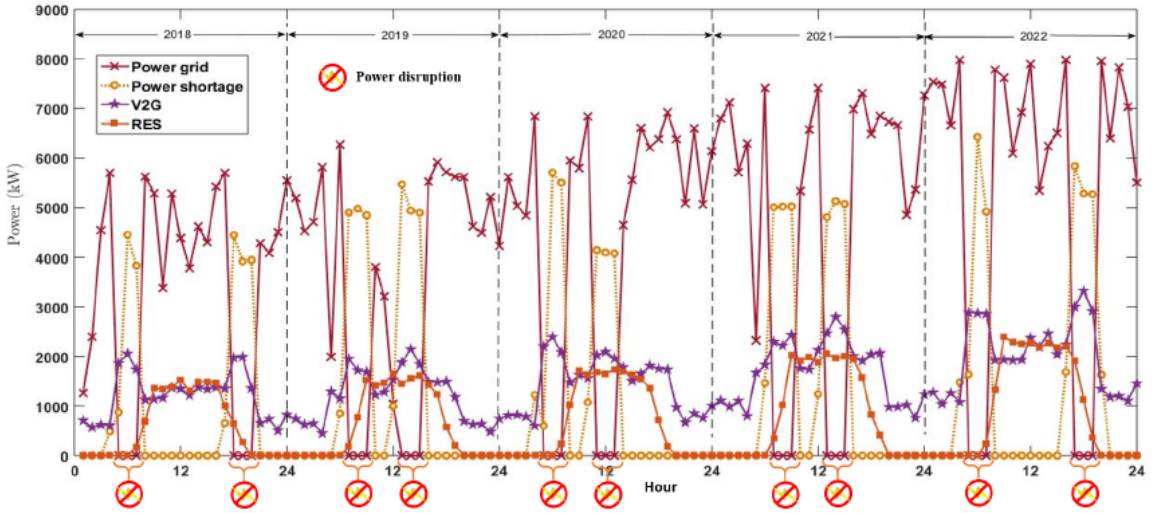

(b) Disrupted model

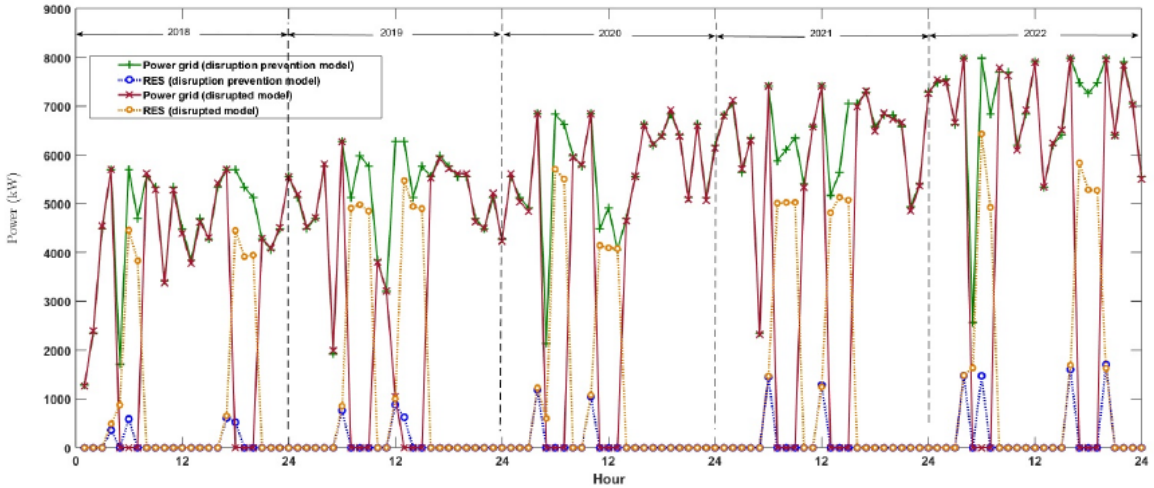

(c) Utilized PG power and power shortage under power disruption prevention model and disrupted model

Figure 4.9: Utilized power resources with and without power disruption management

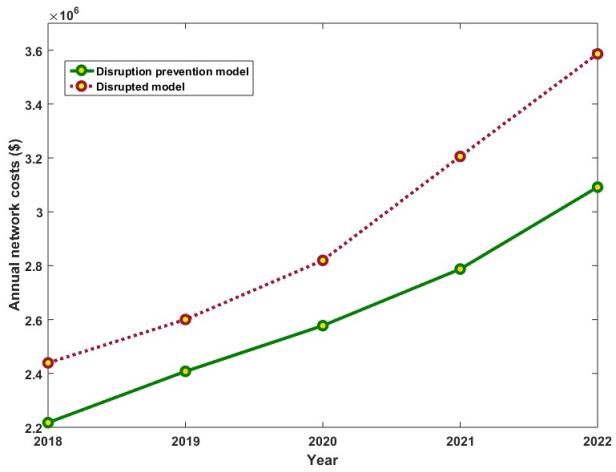

Figure 4.10: Annual network costs with and without power disruption management

i.e, a percentage change with positive number, is shown by solid-line in Figure 4.11. There is an inverse relationship between changes on minimum power requirement to establish a charging station and the total number of established charging stations so that $\sum_{i\in\mathcal{I},k\in\mathcal{K}} Y_{ikt}$ is either increased/decreased or not changed when p^{cs}_{kt} decreases/increases.

Based on the impact of p^{cs}_{1t} and p^{cs}_{2t} on the network design, demonstrated by Figures 4.11a and 4.11b, respectively, the total number of established charging stations is more sensitive to changes in p^{cs}_{1t} in comparison with changes in p^{cs}_{2t}. Figure 4.12 represents the total network cost under different changes in p^{cs}_{1t} and p^{cs}_{2t} separately. Any decrease in p^{cs}_{kt} leads to establish more charging stations and, consequently, satisfy more demands. Contrary, any increase in p^{cs}_{kt} leads to establish less charging stations and, consequently, satisfy less demands. On the other hand, more charging stations result in more network cost due to annual establishment and development cost, while less charging stations result in more network cost due to unsatisfied demands (i.e., power shortage). There is a trade-off between the design (i.e., the number of established charging stations) and the cost of

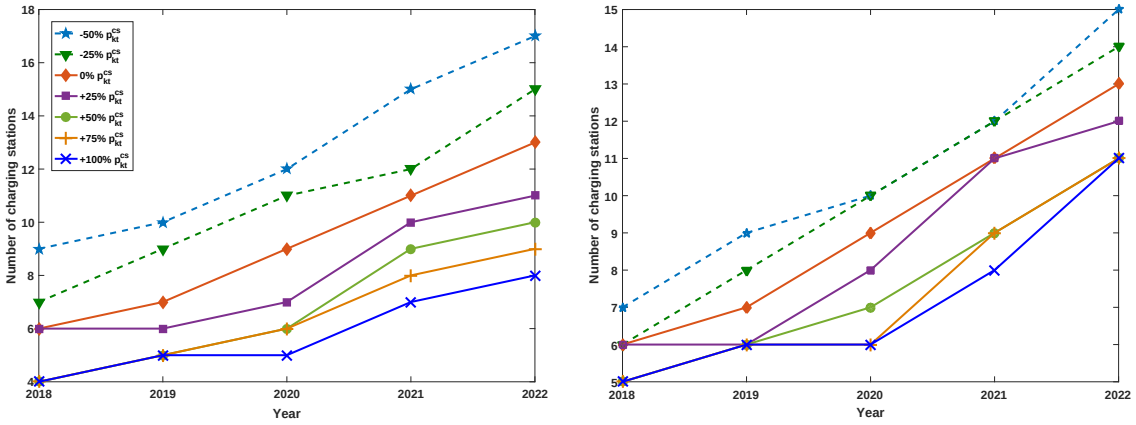

(a) Changes in p_{1t}^{cs}

(b) Changes in p_{2t}^{cs}

Figure 4.11: Impact of p_{kt}^{cs} on established charging stations

electricity supply network, which are known as optimal design under optimal network cost so that any changes on the optimal design (either positive or negative) increases the network cost. The minimum network cost, shown by Figure 4.12, is obtained by 25% and 75% increase in p_{1t}^{cs} and p_{2t}^{cs} related to the base case study, respectively.

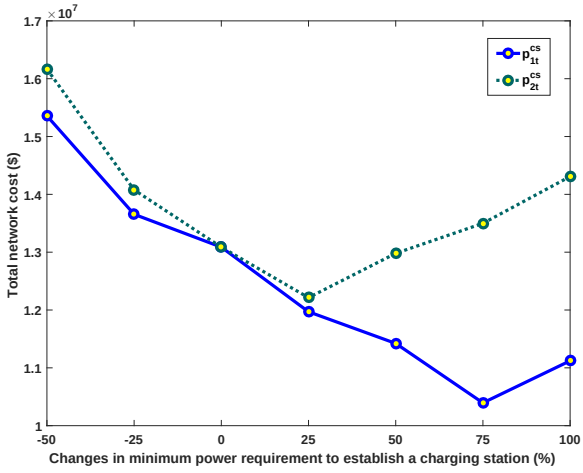

Figure 4.12: Total network cost under different p_{1t}^{cs} and p_{2t}^{cs}

4.4.3 Computational Performance of the Proposed Algorithms

The efficiency and effectiveness of the following algorithms are evaluated by solving model **[LEV3]**: the basic SAA method proposed in Section 4.3.1; the SAA method proposed in Section 4.3.2, where each sub-problem is solved using the SD algorithm; and, the SAA method proposed in Sections 4.3.3, where each sub-problem is solved using the SD algorithm on the basis of the LD scheme. To simplify the definition of proposed solution approaches and obtained results, the following notations are provided.

- **[CPLEX]**: Model **[LEV3]** solved by CPLEX
- **[SAA$_{basic}$]**: The basic SAA method
- **[SAA$_{SD}$]**: The SAA method enhanced with the SD algorithm
- **[SAA$_{SD/LD}$]**: The SAA method enhanced with the SD algorithm on the basis of the LD scheme

In relation to the research problem, there is no benchmark instances available in the literature. Hence, a new set of problem instances are generated with respect to real life case study and computational time required by **[CPLEX]**. Three sets of problem instances have been generated for comparison purpose: small-, medium-, and large-size instances, where the case study proposed on Washington, DC is considered as a medium-size problem. In relation to short term operational decisions, the number of time periods in a year is 12 and 24 hours (around one day) for small-size instances, while it is 24 and 72 hours (1 and 3 days) as well as 168 and 360 hours (7 and 15 days) for medium- and large-size instances,

respectively. Likewise, in relation to long term investment decisions, 2 and 5 years are considered for small-size instances, while it is 5 and 8 years as well as 8 and 10 years for medium- and large-size instances, respectively. All the other parameters are set based on Section (4.4.1). Table 4.1 represents generated instances for each set of problems in terms of the size of $|\mathcal{I}|$, $|\mathcal{H}|$, and $|\mathcal{T}|$, where the deterministic equivalent for model **[LEV3]** is indicated based on the number of variables and constraints for each generated instance.

Table 4.1: Problem size of the deterministic equivalent of the model based on the number of variables and constraints

Size	Instance	$\|\mathcal{I}\|$	$\|\mathcal{H}\|$	$\|\mathcal{T}\|$	Variables				Total
					Binary	Integer	Continuous	Total	constraints
Small	1	25	12	2	3,100	4,800	4,800	12,700	11,550
	2	25	12	5	7,750	12,000	12,000	31,750	28,950
	3	25	24	2	6,100	9,600	9,600	25,300	22,950
	4	25	24	5	15,250	24,000	24,000	63,250	57,450
	5	50	12	2	6,200	9,600	9,600	25,400	23,100
	6	50	12	5	15,500	24,000	24,000	63,500	57,900
	7	50	24	2	12,200	19,200	19,200	50,600	45,900
	8	50	24	5	30,500	48,000	48,000	126,500	114,900
	9	75	12	2	9,300	14,400	14,400	38,100	34,650
	10	75	12	5	23,250	36,000	36,000	95,250	86,850
	11	75	24	2	18,300	28,800	28,800	75,900	68,850
	12	75	24	5	45,750	72,000	72,000	189,750	172,350
Medium	1	100	24	5	61,000	96,000	96,000	253,000	229,800
	2	100	24	8	97,600	153,600	153,600	404,800	367,800
	3	100	72	5	181,000	288,000	288,000	757,000	685,800
	4	100	72	8	289,600	460,800	460,800	1,211,200	1,097,400
	5	132	24	5	80,520	126,720	126,720	333,960	303,336
	6	132	24	8	128,832	202,752	202,752	534,336	485,496
	7	132	72	5	238,920	380,160	380,160	999,240	905,256
	8	132	72	8	382,272	608,256	608,256	1,598,784	1,448,568
	9	150	24	5	91,500	144,000	144,000	379,500	344,700
	10	150	24	8	146,400	230,400	230,400	607,200	551,700
	11	150	72	5	271,500	432,000	432,000	1,135,500	1,028,700
	12	150	72	8	434,400	691,200	691,200	1,816,800	1,646,100
Large	1	175	168	8	1,178,800	1,881,600	1,881,600	4,942,000	4,474,050
	2	175	168	10	1,473,500	2,352,000	2,352,000	6,177,500	5,592,650
	3	175	360	8	2,522,800	4,032,000	4,032,000	10,586,800	9,581,250
	4	175	360	10	3,153,500	5,040,000	5,040,000	13,233,500	11,976,650
	5	200	168	8	1,347,200	2,150,400	2,150,400	5,648,000	5,113,200
	6	200	168	10	1,684,000	2,688,000	2,688,000	7,060,000	6,391,600
	7	200	360	8	2,883,200	4,608,000	4,608,000	12,099,200	10,950,000
	8	200	360	10	3,604,000	5,760,000	5,760,000	15,124,000	13,687,600
	9	225	168	8	1,515,600	2,419,200	2,419,200	6,354,000	5,752,350
	10	225	168	10	1,894,500	3,024,000	3,024,000	7,942,500	7,190,550
	11	225	360	8	3,243,600	5,184,000	5,184,000	13,611,600	12,318,750
	12	225	360	10	4,054,500	6,480,000	6,480,000	17,014,500	15,398,550

A proposed solution approach is evaluated based upon the best lower bound obtained from all solution approaches, i.e., LB_{Best}. In other words, the percentage deviation (gap) between the upper bound of i^{th} solution approach (UB_i) and LB_{Best} is determined as

$\Delta f_i(\%) = (\frac{UB_i - LB_{Best}}{LB_{Best}}) \times 100\% \ \ \forall i \in \mathcal{S}$, where $\mathcal{S} = \{$**[CPLEX]**, **[SAA**$_{basic}$**]**, **[SAA**$_{SD}$**]**, **[SAA**$_{SD/LD}$**]**$\}$ and $LB_{Best} = Max\{LB_i\} \ \ \forall i \in \mathcal{S}$. All proposed solution approaches are terminated when at least one of the following criteria is satisfied: (a) the gap falls below a threshold value ε, i.e., $\Delta f_i(\%) \leq \varepsilon$ and/or (b) the maximum computational time limit, CT^{max}, is reached. In this study, the stopping criteria are set as $\varepsilon = 1\%$ and $CT^{max} = 3600\ s$.

Table 4.2 shows the comparative results obtained for proposed solution approaches in terms of the gap and computational time. Scenario size is set to $N = 1,000$ for **[CPLEX]**, while $\mathcal{N} = 20$ and $\mathcal{N}' = 500$ are set for samples with small- and large-size scenarios, respectively, in relation to **[SAA**$_{basic}$**]**, **[SAA**$_{SD}$**]**, and **[SAA**$_{SD/LD}$**]**. In addition, replication number M is set to 5 for all proposed algorithms. The boldface numbers under $T(s)$ column indicate the best computational time between proposed solution approaches when $\Delta f_i(\%) \leq \varepsilon, \ \exists i \in \mathcal{S}$, while the boldface numbers under $\Delta f(\%)$ column indicate the best gap developed by solution approaches when $T(s) = CT^{max}$. The following results are obtained from Table 4.2 under restricted computational time and pre-determined gap:

- In relation to small-size instances, all solution approaches present results close together based on the gap and computational time.
- The quality of the solutions obtained from **[CPLEX]** is significantly improved by using **[SAA**$_{basic}$**]** for medium-size instances.
- The computational efficiency of the solutions obtained from **[SAA**$_{basic}$**]** is significantly improved by using **[SAA**$_{SD}$**]**, particularly for medium-size instances.

- The quality and computational efficiency of the solutions obtained from **[SAA$_{SD}$]** is significantly improved by using **[SAA$_{SD/LD}$]**, particularly for large-size instances.
- **[SAA$_{SD/LD}$]** reduces overall gap reported by **[CPLEX]** significantly. The overall gap reported by **[SAA$_{SD/LD}$]** is 9% of the gap reported by **[CPLEX]**.
- **[CPLEX]** is capable of solving 13 out of 36 instances optimally within the pre-specified computational time, while **[SAA$_{SD/LD}$]** is capable of solving all generated instances optimally, except two large-size instances.
- A significant improvement in computational efficiency of **[SAA$_{basic}$]** is due to implementing the enhancement technique, which is used to solve sub-problems of **[SAA$_{SD}$]**. Likewise, the computational time reported by **[SAA$_{SD/LD}$]** is significantly improved by incorporating the LD scheme into the SD algorithm in order to solve sub-problems of **[SAA$_{SD}$]**.
- **[SAA$_{SD/LD}$]** is capable of solving problems equal or less than halftime of other solution approaches.
- **[SAA$_{SD/LD}$]** outperforms all other solution approaches and presents high-quality solutions efficiently, particularly for large-size instances.

4.5 Conclusion and Future Studies

This paper proposes a novel disruption prevention optimization framework, which integrate both long-term planning decisions and short-term operational decisions to design and manage electric vehicle charging stations on the electricity supply network, over a pre-determined planning horizon and under a stochastic power demand. A transmission

Table 4.2: Comparison of the results obtained from **[CPLEX]**, **[SAA$_{basic}$]**, **[SAA$_{SD}$]**, and **[SAA$_{SD/LD}$]**

Size		**[CPLEX]**		**[SAA$_{basic}$]**		**[SAA$_{SD}$]**		**[SAA$_{SD/LD}$]**	
	Case	Δf (%)	$T(s)$	Δf (%)	$T(s)$	Δf (%)	$T(s)$	Δf (%)	$T(s)$
Small	1	0.08	**32.51**	0.14	42.74	0.17	45.85	0.10	44.67
	2	0.11	**61.56**	0.24	78.43	0.26	72.51	0.19	79.63
	3	0.09	**58.94**	0.27	76.54	0.25	68.45	0.17	72.58
	4	0.48	378.62	0.58	256.42	0.61	**182.35**	0.36	213.34
	5	0.18	**59.62**	0.15	77.82	0.31	71.25	0.25	77.23
	6	0.62	389.24	0.71	261.47	0.34	**196.54**	0.43	226.47
	7	0.72	377.65	0.69	259.71	0.84	**183.64**	0.52	211.35
	8	0.64	1,045.87	0.71	589.61	0.86	484.57	0.89	**315.68**
	9	0.38	145.58	0.45	165.34	0.54	**123.28**	0.46	136.50
	10	0.75	543.21	0.84	415.61	0.71	364.21	0.63	**284.41**
	11	0.52	554.69	0.71	427.54	0.48	374.25	0.51	**287.64**
	12	0.47	1,854.65	0.89	1,254.62	0.67	1,014.27	0.88	**471.24**
Average		0.42	458.51	0.53	325.49	0.50	265.10	0.45	**201.73**
Medium	1	0.92	28,145.21	0.94	8,745.62	0.54	4,753.21	0.84	**2,654.88**
	2	11.52	CT^{max}	0.84	9,756.58	0.84	5,476.52	0.63	**3,124.50**
	3	18.55	CT^{max}	0.67	16,543.88	0.71	8,542.65	0.82	**4,563.87**
	4	20.61	CT^{max}	0.41	18,524.64	0.94	9,985.65	0.68	**6,025.22**
	5	7.52	CT^{max}	0.88	9,012.54	0.65	5,012.35	0.56	**2,964.55**
	6	8.63	CT^{max}	0.97	10,245.31	0.92	5,687.57	0.68	**3,452.67**
	7	21.65	CT^{max}	0.77	18,635.74	0.57	9,745.64	0.47	**5,047.64**
	8	OM	-	4.62	CT^{max}	0.93	12,354.62	0.82	**8,642.51**
	9	11.89	CT^{max}	0.79	9,825.74	0.87	5,478.61	0.78	**3,254.87**
	10	15.33	CT^{max}	0.78	14,563.87	0.86	7,153.44	0.66	**4,123.51**
	11	23.64	CT^{max}	0.81	19,524.30	0.65	10,632.55	0.89	**6,214.51**
	12	OM	-	12.54	CT^{max}	0.69	13,621.52	0.64	**9,256.66**
Average		14.03	35,214.52	2.09	17,281.52	0.76	8,203.69	0.71	**4,943.78**
Large	1	OM	-	3.54	CT^{max}	0.92	17,523.64	0.64	**9,726.54**
	2	OM	-	OM	-	0.81	29,635.24	0.48	**10,825.43**
	3	OM	-	OM	-	10.35	CT^{max}	0.61	**14,253.68**
	4	OM	-	OM	-	12.65	CT^{max}	0.77	**16,352.47**
	5	OM	-	OM	-	0.89	28,635.41	0.94	**10,235.44**
	6	OM	-	OM	-	4.52	CT^{max}	0.59	**12,635.71**
	7	OM	-	OM	-	11.35	CT^{max}	0.82	**15,234.95**
	8	OM	-	OM	-	OM	-	**1.23**	CT^{max}
	9	OM	-	OM	-	2.35	CT^{max}	0.65	**11,235.96**
	10	OM	-	OM	-	7.65	CT^{max}	0.78	**13,654.52**
	11	OM	-	OM	-	OM	-	0.96	**25,632.40**
	12	OM	-	OM	-	OM	-	**1.42**	CT^{max}
Average		-	-	3.54	CT^{max}	5.72	32,421.59	0.82	**17,648.93**
Total average		7.22	17,836.52	2.05	1,7869.00	2.33	13,630.13	0.66	**7,598.15**

CT^{max} stands for maximum computational time, i.e., 36000(s).
OM stands for out of memory.

network might be disrupted due to power line overheating as a result of excessive power flows in a prolonged time. To the best of our knowledge, this study is the first work that considers power disruption prevention on a transmission network on the basis of a reliable electricity supply network under demand uncertainty.

A reliable two-stage stochastic MINLP model **[NEV]** is formulated to determine the type, location, and time of established charging stations in each year (long-term planning decisions) and manage power resource utilization in each hour (short-term operational decisions) of the planning horizon with the aim of network cost minimization under electricity demand uncertainty. The proposed model **[NEV]** prevents the evolution of excessive

temperature on a power line under stochastic exogenous factors such as outside temperature and air velocity. Power resource management include the hourly operational decisions of electricity flow from the PG, the RES usage, V2G power usage, as well as the number of batteries charged, discharged (electricity flow to the PG), swapped, and stored. Although model **[NEV]** is converted to a linear MILP model **[LEV3]** based on piecewise McCromick relaxation technique of linearization, model **[LEV3]** is computationally very challenging depending upon the number of network cells ($|\mathcal{I}|$), set of time periods as a combination of years ($|\mathcal{T}|$) and hours ($|\mathcal{H}|$), and set of scenarios ($|\omega|$), which are determined by a decision maker(s). To alleviate these challenges and to solve industry-size instances, we develop an Sample Average Approximation (SAA) method accompanied by a Scenario Decomposition (SD) algorithm to solve generated sub-problems. The performance of hybrid SAA method is improved by integrating Lagrangian Decomposition (LD) scheme on the SD algorithm in order to solve sub-problems. Computational results indicate that the SAA method accompanied by SD on the basis of LD is capable of producing consistently high-quality solution to solve realistic large-size instances within reasonable computational times.

Sensitivity analysis, performed on a case study based upon the road network of Washington, DC as a testing ground, provides insightful results about the impact of demand variation, power grid disruption, and minimum power requirement to establish a charging station on the overall electricity supply network cost and design. In addition, computational experiments reveal numerous managerial insights for managers to make operational decisions at the optimum network cost. The following outcome of our data-driven analysis

help decision makers to develop a future sustainable power management decision system related to the electricity supply network with respect to the transmission network failure. With respect to time-dependent parameters such as solar radiation availability, charging prices, and electric vehicle flows, a decision maker is able to provide better hourly operational decisions of utilized power resources to reduce the network cost. A type 2 charging stations with more available batteries and battery activities is capable of reducing the amount of fluctuation on electricity demand and, consequently, demand variations can be under control. The overall electricity supply network cost is reduced more by managing the permissible amount of power transaction among the PG and charging stations with respect to charging prices, particularly through power disruption prevention management. In addition, there are some hidden costs related to customer retention, operator unemployment, and network re-installation as a result of power disruption, which have indirectly impacts the network cost. Finally, there is a trade-off between the number of established charging stations and the electricity supply network cost at the optimum point for the minimum power requirement to establish charging stations so that any variation on the number of established charging stations leads to increase in the network cost. In summary, the management of time-dependent parameters, battery inventory of type 2 charging stations, power transaction among the PG and charging stations, and minimum power requirement to establish charging stations can considerably reduce the overall electricity supply network cost, when the PG utilization is under control.

This study can be further extended in several research directions. Our study ignores the impact of traffic congestion on the electricity supply network design and cost. One

possible extension is the inclusion of the impact of EV congestion at charging stations on a driver charging decision. Apart from this, a more realistic approach can track drivers' behaviors in relation to the congestion at EV charging stations. A disrupted model along with backup scenarios of demand satisfaction can be proposed in comparison with a power disruption prevention model at the high risk aversion level. Furthermore, it is interesting to consider the stochastic nature of other parameters into the model such as the RES.

REFERENCES

[1] Agenbroad J., Hollland B., "EV charging station infrastructure costs. Rocky Mountain Institute.," Available from: http://blog.rmi.org/blog_2014_04_29_pulling_back_the_veil_on_ev_charging_station_costs, 2014.

[2] Ahmed S., "A scenario decomposition algorithm for 0–1 stochastic programs.," *Operations Research Letters*, vol. 41, no. 6, 2013, pp. 565–569.

[3] Alternative Fuels Data Center, "U.S. alternative fueling stations by fuel type.," Available from: http://www.afdc.energy.gov/data/10332, 2016.

[4] American Transmission Company, "Overhead Transmission Line Ampacity Ratings.," Available from: http://www.atc10yearplan.com/2011/documents/CR-0061.pdf, 2012.

[5] Anghel M., Werley K.A., Motter A.E., "Stochastic model for power grid dynamics," *System Sciences, 2007. HICSS 2007. 40th Annual Hawaii International Conference on*, 2007, p. 113.

[6] ArcGIS, "Washington, DC.," Available from: https://www.arcgis.com/home/item.html?id=009fd190135f40e1b4678b73a6ce7ef7, 2016.

[7] Arslan O., Karasan O.E., "A Benders decomposition approach for the charging station location problem with plug-in hybrid electric vehicles.," *Transportation Research Part B: Methodological*, vol. 93, 2016, pp. 670–695.

[8] Avci B., Girotra K., Netessine S., "Electric vehicles with a battery switching station: Adoption and environmental impact.," *Management Science*, vol. 61, no. 4, 2014, pp. 772–794.

[9] Bai H., Miao S., Zhang P., Bai Z., "Reliability evaluation of a distribution network with microgrid based on a combined power generation system.," *Energies*, vol. 8, no. 2, 2015, pp. 1216–1241.

[10] Balas E., "Disjunctive programming.," *Annals of Discrete Mathematics*, vol. 5, 1979, pp. 3–51.

[11] Balasubramanian J., Grossmann I., "Approximation to multistage stochastic optimization in multiperiod batch plant scheduling under demand uncertainty.," *Industrial & Engineering Chemistry Research*, vol. 43, no. 14, 2004, pp. 3695–3713.

[12] Baouche F., Billot R., Trigui R., El Faouzi N.E., "Efficient allocation of electric vehicles charging stations: Optimization model and application to a dense urban network.," *IEEE Intelligent transportation systems magazine*, vol. 6, no. 3, 2014, pp. 33–43.

[13] Basciftci B., Ahmed S., Gebraeel N., Yildirim M., "Integrated Generator Maintenance and Operations Scheduling under Uncertain Failure Times.," 2017, p. .

[14] Bayram I.S., Michailidis G., Devetsikiotis M., Granelli F., "Electric power allocation in a network of fast charging stations.," *IEEE Journal on Selected Areas in Communications*, vol. 31, no. 7, 2013, pp. 1235–1246.

[15] Becker T.A., Sidhu I., Tenderich B., "Electric vehicles in the United States a new model with forecasts to 2030," Tech. rep. Berkeley: Center for Entrepreneurship & Technology, University of California., 2009.

[16] Beer S., Gomez T., Dallinger D., Momber I., Marnay C., Stadler M., Lai J., "An economic analysis of used electric vehicle batteries integrated into commercial building microgrids.," *IEEE Transactions on Smart Grid*, vol. 3, no. 1, 2012, pp. 517–525.

[17] Bhatti S.F., Lim M.K., Mak H.Y., "Alternative fuel station location model with demand learning.," *Annals of Operations Research*, vol. 230, no. 1, 2015, pp. 105–127.

[18] CaroE C.C., Schultz R., "Dual decomposition in stochastic integer programming.," *Operations Research Letters*, vol. 24, no. 1-2, 1999, pp. 37–45.

[19] Castro, P.M., "Tightening piecewise McCormick relaxations for bilinear problems.," *Computers & Chemical Engineering*, vol. 72, 2015, pp. 300–311.

[20] Chang M., Tseng Y., Chen J., "A scenario planning approach for the flood emergency logistics preparation problem under uncertainty.," *Transportation Research Part E: Logistics and Transportation Review*, vol. 43, no. 6, 2007, pp. 737–754.

[21] Chen C.-W., Fan Y., "Bioethanol supply chain system planning under supply and demand uncertainities.," *Transportation Research Part E*, vol. 48, 2012, pp. 150–164.

[22] Chen T.D., Kockelman K.M., Khan M., "The electric vehicle charging station location problem: a parking-based assignment method for Seattle.," *Transportation Research Board 92nd Annual Meeting.*, 2013, pp. 13–1254.

[23] Chung S.H., Kwon C., "Multi-period planning for electric car charging station locations: A case of Korean Expressways.," *European Journal of Operational Research*, vol. 242, 2015, pp. 677–687.

[24] City Light, "The Impact of Electric Vehicles on System Load.," Available from: https://www.seattle.gov/light/news/issues/irp/docs/dbg_538_app_d_3.pdf, 2010.

[25] Clarke A.D., Makram E.B., "A Comprehensive Analysis of Plug in Hybrid Electric Vehicles to Commercial Campus (V2C).," *Applied Energy*, vol. 3, no. 01, 2015, p. 24.

[26] Cordeau J.F., Pasin F., Solomon M.M., "An integrated model for logistics network design.," *Annals of operations research*, vol. 144, no. 1, 2006, pp. 59–82.

[27] Cornuejols G., Nemhauser G.L., Wolsey L.A., "The uncapacitated facility location problem (No. MSRR-493).," *Carnegie-mellon univ pittsburgh pa management sciences research group*, 1983.

[28] Crainic T.G., Fu X., Gendreau M., Rei W., Wallace S.W., "Progressive hedging-based metaheuristics for stochastic network design," *Networks*, vol. 58, 2011, pp. 114–124.

[29] Deilami S., Masoum A.S., Moses P.S., Masoum M.A., "Real-time coordination of plug-in electric vehicle charging in smart grids to minimize power losses and improve voltage profile.," *IEEE Transactions on Smart Grid*, vol. 2, no. 3, 2011, pp. 456–467.

[30] Elhedhli S., Wu, H., "A Lagrangean Heuristic for Hub-and-Spoke System Design with Capacity Selection and Congestion.," *INFORMS Journal on Computing*, vol. 22, no. 2, 2010, pp. 282–296.

[31] Energy Information Administration, "District of Columbia Profile State Profile and Energy Estimates.," Available from: http://www.eia.gov/state/?sid=DC#tabs-3, 2016.

[32] Erdinc O., "Economic impacts of small-scale own generating and storage units, and electric vehicles under different demand response strategies for smart households.," *Applied Energy*, vol. 126, 2014, pp. 142–150.

[33] Fathabadi H., "Utilization of electric vehicles and renewable energy sources used as distributed generators for improving characteristics of electric power distribution systems.," *Energy*, vol. 90, 2015, pp. 1100–1110.

[34] Fisher M.L., "An applications oriented guide to Lagrangian relaxation.," *Interfaces*, vol. 15, no. 2, 1985, pp. 10–21.

[35] Fleet Carma, "Electric Vehicle Sales in the United States: 2016 Final Update.," Available from: http://www.fleetcarma.com/ev-sales-usa-2016-final/, 2016.

[36] Flores R.J., Shaffer B.P., Brouwer J., "Electricity costs for a Level 3 electric vehicle fueling station integrated with a building.," *Applied Energy*, vol. 191, 2017, pp. 367–384.

[37] Gan L., Topcu U., Low S.H., "Optimal decentralized protocol for electric vehicle charging.," *IEEE Transactions on Power Systems*, vol. 28, no. 2, 2013, pp. 940–951.

[38] Ge S., Feng L., Liu H., "The planning of electric vehicle charging station based on Grid partition method.," *2011 International Conference on Electrical and Control Engineering, ICECE 2011 - Proceedings.*, 2011, pp. 2726–2730.

[39] General Algebraic Modeling System (GAMS), ," Available from: http://www.gams.com/, 2013.

[40] Gigaom, "This is Teslas first battery swap station.," Available from: http://gigaom.com/2015/01/29/this-is-teslas-first-battery-swap-station-photos/, 2015.

[41] Gough R., Dickerson C., Rowley P., Walsh C., "Vehicle-to-grid feasibility: A techno-economic analysis of EV-based energy storage.," *Applied Energy*, vol. 192, 2017, pp. 12–23.

[42] Guignard M., "Lagrangean relaxation.," *Top*, vol. 11, no. 2, 2003, pp. 151–200.

[43] Gul S., Denton B.T., Fowler J., "A Multi-Stage Stochastic Integer Programming Model for Surgery Planning," *INFORMS Journal on Computing*, vol. In-press, 2015, pp. 445–456.

[44] Guo Y., Hu J., Su W., "Stochastic optimization for economic operation of plug-in electric vehicle charging stations at a municipal parking deck integrated with on-site renewable energy generation," *2014 IEEE Transportation Electrification Conference and Expo (ITEC)*, 2014, pp. 1–6.

[45] Haddadian G., Khalili N., Khodayar M., Shahidehpour M., "Optimal coordination of variable renewable resources and electric vehicles as distributed storage for energy sustainability.," *Sustainable Energy, Grids and Networks*, vol. 6, 2016, pp. 14–24.

[46] Haddadian G., Khalili N., Khodayar M., Shahiedehpour M., "Security-constrained power generation scheduling with thermal generating units, variable energy resources, and electric vehicle storage for V2G deployment.," *International Journal of Electrical Power & Energy Systems*, vol. 73, 2015, pp. 498–507.

[47] He F., Wu D., Yin Y., Guan Y., "Optimal deployment of public charging stations for plug-in hybrid electric vehicles.," *Transportation Research Part B*, vol. 47, 2013, pp. 87–101.

[48] He Y., Venkatesh B., Guan L., "Optimal Scheduling for Charging and Discharging of Electric Vehicles.," *IEEE Transactions on Smart Grid*, vol. 3, no. 3, 2012, pp. 1095–1105.

[49] Helgason T., Wallace S.W., "Approximate scenario solutions in the progressive hedging algorithm," *Annals of Operations Research*, vol. 31, 1991, pp. 425–444.

[50] Honarmand M., Zakariazadeh A., Jadid S., "Integrated scheduling of renewable generation and electric vehicles parking lot in a smart microgrid.," *Energy Conversion and Management*, vol. 86, 2014, pp. 745–755.

[51] Hong L., Pingliang Z., Jianyi G., Huiyu W., Shaoyun G., "An optimization strategy of controlled electric vehicle charging considering demand side response and regional wind and photovoltaic.," *Journal of Modern Power Systems and Clean Energy*, vol. 2, no. 2, 2015, pp. 232–239.

[52] Hosseini M., MirHassani S.A., "Refueling-station location problem under uncertainty.," *Transportation Research Part E*, vol. 84, 2015, pp. 101–116.

[53] Huang Y., Fan Y., Chen C.-W, "An integrated bio-fuel supply chain against feedstock seasonality and uncertainty.," *Transportation Science*, vol. 48, no. 4, 2014, pp. 540–554.

[54] Hvattum L.M., Lokketangen A., "Using scenario trees and progressive hedging for stochastic inventory routing problems," *Journal of Heuristics*, vol. 15, 2009, pp. 527–557.

[55] Inside EVs, "Electric vehicle sales in the U.S.," Available from: `http://insideevs.com/`, 2016.

[56] International Energy Agency (IEA)., "Global EV Outlook 2017.," Available from: `https://www.iea.org/publications/freepublications/publication/GlobalEVOutlook2017.pdf`, 2017.

[57] Ip A., Fong S., Liu E., "Optimization for allocating BEV recharging stations in urban areas by using hierarchical clustering.," *Advanced Information Management and Service (IMS), 2010 6th International Conference on.*, 2010, pp. 460–465.

[58] Jia L., Hu Z., Song Y., Luo Z., "Optimal siting and sizing of electric vehicle charging stations.," *IEEE International Electric Vehicle Conference*, 2012, pp. 1–6.

[59] Jin C., Sheng X., Ghosh P., "Optimized electric vehicle charging with intermittent renewable energy sources.," *IEEE Journal of Selected Topics in Signal Processing*, vol. 8, no. 6, 2014, pp. 1063–1072.

[60] Karan E., Mohammadpour A., Asadi S., "Integrating building and transportation energy use to design a comprehensive greenhouse gas mitigation strategy.," *Applied Energy*, vol. 165, 2016, pp. 234–243.

[61] Kavousi-Fard A., Khodaei A., "Efficient integration of plug-in electric vehicles via reconfigurable microgrids.," *Energy*, vol. 111, 2016, pp. 653–663.

[62] Kleywegt A.J., Shapiro A., Homem-De-Mello T., "The sample average approximation method for stochastic discrete optimization.," *SIAM Journal of Optimization*, vol. 12, 2001, pp. 479–502.

[63] Kostina A.M., Guillen-Gosalbeza G., Meleb F.D., Bagajewiczc M.J., Jimeneza L., "A novel rolling horizon strategy for the strategic planning of supply chains. Application to the sugar cane industry of Argentina.," *Computers & Chemical Engineering*, vol. 35, 2011, pp. 2540–2563.

[64] Kriett P.O., Salani M., "Optimal control of a residential microgrid.," *Energy*, vol. 42, no. 1, 2012, pp. 321–330.

[65] Kuby M., Lim S., "The flow-refueling location problem for alternative-fuel vehicles.," *Socio-Economic Planning Sciences*, vol. 39, no. 2, 2005, pp. 125–145.

[66] Li J., "Compatibility and Investment in the US Electric Vehicle Market.," Available from: `https://scholar.harvard.edu/files/jingli/files/li_jmp.pdf`, 2017.

[67] Li S., Huang Y., Mason S.J., "A multi-period optimization model for the deployment of public electric vehicle charging stations on network.," *Transportation Research Part C: Emerging Technologies*, vol. 65, 2016, pp. 128–143.

[68] Liu C., Wang J., Botterud A., Zhou Y., Vyas A., "Assessment of Impacts of PHEV Charging Patterns on Wind-Thermal Scheduling by Stochastic Unit Commitment.," *IEEE Transactions on Smart Grid*, vol. 3, no. 2, 2012, pp. 675–683.

[69] Liu N., Chen Q., Liu J., Lu X., Li P., Lei J., Zhang J., "A heuristic operation strategy for commercial building microgrids containing EVs and PV system.," *IEEE Transactions on Industrial Electronics*, vol. 62, no. 4, 2015, pp. 2560–2570.

[70] Liu N., Chen Z., Liu, J., Tang X., Xiao X., Zhang J., "Multi-objective optimization for component capacity of the photovoltaic-based battery switch stations: Towards benefits of economy and environment.," *Energy*, vol. 64, 2014, pp. 779–792.

[71] Liu W., Niu S., Xu H., Li X., "A new method to plan the capacity and location of battery swapping station for electric vehicle considering demand side management.," *Sustainability*, vol. 8, no. 6, 2016, p. 557.

[72] Lopes J.A.P., Soares F.J., Almeida P.M.R., "Integration of electric vehicles in the electric power system.," *Proceedings of the IEEE*, vol. 99, no. 1, 2011, pp. 168–183.

[73] Magnanti T.L., Wong R.T., "Acclerating Benders Decomposition: Algorithmic enhancement and model selection criteria.," *Operations Research*, vol. 29, 1981, pp. 464–484.

[74] Mak H.Y., Rong Y., Shen Z.M., "Infrastructure planning for electric vehicles with battery swapping.," *Management Science*, vol. 59, no. 7, 2013, pp. 1557–1575.

[75] Mak W.K., Morton D.P., Wood R.K., "Monte Carlo bounding techniques for determining solution quality in stochastic programs.," *Operations Research Letters*, vol. 24, 1999, pp. 47–56.

[76] Marino C., Quddus M.A., Marufuzzaman M., Cowan M., Bednar A.E., "A chance-constrained two-stage stochastic programming model for reliable microgrid operations under power demand uncertainty.," *Sustainable Energy, Grids and Networks*, vol. 13, 2018, pp. 66–77.

[77] Marmaras C., Xydas E., Cipcigan L., "Simulation of electric vehicle driver behaviour in road transport and electric power networks.," *Transportation Research Part C: Emerging Technologies*, vol. 80, 2017, pp. 239–256.

[78] McCormick G.P, "Computability of global solutions to factorable nonconvex programs: Part IConvex underestimating problems.," *Mathematical programming*, vol. 10, no. 1, 1976, pp. 147–175.

[79] MirHassani S.A., Ebrazi R., "A flexible reformulation of the refueling station location problem.," *Transportation Science*, vol. 47, no. 4, 2012, pp. 617–628.

[80] Momber I., Gomez T., Venkataramanan G., Stadler M., Beer S., Lai J., Marnay C., Battaglia V., "Plug-in electric vehicle interactions with a small office building: An economic analysis using DER-CAM," *Power and Energy Society General Meeting, 2010 IEEE*, 2010, pp. 1–8.

[81] Mulvey J.M., Ruszczynski A., "A new scenario decomposition method for large-scale stochastic optimization.," *Operations Research*, vol. 43, no. 3, 1995, pp. 477–490.

[82] Mulvey J.M., Vladimirou H., "Applying the progressive hedging algorithm to stochastic generalized networks," *Annals of Operations Research*, vol. 31, 1991, pp. 399–424.

[83] National Renewable Energy Laboratory., "National solar radiation data base.," Available from: http://rredc.nrel.gov/solar/old_data/nsrdb/, 2010.

[84] Nilsson M., "Electric vehicles: The phenomenon of range anxiety.," *ELVIRE, Gif-sur-Yvette Cedex, France, ELVIRE Consortium FP7CICT-2009C4-249105*, 2011.

[85] Norkin V.I., Ermoliev Y.M., Ruszczynski A., "On optimal allocation of indivisibles under uncertainty.," *Operations Research*, vol. 46, 1998, pp. 381–395.

[86] Norkin V.I., Pflug G.C., Ruszczynski A., "A branch and bound method for stochastic global optimization.," *Mathematical Programming*, vol. 83, no. 3, 1998, pp. 425–450.

[87] Nurre S.G., Bent R., Pan F., Sharkey T.C., "Managing operations of plug-in hybrid electric vehicle (PHEV) exchange stations for use with a smart grid.," *Energy Policy*, vol. 67, 2014, pp. 364–377.

[88] Ortega-Vazquez M.A., Bouffard F., Silva V., "Electric Vehicle Aggregator System Operator Coordination for Charging Scheduling and Services Procurement.," *IEEE Transactions on Power Systems*, vol. 28, no. 2, 2013, pp. 1806–1815.

[89] Pan F., Bent R., Berscheid A., Izraelevitz D., "Locating PHEV Exchange Stations in V2G," *2010 First IEEE International Conference on Smart Grid Communications.*, 2010, pp. 173–178.

[90] Pang C., Dutta P., Kezunovic M., "BEVs/PHEVs as dispersed energy storage for V2B uses in the smart grid.," *IEEE Transactions on Smart Grid*, vol. 3, no. 1, 2012, pp. 473–482.

[91] Plug in America, "EV Battery Amortization Costs and Vehicle To Grid.," Available from: http://pluginamerica.org/ev-battery-amortization-costs-and-vehicle-grid/, 2016.

[92] Pluginsites, "Plug In Sites EV Charging Stations.," Available from: http://pluginsites.org/how-many-plug-in-electric-vehicles-are-in-md-va-dc/, 2016.

[93] PlugShare, "PlugShare EV Charging Station Map Find a place to charge your car.," Available from: https://www.plugshare.com/, 2016.

[94] Poudel S., Marufuzzaman M., Quddus M.A., Chowdhury S., Bian L., Smith B., "Designing a Reliable and Congested Multi-Modal Facility Location Problem for Biofuel Supply Chain Network.," *Energies*, vol. 11, no. 7, 2018, p. 1682.

[95] Poudel S.R., Quddus M.A., Chowdhury S., Marufuzzaman M., Bian L., Smith B.K., "Designing a Reliable and Congested Network for Biofuel Supply Chain Network," *Transportation Research Board 96th Annual Meeting*, 2017, number (No. 17-00108).

[96] Poudel S.R., Quddus M.A., Marufuzzaman M., Bian L., Reuben F.B.V., "Managing congestion in a multi-modal transportation network under biomass supply uncertainty.," *Annals of Operations Research*, 2017, pp. 1–43.

[97] Public Service Commission of the District of Columbia, "Report on the Renewable Energy Portfolio Standard for Compliance Year 2015.," Available from: `http://www.dcpsc.org/getmedia/901b3c18-4859-435d-ae1a-ca296584c26b/aharris_542016_831_1_FC_-_945_-_2016_-_E_-_REPORT.aspx`, 2016.

[98] Qian K., Zhou C., Allan M., Yuan Y., "Modeling of load demand due to EV battery charging in distribution systems.," *IEEE Transactions on Power Systems*, vol. 26, no. 2, 2011, pp. 802–810.

[99] Quddus M.A., Chowdhury S., Marufuzzaman M., Yu F., Bian L., "A two-stage chance-constrained stochastic programming model for a bio-fuel supply chain network.," *International Journal of Production Economics*, vol. 195, 2018, pp. 27–44.

[100] Quddus M.A., Hossain N.U.I., Marufuzzaman, M., Jaradat R.M., Roni M.S., "Sustainable network design for multi-purpose pellet processing depots under biomass supply uncertainty.," *Computers & Industrial Engineering*, vol. 110, 2017, pp. 462–483.

[101] Quddus M.A., Shahvari O., Marufuzzaman M., Usher J.M., Jaradat R., "A collaborative energy sharing optimization model among electric vehicle charging stations, commercial buildings, and power grid.," *Applied Energy*, vol. 229, 2018, pp. 841–857.

[102] Raman R., Grossmann I.E., "Modelling and computational techniques for logic based integer programming.," *Computers & Chemical Engineering*, vol. 18, no. 7, 1979, pp. 563–578.

[103] Rockafellar R.T., Wets R.J.-B., "Scenarios and policy aggregation in optimization under uncertainty," *Mathematics of operations research*, vol. 16, 1991, pp. 119–147.

[104] Salt River Project power and water, "Electric Vehicle Price Plan.," Available from: `http:www.srpnet.com/prices/home/electricvehicle.aspx`, 2015.

[105] Santoso T., Ahmed S., Goetschalckx M., Shapiro A., "A stochastic programming approach for supply chain network design under uncertainty.," *European Journal of Operational Research*, vol. 167, 2005, pp. 96–115.

[106] Schutz P., Tomasgard A., Ahmed S., "Supply chain design under uncertainty using sample average approximation and dual decomposition.," *European Journal of Operational Research*, vol. 199, 2009, pp. 409–419.

[107] Sehar F., Pipattanasomporn M., Rahman S., "Demand management to mitigate impacts of plug-in electric vehicle fast charge in buildings with renewables.," *Energy*, vol. 120, 2017, pp. 642–651.

[108] Solar Cell Central, "Solar Electricity Costs," Available from: `http://solarcellcentral.com/cost_page.html`, 2016.

[109] Stadler M., Kloess M., Groissbock M., Cardoso G., Sharma R., Bozchalui M.C., Marnay C., "Electric storage in Californias commercial buildings.," *Applied Energy*, vol. 104, 2013, pp. 711–722.

[110] Su W., Chow M.Y, "Performance evaluation of an EDA-based large-scale plug-in hybrid electric vehicle charging algorithm.," *IEEE Transactions on Smart Grid*, vol. 3, no. 1, 2012, pp. 308–315.

[111] Su W., Eichi H., Zeng W., Chow M.Y., "A survey on the electrification of transportation in a smart grid environment.," *IEEE Transactions on Industrial Informatics*, vol. 8, no. 1, 2012, pp. 1–10.

[112] Sweda T., Klabjan D., "An agent-based decision support system for electric vehicle charging infrastructure deployment.," *Vehicle Power and Propulsion Conference (VPPC), 2011 IEEE.*, 2011, pp. 1–5.

[113] Tang C., "A scenario decomposition-genetic algorithm method for solving stochastic air cargo container loading problems.," *Transportation Research Part E: Logistics and Transportation Review*, vol. 47, no. 4, 2011, pp. 520–531.

[114] Tasdighi M., Ghasemi H., Rahimi-Kian A., "Residential microgrid scheduling based on smart meters data and temperature dependent thermal load modeling.," *IEEE Transactions on Smart Grid*, vol. 5, no. 1, 2014, pp. 349–357.

[115] U.S. Department of Energy, "EV Everywhere Grand Challenge Road to Success.," Available from: `http://energy.gov/sites/prod/files/2014/02/f8/eveverywhere_road_to_success.pdf`, 2014.

[116] U.S. Energy Information Administration., "Energy consumption estimates by sector.," Available from: `https://www.eia.gov/consumption/`, 2017.

[117] U.S. Energy Information Administration., "U.S. CO_2 emissions by sector.," Available from: http://architecture2030.org/buildings_problem_why/, 2017.

[118] U.S. Energy Information Administration., "U.S. daily demand curve.," Available from: https://www.eia.gov/beta/realtime_grid/#/summary/demand?end=20170629&start=20170529, 2017.

[119] U.S. Energy Information Administration (EIA), "How much gasoline does the United States consume.," Available from: https://www.eia.gov/tools/faqs/faq.php?id=23&t=10, 2016.

[120] Verweij B., Ahmed S., Kleywegt A.J., Nemhauser G., Shapiro A., "The sample average approximation method applied to stochastic routing problems: A computational study.," *Computational Optimization and Applications*, vol. 24, 2003, pp. 289–333.

[121] Vidyarthi N., Jayaswal S., "Efficient solution of a class of locationallocation problems with stochastic demand and congestion.," *Computers and Operations Research*, vol. 48, 2014, pp. 20–30.

[122] Vries H.D., Duijzer E., "Incorporating driving range variability in network design for refueling facilities.," *Omega*, vol. 69, 2017, pp. 102–114.

[123] Wallace S.W., Helgason T., "Structural properties of the progressive hedging algorithm," *Annals of Operations Research*, vol. 31, 1991, pp. 445–456.

[124] Wang Y.W., Lin C.C., "Locating multiple types of recharging stations for battery-powered electric vehicle transport.," *Transportation Research Part E*, vol. 58, 2013, pp. 76–87.

[125] Washington State Department of Transportation, "Washington State Electric Vehicle Action Plan.," Available from: http://www.wsdot.wa.gov/NR/rdonlyres/28559EF4-CD9D-4CFA-9886-105A30FD58C4/0/WAEVActionPlan2014.pdf, 2015.

[126] Watson J.P., Woodruff D.L., "Progressive hedging innovations for a class of stochastic mixed-integer resource allocation problems.," *Computational Management Science*, vol. 8, 2011, pp. 355–370.

[127] Widrick R.S., Nurre S.G., Robbins M.J., "Optimal Policies for the Management of an Electric Vehicle Battery Swap Station.," *Transportation Science*, 2016.

[128] Williams J. L., "Information theoretic sensor management.," Available from: http://dspace.mit.edu/handle/1721.1/38534, 2007.

[129] Worley O., Klabjan D., "Optimization of battery charging and purchasing at electric vehicle battery swap stations.," *2011 IEEE Vehicle Power and Propulsion Conference*, 2011, pp. 1–4.

[130] Xi X., Sioshansi R., Marano V., "Simulation-optimization model for location of a public electric vehicle charging infrastructure.," *Transportation Research Part D: Transport and Environment*, vol. 22, 2013, pp. 60–69.

[131] Zanjani M.K., Nourelfath M., Ait-Kadi D., "A scenario decomposition approach for stochastic production planning in sawmills.," *Journal of the Operational Research Society*, vol. 64, no. 1, 2013, pp. 48–59.

[132] Zhang A., Kang J.E., Kwon C., "Incorporating Demand Dynamics in Multi-Period Capacitated Fast-Charging Location Planning for Electric Vehicles.," , 2017.

[133] Zhang P., Qian K., Zhou C., Stewart B.G., Hepburn, D.M., "A methodology for optimization of power systems demand due to electric vehicle charging load.," *IEEE Transactions on Power Systems*, vol. 27, no. 3, 2012, pp. 1628–1636.

[134] Zhang T., Chen W., Han Z., Cao Z., "Charging Scheduling of Electric Vehicles With Local Renewable Energy Under Uncertain Electric Vehicle Arrival and Grid Power Price.," *IEEE Transactions on Vehicular Technology*, vol. 63, no. 6, 2014, pp. 2600–2612.

[135] Zheng Y., Dong Z.Y., Xu Y., Meng K., Zhao J.H., Qiu J., "Electric vehicle battery charging/swap stations in distribution systems: comparison study and optimal planning.," *IEEE Transactions on Power Systems*, vol. 29, no. 1, 2014, pp. 221–229.